Journal of Ophthalmology

Effects of Ageing on the Anterior Segment of the Eye Structure and Function

Lead Guest Editor: Alejandro Cerviño
Guest Editors: Jose F. Alfonso, Hema Radhakrishnan, Jose M. González-Meijome, and Rune Brautaset

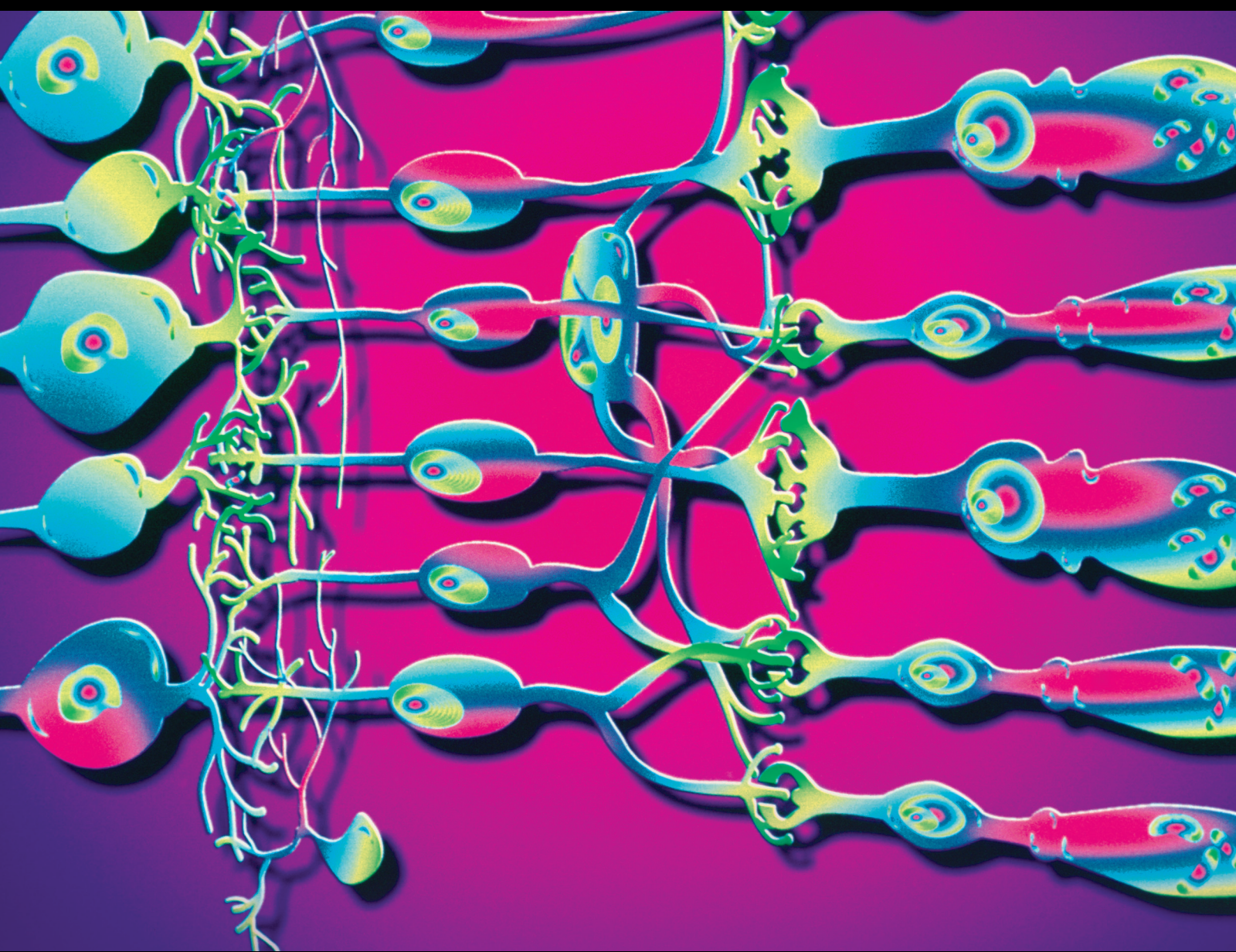

Effects of Ageing on the Anterior Segment of the Eye Structure and Function

Journal of Ophthalmology

Effects of Ageing on the Anterior Segment of the Eye Structure and Function

Special Issue Editor in Chief: Alejandro Cerviño
Guest Editors: Jose F. Alfonso, Hema Radhakrishnan, Jose M. González-Meijome, and Rune Brautaset

Editorial Board

Contents

Effects of Ageing on the Anterior Segment of the Eye Structure and Function
Alejandro Cerviño, Hema Radhakrishnan, José F. Alfonso, Rune Brautaset, and José M. González-Meijome
Editorial (2 pages), Article ID 6260829, Volume 2018 (2018)

Biomaterial Influence on Intraocular Lens Performance: An Overview
Cari Pérez-Vives
Review Article (17 pages), Article ID 2687385, Volume 2018 (2018)

Through-Focus Vision Performance and Light Disturbances of 3 New Intraocular Lenses for Presbyopia Correction
Santiago Escandón-García, Filomena J. Ribeiro, Colm McAlinden, António Queirós, and José M. González-Méijome
Clinical Study (8 pages), Article ID 6165493, Volume 2018 (2018)

Chosen Vascular Risk Markers in Pseudoexfoliation Syndrome: An Age-Related Disorder
Hanna Lesiewska, Agnieszka Łukaszewska-Smyk, Grażyna Odrowąż-Sypniewska, Magdalena Krintus, Aneta Mańkowska-Cyl, and Grażyna Malukiewicz
Research Article (4 pages), Article ID 5231095, Volume 2017 (2018)

Axial Length and Ocular Development of Premature Infants without ROP
Yi Zha, Guangdong Zhu, Jinfei Zhuang, Haihua Zheng, Jianqiu Cai, and Wangqiang Feng
Research Article (4 pages), Article ID 6823965, Volume 2017 (2018)

Molecular Age-Related Changes in the Anterior Segment of the Eye
Luis Fernando Hernandez-Zimbron, Rosario Gulias-Cañizo, María F. Golzarri, Blanca Elizabeth Martínez-Báez, Hugo Quiroz-Mercado, and Roberto Gonzalez-Salinas
Review Article (8 pages), Article ID 1295132, Volume 2017 (2018)

New Objective Refraction Metric Based on Sphere Fitting to the Wavefront
Mateusz Jaskulski, Andreí Martínez-Finkelshtein, and Norberto López-Gil
Research Article (9 pages), Article ID 1909348, Volume 2017 (2018)

Steeper Iris Conicity Is Related to a Shallower Anterior Chamber: The Gutenberg Health Study
Alexander K. Schuster, Norbert Pfeiffer, Stefan Nickels, Andreas Schulz, Philipp S. Wild, Maria Blettner, Karl Lackner, Manfred E. Beutel, Thomas Münzel, and Urs Vossmerbaeumer
Research Article (10 pages), Article ID 2190347, Volume 2017 (2018)

Accommodative Stimulus-Response Curve with Emoji Symbols
Robert Montés-Micó, José J. Esteve Taboada, Paula Bernal-Molina, and Teresa Ferrer-Blasco
Research Article (5 pages), Article ID 4165706, Volume 2017 (2018)

Evaluation of Cholinergic Deficiency in Preclinical Alzheimer's Disease Using Pupillometry
Shaun Frost, Liam Robinson, Christopher C. Rowe, David Ames, Colin L. Masters, Kevin Taddei, Stephanie R. Rainey-Smith, Ralph N. Martins, and Yogesan Kanagasingam
Research Article (8 pages), Article ID 7935406, Volume 2017 (2018)

Changes in Intraocular Straylight and Visual Acuity with Age in Cataracts of Different Morphologies
Sonia Gholami, Nicolaas J. Reus, and Thomas J. T. P. van den Berg
Review Article (12 pages), Article ID 5649532, Volume 2017 (2018)

Intraocular Telescopic System Design: Optical and Visual Simulation in a Human Eye Model
Georgios Zoulinakis and Teresa Ferrer-Blasco
Research Article (8 pages), Article ID 6030793, Volume 2017 (2018)

Hindawi
Journal of Ophthalmology
Volume 2018, Article ID 6260829, 2 pages
https://doi.org/10.1155/2018/6260829

Editorial

Effects of Ageing on the Anterior Segment of the Eye Structure and Function

Alejandro Cerviño,[1] **Hema Radhakrishnan**,[2] **José F. Alfonso**,[3] **Rune Brautaset**,[4] **and José M. González-Meijome**[5]

[1]*Optometry Research Group, Department of Optics & Optometry & Vision Sciences, Universidad de Valencia, Valencia, Spain*
[2]*School of Health Sciences, The University of Manchester, Manchester, UK*
[3]*Fernández-Vega Ophthalmology Institute, Oviedo, Spain*
[4]*Department of Clinical Neuroscience, Karolinska Institutet, Stockholm, Sweden*
[5]*Department of Physics (Optometry), University of Minho, Braga, Portugal*

Correspondence should be addressed to Alejandro Cerviño; alejandro.cervino@uv.es

Received 13 February 2018; Accepted 14 February 2018; Published 9 May 2018

The world will soon have more aged people than children and more people at extreme old age than ever before [1]. Improving quality of life as well as reducing severe disability due to age-related problems has become key for the health systems worldwide. The ageing of the world population has both structural and functional consequences for the human visual system; changes due to ageing occur in all the structures of the eye causing a variety of effects.

Over the last few years, great advances in ophthalmic instrumentation allow the determination of ocular parameters to a level of detail without precedent. Such advances allow researchers to develop specific devices for visual correction and rehabilitation and at the same time guide the clinicians in their decision making and selection of treatment options to convey with the increasing demand of high-quality outcomes of the ageing population.

This special issue aimed at creating a multidisciplinary forum of discussion on recent advances in the knowledge of the effects of ageing in the anterior segment of the human eye's structure and function, and improvements on early detection, treatment, and prognosis of age-related ocular conditions of the anterior segment. As a result, a remarkable compilation of ten articles cover many of these very different aspects of ocular ageing.

Y. Zha et al. report significant biometric differences between preterm infants without retinopathy compared to term infants with interesting implications in refractive development. L. F. Hernandez-Zimbrón et al. carried out an interesting revision of different age-related processes occurring in the different structures of the anterior segment of the eye from a biological perspective and at molecular level. They conclude that the structural and molecular changes observed in the anterior eye segment are caused by molecular changes in intercellular unions, structural arrangements of collagen fibers, overexpression of degradation enzymes, underexpression of inhibitors of metalloproteases in tissues, UV light absorbed, inflammatory cytokines and molecules, and dysregulation of autophagy, among others.

All these changes affect the optical properties of the optical media, and this topic is covered by S. Gholami et al., who investigate the changes in retinal straylight occurring with cataracts of different types and their impact in visual performance, highlighting the importance of including cataract morphology when assessing the visual impact of this age-related condition. M. Jaskulski et al. propose a new refraction metric to better predict spherocylindrical refraction from optical quality metrics for varying pupil sizes. Pupil size determination, on the other side, is suggested by S. Frost

and coauthors as an interesting tool for screening preclinical Alzheimer disease since they report changes in pupil flash response in this preclinical phase of the condition.

Pseudoexfoliation syndrome as an age-related complex systemic disorder and its relationship with vascular disease was explored by H. Lesiewska et al., which has been inconclusive from the outcomes of previous reports.

A. K. Schuster et al. report on the distribution of iris conicity using Scheimpflug imaging in a population-based study, part of the outcomes from the Gutenberg Health Study, and test whether pseudophakia allows the iris to sink back. They conclude that steeper conicity was independently associated with a shallow anterior chamber and thicker crystalline lens, while older persons had flatter iris conicity. They also found that cataract surgery flattens the iris position, therefore reducing the risk of angle closure.

The topic of cataract surgery has also been covered by an extensive review by C. Perez-Vives, particularly on current biomaterials used for intraocular lenses and their benefits and complications. Intraocular corrective systems have evolved dramatically over the last decades, providing with advanced designs for overcoming the functional limitations of crystalline lens ageing, that is, loss of transparency and loss of accommodation. But the high incidence of retinal disease also implies a relatively high prevalence of specific aids for visual remains optimization through customized optical-based devices. Those advances allowed the field to evolve into clinical solutions that offer a satisfactory recovery of the capability to see at different distances with customized extended depth of focus and multifocal intraocular lenses. These devices induce, however, some challenges to the patient with the manifestation of dysphotopsia that can now be measured and quantified in the clinical setting. G. Zoulinakis and T. Ferrer-Blasco present a new intraocular telescopic system designed for magnifying retinal image that would benefit eyes with localized retinal damage.

In addition, the advent of technological progress, increasing dependance on mobile technology, and global use of social networks imply that the accommodative system is exposed to new challenges and demands for longer periods of time at any age. R. Montés-Micó et al. explore the accommodative stimulus curve with emoji symbols in an original study that reveals similar responses than those obtained when reading standard text on smartphones.

To summarize, the present special issue accomplished its main aim, that is, novel approaches to age-related functional problems have been proposed, comprehensive reviews on important issues related with ageing of ocular structures and the solutions to the functional problems involved were addressed, and studies on the changes occurring with ageing from different perspectives and from young to old eyes were presented.

Alejandro Cerviño
Hema Radhakrishnan
José F. Alfonso
Rune Brautaset
José M. González-Meijome

References

[1] World Health Organization, *Global Health and Aging*, US National Institute of Aging, Bethesda, MD, USA, 2011.

Hindawi
Journal of Ophthalmology
Volume 2018, Article ID 2687385, 17 pages
https://doi.org/10.1155/2018/2687385

Review Article

Biomaterial Influence on Intraocular Lens Performance: An Overview

Cari Pérez-Vives

Alcon Management SA, Geneva, Switzerland

Correspondence should be addressed to Cari Pérez-Vives; caridad.perez_vives@alcon.com

Received 8 June 2017; Revised 8 December 2017; Accepted 2 January 2018; Published 15 March 2018

Academic Editor: Jose M. González-Meijome

There is strong evidence that the IOL material is the factor having the greatest impact on posterior capsule opacification (PCO), anterior capsule opacification (ACO) development, and glistening formation after cataract surgery, even though there are other IOL features—such as haptic material and design and edge and optic design—that also have some influence. We reviewed the published literature describing the adverse events that are mainly related to the intraocular lens (IOL) material, such as PCO, ACO, and the subsequent capsule contraction, as well as glistening formation. The adverse events presented in this overview are the most common ones in clinical practice, and therefore, they are generally included in the clinical protocols for IOL evaluation.

1. Introduction

Cataract is at present the second cause of blindness worldwide after age-related macular degeneration; moreover, in Eastern and Central Europe, cataract is still the leading cause [1]. In the United States (US) alone, cataract affects—in at least one eye—an estimated 20.5 million people (17.2%) over 40 years of age, and 6.1 million (5.1%) people have pseudophakia/aphakia. The total number of US people having cataract is predicted to increase up to 30.1 million by 2020, and 9.5 million of them are expected to have pseudophakia/aphakia [2]. Consequently, cataract surgery is one of the most frequent surgical procedures.

Cataract surgery is constantly evolving and improving in terms of the lens material and designs. The first intraocular lenses (IOLs), which were manufactured in 1949, were made of rigid plastic—namely, polymethyl methacrylate (PMMA)—and this biomaterial was the only one available for IOL implantation for over 30 years. The first implanted PMMA IOLs were implanted through an extracapsular surgical technique that resulted in large incisions and induced postoperative astigmatism. Subsequently, the design and the surgical technique have greatly improved. In the early 1970s, Charles Kelman introduced phacoemulsification, thus reducing the incision size, and initiated biomaterial diversification, including foldable materials such as silicone, hydrogel, and acrylic compounds [3, 4]. Today, cataract surgery is mainly performed using phacoemulsification and a foldable IOL, which is implanted through a small incision.

There are many types of IOLs, in terms of both optic features and materials. IOL design and materials are constantly evolving fields, aiming for better refractive outcomes with minimal incision size and trying to minimize host-cell response, since it may cause posterior capsule opacification (PCO), anterior capsular opacification (ACO), and lens epithelial cell (LEC) proliferation. IOL materials vary in water content, chemical composition, refractive index, and tensile strength, while IOL designs have different optic size, edge profiles, and haptic materials and designs, with the main goal of minimizing decentration, dislocations, optical aberrations, and opacifications [5–7].

The literature search was conducted in the Embase®, Medline® and Medline In-process, and the Cochrane databases through Embase and Ovid® platforms from January 2000 to December 2015. A detailed search strategy using terms related to cataract, intraocular lens, posterior capsular opacification, Nd:YAG laser, anterior capsule opacification, capsule contraction, and glistenings was prepared, to identify

published literature reporting evidence that matched our research objectives.

This review provides an overview of the currently available IOL materials and designs and discusses their effect upon PCO, ACO, capsule contraction, and glistening formation.

2. Posterior Capsule Opacification

Surgical trauma during the surgery initially causes blood-aqueous barrier breakdown. This leads to protein leakage and macrophage migration from the blood into the surgical zone, eliciting immediate postoperative inflammation. The cellular reaction consists of two main components. One component comprises large cells, macrophages, and epithelioid cells, which later coalesce to form foreign body type giant cells, which represent uveal biocompatibility. The other comprises LECs, which can be divided into PCO and ACO. The source of the PCO is the equatorial cells originating from the equator of the capsule. These cells go through metaplasia and acquire the ability to migrate and proliferate, causing epithelial ingrowth between the IOL and the posterior capsule, which leads to a reduction in VA. PCO still remains the most frequent complication of modern cataract surgery. Advances in surgical techniques and IOL materials and designs have reduced PCO rates, but it is still a significant problem in clinical practice [8]. PCO can be effectively treated by using a neodymium:YAG (Nd:YAG) laser to cut a hole in the posterior lens capsule. However, this procedure may lead to additional complications, including IOL damage, intraocular pressure (IOP) elevation, glaucoma, cystoid macular edema, or even retinal detachment [9]. The pathophysiology of PCO is multifactorial, varying particularly with the surgical technique, IOL materials, and designs [10–14], but since dissociation of each factor involved in PCO development is almost impossible, it is very difficult to differentiate between the individual elements in clinical practice.

Regarding the IOL material, the Linnola "sandwich theory" states that bioactive materials allow a single LEC to bond to both the IOL and the posterior capsule. This produces a sandwich pattern including the IOL, the LEC monolayer, and the posterior capsule, thus preventing further cell proliferation and capsular bag opacification [15]. Other studies carried out by Linnola et al. evaluated the adhesiveness of fibronectin, vitronectin, laminin, and type-IV collagen to IOL materials (PMMA, silicone, hydrophobic acrylate, and hydrogel), both *in vitro* [16] and in cadaver eyes [17, 18]. They found that fibronectin and laminin bond best to hydrophobic acrylate IOLs, resulting in better attachment to the capsule. This stronger binding could explain the enhanced adhesion of hydrophobic acrylate IOL to the anterior and posterior capsules and, as a result, the lower PCO and Nd:YAG capsulotomy rates [14, 19–34]. However, observational studies in animals [35] and cadaver eyes [36] showed that the IOL having a sharp posterior optic edge may play a more relevant role in this effect than the IOL material.

Table 1 shows the PCO and Nd:YAG rates reported in previous studies carried out for different IOL materials and designs [12–14, 19–34, 37–47]. Hydrophilic acrylic (including those hydrophilic IOLs with the hydrophobic surface) [25] and PMMA IOLs are associated with higher PCO rates, greater PCO severity, and also higher Nd:YAG capsulotomy rates than hydrophobic acrylic IOLs. Several comparative studies showed a superior reduction in PCO and laser capsulotomy rates with hydrophobic acrylic IOLs, compared with hydrophilic acrylic ones.

Auffarth et al. [20] analyzed PCO and Nd:YAG laser treatment as a function of the IOL material (PMMA, silicone, hydrophilic acrylic, and hydrophobic acrylic). After 3 years of follow-up, hydrophobic acrylic IOLs showed a statistically lower incidence of PCO and Nd:YAG rates than the other three materials. A prospective randomized contralateral study [26] reported significantly higher PCO rates in eyes implanted with a hydrophilic hydrogel IOL (Hydroview H60M, B&L) than in eyes having a hydrophobic acrylic IOL (Acrysof MA60BM, Alcon). Moreover, the results revealed that this PCO led to a notably impaired visual acuity. After two years of follow-up, 28% of the eyes in the hydrophilic group and 2% in the hydrophobic acrylic group had required Nd:YAG capsulotomy. Boureau et al., in a retrospective study [23], compared the incidence of Nd:YAG laser treatment for three square-edge IOL models having different design and material compositions. After 3 years of follow-up, the proportion of patients requiring Nd:YAG laser treatment amounted to 12% for the SA60AT (Alcon) group, 25.2% for the AR40e (AMO), and 51% for the XL-Stabi (Zeiss). Gauthier et al. [25] reported 8.8% and 37.2% Nd:YAG rates after 2 years of bilateral implantation of AcrySof ReSTOR (Alcon) and Acri.LISA (Zeiss) multifocal IOLs, respectively. Similarly, Bourdiol Ducasse et al. [22] reported that eyes with AcrySof IOL implants required significantly fewer Nd:YAG laser capsulotomies than those implanted with a Hoya or Akreos IOLs and, therefore, were less prone to Nd:YAG laser treatment complications, thus ensuring better vision at the lowest cost.

All these outcomes could be attributed to the fact that hydrophobic IOLs are capable of adhering to collagen membranes [48], leading to a tighter IOL apposition in the posterior capsular bag and a better adhesiveness—through fibronectin—than other materials [49]. This may result in less space left between the IOL and the posterior capsule for the LECs to migrate. Furthermore, it has been reported that IOLs with hydrophilic surfaces promote proliferation and migration of LECs from the equatorial area to the visual region [50].

The literature shows more controversial results when comparing hydrophobic acrylic versus silicone materials. Several studies [41, 42, 44, 45, 47] have compared PCO and Nd:YAG rates for 3-piece, sharp-edge silicone IOLs (CeeOn 911A, AMO) and 3-piece, sharp-edge hydrophobic acrylic IOLs (AcrySof, Alcon). After 3 years of follow-up, the results showed low PCO and Nd:YAG capsulotomy incidence rates for both IOL groups with no statistically significant differences between them, thus concluding that the sharp-edge foldable IOLs play an important role in preventing PCO irrespective of the material the IOL is made of [41, 44, 47]. However, Vock et al. [45] found significantly higher PCO scores and Nd:YAG capsulotomy rates with hydrophobic acrylic IOLs than with silicone IOLs after 6 years of follow-up. They

Table 1: Posterior capsule opacification (PCO) and neodymium:YAG (Nd:YAG) rates of several scientific articles published between 2000 and 2014.

Authors	IOL model	IOL characteristics	Eyes (n)	Study design	Follow-up	PCO rates (%)	p value	Nd:YAG rates	p value
Kucuksumer et al. [29]	Acrysof MA60BM (Alcon)	3-piece, hydrophobic acrylic	32	Contralateral & randomized study	1 year	93.7% grade 0 6.3% grade 1	<0.001	0%	—
	MemoryLens	3-piece, hydrophilic acrylic	32			40.6% grade 0 28.1 grade 1 25% grade 2 6.3% grade 3		0%	
	Acrysof MA60BM (Alcon)	3-piece, hydrophobic acrylic	21	Contralateral & randomized study	3 years	80.9% grade 0 14.4% grade 1 4.7% grade 2	<0.05	0%	0.46
	MemoryLens	3-piece, hydrophilic acrylic	21			4.7% grade 0 52.4% grade 1 19% grade 2 9.5% grade 3 14.4% grade 4		19%	
Oner et al. [33]	Acrysof MA30BA (Alcon)	3-piece, rectangular-edge hydrophobic acrylic	80	Consecutive series	16–22 months	8.70%	<0.05	14.30%	—
	Opsia-Agena 550	Round-edge, PMMA	77			24.70%		26.30%	
Hayashi et al. [39]	MZ60BD (Alcon)	Single-piece, PMMA	90	Prospective & randomized study	Up to 2 years	—	<0.0001	28.90%	—
	SI-30NB (AMO)	Silicone	83			—		14.40%	
	Acrysof MA60BM (Alcon)	3-piece, hydrophobic acrylic	96			—		4.20%	
Schauersberger et al. [44]	Acrysof (Alcon)	3-piece, square-edge, hydrophobic acrylic	25	Prospective study	3 years	85% grade 0 15% grade 1	0.323	—	—
	CeeOn 911A (AMO)	3-piece, square-edge, silicone	25			95% grade 0 5% grade 1		—	
Abhilakh Missier et al. [19]	AcrySof MA30BA/MA60BM (Alcon)	3-piece, hydrophobic acrylic	107	Retrospective & contralateral study	3 years	19.6% grade 0 53.3% grade 1 16.8% grade 2 10.3% grade 3 6.5% grade 0	<0.0001	2.8%	<0.05
	AA4203VF (Staar)	Plate haptic, silicone	107			26.2% grade 1 22.4% grade 2 44.9% grade 3		23.1%	
Bender et al. [21]	812A/Storz P497UV (Pharmacia)	PMMA	63	Retrospective study	6 months	21.9%/27.2%	<0.0001	—	—
	AcrySof MA30/SA31 (Alcon)	3-piece/1-piece, hydrophobic acrylic	33			10.5%/6.2%			
	SI-31 (AMO)	Silicone	22			15.30%			
	Hydroview H61 (B&L)	Hydrophilic acrylic	22			65.00%			
	812A/Storz P497UV (Pharmacia)	1-piece, PMMA	63	Retrospective study	2 years	32.9%/45.5%		—	—

Table 1: Continued.

Authors	IOL model	IOL characteristics	Eyes (*n*)	Study design	Follow-up	PCO rates (%)	*p* value	Nd:YAG rates	*p* value
	AcrySof MA30/SA31 (Alcon)	3-piece/1-piece, hydrophobic acrylic	33			17.8%/18.4%			
	SI-31 (AMO)	Silicone	22			17.80%			
	Hydroview H61 (B&L)	Hydrophilic acrylic	22			62.20%			
Prosdocimo et al. [42]	CeeOn Edge (AMO)	3-piece, sharp-edge, silicone	40	Prospective study	18 months	10% without VA lost	0.0336	0%	—
	Acrysof (Alcon)	3-piece, square sharp-edge, hydrophobic acrylic	38			29% without VA lost 3% with VA lost		3%	
Auffarth et al. [20]	—	Hydrophilic acrylic	294	Retrospective study	3 years	37%	<0.001	31.10%	<0.001
	—	PMMA	384			28.30%		19.30%	
	—	Hydrophobic acrylic	421			8.90%		7.10%	
	—	Silicone	426			21.60%		16.20%	
K. Hayashi and H. Hayashi [26]	Hydroview H60M (B&L)	3-piece, hydrophilic acrylic	95	Prospective randomized contralateral study	24 months	—	—	28%	<0.0001
	Acrysof MA60BM (Alcon)	3-piece, hydrophobic acrylic	95			—		2%	
Heatley et al. [27]	Centerflex 570H (Rayner)	Single-piece, square-edge, hydrophilic acrylic	53	Prospective randomized contralateral study	1 year	50.30%	<0.001	2.60%	—
	AcrySof SA60AT (Alcon)	Single-piece, square-edge, hydrophobic acrylic	53			4.90%		0%	
Kugelberg et al. [30]	BL27 (B&L)	Single-piece, square-edge, hydrophilic acrylic	60	Prospective randomized study	1 year	18.20%	<0.001	3.50%	>0.05
	AcrySof SA60AT (Alcon)	Single-piece, square-edge, hydrophobic acrylic	60			4.65%		6.80%	
Hancox et al. [13]	AcrySof SN60AT (Alcon)	1-piece, hydrophobic acrylic	36	Prospective randomized contralateral study	24 months	8.83%	<0.0001	—	—
	AF-1 YA-60BB (Hoya)	Hydrophobic acrylic	36			32.44%			
Hayashi et al. [40]	Acrysof MA60AC (Alcon)	3-piece, round optic, hydrophobic acrylic	45	Prospective randomized contralateral study	12 months	—	0.5004	2.20%	>0.999
	AR40e (AMO)	3-piece, round optic, hydrophobic acrylic	45			—		2.20%	
Kohnen et al. [41]	CeeOn Edge 911A (AMO) versus Acrysof MA60BM (Alcon)	Sharp-edge, silicone versus sharp-edge, hydrophobic acrylic	139	Prospective randomized contralateral study	37 months	—	—	2.1% versus 2.1%	
	CeeOn Edge 911A (AMO) versus PhacoFlex SI40NB	Sharp-edge, silicone versus round optic edge, silicone	108			—		5.7% versus 17%	
Kugelberg et al. [31]	BL27 (B&L)	Hydrophlic acrylic	60	Prospective randomized study	2 years	—	—	42%	<0.001
	AcrySof SA60AT (Alcon)	Hydrophobic acrylic	60			—		10%	

Table 1: Continued.

Authors	IOL model	IOL characteristics	Eyes (*n*)	Study design	Follow-up	PCO rates (%)	*p* value	Nd:YAG rates	*p* value
Boureau et al. [23]	AcrySof SA60AT (Alcon)	1-piece, sharp-edge, hydrophobic acrylic	250	Restrospective study	2.9 years	13.60%	<0.001	12%	<0.001
	AR40e (AMO)	3-piece, sharp-edge, acrylic hydrophobic	254			26.80%		25.20%	
	XL-Stabi (Zeiss)	1-piece, sharp-edge, acrylic hydrophilic	263			52.90%		51%	
Ronbeck et al. [43]	809C (Pharmacia)	Round-edge, PMMA	54	Prospective randomized study	5 years	100%		54%	<0.05
	SI-40NB (AMO)	Round-edge, silicone	48			12%		29%	
	Acrysof MA60BM (Alcon)	Sharp-edge, acrylic hydrophobic	50			18%		8%	
Vock et al. [46]	Acrysof MA60BM (Alcon)	3-piece, sharp-edge, hydrophobic acrylic	98	Retrospective study	10 years	91% grade 0 4% grade 1 4% grade 2 1% grade 3	0.000073	42%	0.007
	SI-30NB/SI-40NB (AMO)	3-piece, round optic edge, silicone	44			61% grade 0 30% grade 1 9% grade 2 0% grade 3		18%	
Vock et al. [45]	CeeOn 911A (AMO)	3-piece, sharp-edge, silicone	22	Randomized and contralateral study	6 years	—	0.0016	9%	0.01
	Acrysof MA60BM (Alcon)	3-piece, sharp-edge, hydrophobic acrylic	22			—		27.20%	
Gauthier et al. [25]	AcrySof ReSTOR (Alcon)	Hydrophobic acrylic	160	Retrospective bilateral study	2 years	—	—	8.80%	0.0001
	Acri.Lisa (Zeiss)	Hydrophilic acrylic with hydrophobic surface	152			—		37.20%	
Iwase et al. [28]	AcrySof SA60AT	1-piece, sharp-edge, hydrophobic acrylic	63	Prospective randomized and contralateral study	2 years	—	<0.001	2%	<0.01
	Meridian HP60M (B&L)	1-piece, double square-edge, hydrophilic acrylic	63			—		13%	
Vasavada et al. [34]	Acrysof IQ SN60WF (Alcon) versus C-flex 570C (Rayner)	Hydrophobic acrylic versus hydrophilic acrylic	66	Prospective randomized and contralateral study	3 years	—	0	0% versus 12.9%	0.04
	Acrysof IQ SN60WF (Alcon) versus Akreos Adapt (B&L)	Hydrophobic acrylic versus hydrophilic acrylic	62			—	0	0% versus 16.1%	0.02
Zemaitiene and Jasinskas [47]	Acrysof MA30BA (Alcon)	3-piece, hydrophobic acrylic	31	Prospective randomized study	3 years	—	0.995	9%	NS
	Acrysof SA30AL (Alcon)	1-piece, hydrophobic acrylic	31			—		3.10%	
	CeeOn 911A (AMO)	3-piece, silicone	30			—		0%	
Chang et al. [24]	Acrysof SA60AT (Alcon)	1-piece, hydrophobic acrylic	40	Prospective randomized study	5–7 years	—	0.5535	22%	>0.05
	Sensar AR40e (AMO)	3-piece, hydrophobic acrylic	40			—		10%	

Table 1: Continued.

Authors	IOL model	IOL characteristics	Eyes (*n*)	Study design	Follow-up	PCO rates (%)	*p* value	Nd:YAG rates	*p* value
Leydolt et al. [14]	iMics1 NY-60 (Hoya)	1-piece, sharp-edge optimized, hydrophobic acrylic	100	Prospective, randomized and contralateral study	3 years	—	<0.001	35.60%	0.001
	Acrysof SN60WF (Alcon)	1-piece, sharp-edge, hydrophobic acrylic	100			—		13.70%	
Morgan-Warren and Smith [32]	Hoya FY60AD (HOYA)	3-piece, round-edge, hydrophobic acrylic	315	Retrospective comparative study	2 years	—	—	8.90%	0.03
	Hoya PY60AD (HOYA)	3-piece, sharp-edge, hydrophobic acrylic	254			—		4.30%	
	Acrysof SN60WF (Alcon)	1-piece, sharp hydrophobic acrylic	696			—		1.40%	0.007
Bourdiol Ducasse et al. [22]	Acrysof SN60WF (Alcon)	1-piece, square-edge, hydrophobic acrylic	126	Retrospective study	2-3 years	—	—	10.30%	
	Akreos AO-MI60 (B&L)	1-piece, square-edge, hydrophilic acrylic	89			—		36%	
	Hoya YA-60BB (Hoya)	3-piece, square-edge, hydrophobic acrylic	85			—		24.90%	
Cullin et al. [37]	AcrySof SN60 (Alcon)	Hydrophobic acrylic	375	Retrospective study	41.5 months	—	—	7.50%	<0.001
	Akreos Adapt (B&L)	Hydrophilic acrylic	350			—		17.70%	
	Tecnis Acryl Z9003 (AMO)	Hydrophobic acrylic	801			—		3.70%	
Fong et al. [38]	AcrySof SA60AT (Alcon)	1-piece, square-edge, hydrophobic acrylic	1016	Prospective cohort study	3 years	34.40%	—	—	—
	MA50BM (Alcon)	3-piece, square-edge, hydrophobic acrylic	67			50.80%		—	
	Sensar AR40e (AMO)	3-piece, round-edge, hydrophobic acrylic	156			38.50%		—	
	Akreos Adapt (B&L)/Quatrix (Croma)	Square-edge, hydrophilic acrylic	101			64.40%		—	
Ronbeck and Kugelberg [12]	809C (Pharmacia)	Round-edge, HSM PMMA	61	Prospective randomized study	12 years	—	—	57.40%	
	SI-40NB (AMO)	round-edge, silicone	59			—		28.80%	
	Acrysof MA60BM (Alcon)	Sharp-edge, hydrophobic acrylic	59			—		32.20%	

concluded that aside from the IOL material, differences in the haptic design and the degree of the optic edge sharpness may play a role, and they highlighted the need for longer follow-up studies. In a retrospective and contralateral study, Abhilakh Missier et al. [19] assessed PCO rates in fellow eyes: each patient received one plate-haptic silicone IOL (AA4203VF, Staar) in one eye and a hydrophobic acrylate IOL (AcrySof MA30BA/MA60BM, Alcon) in the contralateral one. After 3 years of follow-up, they found significantly less PCO and lower Nd:YAG laser capsulotomy rates in the eyes implanted with the hydrophobic IOL than in the plate-haptic silicone IOL group. Other studies [12, 21, 39, 43, 45] also compared PCO and Nd:YAG rates resulting from 3-piece, round optic-edge silicone IOL (SI30N/SI40NB, AMO) and 3-piece, sharp-edge hydrophobic acrylic IOL (AcrySof, Alcon) implantation. Most of these studies revealed that following phacoemulsification, PCO rates increased over the years for all groups and that the benefit yielded by the acrylic IOL in terms of showing lower PCO rates faded as the years went by: after a long follow-up period, up to 12 years of follow-up, the PCO and Nd:YAG treatment rates were similar for both groups. These outcomes could be due to the silicone IOL efficiently inhibiting PCO over a long time or to the efficiency drop or loss of the hydrophobic acrylic IOL's sharp edge due to late LEC proliferation, leading to an emerging Soemmering ring in the peripheral capsular bag, which, in its turn, resulted in a reduced or nonexistent PCO preventive effect 4-5 years postoperatively [12].

Regardless of the IOL material, the importance of IOL edge design is widely accepted, and there is considerable agreement among medical communities in favor of a square posterior optic edge for reducing PCO rates and Nd:YAG procedure needs. A systematic review found significantly lower PCO scores for sharp-edge IOLs compared to round-edge models, although there were no clear differences between IOL materials [10]. A square edge on the posterior IOL surface provides a barrier to LEC migration by inducing a capsular bend in the area where it is in contact with the IOL edge [33, 51–54]. Several trials showed no differences in PCO prevention between IOL models that had sharp posterior optic edges—irrespective of IOL material composition or square-edge design—thus indicating that a sharp posterior optic edge is the main factor preventing PCO [13, 41, 55, 56]. Edge sharpness can vary across IOL models. A prospective, single-site, fellow-eye comparative study of two hydrophobic IOLs found higher PCO rates and poorer visual acuity in eyes implanted with the AF-1 YA-60BB IOL (Hoya) versus the AcrySof SN60AT IOL (Alcon) over 24 months of follow-up. The authors attributed these differences to the fact that the AcrySof IOL has a sharper posterior edge profile than the Hoya IOL [13]. Moreover, in a recent 36-month follow-up study [14], the Hoya iMics1 NY-60 IOL showed higher PCO and Nd:YAG capsulotomy rates than AcrySof SN60WF IOL despite the novel Hoya iMics1 NY 60 model with optimized sharp edges, which are even sharper than those of the AcrySof SN60WF IOL (Alcon). These results suggest that the IOL material continues to play an important role in this complication [14].

A meta-analysis performed by Cheng et al. [11] concluded that PCO and Nd:YAG laser capsulotomy rates may be influenced by two parameters: IOL material and optic edge design. Lenses made of acrylic and silicone and those having sharp optic edges lead to lower PCO and laser capsulotomy rates. Morgan-Warren and Smith [32], in a retrospective, comparative 2-year follow-up study, reported lower Nd:YAG procedure rates with the newer sharper Hoya PY60AD IOL than with the Hoya FY60AD IOL model. The one-piece AcrySof SN60WF IOL was also analyzed in this retrospective study, showing the lower Nd:YAG rates than both the three-piece Hoya IOLs in the same period postoperatively. The sharpness of the square edge of the AcrySof IOL lies between the two Hoya models; therefore, the authors concluded that the IOL edge may contribute to reducing the PCO rates, but variations in IOL material composition may influence IOL's susceptibility to PCO development independent of edge sharpness.

The fact that the primary site of late intrusion of LECs is inside the haptic loop [45] reveals the importance of the haptic configuration for PCO formation, such as broad optic-haptic junction [57–59] and haptics angulation [45]. It has been shown that either less angulation, a better haptic memory, a more c-loop shape of the haptic, and/or a thin and perpendicular insertion of the haptic into the optic, or a combination of these seems to result in a more prolonged and permanent barrier effect against late LEC migration [45]. Nixon and Woodcock [60] compared two 1-piece hydrophobic acrylic IOLs; the authors identified Tecnis AAB00 (AMO) as a continuous optic edge and an AcrySof SA60AT (Alcon) as an interrupted optic edge. Their findings, after 2 years of follow-up, showed that those eyes implanted with a continuous 360-degree square-edge IOL had significantly less PCO than those eyes having a square edge with an interrupted optic-haptic junction IOL. These characteristics—360-degree square-edge, angled haptics, increased optic-haptic space, and increased resistance to compression—help position the IOL against the posterior capsule and promote complete circumferential shrink wrapping of the IOL by the capsule. Nonetheless, recent studies [61–63] have shown that after 1 and 3 years of follow-up, the levels of PCO were low for those eyes implanted with an IOL having a continuous sharp and square optic edge (Tecnis ZCB00, AMO) and for those implanted with an IOL having an interrupted square optic edge (AcrySof SA60AT, Alcon) with no statistically significant differences between the two IOL models. However, they did find higher ACO rates in those eyes implanted with the interrupted optic edge IOL.

On the other hand, studies have consistently failed to reach a consensus on the relative merits of one-piece versus three-piece IOLs per se in protecting against PCO development. Some authors reported more PCO [64] and higher Nd:YAG rates [65] in eyes implanted with a one-piece IOLs compared to three-piece models. The thin haptics of the three-piece IOL is believed to allow for better adhesion between the anterior and posterior capsules and bend formation, compared to the bulky haptics of the one-piece models, which enable enhanced posterior LEC

migration. However, other studies showed no significant differences in terms of PCO and Nd:YAG rates between one- and three-piece IOLs [58, 65–70].

There are other features that also exert influence upon PCO formation, such as the presence of aspheric surfaces [71], and optic size [72]. Several studies [73, 74] reported decreased PCO rates when the capsulorhexis is in complete contact with the anterior IOL surface. Meacock et al. [72] reported that larger optic IOLs have a lower PCO; this can be explained by the fact that it is easier to get the capsulorhexis on the IOL with a larger optics. On the other side, the LECs may have an increased ability to migrate from the anterior capsule to the posterior capsule when the anterior capsulorhexis is decentered and the lens is tilted off the posterior capsule [73, 74].

3. Anterior Capsule Opacification

Unlike the equatorial cells, the anterior cells go through fibrous metaplasia but lack the ability to migrate and proliferate and therefore do not appear outside the margins of the capsulorhexis. Capsule opacification may occur on either the anterior or the posterior capsule and is caused by LECs that remain in the evacuated capsular bag [75]. The source of ACO is the anterior epithelial cells, which originate from beneath the anterior lens capsule. These cells can be classified into 2 subpopulations with distinct properties: The equatorial LEC population resides in the equatorial region of the capsular bag, and following capsular bag evacuation, these cells tend to migrate onto the posterior capsule and proliferate. Meanwhile, the anterior LEC population resides on the anterior capsule leaf and has the potential to undergo myofibroblastic transdifferentiation. While PCO has been regeneratory or fibrotic or both, ACO can only be fibrotic. ACO generally occurs at a much earlier stage in comparison to PCO: sometimes, it develops within one month postoperatively [76]. It has been shown that the area of the anterior capsule opening seems to gradually decrease for up to 6 months postoperatively [76, 77].

The process of opacification of the anterior capsule may be split into four stages: (1) fibrosis/opacification of the capsulorhexis margin in some places; (2) the entire anterior capsular edge in contact with the IOL optic's biomaterial; (3) formation of capsular folds; and (4) advanced/excessive and/or asymmetric shrinkage. Such shrinkage may result in some complications, such as eccentric displacement of the continuous curvilinear capsulorhexis (CCC) opening, IOL decentration [78], capsulorhexis phimosis, and capsule contraction [79]. Some authors recommend Nd:YAG laser anterior relaxing incisions in the early postoperative period after cataract surgery in order to prevent capsule contraction in high-risk patients (such as those with primary angle closure, pseudoexfoliation, or diabetic retinopathy) [80, 81].

There are different factors that could influence the level of ACO, such as CCC's initial size; IOL material and design; and some preexisting conditions (e.g., the quality of the zonular support). Some authors reported that if the CCC is smaller than the diameter of the IOL optic, the contact of the optic's biomaterial with the anterior capsule will induce fibrosis/opacification [82, 83]. Tsuboi et al. [84] studied the influence of the CCC and IOL fixation on the blood-aqueous barrier (BAB). They found an unfavorable effect of in-the-bag fixation with a small CCC and thus a broader contact of the IOL optic with the anterior capsule. On the contrary, Gonvers et al. [85] did not find any correlation between the initial CCC size and the postoperative CCC constriction.

Park et al. [86] evaluated the rate at which the area of the anterior capsule opening decreased following CCC for different IOL types. Although this area reduction occurred for all patients, on average, it was significantly lower in the two acrylic-IOL groups than in the silicone-IOL one. They suggested that IOL selection can be important when it comes to reducing anterior capsule opening contraction, especially for patients at risk for contraction. In this sense, the IOL material and design also play a role in ACO, which is a complication that can impair visual function [87]. Werner et al. [88, 89] evaluated the degree of ACO in postmortem human eyes that had been implanted with IOLs of a wide variety of materials and designs. The results of this histopathological study revealed that ACO is more likely to occur with plate-haptic silicone and hydrogel IOLs than with acrylic hydrophobic IOLs. Nagata et al. [90] also reported a marked anterior capsule contraction with a silicone IOL (AQ310NV, Canon) compared to a hydrophobic acrylic IOL, as well as varying rates of capsule contraction across the range of acrylic IOLs under test (AR40e, AMO; AcrySof MA60BM and SA60AT models, Alcon; and YA60BBR, Hoya), being statistically greater with the AR40e. These results suggest that when implanting an IOL with high surface adhesion, a sharp bend is created in the lens capsule at the rectangular, sharp posterior optic edge of the IOL soon after surgery. This suppresses PCO formation and anterior capsule contraction [78, 91]. In a retrospective study, Tsinopoulos et al. [92] reported significantly greater capsule contraction with hydrophilic IOLs (Quatrix and ACR6D, Corneal Laboratories) than with hydrophobic ones (AcrySof SN60AT, Alcon).

K. Hayashi and H. Hayashi [93] reported that the optic material is the most important factor influencing the degree of capsule contraction, whereas the optic design and haptic material and design play a less significant role. Other studies have shown that plate haptics [85], single-piece designs [94], or IOLs that have a thin optics are risk factors for capsule contraction [95]. Among the four silicone IOL groups assessed by Werner et al. [89], plate-haptic silicone ones yielded significantly higher scores than the 3-piece designs. This correlates well with the findings by Gonvers et al. [85] who claimed that the IOL haptic design (loop-haptic versus plate-haptic) has a major effect on the CCCs' size change. The excessive CCC constriction observed with plate-haptic IOLs is probably due to the relatively large contact area between the plate haptic silicone material and the anterior capsule, in sharp contrast to three-piece IOLs, with which the contact is limited to the optic's surface. Thus, the larger surface exposure inherent to plate IOLs may stimulate cell proliferation and fibrosis. Despite these findings, Sacu et al. [96] showed in a recent study that neither the optic material (silicon versus hydrophobic IOLs) nor the haptic design

(one-piece versus three-piece open loop) had any influence on the amount of ACO or capsulorhexis contraction.

Several studies reported that capsule contraction has also been associated with some systemic or ocular conditions, such as diabetes mellitus [97–99], pseudoexfoliation syndrome [100], retinitis pigmentosa [101], and uveitis [79]. It may result in a smaller capsulotomy opening, opening malposition, reduction in equatorial capsular diameter, and displacement of the IOL, this effect being more acute for small capsulorhexis openings and older patient [79]. The Nd:YAG laser can be used to perform anterior capsulotomy to increase the size of the anterior capsule opening, but this treatment can lead to other complications, such as IOP elevation, iritis, corneal edema, and damage to the IOL [9].

4. Glistenings

Glistenings are condensations of water within the IOL polymer matrix that occur when the IOL is in an aqueous environment. They are usually distributed throughout the entire IOL optic. They result from the formation of water vacuoles within the lens due to in-the-eye hydration; they are not caused by the deterioration of the material. The mechanism of glistening formation has been extensively evaluated [102]. The polymers that make up the IOLs have different components, including different monomers, chromophores, and crosslinking agents. Polymers absorb water when immersed in an aqueous environment, and their water absorption rate depends on the specific IOL material and the temperature. If the IOL is placed in warm water and the temperature is then lowered, the water inside the polymer becomes oversaturated [103, 104] and, consequently, it separates into phases and collects in a void, generating glistening [105]. In the clinical practice, glistenings typically begin to appear over a 1- to 16-month period after implantation.

Kato et al. [102] found an association between a reduction in temperature and the rate of glistening formation. They studied the changes undergone by a Wagon Wheel packaged AcrySof IOL at various temperatures, placing the IOLs in 37°C or 70°C water, which was then cooled down to 23°C. Microvacuoles of 1.0 to 20.0 μm diameter formed inside the AcrySof IOL when the temperature dropped from 37° to 34°C (3°C decrease), which was enough to trigger vacuole formation. Vacuole density was higher in the IOL that had undergone cooling from 60°C than in the one cooled from only 37°C. In the same paper, the authors also studied temperature changes on the human ocular surface. The temperature of the ocular surface decreased by approximately 7°C when the outer temperature dropped from 45°C to 0°C. As mentioned above, glistening-like vacuole formation can be triggered by a 3°C decrease in body temperature (37°C). Therefore, glistenings may occur in vivo if the lens experienced small aqueous humor temperature fluctuations. Shiba et al. [106] concluded that immersing AcrySof IOLs in warm water (37°C or 60°C) for a short time may alter the IOL's features. On the contrary, when the lens is left for 6 months in 15°C water, glistening formation is not observed.

Miyata and Yaguchi [107] correlated the degree of glistenings in two different hydrophobic acrylic IOLs, AcrySof MA60BM (Alcon) and Sensar AR40 (AMO), with their equilibrium water content at 30°C, 40°C, and 50°C. The 2 IOLs were also subjected to 3 temperature changes: from 37°C to 35°C, from 39°C to 35°C, and from 41°C to 35°C. IOLs were incubated in a physiological saline solution at the higher temperature for 2 hours and at the lower temperature for 30 days before being assessed for glistening formation. The equilibrium water content was higher in the Sensar IOL than in the AcrySof IOL, but the temperature-related change of the equilibrium water content was greater for the AcrySof IOL. It is in those IOLs whose water content varies significantly with temperature (i.e., temperature-dependent) where phase separation (water and glistenings) occurs. When temperature changed from 37°C to 35°C, glistening formation was not observed in either IOLs, but when it changed from 39°C to 35°C, glistenings were observed in AcrySof IOL, and when it went down from 41°C to 35°C, they were observed in both IOLs.

Glistenings can be evaluated subjectively by means of a slit lamp and by slit lamp photography of the IOL at high magnification. The size and number of glistenings can be quantified by either manual or digital image analysis. Miyata et al. [105] classify glistening into the following grades: 0 = no glistenings; 1 = up to 50/mm^3, 2 = up to 100/mm^3, and 3 = up to 200/mm^3. Some authors also suggested quantifying glistenings employing light scattering. Klos et al. [108] proposed the use of Scheimpflug camera photography for glistening evaluation, as irregularities, damage, or disturbances in the transparency of the IOL material with lower light scattering. Out of the 41 AcrySof IOLs that were evaluated 1 year after implantation, glistenings were observed in all of them and it formed throughout the IOL's volume. No correlation between visual acuity, scotopic vision, or brightness acuity test and the glistening grade was found. Behndig and Monestam [109] described a method for quantifying glistenings that relied on Scheimpflug photography associated with IOL light scattering quantification using an image analysis program. Glistenings were observed in all AcrySof MA60AT or SA60AT IOLs; its grade correlated well with the length of the postoperative period. They also found that glistenings were more prominent near the IOL surfaces, especially the anterior one. Nevertheless, Mackool and Colin [110] consider that Scheimpflug photography is unsuitable for glistening quantification in IOLs, due to the fact that it has not been confirmed yet that the method is able to distinguish between glistening-related light scatter and light scatter due to other variables, such as the aqueous IOL interface, PCO, or the presence of biological materials on the IOL surface. Glistenings are usually distributed throughout the entire IOL optic [111]. Clinically observed glistenings are usually up to 10 μm in diameter [112], although the size of glistenings observed during in vitro studies goes up to 20 μm [113].

There are several factors influencing glistening formation, such as IOL material composition, manufacturing technique, IOL packaging, follow-up period, IOL diopter power, performance of phacotrabeculectomy, condition such as glaucoma or those that break down the BAB, and specific ocular medications (some anti-inflammatory agents). Glistenings have been observed in a variety of

materials [114–118], including silicone, hydrogel, hydrophobic acrylic, and PMMA. However, most of the studies available in the literature on glistening formation describe them in association with hydrophobic acrylic IOLs [114–116]. Tognetto et al. [114] evaluated glistenings in 7 types of foldable IOLs (2 silicone, 3 hydrophilic acrylic, and 2 hydrophobic acrylic). They found varying degrees of glistenings in all IOLs, irrespective of the manufacturing material, but it was the AcrySof group that showed a higher percentage and a greater density of glistenings. Ronbeck et al. [116] assessed lens glistening effects in PMMA, silicone, and hydrophobic acrylic IOLs in a long-term study (11–13 years). The AcrySof hydrophobic acrylic IOL had a significantly higher degree of lens glistenings compared to the silicone and PMMA ones. Although it is likely that the various hydrophobic acrylic materials available on the market exhibit different behaviors in terms of glistening formation [14, 24], most of the peer-reviewed studies found in the literature focus on the AcrySof material, whereas relatively few evaluated other hydrophobic acrylic IOLs.

AcrySof packaging was also found to play an important role in the process of glistening formation. Omar et al. [103] carried out an in vitro study to compare glistening formation in AcrySof acrylic hydrophobic IOLs that relied on either the AcryPack or the Wagon Wheel packaging systems. Glistening formation occurred in both types of packaging, although those AcrySof IOLs packaged in Wagon Wheel did not develop glistenings when kept under constant body temperature. Furthermore, the IOLs in the AcryPack exhibited significantly more microvacuoles. This may be due to the large plastic case that holds the lens and the folding device [103, 111].

Moreno-Montanes et al. [119] studied the clinical factors influencing the frequency and intensity of glistenings by assessing 129 eyes of 94 patients that had undergone phacoemulsification and implantation of an AcrySof MA30BA IOL (Alcon). Glistenings occurred in 38 cases (29.5%) after 20.6 ± 11.5 months postoperatively (range: 1 to 50 months). They found a significant direct correlation between the frequency of glistenings and the following factors: more time elapsed between surgery and evaluation, higher IOL dioptric power, postoperative inflammation, and joint phacotrabeculectomy procedure. As for glistening intensity, it was directly correlated with the time elapsed after the surgery and the presence of postoperative inflammation. Glistenings developed more frequently in cases of phacotrabeculectomy but not after combined phacoemulsification and deep sclerectomy [119]. Other studies also found less glistening formation in lower dioptric power IOLs (≤20.0 D); this could be due to the fact that IOL thickness within a given model usually increases with IOL dioptric power. Therefore, glistenings may be more likely to accumulate in the thicker IOL matrix material in higher power IOLs [120, 121]. Nevertheless, recent studies did not find a significant correlation between the degree of glistenings and the IOL's dioptric power [116, 122]. As for the time evolution of this phenomenon, most studies show that glistenings increase in frequency and size with time up to approximately 3 years postoperatively [105, 117, 123]. A reasonable hypothesis is that the incidence and degree of glistenings may increase until the IOL is completely hydrated and all available voids within the polymer network are visible as glistenings as a result of temperature fluctuations [115]. Contrariwise, other authors found no significant association between glistening grade and duration of the follow-up period [120, 124].

Glistenings have been found to be associated with some conditions such as glaucoma [120] or those that break down the BAB [125], as well as concurrent medications or ophthalmic solutions. Colin et al. [120] assessed the correlation between clinical and demographic factors in 260 eyes implanted with different AcrySof IOL models. They found a potential association between the frequency of glistenings and the incidence of glaucoma. The authors hypothesized that this was due to an interaction of the material with the pathology of glaucoma or to the chronic topical medication used to lower IOP. Active ingredients or preservatives present in glaucoma medications may lead to the rupture of the BAB, thus modifying the aqueous humor composition and increasing the glistening rate [126, 127]. Schweitzer et al. [128] also found a significant association between the increase of glistenings and the number of topical glaucoma medication that the patient instilled on a daily basis.

Regarding clinical impact, most clinical studies show no association between glistening occurrence and a decrease in visual acuity (Table 2) [24, 119–122, 129, 130]. Nevertheless, there are a few reports on the possible impact upon contrast sensitivity function under specific conditions [112, 131, 132] (Table 2). Colin and Orignac [122] evaluated 97 eyes from 65 patients implanted with an AcrySof IOL at 18 ± 17 months of follow-up. They found that 40% of eyes had grade 0 glistenings, 32% had grade 1, and 28% had grade 2 glistenings. There were no statistically significant differences in visual acuity and contrast sensitivity across glistening-grade groups. They concluded that the intensity of glistenings was not associated with a reduction in visual acuity or contrast sensitivity at any spatial frequency evaluated. In a previous study, Colin et al. [120] evaluated the incidence of severe glistenings in a large series of AcrySof IOL wearers (model SN60AT, SN60WF, SA60AT, or MA) and assessed the potential correlation between glistenings and clinical (length of follow-up, IOL model, IOL power, Nd:YAG capsulotomy, visual acuity, spherical equivalent, ocular and systematic diseases, and medication) and demographic (age and gender) factors. In this retrospective evaluation of a series of 260 AcrySof IOLs which found glistenings in approximately 60% of IOLs, the results suggest a potential association between the incidence of glistenings and IOL power and the presence of glaucoma, but not between glistenings and age, gender, IOL model, length of follow-up, visual acuity reduction, or the presence of any of the most common ocular and systemic diseases and medications. Monestam and Behndig [121] followed 103 eyes implanted with the AcrySof IOL for 10 years. The patients were divided into different groups according to the degree of glistenings. They did not find any impact upon visual function or high- and low-contrast visual acuity, even in patients having severe glistening. Chang and Kugelberg [130] compared the development of glistenings after implantation of hydrophobic (AcrySof SA60AT) and

Table 2: Impact of glistenings on visual function with several models of AcrySof intraocular lenses (IOLs).

Author	IOL model	Eyes (n)	Follow-up	Results
Moreno-Montanes et al. [119]	AcrySof MA30BA	129	20 ± 11 months	No impact on visual acuity
Colin et al. [120]	AcrySof SN60AT, SN60WF, SA60AT, or MA	260	0–86 months	No impact on visual acuity
Colin et al. [129]	AcrySof SN60WF	111	±24 months	No impact on visual acuity
Monestam and Behndig [121]	AcrySof MA60BM	103	>10 years	No impact on visual acuity at high and low contrast
Colin and Orignac [122]	Several AcrySof	97	18 months	No impact on visual acuity or contrast sensitivity
Hayashi et al. [133]	AcrySof versus SI30NB versus PMMA	35	>10 years	No impact on visual acuity and aberrometry
Chang et al. [24]	AcrySof SA60AT versus Sensar AR40e	80	5–7 years	No impact on visual acuity or contrast sensitivity
Chang and Kugelberg [130]	AcrySof SA60AT & BL27	120	9 years	No impact on visual acuity or contrast sensitivity
Waite et al. [112]	AcrySof SA & SN60	20	36 months	No impact on visual acuity, aberrometry, and contrast sensitivity but at high spatial frequencies
Gunenc et al. [131]	AcrySof MA30BA & MA60BA	91	7–24 months	Decreased contrast sensitivity at high spatial frequencies
Xi et al. [132]	AcrySof SA60AT	120	2 years	No impact on visual acuity and contrast sensitivity but at high spatial frequencies
Christiansen et al. [124]	AcrySof MA30BA & MA60BM	42	6–46 months	Decreased visual acuity but not glare and contrast sensitivity

hydrophilic IOLs (BL27). Nine years postoperatively, patients with a hydrophobic IOL developed more glistenings than those with the hydrophilic IOL, but glistenings did not affect visual acuity or contrast sensitivity. On the contrary, Gunenc et al. [131] found statistically significant differences in terms of contrast sensitivity at a high spatial frequency (12 cycles per degree) between eyes where glistening formation had occurred and those eyes that had not developed it. Xi et al. [132] concluded that severe glistenings may have an influence on high spatial frequency contrast sensitivity and reduce light sensitivity, but they did not find any impact on visual acuity. Christiansen et al. [124] reported that all patients (42 eyes) implanted with an AcrySof IOL showed some degree of glistenings. They found statistically significant differences in visual acuity in 24% of the eyes—those having severe glistenings (≥2+)—but there was no evidence that contrast sensitivity had been negatively affected by this glistening phenomenon.

Some authors have associated glistenings with intraocular straylight [121, 133–137]. Monestam and Behndig [121] found that most patients that had undergone surgery 10 years before had severe glistening and a high level of light scattering resulting from their IOLs but with no impact on visual acuity at high or low contrast. Hayashi et al. found more glistenings and surface scattering in those eyes implanted with acrylic IOLs versus silicone or PMMA IOLs, but these data were not significantly correlated with visual function or optical aberrations. Recent studies also reported the presence of straylight in eyes implanted with hydrophobic IOLs resulting from subsurface nanoglistenings, but these findings did not lead to visual acuity deterioration [135–137]. In contrast, Colin and Orignac [122] did not show any correlation between glistenings and intraocular light scatter.

Glistenings has decreased noticeably over the last years. A recent study by Thomes and Callaghan [138] reported significantly reduced levels of glistenings, measured in vitro, in newer AcrySof IOL models as a result of the continuous improvements implemented since 2003 in the manufacturing process, including manufacturing equipment, environmental controls, and tightened process controls/specifications. They found an 87% decrease in mean microvacuole density for the AcrySof IOLs manufactured in 2012 versus those produced in 2003. Packer et al. also showed the safety and effectiveness in a glistening-free hydrophobic acrylic IOL (enVista IOL). In a prospective series of 122 subjects, the authors showed no glistenings of any grade for any subject after 6 months of follow-up [139].

5. Conclusions

There is clear evidence that the IOL biomaterial is one of the main factors influencing PCO, ACO, and glistening formation. Most of the studies showed lower PCO rates with hydrophobic than with hydrophilic and PMMA IOL materials due to the effects outlined by Linnola in the "Sandwich theory" [15]. However, there are more controversial findings

when comparing hydrophobic and silicone IOL materials: in this setting, there are additional factors that have an influence on the outcome of the cataract procedure. This is due to the fact that these two materials have both optimal properties to prevent PCO formation and, consequently, secondary factors come into play, such as edge design. Indeed, some authors consider the optic edge as the main factor preventing PCO. It has been shown that sharp edges lead to lower PCO formation than round ones, thanks to the barrier that is created, which hinders LEC migration. Nevertheless, not all square edges are the same. Edge sharpness can vary across IOL models, in the same manner that IOL material composition can vary across IOL designs. PCO and Nd:YAG laser capsulotomy rates are influenced by both IOL biomaterials and optic edge design, the best outcomes being observed for hydrophobic or silicone material IOLs having sharp edges. Other factors, such as haptics design, optic size, and the presence of aspheric surfaces, could also have a minor influence on PCO formation.

As for anterior capsule opacification, most authors have reported that ACO rates are lower for hydrophobic than for silicone and, specifically, for hydrophilic IOL materials. Other factors, such as thin optics, plate-haptics and single-piece IOLs, are additional risk factors for capsule contraction.

Glistening formation seems to be directly related with the IOL material and its composition. Most of the studies showed higher levels of glistening formation with hydrophobic IOLs, than with other materials. Nonetheless, most clinical studies showed no correlation between glistening formation and impaired visual performance.

Additional Points

Precis. Although cataract surgery is one of the most common surgeries performed everyday worldwide and technology and products are constantly improving day after day, we can still find undesirable effects following cataract surgery in some patients.

Conflicts of Interest

The author declares that there is no conflict of interest regarding the publication of this paper.

Acknowledgments

This work was supported by Marie Curie Grant FP7-LIFE-ITN-2013-608049-AGEYE.

References

[1] R. R. A. Bourne, J. B. Jonas, S. R. Flaxman et al., "Prevalence and causes of vision loss in high-income countries and in Eastern and Central Europe: 1990–2010," *The British Journal of Ophthalmology*, vol. 98, no. 5, pp. 629–638, 2014.

[2] N. Congdon, J. R. Vingerling, B. E. Klein et al., "Prevalence of cataract and pseudophakia/aphakia among adults in the United States," *Archives of Ophthalmology*, vol. 122, no. 4, pp. 487–494, 2004.

[3] T. Amzallag and J. Pynson, "Lens biomaterials for cataract surgery," *Journal Français d'Ophtalmologie*, vol. 30, no. 7, pp. 757–767, 2007.

[4] K. Slowinski, M. Misiuk-Hojlo, and M. Szalinski, "Influence of material on biocompatibility of intraocular lenses," *Polimery w Medycynie*, vol. 37, no. 1, pp. 35–45, 2007.

[5] K. T. Doan, R. J. Olson, and N. Mamalis, "Survey of intraocular lens material and design," *Current Opinion in Ophthalmology*, vol. 13, no. 1, pp. 24–29, 2002.

[6] J. P. McCulley, "Biocompatibility of intraocular lenses," *Eye & Contact Lens*, vol. 29, no. 3, pp. 155–163, 2003.

[7] L. Werner, "Biocompatibility of intraocular lens materials," *Current Opinion in Ophthalmology*, vol. 19, no. 1, pp. 41–49, 2008.

[8] N. Awasthi, S. Guo, and B. J. Wagner, "Posterior capsular opacification: a problem reduced but not yet eradicated," *Archives of Ophthalmology*, vol. 127, no. 4, pp. 555–562, 2009.

[9] C. Billotte and G. Berdeaux, "Adverse clinical consequences of neodymium:YAG laser treatment of posterior capsule opacification," *Journal of Cataract & Refractive Surgery*, vol. 30, no. 10, pp. 2064–2071, 2004.

[10] O. Findl, W. Buehl, P. Bauer, and T. Sycha, "Interventions for preventing posterior capsule opacification," *Cochrane Database of Systematic Reviews*, vol. 2, article CD003738, 2010.

[11] J. W. Cheng, R. L. Wei, J. P. Cai et al., "Efficacy of different intraocular lens materials and optic edge designs in preventing posterior capsular opacification: a meta-analysis," *American Journal of Ophthalmology*, vol. 143, no. 3, pp. 428–436.e3, 2007.

[12] M. Ronbeck and M. Kugelberg, "Posterior capsule opacification with 3 intraocular lenses: 12-year prospective study," *Journal of Cataract & Refractive Surgery*, vol. 40, no. 1, pp. 70–76, 2014.

[13] J. Hancox, D. Spalton, G. Cleary et al., "Fellow-eye comparison of posterior capsule opacification with AcrySof SN60AT and AF-1 YA-60BB blue-blocking intraocular lenses," *Journal of Cataract & Refractive Surgery*, vol. 34, no. 9, pp. 1489–1494, 2008.

[14] C. Leydolt, S. Schriefl, E. Stifter, A. Haszcz, and R. Menapace, "Posterior capsule opacification with the iMics1 NY-60 and AcrySof SN60WF 1-piece hydrophobic acrylic intraocular lenses: 3-year results of a randomized trial," *American Journal of Ophthalmology*, vol. 156, no. 2, pp. 375–381.e2, 2013, e372.

[15] R. J. Linnola, "Sandwich theory: bioactivity-based explanation for posterior capsule opacification," *Journal of Cataract & Refractive Surgery*, vol. 23, no. 10, pp. 1539–1542, 1997.

[16] R. J. Linnola, M. Sund, R. Ylonen, and T. Pihlajaniemi, "Adhesion of soluble fibronectin, laminin, and collagen type IV to intraocular lens materials," *Journal of Cataract & Refractive Surgery*, vol. 25, no. 11, pp. 1486–1491, 1999.

[17] R. J. Linnola, L. Werner, S. K. Pandey, M. Escobar-Gomez, S. L. Znoiko, and D. J. Apple, "Adhesion of fibronectin, vitronectin, laminin, and collagen type IV to intraocular lens materials in pseudophakic human autopsy eyes. Part 2: explanted intraocular lenses," *Journal of Cataract & Refractive Surgery*, vol. 26, no. 12, pp. 1807–1818, 2000.

[18] R. J. Linnola, L. Werner, S. K. Pandey, M. Escobar-Gomez, S. L. Znoiko, and D. J. Apple, "Adhesion of fibronectin, vitronectin, laminin, and collagen type IV to intraocular lens

materials in pseudophakic human autopsy eyes. Part 1: histological sections," *Journal of Cataract & Refractive Surgery*, vol. 26, no. 12, pp. 1792–1806, 2000.

[19] K. A. Abhilakh Missier, R. M. M. A. Nuijts, and K. F. Tjia, "Posterior capsule opacification: silicone plate-haptic versus AcrySof intraocular lenses," *Journal of Cataract & Refractive Surgery*, vol. 29, no. 8, pp. 1569–1574, 2003.

[20] G. Auffarth, A. Brezin, A. Caporossi et al., "Comparison of Nd : YAG capsulotomy rates following phacoemulsification with implantation of PMMA, silicone, or acrylic intraocular lenses in four European countries," *Ophthalmic Epidemiology*, vol. 11, no. 4, pp. 319–329, 2004.

[21] L. E. Bender, D. J. Spalton, W. Meacock, R. Jose, and J. Boyce, "Predicting posterior capsule opacification: value of early retroillumination imaging," *Journal of Cataract & Refractive Surgery*, vol. 29, no. 3, pp. 526–531, 2003.

[22] A. M. Bourdiol Ducasse, V. Guerzider, L. Velasque, M. Dominguez, A. Lafuma, and J. Robert, "Comparison of clinical efficacy: Nd:YAG laser rates after implantation of AcrySof® SN60WF, Akreos® AO-MI60 and Hoya® YA-60BB," *Journal Français d'Ophtalmologie*, vol. 36, no. 7, pp. 575–582, 2013.

[23] C. Boureau, A. Lafuma, V. Jeanbat, G. Berdeaux, and A. F. Smith, "Incidence of Nd:YAG laser capsulotomies after cataract surgery: comparison of 3 square-edged lenses of different composition," *Canadian Journal of Ophthalmology*, vol. 44, no. 2, pp. 165–170, 2009.

[24] A. Chang, A. Behndig, M. Ronbeck, and M. Kugelberg, "Comparison of posterior capsule opacification and glistenings with 2 hydrophobic acrylic intraocular lenses: 5- to 7-year follow-up," *Journal of Cataract & Refractive Surgery*, vol. 39, no. 5, pp. 694–698, 2013.

[25] L. Gauthier, A. Lafuma, C. Laurendeau, and G. Berdeaux, "Neodymium:YAG laser rates after bilateral implantation of hydrophobic or hydrophilic multifocal intraocular lenses: twenty-four month retrospective comparative study," *Journal of Cataract & Refractive Surgery*, vol. 36, no. 7, pp. 1195–1200, 2010.

[26] K. Hayashi and H. Hayashi, "Posterior capsule opacification after implantation of a hydrogel intraocular lens," *The British Journal of Ophthalmology*, vol. 88, no. 2, pp. 182–185, 2004.

[27] C. J. Heatley, D. J. Spalton, A. Kumar, R. Jose, J. Boyce, and L. E. Bender, "Comparison of posterior capsule opacification rates between hydrophilic and hydrophobic single-piece acrylic intraocular lenses," *Journal of Cataract & Refractive Surgery*, vol. 31, no. 4, pp. 718–724, 2005.

[28] T. Iwase, Y. Nishi, B. C. Oveson, and Y. J. Jo, "Hydrophobic versus double-square-edged hydrophilic foldable acrylic intraocular lens: effect on posterior capsule opacification," *Journal of Cataract & Refractive Surgery*, vol. 37, no. 6, pp. 1060–1068, 2011.

[29] Y. Kucuksumer, S. Bayraktar, S. Sahin, and O. F. Yilmaz, "Posterior capsule opacification 3 years after implantation of an AcrySof and a MemoryLens in fellow eyes," *Journal of Cataract & Refractive Surgery*, vol. 26, no. 8, pp. 1176–1182, 2000.

[30] M. Kugelberg, G. Wejde, H. Jayaram, and C. Zetterstrom, "Posterior capsule opacification after implantation of a hydrophilic or a hydrophobic acrylic intraocular lens: one-year follow-up," *Journal of Cataract & Refractive Surgery*, vol. 32, no. 10, pp. 1627–1631, 2006.

[31] M. Kugelberg, G. Wejde, H. Jayaram, and C. Zetterstrom, "Two-year follow-up of posterior capsule opacification after implantation of a hydrophilic or hydrophobic acrylic intraocular lens," *Acta Ophthalmologica*, vol. 86, no. 5, pp. 533–536, 2008.

[32] P. J. Morgan-Warren and J. A. Smith, "Intraocular lens-edge design and material factors contributing to posterior-capsulotomy rates: comparing Hoya FY60aD, PY60aD, and AcrySof SN60WF," *Clinical Ophthalmology*, vol. 7, pp. 1661–1667, 2013.

[33] F. H. Oner, U. Gunenc, and S. T. Ferliel, "Posterior capsule opacification after phacoemulsification: foldable acrylic versus poly(methyl methacrylate) intraocular lenses," *Journal of Cataract & Refractive Surgery*, vol. 26, no. 5, pp. 722–726, 2000.

[34] A. R. Vasavada, S. M. Raj, A. Shah, G. Shah, V. Vasavada, and V. Vasavada, "Comparison of posterior capsule opacification with hydrophobic acrylic and hydrophilic acrylic intraocular lenses," *Journal of Cataract & Refractive Surgery*, vol. 37, no. 6, pp. 1050–1059, 2011.

[35] O. Nishi, "Posterior capsule opacification. Part 1: experimental investigations," *Journal of Cataract & Refractive Surgery*, vol. 25, no. 1, pp. 106–117, 1999.

[36] J. Ram, D. J. Apple, Q. Peng et al., "Update on fixation of rigid and foldable posterior chamber intraocular lenses. Part II: choosing the correct haptic fixation and intraocular lens design to help eradicate posterior capsule opacification," *Ophthalmology*, vol. 106, no. 5, pp. 891–900, 1999.

[37] F. Cullin, T. Busch, and M. Lundstrom, "Economic considerations related to choice of intraocular lens (IOL) and posterior capsule opacification frequency – a comparison of three different IOLs," *Acta Ophthalmologica*, vol. 92, no. 2, pp. 179–183, 2014.

[38] C. S.-U. Fong, P. Mitchell, E. Rochtchina, S. Cugati, T. Hong, and J. J. Wang, "Three-year incidence and factors associated with posterior capsule opacification after cataract surgery: the Australian Prospective Cataract Surgery and Age-related Macular Degeneration Study," *American Journal of Ophthalmology*, vol. 157, no. 1, pp. 171–179.e1, 2014, e171.

[39] K. Hayashi, H. Hayashi, F. Nakao, and F. Hayashi, "Changes in posterior capsule opacification after poly(methyl methacrylate), silicone, and acrylic intraocular lens implantation," *Journal of Cataract & Refractive Surgery*, vol. 27, no. 6, pp. 817–824, 2001.

[40] K. Hayashi, M. Yoshida, and H. Hayashi, "Comparison of posterior capsule opacification between fellow eyes with two types of acrylic intraocular lens," *Eye*, vol. 22, no. 1, pp. 35–41, 2008.

[41] T. Kohnen, E. Fabian, R. Gerl et al., "Optic edge design as long-term factor for posterior capsular opacification rates," *Ophthalmology*, vol. 115, no. 8, pp. 1308–1314.e3, 2008.

[42] G. Prosdocimo, G. Tassinari, M. Sala et al., "Posterior capsule opacification after phacoemulsification: silicone CeeOn Edge versus acrylate AcrySof intraocular lens," *Journal of Cataract & Refractive Surgery*, vol. 29, no. 8, pp. 1551–1555, 2003.

[43] M. Ronbeck, C. Zetterstrom, G. Wejde, and M. Kugelberg, "Comparison of posterior capsule opacification development with 3 intraocular lens types: five-year prospective study," *Journal of Cataract & Refractive Surgery*, vol. 35, no. 11, pp. 1935–1940, 2009.

[44] J. Schauersberger, M. Amon, A. Kruger, C. Abela, G. Schild, and J. Kolodjaschna, "Comparison of the biocompatibility

of 2 foldable intraocular lenses with sharp optic edges," *Journal of Cataract & Refractive Surgery*, vol. 27, no. 10, pp. 1579–1585, 2001.

[45] L. Vock, A. Crnej, O. Findl et al., "Posterior capsule opacification in silicone and hydrophobic acrylic intraocular lenses with sharp-edge optics six years after surgery," *American Journal of Ophthalmology*, vol. 147, no. 4, pp. 683–690.e2, 2009, e682.

[46] L. Vock, R. Menapace, E. Stifter, M. Georgopoulos, S. Sacu, and W. Buhl, "Posterior capsule opacification and neodymium:YAG laser capsulotomy rates with a round-edged silicone and a sharp-edged hydrophobic acrylic intraocular lens 10 years after surgery," *Journal of Cataract & Refractive Surgery*, vol. 35, no. 3, pp. 459–465, 2009.

[47] R. Zemaitiene and V. Jasinskas, "Prevention of posterior capsule opacification with 3 intraocular lens models: a prospective, randomized, long-term clinical trial," *Medicina*, vol. 47, no. 11, pp. 595–599, 2011.

[48] T. Nagata, A. Minakata, and I. Watanabe, "Adhesiveness of AcrySof to a collagen film," *Journal of Cataract & Refractive Surgery*, vol. 24, no. 3, pp. 367–370, 1998.

[49] M. Ong, L. Wang, and M. Karakelle, "Fibronectin adhesive properties of various intraocular lens materials," *Investigative Ophthalmology & Visual Science*, vol. 54, no. 15, p. 819, 2013.

[50] M. W. Dorey, S. Brownstein, V. E. Hill et al., "Proposed pathogenesis for the delayed postoperative opacification of the hydroview hydrogel intraocular lens," *American Journal of Ophthalmology*, vol. 135, no. 5, pp. 591–598, 2003.

[51] Q. Peng, N. Visessook, D. J. Apple et al., "Surgical prevention of posterior capsule opacification. Part 3: intraocular lens optic barrier effect as a second line of defense," *Journal of Cataract & Refractive Surgery*, vol. 26, no. 2, pp. 198–213, 2000.

[52] G. U. Auffarth, A. Golescu, K. A. Becker, and H. E. Volcker, "Quantification of posterior capsule opacification with round and sharp edge intraocular lenses," *Ophthalmology*, vol. 110, no. 4, pp. 772–780, 2003.

[53] N. Li, X. Chen, J. Zhang et al., "Effect of AcrySof versus silicone or polymethyl methacrylate intraocular lens on posterior capsule opacification," *Ophthalmology*, vol. 115, no. 5, pp. 830–838, 2008.

[54] O. Nishi, K. Nishi, J. Akura, and T. Nagata, "Effect of round-edged acrylic intraocular lenses on preventing posterior capsule opacification," *Journal of Cataract & Refractive Surgery*, vol. 27, no. 4, pp. 608–613, 2001.

[55] O. Nishi, K. Nishi, and Y. Osakabe, "Effect of intraocular lenses on preventing posterior capsule opacification: design versus material," *Journal of Cataract & Refractive Surgery*, vol. 30, no. 10, pp. 2170–2176, 2004.

[56] O. Nishi, K. Nishi, and K. Wickstrom, "Preventing lens epithelial cell migration using intraocular lenses with sharp rectangular edges," *Journal of Cataract & Refractive Surgery*, vol. 26, no. 10, pp. 1543–1549, 2000.

[57] G. Cleary, D. J. Spalton, J. Hancox, J. Boyce, and J. Marshall, "Randomized intraindividual comparison of posterior capsule opacification between a microincision intraocular lens and a conventional intraocular lens," *Journal of Cataract & Refractive Surgery*, vol. 35, no. 2, pp. 265–272, 2009.

[58] S. Sacu, O. Findl, R. Menapace, W. Buehl, and M. Wirtitsch, "Comparison of posterior capsule opacification between the 1-piece and 3-piece Acrysof intraocular lenses: two-year results of a randomized trial," *Ophthalmology*, vol. 111, no. 10, pp. 1840–1846, 2004.

[59] L. Werner, N. Mamalis, A. M. Izak et al., "Posterior capsule opacification in rabbit eyes implanted with 1-piece and 3-piece hydrophobic acrylic intraocular lenses," *Journal of Cataract & Refractive Surgery*, vol. 31, no. 4, pp. 805–811, 2005.

[60] D. R. Nixon and M. G. Woodcock, "Pattern of posterior capsule opacification models 2 years postoperatively with 2 single-piece acrylic intraocular lenses," *Journal of Cataract & Refractive Surgery*, vol. 36, no. 6, pp. 929–934, 2010.

[61] C. Leydolt, K. Kriechbaum, S. Schriefl, M. Pachala, and R. Menapace, "Posterior capsule opacification and neodymium:YAG rates with 2 single-piece hydrophobic acrylic intraocular lenses: three-year results," *Journal of Cataract & Refractive Surgery*, vol. 39, no. 12, pp. 1886–1892, 2013.

[62] G. Kahraman, H. Schrittwieser, M. Walch et al., "Anterior and posterior capsular opacification with the Tecnis ZCB00 and AcrySof SA60AT IOLs: a randomised intraindividual comparison," *The British Journal of Ophthalmology*, vol. 98, no. 7, pp. 905–909, 2014.

[63] G. Kahraman, M. Amon, C. Ferdinaro, K. Nigl, and M. Walch, "Intraindividual comparative analysis of capsule opacification after implantation of 2 single-piece hydrophobic acrylic intraocular lenses models: three-year follow-up," *Journal of Cataract & Refractive Surgery*, vol. 41, no. 5, pp. 990–996, 2015.

[64] T. R. Wallin, M. Hinckley, C. Nilson, and R. J. Olson, "A clinical comparison of single-piece and three-piece truncated hydrophobic acrylic intraocular lenses," *American Journal of Ophthalmology*, vol. 136, no. 4, pp. 614–619, 2003.

[65] S. I. Mian, K. Fahim, A. Marcovitch, H. Gada, D. C. Musch, and A. Sugar, "Nd:YAG capsulotomy rates after use of the AcrySof acrylic three piece and one piece intraocular lenses," *The British Journal of Ophthalmology*, vol. 89, no. 11, pp. 1453–1457, 2005.

[66] R. Nejima, K. Miyata, M. Honbou et al., "A prospective, randomised comparison of single and three piece acrylic foldable intraocular lenses," *The British Journal of Ophthalmology*, vol. 88, no. 6, pp. 746–749, 2004.

[67] L. E. Bender, C. Nimsgern, R. Jose et al., "Effect of 1-piece and 3-piece AcrySof intraocular lenses on the development of posterior capsule opacification after cataract surgery," *Journal of Cataract & Refractive Surgery*, vol. 30, no. 4, pp. 786–789, 2004.

[68] C. Leydolt, S. Davidovic, S. Sacu et al., "Long-term effect of 1-piece and 3-piece hydrophobic acrylic intraocular lens on posterior capsule opacification: a randomized trial," *Ophthalmology*, vol. 114, no. 9, pp. 1663–1669, 2007.

[69] R. Zemaitiene, V. Jasinskas, and G. U. Auffarth, "Influence of three-piece and single-piece designs of two sharp-edge optic hydrophobic acrylic intraocular lenses on the prevention of posterior capsule opacification: a prospective, randomised, long-term clinical trial," *The British Journal of Ophthalmology*, vol. 91, no. 5, pp. 644–648, 2007.

[70] P. J. Ness, L. Werner, S. Maddula et al., "Pathology of 219 human cadaver eyes with 1-piece or 3-piece hydrophobic acrylic intraocular lenses: capsular bag opacification and sites of square-edged barrier breach," *Journal of Cataract & Refractive Surgery*, vol. 37, no. 5, pp. 923–930, 2011.

[71] J. M. Biber, H. P. Sandoval, R. H. Trivedi, L. E. Fernández de Castro, J. W. French, and K. D. Solomon, "Comparison of the

incidence and visual significance of posterior capsule opacification between multifocal spherical, monofocal spherical, and monofocal aspheric intraocular lenses," *Journal of Cataract & Refractive Surgery*, vol. 35, no. 7, pp. 1234–1238, 2009.

[72] W. R. Meacock, D. J. Spalton, J. F. Boyce, and R. M. Jose, "Effect of optic size on posterior capsule opacification: 5.5 mm versus 6.0 mm AcrySof intraocular lenses," *Journal of Cataract & Refractive Surgery*, vol. 27, no. 8, pp. 1194–1198, 2001.

[73] G. Wejde, M. Kugelberg, and C. Zetterstrom, "Position of anterior capsulorhexis and posterior capsule opacification," *Acta Ophthalmologica Scandinavica*, vol. 82, no. 5, pp. 531–534, 2004.

[74] S. M. E. Wren, D. J. Spalton, R. Jose, J. Boyce, and C. J. Heatley, "Factors that influence the development of posterior capsule opacification with a polyacrylic intraocular lens," *American Journal of Ophthalmology*, vol. 139, no. 4, pp. 691–695, 2005.

[75] T. Ishibashi, H. Araki, S. Sugai, A. Tawara, Y. Ohnishi, and H. Inomata, "Anterior capsule opacification in monkey eyes with posterior chamber intraocular lenses," *Archives of Ophthalmology*, vol. 111, no. 12, pp. 1685–1690, 1993.

[76] C. K. Joo, J. A. Shin, and J. H. Kim, "Capsular opening contraction after continuous curvilinear capsulorhexis and intraocular lens implantation," *Journal of Cataract & Refractive Surgery*, vol. 22, no. 5, pp. 585–590, 1996.

[77] K. Hayashi, H. Hayashi, F. Nakao, and F. Hayashi, "Reduction in the area of the anterior capsule opening after polymethylmethacrylate, silicone, and soft acrylic intraocular lens implantation," *American Journal of Ophthalmology*, vol. 123, no. 4, pp. 441–447, 1997.

[78] S. Sacu, R. Menapace, W. Buehl, G. Rainer, and O. Findl, "Effect of intraocular lens optic edge design and material on fibrotic capsule opacification and capsulorhexis contraction," *Journal of Cataract & Refractive Surgery*, vol. 30, no. 9, pp. 1875–1882, 2004.

[79] J. A. Davison, "Capsule contraction syndrome," *Journal of Cataract & Refractive Surgery*, vol. 19, no. 5, pp. 582–589, 1993.

[80] K. Hayashi, M. Yoshida, A. Hirata, and H. Hayashi, "Anterior capsule relaxing incisions with neodymium:YAG laser for patients at high-risk for anterior capsule contraction," *Journal of Cataract & Refractive Surgery*, vol. 37, no. 1, pp. 97–103, 2011.

[81] K. Hayashi, M. Yoshida, F. Nakao, and H. Hayashi, "Prevention of anterior capsule contraction by anterior capsule relaxing incisions with neodymium:yttrium–aluminum–garnet laser," *American Journal of Ophthalmology*, vol. 146, no. 1, pp. 23–30.e1, 2008.

[82] S. O. Hansen, A. S. Crandall, and R. J. Olson, "Progressive constriction of the anterior capsular opening following intact capsulorhexis," *Journal of Cataract & Refractive Surgery*, vol. 19, no. 1, pp. 77–82, 1993.

[83] O. Nishi and K. Nishi, "Intraocular lens encapsulation by shrinkage of the capsulorhexis opening," *Journal of Cataract & Refractive Surgery*, vol. 19, no. 4, pp. 544-545, 1993.

[84] S. Tsuboi, M. Tsujioka, T. Kusube, and S. Kojima, "Effect of continuous circular capsulorhexis and intraocular lens fixation on the blood-aqueous barrier," *Archives of Ophthalmology*, vol. 110, no. 8, pp. 1124–1127, 1992.

[85] M. Gonvers, M. Sickenberg, and G. van Melle, "Change in capsulorhexis size after implantation of three types of intraocular lenses," *Journal of Cataract & Refractive Surgery*, vol. 23, no. 2, pp. 231–238, 1997.

[86] T. K. Park, S. K. Chung, and N. H. Baek, "Changes in the area of the anterior capsule opening after intraocular lens implantation," *Journal of Cataract & Refractive Surgery*, vol. 28, no. 9, pp. 1613–1617, 2002.

[87] K. Hayashi and H. Hayashi, "Effect of anterior capsule contraction on visual function after cataract surgery," *Journal of Cataract & Refractive Surgery*, vol. 33, no. 11, pp. 1936–1940, 2007.

[88] L. Werner, S. K. Pandey, D. J. Apple, M. Escobar-Gomez, L. McLendon, and T. A. Macky, "Anterior capsule opacification: correlation of pathologic findings with clinical sequelae," *Ophthalmology*, vol. 108, no. 9, pp. 1675–1681, 2001.

[89] L. Werner, S. K. Pandey, M. Escobar-Gomez, N. Visessook, Q. Peng, and D. J. Apple, "Anterior capsule opacification: a histopathological study comparing different IOL styles," *Ophthalmology*, vol. 107, no. 3, pp. 463–471, 2000.

[90] M. Nagata, H. Matsushima, K. Mukai, W. Terauchi, N. Gotoh, and E. Matsui, "Comparison of anterior capsule contraction between 5 foldable intraocular lens models," *Journal of Cataract & Refractive Surgery*, vol. 34, no. 9, pp. 1495–1498, 2008.

[91] O. Nishi, K. Nishi, and K. Sakanishi, "Inhibition of migrating lens epithelial cells at the capsular bend created by the rectangular optic edge of a posterior chamber intraocular lens," *Ophthalmic Surgery, Lasers and Imaging Retina*, vol. 29, no. 7, pp. 587–594, 1998.

[92] I. T. Tsinopoulos, K. T. Tsaousis, G. D. Kymionis et al., "Comparison of anterior capsule contraction between hydrophobic and hydrophilic intraocular lens models," *Graefe's Archive for Clinical and Experimental Ophthalmology*, vol. 248, no. 8, pp. 1155–1158, 2010.

[93] K. Hayashi and H. Hayashi, "Intraocular lens factors that may affect anterior capsule contraction," *Ophthalmology*, vol. 112, no. 2, pp. 286–292, 2005.

[94] G. Savini, P. Barboni, P. Ducoli, E. Borrelli, and K. J. Hoffer, "Influence of intraocular lens haptic design on refractive error," *Journal of Cataract & Refractive Surgery*, vol. 40, no. 9, pp. 1473–1478, 2014.

[95] M. Sickenberg, M. Gonvers, and G. van Melle, "Change in capsulorhexis size with four foldable loop-haptic lenses over 6 months," *Journal of Cataract & Refractive Surgery*, vol. 24, no. 7, pp. 925–930, 1998.

[96] S. Sacu, R. Menapace, and O. Findl, "Effect of optic material and haptic design on anterior capsule opacification and capsulorrhexis contraction," *American Journal of Ophthalmology*, vol. 141, no. 3, pp. 488–493.e2, 2006.

[97] H. Hayashi, K. Hayashi, F. Nakao, and F. Hayashi, "Area reduction in the anterior capsule opening in eyes of diabetes mellitus patients," *Journal of Cataract & Refractive Surgery*, vol. 24, no. 8, pp. 1105–1110, 1998.

[98] S. Kato, T. Oshika, J. Numaga et al., "Anterior capsular contraction after cataract surgery in eyes of diabetic patients," *The British Journal of Ophthalmology*, vol. 85, no. 1, pp. 21–23, 2001.

[99] Y. Takamura, T. Tomomatsu, S. Arimura et al., "Anterior capsule contraction and flare intensity in the early stages after cataract surgery in eyes with diabetic retinopathy,"

Journal of Cataract & Refractive Surgery, vol. 39, no. 5, pp. 716–721, 2013.

[100] H. Hayashi, K. Hayashi, F. Nakao, and F. Hayashi, "Anterior capsule contraction and intraocular lens dislocation in eyes with pseudoexfoliation syndrome," *The British Journal of Ophthalmology*, vol. 82, no. 12, pp. 1429–1432, 1998.

[101] K. Hayashi, H. Hayashi, K. Matsuo, F. Nakao, and F. Hayashi, "Anterior capsule contraction and intraocular lens dislocation after implant surgery in eyes with retinitis pigmentosa," *Ophthalmology*, vol. 105, no. 7, pp. 1239–1243, 1998.

[102] K. Kato, M. Nishida, H. Yamane, K. Nakamae, Y. Tagami, and K. Tetsumoto, "Glistening formation in an AcrySof lens initiated by spinodal decomposition of the polymer network by temperature change," *Journal of Cataract & Refractive Surgery*, vol. 27, no. 9, pp. 1493–1498, 2001.

[103] O. Omar, A. Pirayesh, N. Mamalis, and R. J. Olson, "In vitro analysis of AcrySof intraocular lens glistenings in AcryPak and Wagon Wheel packaging," *Journal of Cataract & Refractive Surgery*, vol. 24, no. 1, pp. 107–113, 1998.

[104] P. Tyagi, N. Shah, and M. Jabir, "Intraoperative clouding of a posterior chamber intraocular lens," *International Ophthalmology*, vol. 31, no. 6, pp. 483-484, 2011.

[105] A. Miyata, N. Uchida, K. Nakajima, and S. Yaguchi, "Clinical and experimental observation of glistening in acrylic intraocular lenses," *Japanese Journal of Ophthalmology*, vol. 45, no. 6, pp. 564–569, 2001.

[106] T. Shiba, K. Mitooka, and H. Tsuneoka, "In vitro analysis of AcrySof intraocular lens glistening," *European Journal of Ophthalmology*, vol. 13, no. 9-10, pp. 759–763, 2003.

[107] A. Miyata and S. Yaguchi, "Equilibrium water content and glistenings in acrylic intraocular lenses," *Journal of Cataract & Refractive Surgery*, vol. 30, no. 8, pp. 1768–1772, 2004.

[108] K. M. Klos, R. Richter, O.-E. Schnaudigel, and C. Ohrloff, "Image analysis of implanted rigid and foldable intraocular lenses in human eyes using Scheimpflug photography," *Ophthalmic Research*, vol. 31, no. 2, pp. 130–133, 1999.

[109] A. Behndig and E. Monestam, "Quantification of glistenings in intraocular lenses using Scheimpflug photography," *Journal of Cataract & Refractive Surgery*, vol. 35, no. 1, pp. 14–17, 2009.

[110] R. J. Mackool and J. Colin, "Limitations of Scheimpflug photography in quantifying glistenings," *Journal of Cataract & Refractive Surgery*, vol. 35, no. 8, pp. 1480-1481, 2009.

[111] D. K. Dhaliwal, N. Mamalis, R. J. Olson et al., "Visual significance of glistenings seen in the AcrySof intraocular lens," *Journal of Cataract & Refractive Surgery*, vol. 22, no. 4, pp. 452–457, 1996.

[112] A. Waite, N. Faulkner, and R. J. Olson, "Glistenings in the single-piece, hydrophobic, acrylic intraocular lenses," *American Journal of Ophthalmology*, vol. 144, no. 1, pp. 143-144, 2007.

[113] M. Miura, M. Osako, A. E. Elsner, H. Kajizuka, K. Yamada, and M. Usui, "Birefringence of intraocular lenses," *Journal of Cataract & Refractive Surgery*, vol. 30, no. 7, pp. 1549–1555, 2004.

[114] D. Tognetto, L. Toto, G. Sanguinetti, and G. Ravalico, "Glistenings in foldable intraocular lenses," *Journal of Cataract & Refractive Surgery*, vol. 28, no. 7, pp. 1211–1216, 2002.

[115] L. Werner, "Glistenings and surface light scattering in intraocular lenses," *Journal of Cataract & Refractive Surgery*, vol. 36, no. 8, pp. 1398–1420, 2010.

[116] M. Ronbeck, A. Behndig, M. Taube, A. Koivula, and M. Kugelberg, "Comparison of glistenings in intraocular lenses with three different materials: 12-year follow-up," *Acta Ophthalmologica*, vol. 91, no. 1, pp. 66–70, 2013.

[117] E. Wilkins and R. J. Olson, "Glistenings with long-term follow-up of the Surgidev B20/20 polymethylmethacrylate intraocular lens," *American Journal of Ophthalmology*, vol. 132, no. 5, pp. 783–785, 2001.

[118] T. Maki, S. Izumi, M. Ayaki, and R. Koide, "Glistenings in PMMA intraocular lenses," *The Showa University Journal of Medical Sciences*, vol. 16, no. 1, pp. 75–82, 2004.

[119] J. Moreno-Montanes, A. Alvarez, R. Rodriguez-Conde, and A. Fernandez-Hortelano, "Clinical factors related to the frequency and intensity of glistenings in AcrySof intraocular lenses," *Journal of Cataract & Refractive Surgery*, vol. 29, no. 10, pp. 1980–1984, 2003.

[120] J. Colin, I. Orignac, and D. Touboul, "Glistenings in a large series of hydrophobic acrylic intraocular lenses," *Journal of Cataract & Refractive Surgery*, vol. 35, no. 12, pp. 2121–2126, 2009.

[121] E. Monestam and A. Behndig, "Impact on visual function from light scattering and glistenings in intraocular lenses, a long-term study," *Acta Ophthalmologica*, vol. 89, no. 8, pp. 724–728, 2011.

[122] J. Colin and I. Orignac, "Glistenings on intraocular lenses in healthy eyes: effects and associations," *Journal of Refractive Surgery*, vol. 27, no. 12, pp. 869–875, 2011.

[123] E. Peetermans and R. Hennekes, "Long-term results of wagon wheel packed acrylic intra-ocular lenses (AcrySof)," *Bulletin de la Société Belge d'Ophtalmologie*, vol. 271, pp. 45–48, 1999.

[124] G. Christiansen, F. J. Durcan, R. J. Olson, and K. Christiansen, "Glistenings in the AcrySof intraocular lens: pilot study," *Journal of Cataract & Refractive Surgery*, vol. 27, no. 5, pp. 728–733, 2001.

[125] H. B. Dick, R. J. Olson, A. J. Augustin, O. Schwenn, G. Magdowski, and N. Pfeiffer, "Vacuoles in the Acrysof™ intraocular lens as factor of the presence of serum in aqueous humor," *Ophthalmic Research*, vol. 33, no. 2, pp. 61–67, 2001.

[126] M. Ayaki, H. Nishihara, S. Yaguchi, and R. Koide, "Surfactant induced glistenings: surface active ingredients in ophthalmic solutions may enhance water entry into the voids of implanted acrylic intraocular lenses," *Journal of Long-Term Effects of Medical Implants*, vol. 16, no. 6, pp. 451–457, 2006.

[127] M. Ayaki, H. Nishihara, S. Yaguchi, and R. Koide, "Effect of ophthalmic solution components on acrylic intraocular lenses," *Journal of Cataract & Refractive Surgery*, vol. 33, no. 1, pp. 122–126, 2007.

[128] C. Schweitzer, I. Orignac, D. Praud, O. Chatoux, and J. Colin, "Glistening in glaucomatous eyes: visual performances and risk factors," *Acta Ophthalmologica*, vol. 92, no. 6, pp. 529–534, 2014.

[129] J. Colin, D. Praud, D. Touboul, and C. Schweitzer, "Incidence of glistenings with the latest generation of yellow-tinted hydrophobic acrylic intraocular lenses," *Journal of Cataract & Refractive Surgery*, vol. 38, no. 7, pp. 1140–1146, 2012.

[130] A. Chang and M. Kugelberg, "Glistenings 9 years after phacoemulsification in hydrophobic and hydrophilic acrylic intraocular lenses," *Journal of Cataract & Refractive Surgery*, vol. 41, no. 6, pp. 1199–1204, 2015.

[131] U. Gunenc, F. H. Oner, S. Tongal, and M. Ferliel, "Effects on visual function of glistenings and folding marks in AcrySof

intraocular lenses," *Journal of Cataract & Refractive Surgery*, vol. 27, no. 10, pp. 1611–1614, 2001.

[132] L. Xi, Y. Liu, F. Zhao, C. Chen, and B. Cheng, "Analysis of glistenings in hydrophobic acrylic intraocular lenses on visual performance," *International Journal of Ophthalmology*, vol. 7, no. 3, pp. 446–451, 2014.

[133] K. Hayashi, A. Hirata, M. Yoshida, K. Yoshimura, and H. Hayashi, "Long-term effect of surface light scattering and glistenings of intraocular lenses on visual function," *American Journal of Ophthalmology*, vol. 154, no. 2, pp. 240–251.e2, 2012.

[134] M. van der Mooren, L. Franssen, and P. Piers, "Effects of glistenings in intraocular lenses," *Biomedical Optics Express*, vol. 4, no. 8, pp. 1294–1304, 2013.

[135] S. Beheregaray, T. Yamamoto, T. Hiraoka, and T. Oshika, "Influence on visual function of forward light scattering associated with subsurface nanoglistenings in intraocular lenses," *Journal of Cataract & Refractive Surgery*, vol. 40, no. 7, pp. 1147–1154, 2014.

[136] B. S. Henriksen, K. Kinard, and R. J. Olson, "Effect of intraocular lens glistening size on visual quality," *Journal of Cataract & Refractive Surgery*, vol. 41, no. 6, pp. 1190–1198, 2015.

[137] L. Werner, J. C. Stover, J. Schwiegerling, and K. K. Das, "Light scattering, straylight, and optical quality in hydrophobic acrylic intraocular lenses with subsurface nanoglistenings," *Journal of Cataract & Refractive Surgery*, vol. 42, no. 1, pp. 148–156, 2016.

[138] B. E. Thomes and T. A. Callaghan, "Evaluation of in vitro glistening formation in hydrophobic acrylic intraocular lenses," *Clinical Ophthalmology*, vol. 7, pp. 1529–1534, 2013.

[139] M. Packer, L. Fry, K. T. Lavery et al., "Safety and effectiveness of a glistening-free single-piece hydrophobic acrylic intraocular lens (enVista)," *Clinical Ophthalmology*, vol. 7, pp. 1905–1912, 2013.

Hindawi
Journal of Ophthalmology
Volume 2018, Article ID 6165493, 8 pages
https://doi.org/10.1155/2018/6165493

Clinical Study

Through-Focus Vision Performance and Light Disturbances of 3 New Intraocular Lenses for Presbyopia Correction

Santiago Escandón-García,[1] Filomena J. Ribeiro,[2] Colm McAlinden,[3,4] António Queirós,[1] and José M. González-Méijome[1]

[1]*Clinical & Experimental Optometry Research Lab (CEORLab), Center of Physics, University of Minho, Braga, Portugal*
[2]*Hospital da Luz, Lisboa, Portugal*
[3]*Department of Ophthalmology, Glangwili Hospital, Hywel Dda University Hospital Board, Carmarthen, UK*
[4]*School of Ophthalmology and Optometry, Wenzhou Medical University, Wenzhou, Zhejiang, China*

Correspondence should be addressed to António Queirós; aqp@fisica.uminho.pt

Received 26 April 2017; Revised 7 December 2017; Accepted 14 December 2017; Published 31 January 2018

Academic Editor: Tamer A. Macky

Purpose. To compare the through-focus visual performance in a clinical population of pseudophakic patients implanted with two new trifocal intraocular lenses (IOLs) and one extended depth of focus IOL. *Methods.* Prospective, nonrandomized, examiner-masked case series. Twenty-three patients received the FineVision® and seven patients received the PanOptix™ trifocal IOLs. Fifteen patients received the Symfony extended depth of focus IOL. Mean age of patients was 63 ± 8 years. Through-focus visual acuity was measured from −3.00 to +1.00 D vergences. Contrast sensitivity was measured with and without a source of glare. Light disturbances were evaluated with the Light Distortion Analyzer. *Results.* Though-focus evaluation showed that trifocal IOLs performed significantly better at near distance (33 and 40 cm), and extended depth of focus performed significantly better at intermediate distance (1.0 m). Contrast sensitivity function with glare and dysphotopsia was similar between the three IOLs and subjective response to questionnaire showed a significantly higher score (worse performance) for the extended depth of focus IOL compared to both trifocal IOLs in the bothersome subscale ($p < 0.05$). *Conclusions.* Trifocal IOLs grant better performance at near distance while extended depth of focus IOL performs better at intermediate distance. Objective dysphotopsia measured with the Light Distortion Analyzer is not reduced in extended depth of focus IOL compared to trifocal IOLs.

1. Introduction

Multifocal intraocular lenses (IOLs) are increasingly implanted in pseudophakic patients to increase spectacle independence. In the recent years, the number of new optical designs available has increased. Bifocal and trifocal diffractive IOLs are the most commonly implanted and provide a range of vision from distance to intermediate and near distance. These IOLs allow independence of spectacle correction for intermediate and near vision [1]. However, the simultaneous focusing of objects from different distances across a distance of approximately 1 mm in front of the retina along the optical axis induces formation of haloes and other visual phenomena around the best focused image [2]. Complaints of night vision disturbances or photic phenomena are common with these devices causing some degree of dissatisfaction with the outcomes, which accounts for more than a third of the main reasons for IOL explantation [3, 4].

Considering the potential medical impact of photic phenomena, there have been efforts to investigate and quantify these complaints. Several instruments have been used including halometers [5] and subjective questionnaires [6, 7]. Mastropasqua et al. [8] used some subcategories of the National Eye Institute Refractive Error Quality of Life

Instrument-42 (NEI-RQL42) questionnaire comparing three groups of 20 patients each implanted bilaterally with bifocal 2.5 D, bifocal 3.0 D, and mixed contralateral implantation of each lens. Gundersen and Potvin [9] used the National Eye Institute Visual Function Questionnaire (NEI-VFQ) in two cohorts of 11 patients each implanted with diffractive bifocal toric and trifocal toric IOLs. The recently developed Quality of Vision (QoV) questionnaire by McAlinden et al. [10, 11] includes specific categories for dysphotopic phenomena with simulation images and might be a more adequate instrument to subjectively assess the performance of multifocal IOLs.

In a further attempt to get objective metrics of the photic phenomena, different instruments and devices have been engineered. Systems aiming to measure the size of the distortion by analyzing a certain area of the visual field only and expanding the results to 360° of the field usually assume that the distortion might be circular and symmetric in shape [2, 12], which is not actually the case for most people describing such phenomena. More recently, Puell et al. [13] investigated the size of the halo in the general population using the commercial Vision Monitor device. This device measures the ability to recognize letters in three semimeridians around a source of glare at 2.5 m. Indeed, the systems described provide a single value of size around the central source of light. Other experimental devices have been described for use in clinical practice that present peripheral detection stimuli in the form of fluorescent paint which might limit their use as uniform methods for visual assessment [14].

The Light Distortion Analyzer (LDA) is a device consisting of 240 individual light-emitting diodes (LEDs) surrounding a central larger LED acting as source of glare [15]. The exam is performed in a darkened room at 2.0 ms, and it provides different morphological metrics of light disturbances in 30 to 90 seconds per exam [16, 17] which are sensitive to small changes in optical higher-order aberrations [18].

With the aim to reduce the complaints of photic phenomena, the concept of extended depth of focus IOLs has been developed to provide more consistent distance and intermediate vision with less photic phenomena, at the expense of some loss of near vision [19]. Trifocal IOLs have also showed better performance in terms of halo formation compared to bifocal IOLs [20].

Considering the existing concern of photic phenomena with modern IOLs, the potential benefit of new devices in terms of reduction of visual complaints, and the existence of newly developed systems to capture quantitative metrics of such phenomenon, the main goal of the present study is to compare the visual performance of three multifocal IOLs with particular attention to the subjective complaints and the quantitative measurement of the photic phenomena in pseudophakic patients after cataract extraction.

2. Material and Methods

This was a prospective study involving patients bilaterally implanted with one brand of multifocal IOL (the same IOL implanted in both eyes). These IOLS were implanted following cataract extraction with phacoemulsification and targeted for emmetropia. Inclusion criteria for enrollment in the present study included no active ocular disease except cataract, nonsevere dry eye, uneventful cataract surgery and postoperative healing process, clear posterior capsule and lens implant, no pupillary abnormality, postop refractive error within ±1.00 diopters (D), and an unaided postoperative visual acuity of 0.10 logMAR or better. Exclusion criteria were IOL dislocation, posterior capsule opacification, or any vitreous or retinal disease. In agreement with the Declaration of Helsinki, the protocol of the study was reviewed and approved by the Ethics Committee of Hospital da Luz (Lisbon, Portugal). Before data collection, patients were instructed on the purpose of the study and procedures used and signed a consent form before formal enrollment.

Surgical procedures were conducted by the same experienced surgeon (FR) under local anesthesia through a microincision of 2.2 mm. Prior to surgery, patients underwent a comprehensive ophthalmological examination including optical biometry and anterior surface optical tomography for the calculation of the power of the IOL using a semicustomized ray-tracing method [21]. Surgical procedures with IOL implantation were conducted with a difference of 7 days between eyes. A summary of the technical details of the IOLs implanted is presented in Table 1.

The AcrySof® IQ PanOptix (TFNT00) is a single-piece copolymer acrylate-methacrylate trifocal IOL (Alcon Laboratories, Texas, USA). The posterior lens surface is spherical, and the anterior surface is aspheric with a diffractive/refractive surface. The lens incorporates a blue-violet filter with an intermediate addition power of +2.17 D and a maximum addition power of +3.25 D. The lens received a CE mark in June 2015.

The FineVision Pod F (PhysIOL, Liège, BE) is a single-piece 25% hydrophilic acrylic ultraviolet (UV) and blue filter trifocal IOL with an intended intermediate addition power of +1.75 D and a maximum addition power of +3.5 D. The optic zone diameter is 6.15 mm and incorporates a diffractive aspheric front surface and a posterior aspheric surface with a negative spherical aberration of −0.11 microns for a 6.0 mm pupil diameter. The IOL claims reduced halo and glare perception under mesopic conditions due to the maximization of distance vision for larger pupils. The lens received a CE mark in February 2010.

The TECNIS® Symfony model ZXR00 (Abbott Medical Optics, Santa Ana, USA) is a biconvex and pupil-independent diffractive IOL combining an achromatic diffractive surface with an echelette design. The achromatic surface is aimed to correct chromatic aberrations and enhance contrast sensitivity. The echelette design which is a specific type of diffraction grating aims to extend the range of vision. Its overall diameter is 13.0 mm and its optical zone diameter is 6.0 mm. The power spectrum available ranges from +5.0 to +34.0 D and incorporates an UV light-absorbing filter. The lens received a CE mark in June 2014.

The main outcome measures were binocular high-contrast visual acuity for different levels of defocus from +1.00 to −3.00 in 0.50 step. The contrast sensitivity function (CSF) with the Functional Acuity Contrast Test® for 1.5, 3.0, 6.0, 12.0, and 18.0 cycles per degree (cpd) under photopic

Table 1: Technical specifications of the IOLs implanted.

	PanOptix	Symfony	FineVision
Technology/design	Trifocal	Extended depth of focus	Trifocal
Diffractive area	4.50 mm	6.00 mm	6.15 mm
Geometry of central zone	Diffractive	Aspheric anterior surface/posterior achromatic diffractive surface	Diffractive
Optic type	Nonapodized	Nonapodized	Apodized
Refractive index	1.55	1.47	1.46
Near add powers in the IOL plane and spectacle plane	3.25 D (2.6 D)	—	3.50 D (2.8 D)
Intermediate add powers in the IOL plane and spectacle plane	2.17 D (1.74 D)	—	1.75 D (1.4 D)
Spherical aberration	−0.10 μm	−0.27 μm	−0.10 μm
Material	Copolymer acrylate-methacrylate	UV-blocking hydrophobic acrylic	26% hydrophilic acrylic
Lens color	Yellow	No pigment	Yellow

(85 cd/m^2) and scotopic (5 cd/m^2) conditions with glare (28 lux–glare II) was evaluated using the Functional Visual Analyzer (FVA, Stereo Optical Company Inc., USA). Subjective quality of vision was assessed with the Quality of Vision (QoV) questionnaire [6, 10, 22]. The questionnaire consists of 10 items with visual pictures to simulate the visual symptoms for the first 7 items and has three subscales: frequency, severity, and bothersome. The questionnaire has been previously developed and validated with the Rasch analysis. The Rasch-scaled scoring is on a 0–100 scale with higher scores indicating worse quality of vision [23]. There are three scores, one for each of the three subscales. Light distortion analysis for size, shape, and regularity of the halo surrounding a source of glare was assessed with a custom-made device (Light Distortion Analyzer, CEORLab-University of Minho, Portugal). The characteristics of this device, examination routines, and main outcome measures have been previously described and validated in clinical populations [15–17] including pseudophakic patients [20, 24]. The size of the light distortion compared to the total area under evaluation, also known as the light distortion index (LDI%), was calculated. Considering the symmetric bilateral implantation, for monocular analysis, only the right eye was considered. Binocular summation was calculated as the % decrease or increase in light distortion under binocular conditions compared to the average monocular value. Patients were evaluated once between 1 and 3 months after surgery.

Statistical analysis was conducted using SPSS v21.0 (IBM Inc., IL). Normality of data distribution was assessed using the Shapiro-Wilk test. Comparison between monocular and binocular values was evaluated by paired sample t-test or nonparametric Wilcoxon signed-rank test, while comparisons between clusters of patients with different IOLs implanted were evaluated with independent sample t-test or the nonparametric Mann-Whitney test. Correlations were assessed using Pearson correlation or nonparametric Spearman correlation. ANOVA or Kruskal-Wallis with multiple post-hoc comparisons was used to compare the outcomes among different IOL groups. The level of statistical significance has been set at $p < 0.050$.

3. Results

Demographic data of patients enrolled in each group are presented in Table 2 along with pre- and postoperative clinical data. There was a statistically significant difference in J0 between the three groups postoperatively (Kruskal-Wallis test), but the differences were not clinically different. Comparisons for all other parameters indicated no statistically significant differences between groups ($p > 0.050$).

Postoperative uncorrected distance visual acuity was 0.08 ± 0.12 logMAR for the whole sample, and there were no statistically significant differences between the IOL groups ($p = 0.780$). Best-corrected distance visual acuity improved to -0.16 ± 0.27 logMAR for the whole group.

Figure 1 presents the defocus curves for the three lenses under comparison. The three lenses performed similarly for all vergences with the exception of intermediate vision at −1.00 D/1 m ($p = 0.030$) and near vision at −2.5 D/0.4 m ($p = 0.007$) and −3.0 D/0.33 m ($p = 0.014$). The extended depth of focus (EDOF) IOL (Symfony) provided a range of stable maximum visual acuity from infinity to approximately 1 m, dropping almost 1 line in visual acuity (0.18 logMAR) at 67 cm and to 0.44 logMAR at 33 cm. Conversely, the two trifocal IOLs (FineVision and PanOptix) showed a similar behavior, with a worse intermediate vision at 1 m compared to the EDOF IOL being 0.12 logMAR for Symfony and 0.18-0.19 logMAR for FineVision and PanOptix, respectively ($p < 0.050$). The three lenses showed a similar behavior between 67 and 50 cm ($p > 0.050$), and at near vision, both trifocal IOLs showed significantly better performance compared with EDOF IOL ($p < 0.050$).

Contrast sensitivity function under photopic and scotopic conditions is presented in Figure 2. Differences between IOLs were not significantly different at any spatial frequency under both conditions ($p > 0.050$). Under photopic conditions (Figure 2(a)), the three IOLs are above the inferior limit of normality for 3, 12, and 18 cpd. Conversely, the three lenses dropped below the inferior limit of normality for 6 cpd, and the PanOptix was below the inferior limit for 1.5 cpd. Only for the lowest frequency,

Table 2: Preoperative demographic data (mean ± SD) of the patients enrolled in this study.

	PanOptix	Symfony	FineVision	Significance (p)†
Number of patients	7	15	23	
Male : female	1 : 6	2 : 13	7 : 16	
Age ± SD (years)	62.3 ± 9.0	63.5 ± 9.4	62.6 ± 8.0	0.746
Axial length	23.2 ± 0.6	23.2 ± 1.7	24.0 ± 4.4	0.822
IOL power (D)*	21.6 ± 1.4	22.9 ± 4.2	22.0 ± 3.4	0.499
M preoperatively	−0.71 ± 3.21	0.80 ± 3.85	0.96 ± 2.21	0.891
J0 preoperatively	−0.06 ± 0.36	0.20 ± 0.43	−0.19 ± 0.46	0.069
J45 preoperatively	−0.04 ± 0.11	0.01 ± 0.38	−0.01 ± 0.12	0.640
Time ± SD since surgery (days)	42 ± 29	39 ± 13	50 ± 20	0.145
Distance binocular UCVA (postoperatively)	0.07 ± 0.10	0.08 ± 0.10	0.08 ± 0.09	0.780
Distance binocular BSCVA (postoperatively)	−0.07 ± 0.19	−0.10 ± 0.19	−0.24 ± 0.14	0.613
Pupil diameter (mm)	4.6 ± 1.5	4.7 ± 1.3	4.9 ± 1.5	0.406
M postoperatively	0.13 ± 0.24	0.02 ± 0.80	0.27 ± 0.86	0.178
J0 postoperatively	−0.06 ± 0.34	−0.11 ± 0.48	−0.09 ± 1.12	**0.022**
J45 postoperatively	−0.05 ± 0.18	−0.03 ± 0.48	−0.09 ± 1.12	0.891

SD: standard deviation; IOL: intraocular lens; UCVA: uncorrected distance visual acuity; BSCVA: best distance spectacle-corrected visual acuity; M: spherical equivalent; J0 and J45: horizontal and oblique components of the vector decomposition of cylindrical refraction. *Right eye only (interocular difference ≤ 1.00 D). †Kruskal-Wallis Test.

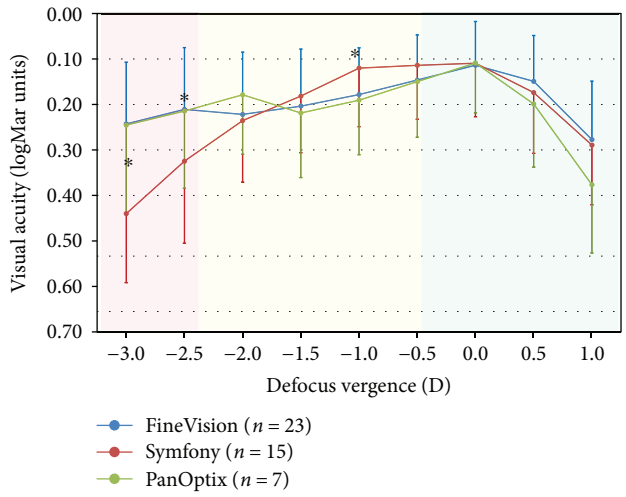

Figure 1: Defocus curves for the three lenses under comparison in this study. Error bars represent 1 × SD. *Statistically significantly different at 0.05 level (Kruskal-Wallis).

the PanOptix lens performed worse than the other two lenses ($p = 0.049$).

The light distortion analysis (Figure 3) showed that the EDOF IOL had larger values of LDI (34.6 ± 16.0) compared with the two trifocal IOLs but this difference was not statistically significant ($p = 0.237$).

The results of the subjective questionnaire are presented in Figure 4. While the Symfony IOL presented higher values showing worse performance in all categories, differences were only statistically significant ($p = 0.011$) for the bothersome subscale that reached an average value of 47.2 ± 16.0 compared with that of FineVision (32.8 ± 16.0) or PanOptix (37.9 ± 12.0).

4. Discussion

In the present study, we report comparative performance of the three newly designed IOLs for the correction of presbyopia in patients successfully implanted and with optical distance vision correction as shown in the through-focus curves. For distance vision, our uncorrected visual acuity was inferior to the values reported by other authors that might be related to the residual refractive errors reported in Table 2. Discrepancies with the outcomes of other studies [25, 26] might be also related to the methodologies used to record acuity using targets at infinity in devices such as the Functional Visual Analyzer as we used or real targets at shorter distances as the ETDRS charts. However, several other studies do not report the tests used that makes it difficult to compare the results. Visual performance at different vergences showed a similar behavior for both trifocal lenses, as expected. In contrast, the EDOF lens provided a consistent visual performance from distance and intermediate distance, worsening below the performance of the trifocal lenses for 50 cm and closer distances. The uniform range of vision near the 0 vergence might imply that this lens is more robust to errors in the power calculation or in the final position of the lens, without reducing distance vision significantly. This is in disagreement with results presented recently by Gatinel and Loicq [27] reporting optical bench measurements in the Symfony EDOF IOL compared with a bifocal and a trifocal IOL that predict a drop in modulation transfer function (MTF) for the EDOF lens at intermediate vision for pupil sizes larger than 2 mm. Considering that the pupil size of our sample (4.35 mm) is larger than the 3.75 mm of the maximum pupil evaluated by Gatinel and Loicq, a worse performance at intermediate vision would be expected based on optical bench measurements. Our clinical results are much better than those predicted. On the other hand, the

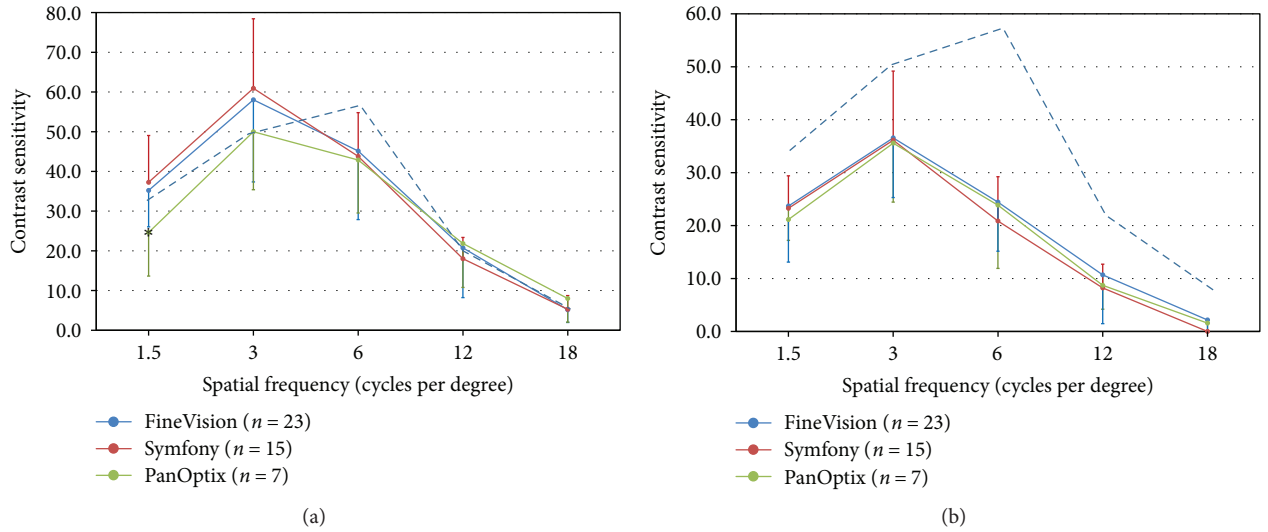

Figure 2: Contrast sensitivity function under photopic (a) and scotopic (b) conditions measured with the Functional Visual Analyzer. Error bars represent 1 × SD. *Statistically significantly different at 0.05 level (Kruskal-Wallis). To avoid collapsing the lines, only the lower limit of normality is shown (dashed line).

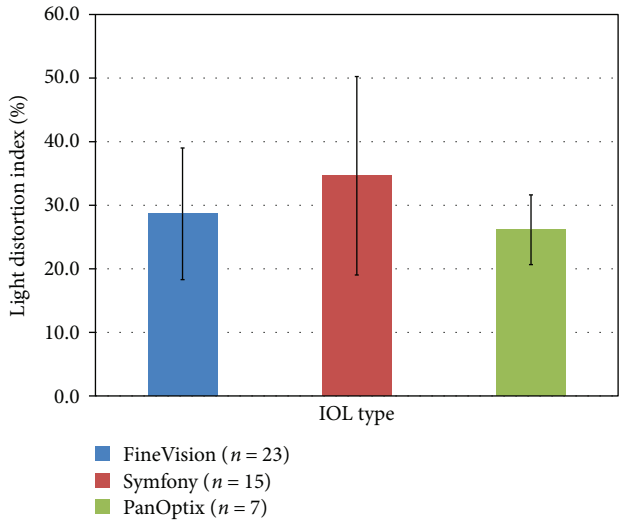

Figure 3: Light distortion index (%) for the three IOLs under evaluation. Error bars represent 1 × SD.

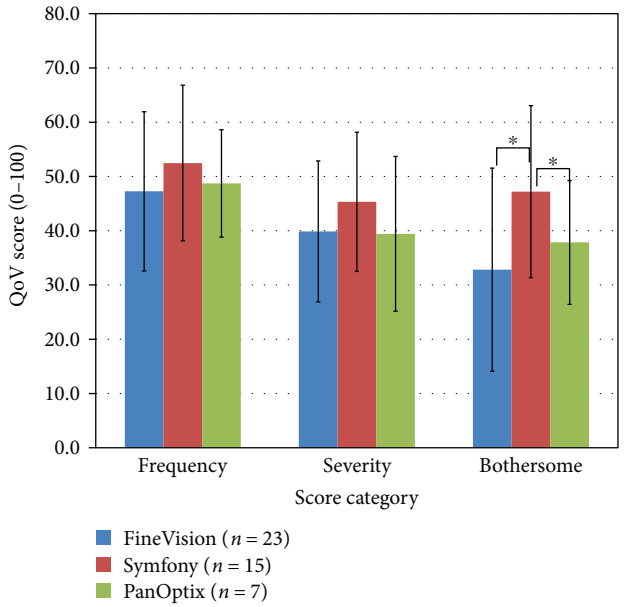

Figure 4: Quality of Vision (QoV) questionnaire scores for the three IOL groups across the three subscales of the questionnaire (frequency, severity, and bothersome). Error bars represent 1 × SD. *Statistically significantly different at 0.05 level (Kruskal-Wallis).

results of Domínguez-Vicent predict a better performance for the EDOF lens at 50 cm (vergence +2.00 D) compared with 100 cm (vergence +1.00 D). Our clinical results showing good performance for distance and intermediate vision up to 100 and 70 cm do not agree with previous experimental predictions based on simulation analysis. For example, Gatinel and Loicq [27] obtained a maximum peak of performance based on MTF values at 70 cm accordingly, while Domínguez-Vicent et al. [19] found the best intermediate performance for 50 cm. These differences might be related to the fact that in vitro measurements are obtained with monochromatic light under nonrealistic conditions compared to clinical measurements and the adaptation effects that the patient might undergo over time. Comparing the trifocal IOLs, the PanOptix IOL shows a second peak of improved visual acuity at +2.00 D vergence compared with the FineVision. This might be explained by the intermediate addition provided in the PanOptix (+2.17 D) compared to the FineVision (+1.75 D). This provides a wide range of good vision for the PanOptix from distance to 40 cm as we report, and this is in agreement with preliminary data reported by Kohnen [28] on the first six eyes implanted with this lens. The previous should not be understood as a direct justification of the visual outcomes found in this study as the MTF has shown to be not a good predictor of the clinical visual acuity outcomes [29].

The present study showed also for the first time for the IOLs investigated that the light distortion, as measured with the Light Distortion Analyzer, affects a significant proportion of patients, showing an increase compared to the mean and median values of approximately 15–23% previously reported for monofocal IOLs [20, 24]. These monofocal IOL studies were for older populations (64–70 years of age) compared to the present study (62-63 years). This is in agreement with the common clinical knowledge and also with the preliminary data recently published by Brito et al. [20] with the AT Lisa bifocal and trifocal IOLs. In their investigation of light distortion with the trifocal AT Lisa 839M and bifocal AT Lisa 909MP, the authors reported an average binocular LDI of 29.29% and 40.49%, respectively, compared with 15.28% for the monofocal control group. Our results for the trifocal IOLs (PanOptix and FineVision) agree with those reported by Brito et al. In contrast with the expected, the EDOF IOL showed higher average values compared with the trifocal IOLs.

Despite the fact that average values of light distortion were higher in patients with poorer low-contrast visual acuity and lower contrast sensitivity postoperatively, the correlations between light distortion and the remaining visual functions were generally poor (correlation coefficient < 0.400). This suggests that the CSF and LDA measure different aspects of quality of vision in patients implanted with multifocal IOLs. In IOL patients, contrast sensitivity may be reduced due to decreased visual quality, residual refractive error, split of light into different foci, or intraocular light scatter. In the present study, we found CS values within the normal range expected for the age of the patients under photopic conditions. However, under scotopic conditions with glare, the CS was reduced for all lenses. The three lenses performed similarly in terms of contrast sensitivity. This might be explained by the fact that we measured CSF at distance where the three lenses show accurate refractive outcomes as seen in the defocus curves. The lower values for the PanOptix at lower frequencies compared with the other two lenses might be related to the limited sample in this group compared with the other two.

Mastropasqua et al. evaluated the patient satisfaction after bilateral implantation and combination of two similar multifocal IOLs using the National Eye Institute Refractive Error Quality of Life Instrument-42 questionnaire. Though this questionnaire has not been specifically devised to evaluate dysphotopic phenomena and contains some serious psychometric flaws [30, 31], it includes some questions such as glare. While the 2.5 D addition subgroup showed a higher glare score (better performance) compared with the higher addition, this was not statistically significant [8]. Our results with the QoV questionnaire agree with those with the LDA measurements showing a slightly worse performance with the Symfony compared with the trifocal IOLs, and this difference was statistically significant for the bothersome subscale. As said, this was not expected as this IOL should reduce halo perception. However, in vitro measurements obtained by Gatinel and Loicq show that this lens is expected to show a more intense first halo compared with other trifocal and bifocal lenses. They also report the spherical aberration for this lens and show that for a 4.5 mm pupil (similar to the one shown by our patients), the lens will induce high negative spherical aberration (−0.24 micron). In a recent study, Macedo-de-Araújo et al. [18] showed that inducing positive or negative spherical aberration in a nonaccommodating eye will increase significantly the light distortion size. This negative spherical aberration is necessary to create the EDOF effect, but the consequence might be a larger halo perception under night vision conditions. In contrast, according to Table 1, the remaining two lenses induce a slightly negative spherical aberration that counterbalances the aberration of the cornea in the pseudophakic patient and improves quality of vision. Therefore, we hypothesize that the increase in light distortion in the trifocal lenses is due to the superposition of the near, intermediate, and distance focused and defocused images in the retinal plane, while with the EDOF lens, the increase in negative spherical aberration along with the diffractive optics for the achromatizing purpose that might create some scattering phenomena might add to each other to generate a larger distortion under the conditions of our measurements with this experimental device. This observation is also supported by the QoV questionnaire results, particularly for the bothersome score. In trifocal IOLs, this phenomenon can be explained by the superposition of the near and distance foci [32] but the same mechanism should not explain the findings in the extended depth of focus IOL. The potential involvement of scattered light in the echelletes of the diffractive achromatizing surface is a hypothesis that should be investigated in future studies.

One limitation of the present study is the limited sample. The sample might also be underpowered to detect differences in the light distortion and the subjective QoV questionnaire. This is even more relevant in the PanOptix group with only 7 subjects. Assuming that one of the IOLs under comparison would be hypothesized not to induce haloes, this small sample should warrant 80% statistical power to detect differences in light disturbance of 30 units between lenses on a parallel study design. Instead, we found that all IOLs under comparison induce similar light disturbance as measured with this experimental device with a nonstatistically significant trend for the EDOF IOL to show a worse performance in terms of light distortion and subjective performance (statistically significant in the bothersome domain). Residual refractive errors might also justify differences in performance in terms of light disturbances and visual complaints, but we have not observed significant differences in this domain either in the spherical equivalent or in the astigmatic components (see Table 2). However, even under good refractive outcomes, it is expected that the complaints of dysphotopsia can be present. In a recent large study involving several thousands of patients, nearly 40% of the patients complained of worse night vision after implantation, despite their good uncorrected distance visual acuity [26]. A recent study showed that the first halo estimated in an optical bench for the Symphony lens was more intense compared with that for the trifocal FineVision and a bifocal IOL [23]. This should be further investigated in future studies involving larger sample sizes, including the potential relationship between the size and intensity of the haloes

measured in an optical bench and those measured after lens implantation with a psychophysical method such as the LDA used in this work.

Conflicts of Interest

José M. González-Méijome is a coinventor in patent application involving one experimental device used in this study. The remaining authors do not have any financial interest in the methods used in the study. Funding received does not lead to any conflict of interests regarding the publication of this manuscript.

Acknowledgments

This study has been funded by FEDER through the COMPTETE Program and by the Portuguese Foundation for Science and Technology (FCT) in the framework of projects PTDC/SAU-BEB/098391/2008 and PTDC/SAU-BEB/098392/2008 and the Strategic Project PEST-C/FIS/UI607/2011.

References

[1] N. E. de Vries and R. M. M. A. Nuijts, "Multifocal intraocular lenses in cataract surgery: literature review of benefits and side effects," *Journal of Cataract & Refractive Surgery*, vol. 39, no. 2, pp. 268–278, 2013.

[2] S. Pieh, B. Lackner, G. Hanselmayer et al., "Halo size under distance and near conditions in refractive multifocal intraocular lenses," *The British Journal of Ophthalmology*, vol. 85, no. 7, pp. 816–821, 2001.

[3] K. Kamiya, K. Hayashi, K. Shimizu et al., "Multifocal intraocular lens explantation: a case series of 50 eyes," *American Journal of Ophthalmology*, vol. 158, no. 2, pp. 215–220.e1, 2014.

[4] N. E. de Vries, C. A. B. Webers, W. R. H. Touwslager et al., "Dissatisfaction after implantation of multifocal intraocular lenses," *Journal of Cataract & Refractive Surgery*, vol. 37, no. 5, pp. 859–865, 2011.

[5] P. J. Buckhurst, S. A. Naroo, L. N. Davies et al., "Tablet app halometer for the assessment of dysphotopsia," *Journal of Cataract & Refractive Surgery*, vol. 41, no. 11, pp. 2424–2429, 2015.

[6] J. Khadka, C. McAlinden, and K. Pesudovs, "Quality assessment of ophthalmic questionnaires: review and recommendations," *Optometry and Vision Science*, vol. 90, no. 8, pp. 720–744, 2013.

[7] G. Cillino, A. Casuccio, M. Pasti, V. Bono, R. Mencucci, and S. Cillino, "Working-age cataract patients: visual results, reading performance, and quality of life with three diffractive multifocal intraocular lenses," *Ophthalmology*, vol. 121, no. 1, pp. 34–44, 2014.

[8] R. Mastropasqua, E. Pedrotti, M. Passilongo, G. Parisi, I. Marchesoni, and G. Marchini, "Long-term visual function and patient satisfaction after bilateral implantation and combination of two similar multifocal IOLs," *Journal of Refractive Surgery*, vol. 31, no. 5, pp. 308–314, 2015.

[9] K. G. Gundersen and R. Potvin, "Comparison of visual outcomes after implantation of diffractive trifocal toric intraocular lens and a diffractive apodized bifocal toric intraocular lens," *Clinical Ophthalmology*, vol. 10, pp. 455–461, 2016.

[10] C. McAlinden, K. Pesudovs, and J. E. Moore, "The development of an instrument to measure quality of vision: the Quality of Vision (QoV) questionnaire," *Investigative Ophthalmology & Visual Science*, vol. 51, no. 11, pp. 5537–5545, 2010.

[11] C. McAlinden, E. Skiadaresi, K. Pesudovs, and J. E. Moore, "Quality of vision after myopic and hyperopic laser-assisted subepithelial keratectomy," *Journal of Cataract & Refractive Surgery*, vol. 37, no. 6, pp. 1097–1100, 2011.

[12] B. Lackner, S. Pieh, G. Schmidinger et al., "Glare and halo phenomena after laser in situ keratomileusis," *Journal of Cataract & Refractive Surgery*, vol. 29, no. 3, pp. 444–450, 2003.

[13] M. C. Puell, M. J. Perez-Carrasco, A. Barrio, B. Antona, and C. Palomo-Alvarez, "Normal values for the size of a halo produced by a glare source," *Journal of Refractive Surgery*, vol. 29, no. 9, pp. 618–622, 2013.

[14] T. Kojima, A. Hasegawa, S. Hara et al., "Quantitative evaluation of night vision and correlation of refractive and topographical parameters with glare after orthokeratology," *Graefe's Archive for Clinical and Experimental Ophthalmology*, vol. 249, no. 10, pp. 1519–1526, 2011.

[15] J. M. M. Linhares, H. Neves, D. Lopes-Ferreira, M. Faria-Ribeiro, S. C. Peixoto-de-Matos, and J. M. González-Méijome, "Radiometric characterization of a novel led array system for visual assessment," *Journal of Modern Optics*, vol. 60, no. 14, pp. 1136–1144, 2013.

[16] H. Ferreira-Neves, R. Macedo-de-Araújo, L. Rico-del-Viejo, A. C. da-Silva, A. Queirós, and J. M. González-Méijome, "Validation of a method to measure light distortion surrounding a source of glare," *Journal of Biomedical Optics*, vol. 20, no. 7, article 075002, 2015.

[17] E. S. Santolaria, A. Cerviño, A. Queiros, C. Villa-Collar, D. Lopes-Ferreira, and J. M. González-Méijome, "Short-term changes in light distortion in orthokeratology subjects," *BioMed Research International*, vol. 2015, Article ID 278425, 7 pages, 2015.

[18] R. Macedo-de-Araújo, H. Ferreira-Neves, L. Rico-del-Viejo, S. C. Peixoto-de-Matos, and J. M. González-Méijome, "Light distortion and spherical aberration for the accommodating and nonaccommodating eye," *Journal of Biomedical Optics*, vol. 21, no. 7, article 075003, 2016.

[19] A. Domínguez-Vicent, J. J. Esteve-Taboada, A. J. Del Águila-Carrasco, T. Ferrer-Blasco, and R. Montés-Micó, "In vitro optical quality comparison between the Mini WELL Ready progressive multifocal and the TECNIS Symfony," *Graefe's Archive for Clinical and Experimental Ophthalmology*, vol. 254, no. 7, pp. 1387–1397, 2016.

[20] P. Brito, J. Salgado-Borges, H. Neves, J. Gonzalez-Meijome, and M. Monteiro, "Light-distortion analysis as a possible indicator of visual quality after refractive lens exchange with diffractive multifocal intraocular lenses," *Journal of Cataract & Refractive Surgery*, vol. 41, no. 3, pp. 613–622, 2015.

[21] F. J. Ribeiro, A. Castanheira-Dinis, and J. M. Dias, "Personalized pseudophakic model for refractive assessment," *PLoS One*, vol. 7, no. 10, article e46780, 2012.

[22] C. McAlinden, E. Skiadaresi, D. Gatinel, F. Cabot, J. Huang, and K. Pesudovs, "The Quality of Vision questionnaire: subscale interchangeability," *Optometry and Vision Science*, vol. 90, no. 8, pp. 760–764, 2013.

[23] E. Skiadaresi, C. McAlinden, K. Pesudovs, S. Polizzi, J. Khadka, and G. Ravalico, "Subjective quality of vision before and after

cataract surgery," *Archives of Ophthalmology*, vol. 130, no. 11, pp. 1377–1382, 2012.

[24] J. Salgado-Borges, L. Dias, J. Costa, H. Ferreira-Neves, S. C. Peixoto-de-Matos, and J. M. González-Méijome, "Light distortion and ocular scattering with glistening and aberration-free pseudophakic IOL: a pilot study," *Journal of Emmetropia*, vol. 3, pp. 127–132, 2015.

[25] M. S. A. Attia, G. U. Auffarth, F. T. A. Kretz et al., "Clinical evaluation of an extended depth of focus intraocular lens with the Salzburg reading desk," *Journal of Refractive Surgery*, vol. 33, no. 10, pp. 664–669, 2017.

[26] R. Bilbao-Calabuig, A. Llovet-Rausell, J. Ortega-Usobiaga et al., "Visual outcomes following bilateral lmplantation of two diffractive trifocal intraocular lenses in 10 084 eyes," *American Journal of Ophthalmology*, vol. 179, pp. 55–66, 2017.

[27] D. Gatinel and J. Loicq, "Clinically relevant optical properties of bifocal, trifocal, and extended depth of focus intraocular lenses," *Journal of Refractive Surgery*, vol. 32, no. 4, pp. 273–280, 2016.

[28] T. Kohnen, "First implantation of a diffractive quadrafocal (trifocal) intraocular lens," *Journal of Cataract & Refractive Surgery*, vol. 41, no. 10, pp. 2330–2332, 2015.

[29] A. Alarcon, C. Canovas, R. Rosen et al., "Preclinical metrics to predict through-focus visual acuity for pseudophakic patients," *Biomedical Optics Express*, vol. 7, no. 5, pp. 1877–1888, 2016.

[30] C. McAlinden, E. Skiadaresi, J. Moore, and K. Pesudovs, "Subscale assessment of the NEI-RQL-42 questionnaire with Rasch analysis," *Investigative Ophthalmology & Visual Science*, vol. 52, no. 8, pp. 5685–5694, 2011.

[31] C. McAlinden, J. Khadka, J. de Freitas Santos Paranhos, P. Schor, and K. Pesudovs, "Psychometric properties of the NEI-RQL-42 questionnaire in keratoconus," *Investigative Ophthalmology & Visual Science*, vol. 53, no. 11, pp. 7370–7374, 2012.

[32] F. Alba-Bueno, N. Garzón, F. Vega, F. Poyales, and M. S. Millán, "Patient-perceived and laboratory-measured halos associated with diffractive bifocal and trifocal intraocular lenses," *Current Eye Research*, vol. 43, no. 1, pp. 35–42, 2017.

Hindawi
Journal of Ophthalmology
Volume 2017, Article ID 5231095, 4 pages
https://doi.org/10.1155/2017/5231095

Research Article

Chosen Vascular Risk Markers in Pseudoexfoliation Syndrome: An Age-Related Disorder

Hanna Lesiewska,[1] Agnieszka Łukaszewska-Smyk,[1] Grażyna Odrowąż-Sypniewska,[2] Magdalena Krintus,[2] Aneta Mańkowska-Cyl,[2] and Grażyna Malukiewicz[1]

[1]*Department of Ophthalmology, The Nicolaus Copernicus University, Ludwik Rydygier's Collegium Medicum, Bydgoszcz, Poland*
[2]*Department of Laboratory Medicine, The Nicolaus Copernicus University, Ludwik Rydygier's Collegium Medicum, Bydgoszcz, Poland*

Correspondence should be addressed to Hanna Lesiewska; hanjot@op.pl

Received 23 April 2017; Accepted 11 October 2017; Published 31 October 2017

Academic Editor: Alejandro Cerviño

Purpose. To evaluate lipids and C-reactive protein serum levels in patients with pseudoexfoliation syndrome (PEX) in the Polish population. *Methods*. 96 patients were studied with PEX and 79 control subjects. Total cholesterol, triglycerides, high-density lipoprotein (HDL)-cholesterol, low-density lipoprotein (LDL)-cholesterol, non-HDL-cholesterol and CRP serum levels, and TG/HDL-C and TC/HDL-C indexes were assessed. *Results*. There were no significant differences in concentration of lipids and values of TC/HDL-C, TG/HDL-C, and non-HDL-C between PEX and control groups. High-sensitivity C-reactive protein was not increased in patients with PEX. *Conclusions*. Our results cast doubt on the opinion on the possible PEX and vascular diseases relation. Further studies on this subject are mandatory.

1. Introduction

Pseudoexfoliation syndrome (PEX) is an age-related complex systemic disorder of the extracellular matrix affecting the eye and visceral organs. The average worldwide prevalence of PEX is 10%–20% of the general population over the age of 60 years [1, 2]. A population-based study in the Northeastern USA found prevalence of 0.67% in people aged 52–64 years, 2.6% in people aged 65–74 years, and 5% in people aged 78–85 years. In a survey conducted in Iceland, the prevalence of PEX increased from 2.5% in the patients aged 50–59 years to 40.6% in those aged > 80 years [3].

Originally, PEX was thought to be limited to the anterior segment of the eye; some studies have indicated, however, that pseudoexfoliative material may be present in blood vessels and impaired endothelial function can be observed [1, 2]. Since endothelial dysfunction is an independent predictor of future cardiovascular and cerebrovascular events, it might suggest an increased vascular risk in PEX patients [4–6]. Dyslipidemia is a well-established risk factor for cardiovascular and cerebrovascular diseases. Many studies have shown a strong correlation between serum lipids levels and risk of developing vascular events [6–8]. It was found that C-reactive protein (CRP) is significantly associated with cardiovascular disease [9].

The relationship between PEX and vascular diseases has been investigated in many studies [10–16]. Some authors have observed a connection between PEX and cardiovascular or cerebrovascular diseases [4, 10–12, 14, 15]. However, there are also studies reporting that PEX is not associated with arterial hypertension, ischemic heart disease, and cerebrovascular diseases [2, 17–21]. This discrepancy in opinions gave us a spur to assess the relation between PEX syndrome and chosen vascular risk markers in the Polish population.

2. Material and Methods

The subjects for this study were recruited from patients who presented to the Department of Ophthalmology, Collegium Medicum, UMK in Bydgoszcz, Poland for cataract surgery. Exclusion criteria were any other ocular diseases except PEX and cataract. Pseudoexfoliation changes were identified

by slit lamp examination after pupil dilation as the presence of typical PEX material on the anterior lens surface, iris, or corneal endothelium in either eye. The individuals without any evidence of pseudoexfoliation deposits were taken as the control group. This study has been approved by the local bioethical committee. All patients gave their informed consent for this study.

We followed the methods described in our previous study [22]. Blood samples were collected in all patients after an overnight fast. Plasma was obtained within less than 1 hour to avoid proteolysis and stored deep-frozen (−80°C) in small aliquots until assayed but no longer than 8 months. Total cholesterol (TC), high-density lipoprotein (HDL)-cholesterol, and triglyceride (TG) levels were measured by an autoanalyzer (ARCHITECT ci8200, Abbott Diagnostics, Wiesbaden, Germany) using enzymatic methods. Low-density lipoprotein (LDL)-cholesterol levels were calculated using the Friedewald formula. Moreover, TG/HDL-C, TC/HDL-C, and non-HDL-C as atherogenic indexes were calculated. High-sensitivity CRP (hs-CRP) level was measured using the BN II System nephelometer (High-Sensitivity CRP; Siemens Healthcare Diagnostics, Deerfield, IL, USA), providing excellent precision with the coefficient of variation (CV) reported by the manufacturer of less than 10%. CVs for hs-CRP estimated in our laboratory were below 3.5% and below 4.5% for hs-CRP concentrations below 1 mg/L and above 3 mg/L, respectively. The lower limit of hs-CRP detection was 0.175 mg/L. We divided the patients with PEX into three groups: group A with low risk (hs-CRP concentration less than 1.0 mg/L), group B with average risk (hs-CRP concentration 1.0 to 3.0 mg/L), and group C with high risk of cardiovascular disease (hs-CRP concentration above 3.0 mg/L) according to the American Heart Association and U.S. Centers for Disease Control and Prevention.

The statistical analysis of results was performed using the Kolmogorov-Smirnov test to assess normality of distribution of investigated parameters. Data were expressed as medians with the interquartile range (25th–75th percentiles) according to the distributions of the continuous variables. Differences between the PEX and control groups were analyzed by the Mann–Whitney U test for independent samples of nonparametric data. Comparisons of median values between groups were done by ANOVA. The significance level for all statistical tests was 0.05. Statistical analysis was performed using Statistica software (version 8).

3. Results

We studied 96 patients with PEX (26 males and 70 females), median age 76 years ($Q_1 = 72$; $Q_3 = 82$), and 79 age- and sex-matched controls (28 males and 51 females), median age 75 years ($Q_1 = 70$; $Q_3 = 80$). The concentrations of serum lipids, hs-CRP, and values of atherogenic indexes constituting one of the major cardiovascular risk factors are shown in Table 1. There were no significant differences in concentration of lipids between PEX and control groups. Moreover, we did not observe significant differences for other calculated parameters like TC/HDL-C, TG/HDL-C, and non-HDL-C. High-sensitivity C-reactive protein level was not increased in patients with PEX and was found to be similar to that of controls.

Table 1: Biochemical parameters in PEX patients and controls.

Parametres	PEX patients' median (Q_1–Q_3) $n = 96$	Control median (Q_1–Q_3) $n = 79$	p
TC (mg/dL)	199 (176–240)	213 (178–245)	0.25
HDL-C (mg/dL)	55 (45–66)	53 (46–64)	0.39
TG (mg/dL)	125.5 (83.5–161.5)	114 (88–152)	0.61
LDL-C (mg/dL)	114.5 (93.5–152)	128 (103–156)	0.14
Non-HDL-C (mg/dL)	139 (115.5–181)	158 (128–193)	0.13
TC/HDL-C	3.73 (2.95–4.50)	3.78 (3.28–4.54)	0.26
TG/HDL-C	2.2 (1.39–3.30)	2.07 (1.45–3.45)	0.83
hs-CRP mg/l	1.53 (0.75–3.71)	1.57 (0.74–3.44)	0.90

The HDL-C concentration in the PEX female subgroup was statistically higher than in males: 58 mg/dL (Q_1:48; Q_3:67) versus 52 mg/dL (Q_1:40; Q_3:58), $p = 0.02$. In the control group, we did not find such correlation. The concentrations of other serum lipids, hs-CRP, and values of atherogenic indexes did not differ between males and females, both in PEX and control groups.

We did not observe any significant differences for lipids and atherogenic indexes between the following subgroups: group A with low risk, group B with average risk, and group C with high risk of cardiovascular disease (Table 2).

4. Discussion

There are some studies on the possible association between PEX and vascular diseases although their results are inconclusive [10–16]. The risk for cardiovascular and cerebrovascular diseases might be ascribed to the accumulation of pseudoexfoliative fibrils in the arterial wall [2].

It has been proven that one of the several tests in a vascular risk profile, along with tests for cholesterol and triglycerides, is high-sensitivity CRP [6–9].

Studies, that analyzed serum lipids levels and PEX association, provided conflicting results. All these studies are difficult to compare as they vary in size and design. Türkyılmaz et al. found that the mean total cholesterol and triglycerides levels were significantly higher, and mean serum HDL level was lower in the PEX group of 40 patients compared to the controls [23]. We were unable to show an association between the serum lipid levels and PEX syndrome. Our findings are in accordance with the results of Atalar et al. (23 PEX patients) and Spečkauskas et al. (152 PEX patients), who did not reveal the differences in lipid levels in PEX patients [2, 24]. The latter authors found no clear PEX association with triglyceride and HDL cholesterol levels as well as ischemic heart disease after controlling for effect of age in the population-based study. Presence of PEX was not significantly associated with the blood concentration of high-density lipoproteins and cholesterol in the study of Jonas et al. comprising 69 PEX patients [25].

There is also discrepancy regarding CRP levels in PEX. Elevated plasma hs-CRP levels have been reported in patients

Table 2: Lipid concentration and atherogenic indexes in relation to hs-CRP levels in patients with PEX.

	Group A median (Q_1–Q_3) $n = 34$	Group B median (Q1–Q3) $n = 35$	Group C median (Q1–Q3) $n=27$	p
TC (mg/dL)	200 (182–245)	190 (164–217)	204 (161–244)	0.18
TG (mg/dL)	114 (83–181)	115 (81–148)	130 (114–156)	0.95
HDL-C (mg/dL)	59 (48–68)	54 (45–66)	51 (44–58)	0.35
LDL-C (mg/dL)	115 (95–152)	104 (92–142)	130 (98–161)	0.24
non-HDL-C (mg/dL)	154 (127–190)	126 (115–172)	157 (118–191)	0.26
TC/HDL-C	3.9 (3.4–4.5)	3.3 (2.7–4.8)	4.1 (3.2–4.8)	0.63
TG/HDL-C	2.1 (1.4–3.4)	2.2 (1.5–3.1)	2.6 (1.7–3.5)	0.70

with PEX by Sorkhabi et al. [26]. Nevertheless, the study of Kymionis et al. as well as Yüksel et al. revealed that serum CRP levels were not elevated in patients with PEX [27, 28]. This is in accordance with our results which showed that serum CRP levels were not increased in patients with PEX and were found to be similar to that of controls. The conflicting results of these studies may be due to the selection bias. Similarly to Sorkhabi et al., in our study, we strictly excluded all conditions which may affect the levels of inflammatory biomarkers [26].

Our research casts doubt on the possibility of PEX and cardiovascular and cerebrovascular disease association. These findings suggest that patients with this syndrome do not suffer from increased comorbidity and mortality.

5. Conclusions

Serum lipids and hs-CRP levels nor values of atherogenic index hs-CRP were elevated in PEX patients in the Polish population. These findings raise doubt on the opinion on the possible PEX and vascular disease relation. As ours and other studies results are inconclusive, the causes and connections of PEX still remain unexplained and further studies on this subject are required.

Conflicts of Interest

The authors declare that they have no conflicts of interest.

References

[1] S. Schumacher, U. Schlötzer-Schrehardt, P. Martus, W. Lang, and G. O. Naumann, "Pseudoexfoliation syndrome and aneurysms of the abdominal aorta," *The Lancet*, vol. 357, no. 9253, pp. 359-360, 2001.

[2] P. T. Atalar, E. Atalar, H. Kilic et al., "Impaired systemic endothelial function in patients with pseudoexfoliation syndrome," *International Heart Journal*, vol. 47, no. 1, pp. 77–84, 2006.

[3] A. Tarkkanen, "Is exfoliation syndrome a sign of systemic vascular disease?," *Acta Ophthalmologica*, vol. 86, no. 8, pp. 832–836, 2008.

[4] P. Mitchell, J. J. Wang, and W. Smith, "Association of pseudoexfoliation syndrome with increased vascular risk," *American Journal of Ophthalmology*, vol. 124, no. 5, pp. 685–687, 1997.

[5] T. Neunteufl, S. Heher, R. Katzenschlager et al., "Late prognostic value of flow-mediated dilation in the brachial artery of patients with chest pain," *The American Journal of Cardiology*, vol. 86, no. 2, pp. 207–210, 2000.

[6] V. Schachinger, M. B. Britten, and A. M. Zeiher, "Prognostic impact of coronary vasodilator dysfunction on adverse long-term outcome of coronary heart disease," *Circulation*, vol. 101, no. 16, pp. 1899–1906, 2000.

[7] I. H. Yusuf, "Pseudoexfoliation syndrome and cardiovascular disease: studies must control for all cardiovascular risk factors," *Eye*, vol. 27, no. 11, pp. 1328-1329, 2013.

[8] H. Liu and J. Li, "Aging and dyslipidemia: a review of potential mechanisms," *Ageing Research Reviews*, vol. 19, pp. 43–52, 2015.

[9] E. Coffman and J. Richmond-Bryant, "Multiple biomarker models for improved risk estimation of specific cardiovascular diseases related to metabolic syndrome: a cross-sectional study," *Population Health Metrics*, vol. 13, no. 7, 2015.

[10] J. S. Ritland, K. Egge, S. Lydersen, R. Juul, and S. O. Semb, "Exfoliative glaucoma and primary open-angle glaucoma: associations with death causes and comorbidity," *Acta Ophthalmologica Scandinavica*, vol. 82, no. 4, pp. 401–404, 2004.

[11] C. Akarsu and B. Unal, "Cerebral haemodynamics in patients with pseudoexfoliation glaucoma," *Eye*, vol. 19, no. 12, pp. 1297–1300, 2005.

[12] L. Bojic, R. Ermacora, S. Polic et al., "Pseudoexfoliation syndrome and asymptomatic myocardial dysfunction," *Graefe's Archive for Clinical and Experimental Ophthalmology*, vol. 243, no. 5, pp. 446–449, 2005.

[13] N. Yüksel, Y. Anik, O. Altintaş, I. Onur, Y. Cağlar, and A. Demirci, "Magnetic resonance imaging of the brain in patients with pseudoexfoliation syndrome and glaucoma," *Ophthalmologica*, vol. 220, no. 2, pp. 125–130, 2006.

[14] M. Citirik, G. Acaroglu, C. Batman, L. Yildiran, and O. Zilelioglu, "A possible link between the pseudoexfoliation syndrome and coronary artery disease," *Eye*, vol. 21, no. 1, pp. 11–15, 2007.

[15] M. R. Praveen, S. K. Shah, A. R. Vasavada et al., "Pseudoexfoliation as a risk factor for peripheral vascular disease: a case-control study," *Eye*, vol. 25, no. 2, pp. 174–179, 2011.

[16] K. A. Gonen, T. Gonen, and B. Gumus, "Renal artery stenosis and abdominal aorta aneurysm in patients with pseudoexfoliation syndrome," *Eye*, vol. 27, no. 6, pp. 735–741, 2013.

[17] A. Ringvold, S. Blika, and L. Sandvik, "Pseudo-exfoliation and mortality," *Acta Ophthalmologica Scandinavica*, vol. 75, no. 3, pp. 255-256, 1997.

[18] K. R. Shrum, M. G. Hattenhauer, and D. Hodge, "Cardiovascular and cerebrovascular mortality associated with ocular

pseudoexfoliation," *American Journal of Ophthalmology*, vol. 129, no. 1, pp. 83–86, 2000.

[19] R. Allingham, M. Loftsdottir, M. S. Gottfredsdottir et al., "Pseudoexfoliation syndrome in Icelandic families," *British Journal of Ophthalmology*, vol. 85, no. 6, pp. 702–707, 2001.

[20] B. J. Shingleton, J. Heltzer, and M. W. O'Donoghue, "Outcomes of phacoemulsification in patients with and without pseudoexfoliation syndrome," *Journal of Cataract & Refractive Surgery*, vol. 29, no. 6, pp. 1080–1086, 2003.

[21] A. Tarkkanen, A. Reunanen, and T. Kivelä, "Frequency of systemic vascular diseases in patients with primary open-angle glaucoma and exfoliation glaucoma," *Acta Ophthalmologica*, vol. 86, no. 6, pp. 598–602, 2008.

[22] H. Lesiewska, G. Malukiewicz, A. Mańkowska-Cyl, and G. Odrowąż-Sypniewska, "Lipids and C-reactive protein as vascular risk markers in pseudoexfoliation syndrome," *Acta Ophthalmologica*, vol. 94, no. 5, pp. e380–e381, 2016.

[23] K. Türkyılmaz, V. Oner, A. Kırbas et al., "Serum YKL-40 levels as a novel marker of inflammation and endothelial dysfunction in patients with pseudoexfoliation syndrome," *Eye*, vol. 27, no. 7, pp. 854–859, 2013.

[24] M. Spečkauskas, A. Tamošiūnas, and V. Jašinskas, "Association of ocular pseudoexfoliation syndrome with ischaemic heart disease, arterial hypertension and diabetes mellitus," *Acta Ophthalmologica*, vol. 90, no. 6, pp. e470–e475, 2012.

[25] J. B. Jonas, V. Nangia, A. Matin et al., "Pseudoexfoliation: normative data and associations. The Central India Eye and Medical Study," *PLoS One*, vol. 8, no. 10, article e76770, 2013.

[26] R. Sorkhabi, A. Ghorbanihaghjo, M. Ahoor, M. Nahaei, and N. Rashtchizadeh, "High-sensitivity C-reactive protein and tumor necrosis factor alpha in pseudoexfoliation syndrome," *Oman Medical Journal*, vol. 28, no. 1, pp. 16–19, 2013.

[27] G. D. Kymionis, V. P. VP Kankariya, and G. A. Kontadakis, "Serum C-reactive protein levels in exfoliation syndrome and exfoliative glaucoma," *Eye*, vol. 25, no. 10, pp. 1383-1384, 2011.

[28] N. Yüksel, D. Pirhan, O. Altintaş, and Y. Cağlar, "Systemic high-sensitivity C-reactive protein level in pseudoexfoliation syndrome and pseudoexfoliation glaucoma," *Journal of Glaucoma*, vol. 19, no. 6, pp. 373–376, 2010.

Hindawi
Journal of Ophthalmology
Volume 2017, Article ID 6823965, 4 pages
https://doi.org/10.1155/2017/6823965

Research Article

Axial Length and Ocular Development of Premature Infants without ROP

Yi Zha, Guangdong Zhu, Jinfei Zhuang, Haihua Zheng, Jianqiu Cai, and Wangqiang Feng

The 2nd Affiliated Hospital and Yuying Children's Hospital of Wenzhou Medical University, 109 Xueyuan Road, Wenzhou, Zhejiang 325027, China

Correspondence should be addressed to Wangqiang Feng; cy@wzhealth.com

Received 1 March 2017; Revised 24 July 2017; Accepted 17 August 2017; Published 15 October 2017

Academic Editor: Rune Brautaset

Purpose. To investigate the ocular parameters of premature infants without ROP at gestational age (GA) more than 28 weeks and their relationship with growth parameters. *Methods*. 76 preterm infants without ROP and 65 term infants were involved to undergo portable slit lamp, RetCam3, ultrasonic A-scan biometry, and cycloplegic streak examination at their 40 weeks' postconceptional ages (PCA). Ocular parameters of infants' right eye and growth parameters were used for analysis. *Results*. All the infants were examined at 40 weeks' PCA. No significant difference was found between male and female in axial length of preterm infants ($p = 0.993$) and term infants ($p = 0.591$). Significant differences were found in axial length (AL), anterior chamber depth (ACD), lens thickness (LT), and vitreous depth (VD) between preterm and term infants. No significant correlation was found between AL and spherical equivalent in preterm infants' group. In preterm group, AL was significantly correlated with gestational age (GA), birth weight (BW), and head circumference (HC). *Conclusions*. Preterm infants had shorter AL, shallow ACD, thicker LT, and thinner VD compared to term infants. Refractive error in preterm infants at GA between 28 to 37 weeks was not related to axial length. Among all the growth parameters of preterm infants, GA, BW, and HC had effect on axial length.

1. Introduction

Due to the rapid prevalence of myopia, refractive error has long been the most important eye problem throughout the world especially in Asian countries [1]. Prematurity, with childbirth before 37 weeks of pregnancy, is associated with many ocular abnormalities, such as retinopathy of prematurity (ROP), refractive error, and amblyopia. Refractive error, on the other hand, is found to be related to not only prematurity but also increasing severity of retinopathy of prematurity (ROP) as well [2]. The increasing risk of refractive error in prematurely born infants is nowadays urgent to be solved.

The major proportion of eye growth occurs within the first 12 months after birth [3]. It is well known that term infants are commonly hypermetropic, while preterm infants are always associated with myopia [4–7]. Many researchers have found that the development of myopia in premature infants may be related to ocular parameters, such as axial length and anterior chamber depth [6, 8, 9]. Others tended to believe its association with the corneal curvature and refractive power of the lens [10–12]. Current studies focused more on premature infants with gestational age (GA) lower than 28 weeks, who were apt to suffer from ROP. In the present study, we investigated the ocular parameters of premature infants with GA more than 28 weeks and their relationship with growth parameters.

2. Materials and Methods

All the infants involved were recruited from the Department of Neonatology of the 2nd Affiliated Hospital of Wenzhou Medical University. Regional ethics committee approval and parental consent were obtained. Exclusion criteria included ocular anomalies such as microphthalmos, anophthalmos, craniofacial deformities, congenital glaucoma, cornea, and lens, or any other fundus abnormalities (such as ROP) and a history of cerebral damage. Premature infants with GA of less than 28 weeks were also excluded in the study. There was no geographic or ethnic dissimilarity in this study. All the infants were Chinese.

At the first visit, growth parameters such as GA, length, birth weight (BW), and head circumference (HC) at birth were obtained. At 40 weeks' postconceptional ages (PCA) (defined as the gestational age at birth plus the age in weeks at the time of examination), all the infants including premature and term infants underwent portable slit lamp, RetCam3 (Clarity Medical System, USA), ultrasonic A-scan biometry, and cycloplegic streak retinoscopy (cyclopentolate 0.5%) instilled at 10-minute intervals three times, 40 minutes before retinoscopy. RetCam3 was used to exclude ROP or other retinal disease. Cycloplegic streak retinoscopy was used to get the refractive status of each infant. The ultrasonic examination was performed using an A-scan biometer (Carl Zeiss Meditec, Oberkochen, Germany) to measure the axial length (AL), anterior chamber depth (ACD), lens thickness (LT), and vitreous depth (VD). The probe was placed lightly on the center of the cornea, perpendicular to its axis. The probe was maintained in this position until three clear traces were obtained on the screen. The average value from the three images was recorded.

All the data obtained were analyzed using SPSS (version 17.0; SPSS Inc., Chicago, IL, USA). The values obtained for all parameters were expressed as mean ± SD. *t*-test was used to compare parameters between two groups. Simple linear regression analysis was performed to get the association of axial length with each of the variables, namely, spherical equivalent (SE), GA, length, BW, and HC. A p value below 0.05 was considered significant.

3. Results

76 premature infants (with 27 female and 49 male) and 65 term infants (with 32 female and 33 male) were involved in the research. The data of infants' right eye were chosen for analysis. The GA in the preterm group was 32.97 ± 2.15 w and in the term group, 39.29 ± 1.30 w. All the growth parameters for preterm and term infants were shown in Table 1. No significant difference was found between male and female in axial length of preterm infants ($p = 0.993$) and term infants ($p = 0.591$). The mean and SD of infants' SE, AL, ACD, LT, and VD were shown in Table 2. Significant differences were found in AL, ACD, LT, and VD between preterm and term infants' groups.

In preterm group, AL was significantly correlated with GA ($r = 0.312$, $p = 0.006$), BW ($r = 0.344$, $p = 0.002$), and HC ($r = 0.241$, $p = 0.041$) but not correlated with SE ($r = -0.226$, $p = 0.05$) and length ($r = 0.229$, $p = 0.053$).

4. Discussion

This research focused on Chinese premature infants born at GA between 28 to 37 weeks without ROP or other ocular disease and evaluated the association of AL with other ocular and growth parameters. Our study showed that with a GA of 28 to 37 weeks, premature infants did have lower AL, shallow ACD, thicker lens, and shorter VD (Table 2). AL was significantly correlated with GA, BW, and HC.

Fieß A et al. [13] once compared the axial length and anterior segment alterations in preterm infants with those of full-term infants and found significant differences between preterm and full-term infants aged ≤ 7 years for spherical equivalent, astigmatism, corneal diameter, and axial length. Tian et al. [14] investigated the development of the refractive status in premature infants aged 0 to 6 years old and found that the axial length in preterm infants was significant shorter than that in term infants. Ecsedy et al. [15] compared the ocular geometry and refraction in children with a history of preterm birth and found that in the premature eyes, anterior chamber depth was marginally smaller, the lens was significantly thicker, and axial length was significantly shorter. All the research above focused on older preterm children. In our research, we measured the ocular parameters in preterm infants with GA between 28 and 37 weeks without ROP and found that preterm infant had shorter AL, smaller ACD, thicker lens, and shorter VD. As we know, ocular structures go through a continuous development and remodeling process after birth [16]. Premature departure from the intrauterine environment may affect ocular development [17]. We believe that premature birth even with GA older than 28 weeks delays the development of ocular structures, which happens sooner after birth.

Table 1: Growth parameters and age for both preterm and term infants.

Growth parameters	Preterm infants (mean ± SD)	Term infants (mean ± SD)
Gestational age (weeks)	32.97 ± 2.15	39.29 ± 1.30
Birth weight (g)	1930 ± 525	3232 ± 475
Head circum. (cm)	30.68 ± 1.98	33.93 ± 1.35
Length (cm)	42.83 ± 4.38	49.98 ± 2.50

Preterm infants were thought to be more myopic than term infants [8]. However, ocular biometry and the mechanism of myopia in preterm children were somewhat different from those in full-term children. Anterior segment components were thought to contribute more to myopia progression in preterm children [8, 18–20]. Axial length, on the other hand, changed differently [18–21]. According to our result, axial length had no significant relationship with spherical equivalent. It was considered that early refractive errors may not provide enough information in predicting the later refractive and axial length outcome.

Fieß A et al. [13] detected axial length associated with birth weight and age. Modrzejewska et al. [9] found a correlation between axial length and birth weight. In our research, AL was significantly correlated with GA, BW, and HC. As the major proportion of eye growth occurs within the first year after birth, our observation suggested that ocular growth be affected by prematurity and led to shorter axial length, especially in the first years of life.

The prematurely born children had a higher prevalence of hypermetropia (>3 D) and clinically significant myopia (≤−1 D) than those born at term. Moderate or high myopia (<−3 D) was found only in preterm group. In our preterm group, take the right eye for granted, there were 22.37% (17/76) of hypermetropia (>3 D) and 15.78% (12/76) of significant myopia (≤−1 D). Four infants had moderate or high

Table 2: Parameter analysis of variance between preterm and term infants at 40 weeks' PCA.

Parameter for right eye	Term infants (mean ± SD)	Preterm infants (mean ± SD)	p
Number	65	76	
Spherical equivalent (SE, D)	2.19 ± 2.22	1.96 ± 2.12	0.50
Axial length (AL, mm)	17.34 ± 0.55	17.08 ± 0.67	*0.02
Anterior chamber depth (ACD, mm)	2.55 ± 0.26	2.38 ± 0.25	*0.000
Lens thickness (LT, mm)	3.72 ± 0.18	3.99 ± 0.15	*0.000
Vitreous depth (VD, cm)	11.03 ± 0.46	10.79 ± 0.56	*0.01

*$p < 0.05$ significant difference between two groups.

myopia (≤−3 D). The percentages of hypermetropia and significant myopia were higher than those of our term group (with 10/65 of hypermetropia and 5/65 of significant myopia). Due to the limitation of sample size, further studies were needed for larger sample investigation.

In this research, we investigated the axial length and refractive status of preterm infants with a GA of more than 28 weeks without ROP and found that preterm infants had shorter AL, shallow ACD, thicker LT, and thinner VD. Axial length in preterm infants was significantly correlated with gestational age, birth weight, and head circumference.

Conflicts of Interest

The authors declare that there is no conflict of interest regarding the publication of this paper.

Acknowledgments

The authors thank Professor Mingguang Shi for his helpful comments and suggestions.

References

[1] P. J. Foster and Y. Jiang, "Epidemiology of myopia," *Eye*, vol. 28, no. 2, pp. 202–208, 2014.

[2] A. Moskowitz, R. M. Hansen, and A. B. Fulton, "Retinal, visual, and refractive development in retinopathy of prematurity," *Eye Brain*, vol. 8, pp. 103–111, 2016.

[3] M. E. Hartnett and J. S. Penn, "Mechanisms and management of retinopathy of prematurity," *The New England Journal of Medicine*, vol. 367, no. 26, pp. 2515–2526, 2012.

[4] A. R. O'Connor, C. M. Wilson, and A. R. Fielder, "Ophthalmological problems associated with preterm birth," *Eye*, vol. 21, no. 10, pp. 1254–1260, 2007.

[5] R. M. Varghese, V. Sreenivas, J. M. Puliyel, and S. Varughese, "Refractive status at birth: its relation to newborn physical parameters at birth and gestational age," *PLoS One*, vol. 4, no. 2, article e4469, 2009.

[6] S. Bhatti, E. A. Paysse, M. P. Weikert, and L. Kong, "Evaluation of structural contributors in myopic eyes of preterm and full-term children," *Graefe's Archive for Clinical and Experimental Ophthalmology*, vol. 254, no. 5, pp. 957–962, 2016.

[7] H. C. Fledelius, R. Bangsgaard, C. Slidsborg, and M. laCour, "Refraction and visual acuity in a national Danish cohort of 4-year-old children of extremely preterm delivery," *Acta Ophthalmologica*, vol. 93, no. 4, pp. 330–338, 2015.

[8] T. C. Chen, T. H. Tsai, Y. F. Shih et al., "Long-term evaluation of refractive status and optical components in eyes of children born prematurely," *Investigative Ophthalmology & Visual Science*, vol. 51, no. 12, pp. 6140–6148, 2010.

[9] M. Modrzejewska, W. Grzesiak, D. Karczewicz, and D. Zaborski, "Refractive status and ocular axial length in preterm infants without retinopathy of prematurity with regard to birth weight and gestational age," *Journal of Perinatal Medicine*, vol. 38, no. 3, pp. 327–331, 2010.

[10] C. S. Yang, A. G. Wang, Y. F. Shih, and W. M. Hsu, "Astigmatism and biometric optic components of diode laser-treated threshold retinopathy of prematurity at 9 years of age," *Eye*, vol. 27, no. 3, pp. 374–381, 2013.

[11] M. Snir, R. Friling, D. Weinberger, I. Sherf, and R. Axer-Siegel, "Refraction and keratometry in 40 week old premature (corrected age) and term infants," *The British Journal of Ophthalmology*, vol. 88, no. 7, pp. 900–904, 2004.

[12] C. S. Yang, A. G. Wang, Y. F. Shih, and W. M. Hsu, "Long-term biometric optic components of diode laser-treated threshold retinopathy of prematurity at 9 years of age," *Acta Ophthalmologica*, vol. 91, no. 4, pp. e276–e282, 2013.

[13] A. Fieß, R. Kölb-Keer, M. Knuf et al., "Axial length and anterior segment alterations in former preterm infants and full-term neonates analyzed with Scheimpflug imaging," *Cornea*, vol. 36, no. 7, pp. 821–827, 2017.

[14] M. Tian, L. Zhou, Q. Luo, Y. M1, and Y. Xu, "Study of refractive state in premature infants without retinopathy of prematurity and full-term children at the age of 0 to 6," *Zhonghua Yan Ke Za Zhi*, vol. 51, no. 7, pp. 505–509, 2015.

[15] M. Ecsedy, I. Kovacs, K. Mihaltz et al., "Scheimpflug imaging for long-term evaluation of optical components in Hungarian children with a history of preterm birth," *Journal of Pediatric Ophthalmology and Strabismus*, vol. 51, no. 4, pp. 235–241, 2014.

[16] D. J. De Silva, K. D. Cocker, G. Lau, S. T. Clay, A. R. Fielder, and M. J. Moseley, "Optic disk size and optic disk-to-fovea distance in preterm and full-term infants," *Investigative Ophthalmology & Visual Science*, vol. 47, no. 11, pp. 4683–4686, 2006.

[17] K. J. Saunders, D. L. McCulloch, A. J. Shepherd, and A. G. Wilkinson, "Emmetropisation following preterm birth," *The British Journal of Ophthalmology*, vol. 86, no. 9, pp. 1035–1040, 2002.

[18] A. Cook, S. White, M. Batterbury, and D. Clark, "Ocular growth and refractive error development in premature infants with or without retinopathy of prematurity," *Investigative Ophthalmology & Visual Science*, vol. 49, no. 12, pp. 5199–5207, 2008.

[19] A. R. O'Connor, T. J. Stephenson, A. Johnson, M. J. Tobin, S. Ratib, and A. R. Fielder, "Change of refractive state and eye size in children of birth weight less than 1701 g," *The British Journal of Ophthalmology*, vol. 90, no. 4, pp. 456–460, 2006.

[20] A. R. O'Connor, C. M. Wilson, and A. R. Fielder, "Ophthalmological problems associated with preterm birth," *Eye*, vol. 21, no. 10, pp. 1254–1260, 2007.

[21] M. Kaya, A. T. Berk, and A. Yaman, "Long-term evaluation of refractive changes in eyes of preterm children: a 6-year follow-up study," *International Ophthalmology*, pp. 1–8, 2017.

Hindawi
Journal of Ophthalmology
Volume 2017, Article ID 1295132, 8 pages
https://doi.org/10.1155/2017/1295132

Review Article

Molecular Age-Related Changes in the Anterior Segment of the Eye

Luis Fernando Hernandez-Zimbron,[1] Rosario Gulias-Cañizo,[1,2] María F. Golzarri,[3] Blanca Elizabeth Martínez-Báez,[3] Hugo Quiroz-Mercado,[1,4] and Roberto Gonzalez-Salinas[1]

[1]*Research Department, Asociación para Evitar la Ceguera "Hospital Luis Sanchez Bulnes", I.A.P., 04030 México City, Mexico*
[2]*Cell Biology Department, Centro de Investigación y de Estudios Avanzados del IPN, 07360 México City, Mexico*
[3]*Anterior Segment Surgery Department, Asociación para Evitar la Ceguera "Hospital Luis Sanchez Bulnes", I.A.P., 04030 México City, Mexico*
[4]*University of Colorado, Denver, CO, USA*

Correspondence should be addressed to Roberto Gonzalez-Salinas; dr.gonzalezsalinas@gmail.com

Received 29 April 2017; Revised 9 July 2017; Accepted 30 August 2017; Published 24 September 2017

Academic Editor: Alejandro Cerviño

Purpose. To examine the current knowledge about the age-related processes in the anterior segment of the eye at a biological, clinical, and molecular level. *Methods*. We reviewed the available published literature that addresses the aging process of the anterior segment of the eye and its associated molecular and physiological events. We performed a search on PubMed, CINAHL, and Embase using the MeSH terms "eye," "anterior segment," and "age." We generated searches to account for synonyms of these keywords and MESH headings as follows: (1) "Eye" AND "ageing process" OR "anterior segment ageing" and (2) "Anterior segment" AND "ageing process" OR "anterior segment" AND "molecular changes" AND "age." *Results*. Among the principal causes of age-dependent alterations in the anterior segment of the eye, we found the mutation of the TGF-β gene and loss of autophagy in addition to oxidative stress, which contributes to the pathogenesis of degenerative diseases. *Conclusions*. In this review, we summarize the current knowledge regarding some of the molecular mechanisms related to aging in the anterior segment of the eye. We also introduce and propose potential roles of autophagy, an important mechanism responsible for maintaining homeostasis and proteostasis under stress conditions in the anterior segment during aging.

1. Introduction

According to the Global Health Estimates (WHO 2014) by 2017, for the first time in history, the number of people aged 65 years and older globally will outnumber children younger than 5 years of age (World Health Organization, [1]). Specifically in Latin America (according to the World Population Aging report from the World Health Organization, 2015), over the next 15 years, the number of elderly population is expected to grow faster in this region, with a projected 71 percent increase in the population aged 60 years or over [1, 2].

The anterior segment of the eye comprises all the structures located between the corneal epithelium and the posterior capsule of the lens. This review aims to revise the main molecular, physiological, and age-related changes in the anterior segment of the eye.

2. Methods

This review focuses on published articles that address the subject of the aging process in the anterior segment of the eye and the associated molecular and physiological events. We performed a search on PubMed, CINAHL, and Embase for the published literature available using the MeSH terms "eye," "anterior segment," and "age." We used no language restrictions. We generated searches to account for synonyms of these keywords and MESH headings as follows: (1) "Eye"

AND "ageing process" OR "anterior segment ageing" and (2) "Anterior segment" AND "ageing process" OR "anterior segment" AND "molecular changes" AND "age". The search encompassed manuscripts published up to March 2017, and it generated 531 individual references. Abstracts from meetings were not included, as they usually do not contain enough information to perform a proper evaluation. Two researchers (LFHZ and RGS) identified 78 published studies that met the inclusion criteria.

3. Results

3.1. Primary Age-Related Changes in the Anterior Segment

3.1.1. Ocular Surface and Cornea. Meibomian glands, responsible for the oily component of the tear film, become dysfunctional in most patients aged 60 and older, causing rapid evaporation of the tear film with subsequent dry eye symptoms, discomfort, and visual disturbances [3]. In addition, the cornea suffers changes in its shape and optical properties, including corneal steepening measurable by keratometry and a shift in toricity from with-the-rule to against-the-rule astigmatism and increased collagen interfibrillar spacing, as well as an increased thickness of Descemet's membrane [4]. It also becomes more prone to infections, mainly due to increased epithelial permeability and impaired barrier function secondary to the focal loss of hemidesmosomes that occurs with age [5], as well as decreased phagocytic ability of neutrophils. Within the corneal stroma, the senescent keratocytes overexpress collagenase, stromelysin, and elastase [6]. Increased levels of lipofuscin and endogenous ceramide have been reported. With time, there is an asymptomatic deposition of lipids concentrically to the limbus (cholesterol esters, cholesterol, and neutral glycerides), which is the most frequent age-related corneal change, known as arcus senilis or gerontoxon [7]. Another corneal age-related change is the Hassall-Henle bodies, which consist of localized thickenings in the posterior surface of Descemet's membrane, at the periphery of the cornea, that contain a material thought to be collagen, in which several fissures are filled with extrusions of the corneal endothelium. Although these bodies are present in degenerations and chronic inflammation, they are also associated with the aging cornea [7]. Finally, endothelial cells decrease with increasing age at an annual rate of 0.6%, and since they do not have the ability to regenerate, endothelial cell loss is an important aspect to consider in the aging eye, due to their importance on corneal homeostasis maintenance.

3.1.2. Trabecular Meshwork. As the human eye ages, there are structural changes in the anterior segment of the eye that increase the incidence of glaucoma in this age group. For example, some structural changes that increase the resistance to aqueous outflow occur more commonly in older adults. These changes include thickened trabecular sheets due to accumulation of "curly" collagen and pigment in the trabecular meshwork, decrease of proteoglycans (chondroitin and dermatan sulphates) [8], loss of trabecular endothelial cells, reduction of open pores and spaces of the trabecular meshwork, and accumulation of laminin beneath the endothelial lining of Schlemm's canal [9]. In addition, the loss of trabecular endothelial cells allows the fusion of trabecular beams through hyalinization that results in dysfunctional phagocytosis, as well as macromolecules synthesis and/or degradation that alter physiologic processes.

3.1.3. Lens. Cataracts, the most common cause of vision loss in older people worldwide, are a well-known age-related change. Cataract formation includes the deposition of aggregated proteins in the lens and damage to the plasmatic membrane of lens fiber cells. One of the primary changes during aging is the increase of the relative thickness of the lens' cortex throughout a person's life [10]. This change increases the curvature and therefore the refractive power of the lens, with the concomitant deposition of insoluble particles, which at the same time decreases the refractive index. Therefore, the eye may become more hyperopic or more myopic with age, depending on the predominant change [10].

Chaperone proteins contribute to ensure quality control mechanisms in other to achieve an adequate protein function under normal and stress circumstances [11]. Mitochondria contain two particular chaperones: human heat shock proteins (Hsp) 60 and 70, which protect damaged proteins in the aging eye [12]. The Hsp alpha-crystallin is made of two polypeptides, alpha A crystallin and alpha B crystallin, which are the predominant proteins of the eye lens in vertebrate animals. Alpha A is key for lens transparency, ensuring that alpha B or other close related proteins remain soluble [13]. Nevertheless, as the cell fibers of the lens grow, a proteolytic cleavage of crystallins represents a gradual conversion from water-soluble into water-insoluble proteins. This change induces their aggregation, which in turn provokes subsequent light scattering and lens opacity.

Recently, Augusteyn described a lens increase of 1.3 mg of lens tissue/year during the adult life [14]. However, once polypeptides are synthesized and integrated into mature fiber cells, the capacity to break down proteins using proteases such as caspase presumably persists for some time afterwards to allow organelle degradation [14–16]. Other age-related changes in the lens include decreased concentrations of glutathione and potassium and increased concentrations of sodium and calcium in the cytoplasm of the lens' cells [17].

All the aforementioned age-related changes in the structures of the anterior segment are depicted in Figure 1.

4. Biomarkers

The term biomarker of aging has been defined as a "biological parameter of an organism that either alone or in some multivariate composite will better predict functional capability at some late age than will chronological age" [18].

4.1. Inflammatory Markers. Evidence shows that inflammation plays an important role in the aging process; therefore, inflammation biomarkers could be suitable determinants of the aging processes [19]. In the anterior segment of the eye, dysregulation of the complement pathway with altered levels of both intrinsic complement proteins and activated

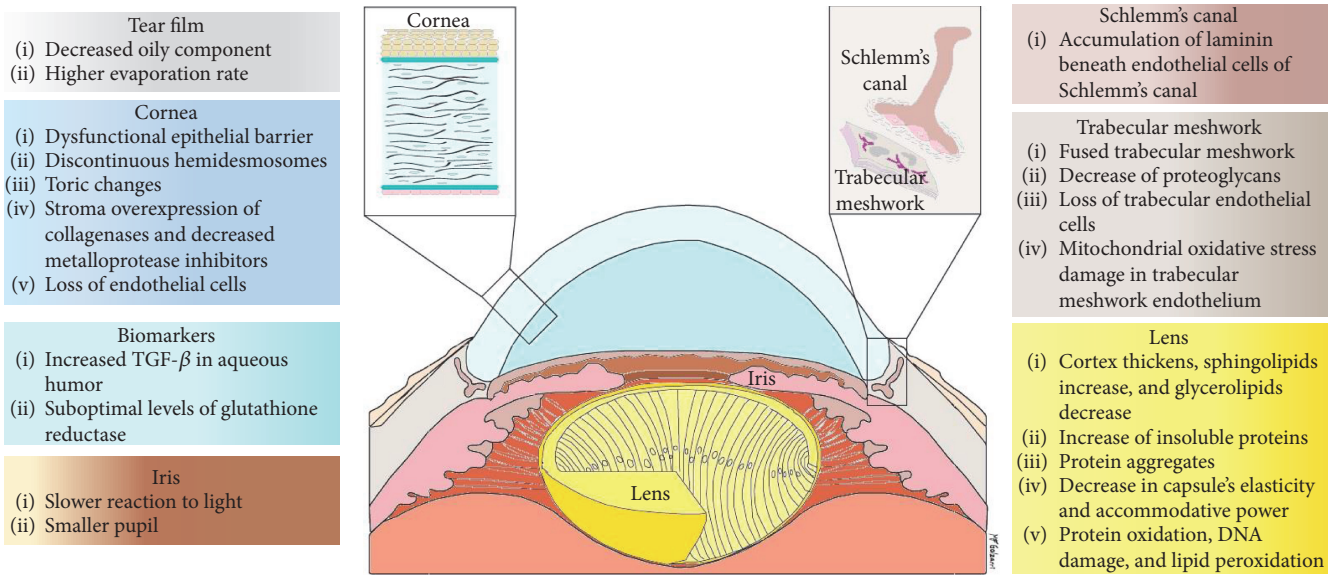

Figure 1: Illustration depicting the most relevant structural changes that occur with aging in the anterior segment of the eye.

products triggered by oxidative stress has been associated as key players in the aging process [20]. Complement components contribute to pathogenic processes by damaging tissues and being highly chemotactic and capable of facilitating neovascularization [21]. Montalvo et al. recently established an association between C1q, C3, and C4 and corneal and lens anterior capsule damage without inflammation [22], suggesting that molecules released by inflammatory cells and inflamed tissues may affect adjacent tissues not directly involved in the pathogenic process [23].

4.2. AGEs. Another cluster of age-related biomarkers is constituted by the advanced glycation end products (AGEs), which are a heterogeneous group of macromolecules formed by nonenzymatic glycation of proteins, lipids, and nucleic acids, where sugars such as glucose react with amino groups in proteins, lipids, and nucleic acids [24]. Aging relates to the presence of AGEs in the cornea, lens, and other ocular structures [24–26]. In the lens, epithelial cell glycation occurs as a reaction of aldo and keto groups of carbohydrates with amino groups of proteins (mostly lysine and arginine residues) [27].

Nevertheless, the lens itself is not only affected by AGEs. Similar to other basal membranes (BM), the lens capsule, a BM secreted by the lens epithelial cells, tends to accumulate posttranslational modifications with age, since the proteins that constitute BMs usually present a low turnover rate [26]. Raghavan et al. reported AGE accumulation in the human lens capsule with increasing age, which in turn is associated with a higher incidence of cataract [28].

In addition, recent studies suggest that AGEs bind to a cell surface receptor known as RAGE. RAGE belongs to the immunoglobulin family of receptors [29]. AGE-RAGE interaction increases intracellular oxidative stress by activation of NADPH-oxidase, a key mediator in superoxide radical production [29]. Therefore, AGEs are linked to another hallmark of aging: oxidative stress.

5. Oxidative Stress

Oxidation-reduction mechanisms are of paramount importance in the eye, since oxidative damage can result in specific molecular changes that contribute to the development of age-related sight-threatening diseases such as glaucoma and cataracts.

5.1. Reactive Oxygen Species—Reducing Agents. Reactive oxygen species (ROS) comprise a group of molecules formed by the partial reduction of oxygen. They generate in the intracellular space as by-products of cellular aerobic metabolism or may be acquired from exogenous sources due to the exposure of cells to the environment. ROS play an essential role in cell signaling and regulation; however, when their production exceeds the intrinsic antioxidant capacity, they induce damage to cell components such as DNA, proteins, and lipids [30].

The production of ROS, such as hydroxyl radical (-OH), single oxygen (O2), hydrogen peroxide (H2O2), and peroxynitrite (OONO-), has to be balanced with the primary antioxidants and chaperones, reducing agents, antioxidant enzymes, and protein repair systems which protect the tissues against oxidative stress [12]. These reducing systems use electron donors such as glutathione (GSH), NADPH, NADH, FADH2, and thioredoxin.

The main reducing system in the eye is the glutathione system that includes reduced GSH, oxidized glutathione (GSSG), and a number of related enzymes [12, 31]. Glutathione peroxidase reduces H2O2 to water and leads to the oxidation of GSH to GSSG. The reduced state of GSH is maintained by glutathione reductase in which NADPH is needed, hence the importance of glucose-6-phosphate dehydrogenase as well. This system is capable of detoxifying H2O2, dehydroascorbic acid, and lipid peroxides and maintains protein thiols in a reduced state. Other reducing agents include thioltransferase that reduces protein thiols by using

reduced GSH [32] and thioredoxin that uses NADPH to maintain mitochondrial proteins in a reduced state [33]. Antioxidant enzymes contribute to the protective role against ROS, like superoxide dismutase, especially SOD2 that converts O2- to hydrogen peroxide. Studies have shown that SOD2 is helpful to protect lens epithelial cells, since cells with high-level expression of this enzyme show resistance to the cytotoxic effects of H2O2, O2-, and UVB radiation [34]. On the contrary, SOD2-deficient cells show mitochondrial damage, leakage of cytochrome C, caspase 3 activation, and increased apoptosis when exposed to O2- [35].

Based on this data, one can conclude that this system is of great significance to ocular and general health maintenance. Therefore, as its efficacy decreases with age, several eye diseases may develop.

5.2. ROS in the Lens. As previously mentioned, ROS are generated from intrinsic and extrinsic sources. Through the years, the lens becomes a tissue highly susceptible to oxidative damage since the proteins that constitute it are never replaced. Consequently, protein oxidation, DNA damage, and lipid peroxidation are all found in the process of cataractogenesis [36]. Nevertheless, since the lens has a high concentration of reduced glutathione as previously mentioned, it helps to maintain reduced thiol groups, leading to transparency of the lens and cornea [31].

Phospholipid composition of lens membranes is of particular interest: sphingolipids increase with age, whereas glycerolipids decrease. The decrease in glycerolipids might correlate with the fact that glycerolipids are more prone to oxidation, and at the same time, the growing numbers of oxidized sphingolipids increase membrane stiffness. Studies show that both findings are exacerbated in cataractous lenses [37].

As previously mentioned, concentration of nuclear glutathione (GSH) helps to prevent oxidation. In the lens, epithelial cells are the only ones that accomplish aerobic metabolism and thus the only cells containing mitochondria aside from newly differentiated fiber cells. Damage to these mitochondria leads to a redox imbalance that affects proteins and lipid plasma cell membranes of the fiber cells [30].

The lens has a high metabolic demand mainly in the equatorial regions of the lens epithelium, where cell division and differentiation usually occur [38]. An extensive gap junction network meets metabolic fiber cell demands, from which one can deduce that epithelial cell dysfunction has an important role in lens damage [36]. Recent studies on bovine lenses show metabolically active mitochondria in both epithelial cell and superficial cortical fiber cells [39].

5.3. ROS in Glaucoma. Oxidative stress contributes to the pathogenesis of neurodegenerative diseases, including apoptosis of retinal ganglion cells characteristic of glaucoma. The exact molecular physiopathology of POAG is unknown; however, it relates to cellular damage by ROS through direct cytotoxicity and specific amino acid enzymatic oxidation. These protein modifications may lead to glial dysfunction, which spreads neuronal damage by secondary degeneration [40]. Another important structure damaged by oxidative stress is the trabecular meshwork. It has a particular susceptibility to mitochondrial oxidative injury that affects its endothelium. This damage induces cell decay, subclinical inflammation, changes in the extracellular matrix and cytoskeleton, reduced aqueous outflow, and consequently, increased intraocular pressure [41].

6. Autophagy and Aging in the Anterior Segment

Cellular homeostasis depends on the proteostasis network that under normal conditions senses and rectifies disturbances in the proteome to restore homeostasis in the cells. Proteostasis maintenance is achieved mainly by two proteolytic systems: the ubiquitin-proteasome and the autophagic system. There are some differences between them: while substrates of the ubiquitin-proteasome pathway are predominantly short-lived proteins, autophagy substrates are long-lived proteins and multiple proteins organized into oligomeric complexes or aggregates not suitable for degradation by other systems [42].

In this regard, autophagy is a catabolic process that "eats" different products (aberrant organelles, misfolded proteins, and protein aggregates) into double membrane autophagosomes and delivers them to lysosomes [43]. The proper function of this process is important because it is the only currently known mechanism that eukaryotic cells possess not only to degrade protein aggregates but also to recycle entire organelles such as mitochondria and peroxisomes [44]. In addition, cell survival is highly dependent on autophagy: loss of autophagy causes accumulation of ubiquitin-positive inclusion bodies and triggers degeneration processes [45].

Although initially autophagy was described as a catabolic process that regulates nutritional homeostasis under stress conditions, currently, autophagy is recognized as a fundamental participant in homeostasis that degrades components that are toxic for the cell. Autophagy is a very complex process and requires a series of coordinated steps. The first step involves the formation of an isolation vesicle called phagophore (Figure 2).

After phagophore formation, it elongates around the cytoplasmic components selected for degradation. The recognition of the components for degradation and the closing of the vesicle are dependent on the lipidated form of LC3 protein (microtubule-associated protein light chain 3). The lipidated form of LC3 is associated with the outer and inner membranes of the autophagosome [46, 47]. A specific pathway that requires at least twenty proteins called ATG (autophagy-related proteins) forms these autophagosomes [47]. Finally, the late stage of autophagy (maturation) depends on the fusion of the autophagosome with the lysosome. This allows contact of the autophagosome cargo with the lysosomal hydrolases and consequently degradation of the components that could be recycled (Figure 2(b)). These steps are fundamental for the autophagic flux (the continuous series of events since the cargo is engulfed until it is degraded). Any event that alters this flux also impairs the

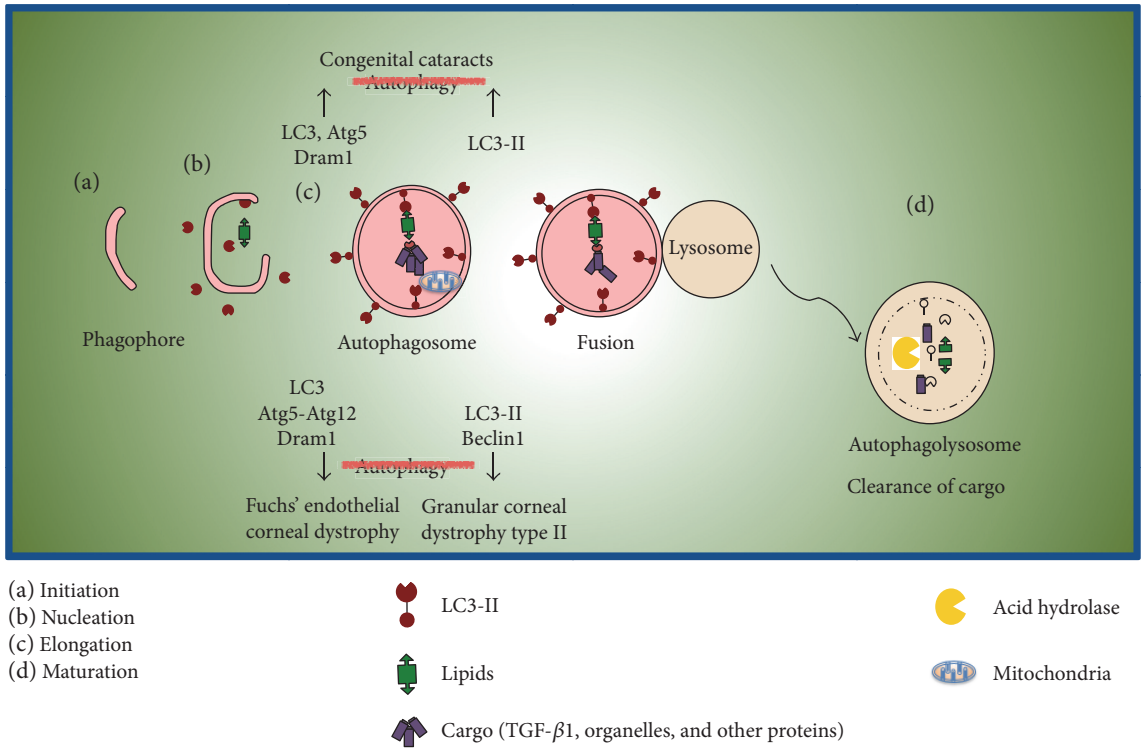

Figure 2: Autophagy elimination of cargo (any protein and/or organelle to be degraded) and autophagy disturbances in the eye are represented in this diagram of corneal and lens cells, displaying autophagy proteins altered in various stages of autophagic processes and the consequences of these modifications.

degradation process and leads to accumulation of autophagosomes [45–47].

There are some particular stages of the autophagy process. There is an initial stage called initiation that requires a complex formed by the kinase ULK1 (UNC51-like kinase) and its substrates: Atg13 and FIP200. ULK1 may be regulated in two main ways: inhibition by mTOR (target of rapamycin complex 1) and stimulation by AMPK (AMP-activated protein kinase) [47]. During nucleation, the participation of Beclin1 protein, as well as Vsp34 and Atg14, is critical. These proteins form a complex to recruit WIPI1 and Atg2, aiding to form a new autophagosome. Subsequently, elongation and closure of the autophagosome occur. This event involves the formation of an Atg7-dependent conjugated system (Atg12-Atg5), which is responsible for LC3 lipidation by phosphatidylethanolamine. The expansion of this autophagosome membrane is a consequence of the participation of Atg9, and the closure of the autophagosome is a process that helps to include proteins to be degraded (cargo). In the end, cargo degradation is dependent on the interplay between lysosomes and autophagosomes, the so-called autolysosome. One key participant in the transport of autophagic vacuoles is FYCO1 protein [46–47].

In the eye, all cells undergo autophagy in order to maintain a specific and normal function contributing to healthy vision. These cells express differential autophagy-related proteins, but when they harbor gene mutations, they activate stress-induced autophagic pathways and induce the development of ocular diseases [48].

This section of the review summarizes the current knowledge about the role of autophagy in ocular health and disease (specifically cornea and lens), as well as the potential molecules that could be used as a protective therapy against anterior segment degeneration in aging.

6.1. Autophagy in Cornea. During aging, there is an overaccumulation of abnormal aggregated proteins in the corneal epithelium and stroma. Among the principal causes of age-dependent accumulation of aggregated proteins in these regions is the mutation of the TGF-β gene that affects corneal transparency. This growth factor participates in cell adhesion and migration. In addition, it is recognized as a component of extracellular matrix. The mutant TGF-β1 protein is more prone to aggregation, and it is eliminated specifically by autophagy through the interaction between TGF-β and LC3. The abnormal accumulation of mutant TGF-β1 and the dysregulation of the autophagic process relates to the development of granular corneal dystrophy type II (GCd2) [49, 50]. Indeed, an autophagic inductor suggested for the treatment of GCD2 is lithium. Lithium enhances autophagy by an mTOR-independent pathway, reduces the expression of TGF-β1, and increases LC3-II levels [48].

In a mice model of Fuchs' endothelial corneal dystrophy (FECD), the authors observed an increase of LC3 and macroautophagy [49], as well as a decrease in Atg12-Atg5 that affects the complete degradation of different organelles [48].

In addition, in the cornea and conjunctiva, there are infectious (HSV-1 infection) and non-infectious (keratoconus)

inhibitors of autophagy, but the mechanisms involved have not been fully understood [48, 51]. The cornea is a target for HSV-1, and after the internalization of the virion and membrane fusion, the viral genome is delivered to the endothelial cell nucleus. As we previously mentioned, Beclin1 is necessary for autophagosome formation through the interaction with Vsp34. In this infection, the virus interacts directly with Beclin1. Some authors have reported different synthetic inductors of autophagy such as the preservative benzalkonium chloride (BAC) [51].

There are several reports describing the participation of autophagy in other pathologies like age-related macular degeneration, diabetic retinopathy (DR), thyroid-associated ophthalmopathy (TAO), chloroquine retinopathy, and glaucoma [52]; however, there are comparatively less reports explaining the autophagy-related mechanisms in the lens.

6.2. Autophagy in the Lens. As we mentioned before, during normal aging, the lens losses its clarity and its refractive power diminishes. During maturation of the lens, proteostasis, degradation of the organelles, and nucleic acids produce the organelle free zone (OFZ), contributing to lens transparency. The abnormal growth of lens epithelial cells (LECs) towards the nucleus forms senile cataracts and is a normal process in aging.

Autophagy in the lens normally occurs as a physiologic process to eliminate cytoplasmic components and nucleic acids, indicative of a normal expression of LC3 protein [53, 54]. All the autophagy-related genes and proteins are present in the lens. Some of them, like FYCO1 gene, are involved in lens development and differentiation; also, mutations in FYCO1 gene relate to the development of congenital cataracts [55, 56]. Loss of FYCO1's homeostatic function disrupts the fusion of lysosomes to autophagosomes, resulting in the accumulation of LC3-II vesicles and thus affecting mitophagy [48, 57]. Recently, mitophagy [50] has been extensively studied, but the mechanisms related to nucleophagy and the way they participate in lens transparency with aging have not been fully described [55, 57]. Alterations in some autophagy-related proteins such as Atg5 and Vsp34 are involved in autophagy failure that induces defective lens development, promoting formation of congenital cataracts. However, as we have discussed, there is not enough evidence in the literature to explain thoroughly the autophagic process in lens aging [57].

6.3. Autophagy Induction as a Treatment for Anterior Segment Pathologies. A wide variety of molecules can induce autophagy to eliminate accumulated proteins from different cells in the anterior segment. Among autophagy inducers, we find trehalose, metformin, and rapamycin. Trehalose is a disaccharide of glucose (a natural disaccharide that blocks glucose transporters) which "rescues" different products accumulated in corneal endothelium and retina [58]. Several organisms produce it under stress conditions, but it is not a naturally occurring substance in mammals. Specifically in cornea, this sugar suppresses inflammation and neovascularization [58, 59]. In dry eye disease, it helps to decrease cell death as well as inflammation [59]. The literature shows that trehalose prevents neurodegenerative disorders by promoting autophagy, thus reducing the presence of toxic proteins or peptides [59, 60]. Besides, it is not toxic and it can be safely administered in humans [51, 53, 54], like the marketed trehalose eye drops used to preserve viability and function of corneal epithelial cells during desiccation [56, 61]. However, its role in autophagic activation related to anterior segment diseases has not been completely studied.

7. Conclusions

Changes in the anterior segment of the eye are responsible for half of the four most common causes of age-related vision impairing diseases (glaucoma, cataracts, age-related macular degeneration, and diabetic retinopathy). The burden of these ocular diseases will not only affect developed countries but also developing regions with limited resources. The structural and molecular changes observed in the anterior eye segment are caused by molecular changes in intercellular unions, structural arrangements of collagen fibers, overexpression of degradation enzymes, underexpression of inhibitors of metalloproteases in tissues, UV light absorbed that produces ROS, inflammatory cytokines and molecules (such as TGF beta), and dysregulation of autophagy, among others. As the global population ages, diseases related to cell and tissue senescence are becoming more prevalent, so it is important to be familiar with these changes in order to tackle their consequences as best as possible.

Conflicts of Interest

The authors have declared no conflict of interest.

References

[1] World Health Organization, "Global health and aging US National Institute of Aging," October 2011, http://www.who.int/ageing/publications/global_health.pdf.

[2] Instituto Nacional de Estadística y Geografía, *Estadísticas a propósito del día internacional de las personas con edad*, 2016.

[3] G. J. Chader and A. Taylor, "Preface: the aging eye: normal changes, age-related diseases, and sight-saving approaches," *Investigative Ophthalmology & Visual Science*, vol. 54, no. 14, pp. ORSF1–ORSF4, 2013.

[4] R. G. A. Faragher, B. Mulholland, S. J. Tuft, S. Sandeman, and P. T. Khaw, "Aging and the cornea," *British Journal of Ophthalmology*, vol. 81, pp. 814–817, 1997.

[5] V. Trinkaus-Randall, M. Tong, P. Thomas, and A. Cornell-Bell, "Confocal imaging of the alpha 6 and beta 4 integrin subunits in the human cornea with aging," *Investigative Ophthalmology & Visual Science*, vol. 34, pp. 3103–3109, 1993.

[6] A. J. Millis, M. Hoyle, H. M. McCue, and H. Martini, "Differential expression of metalloproteinase and tissue inhibitor of metalloproteinase genes in aged human fibroblasts," *Experimental Cell Research*, vol. 201, pp. 373–379, 1992.

[7] C. A. P. Cavallotti and L. Cerulli, Eds., *Age-Related Changes of the Human Eye*, Humana Press, 2008.

[8] M. F. Gaballah and Z. H. Badawy, *Anatomy of the Orbit and Eye. A Diagrammatic Atlas, Vol. II*, 2014.

[9] R. Stamper, M. Lieberman, and M. Drake, *Becker-Shaffer's Diagnosis and Therapy of the Glaucomas*, Elsevier, Cambridge, MA, USA, 8th edition, 2009.

[10] M. Dubbelman, G. L. Van der Heijde, H. A. Weeber, and G. F. J. M. Vrensen, "Changes in the internal structure of the human crystalline lens with age and accommodation," *Vision Research*, vol. 43, pp. 2363–2375, 2003.

[11] T. Bender, C. Leidhold, T. Ruppert, S. Franken, and W. Voos, "The role of protein quality control in mitochondrial protein homeostasis under oxidative stress," *Proteomics*, vol. 10, 2010.

[12] L. A. Brennan and M. Kantorow, "Mitochondrial function and redox control in the aging eye: role of MsrA and other repair systems in cataract and macular degenerations," *Experimental Eye Research*, vol. 88, no. 2, pp. 195–203, 2009.

[13] J. P. Brady, D. Garland, Y. Duglas-Tabor, W. G. Robison Jr., A. Groome, and E. F. Wawrousek, "Targeted disruption of the mouse alpha A-crystallin gene induces cataract and cytoplasmic inclusion bodies containing the small heat shock protein alpha B-crystallin," *Proceedings of the National Academy of Sciences of the United States of America*, vol. 94, no. 3, pp. 884–889, 1997.

[14] R. C. Augusteyn, "On the growth and internal structure of the human lens," *Experimental Eye Research*, vol. 90, no. 6, pp. 643–654, 2010.

[15] X. Zhu, A. Korlimbinis, and R. J. Truscott, "Age-dependent denaturation of enzymes in the human lens: a paradigm for organismic aging?," *Rejuvenation Research*, vol. 13, no. 5, pp. 553–560, 2010.

[16] I. M. Wormstone and M. A. Wride, "The ocular lens: a classic model for development, physiology and disease," *Philosophical Transactions of the Royal Society B: Biological Sciences*, vol. 366, 2011.

[17] S. M. Salvi, S. Akhtar, and Z. Currie, "Ageing changes in the eye," *Postgraduate Medical Journal*, vol. 82, pp. 581–587, 2006.

[18] E. Song, H. Sun, Y. Xu, Y. Ma, H. Zhu, and C. W. Pan, "Age-related cataract, cataract surgery and subsequent mortality: a systematic review and meta-analysis," *PLoS One*, vol. 9, 2014.

[19] H. Xu, M. Chen, and J. V. Forrester, "Para-inflammation in the aging retina," *Progress in Retinal and Eye Research*, vol. 28, no. 5, pp. 348–368, 2009.

[20] M. Chen, E. Muckersie, J. V. Forrester, and H. Xu, "Immune activation in retinal aging: a gene expression study," *Investigative Ophthalmology & Visual Science*, vol. 51, no. 11, pp. 5888–5896, 2010.

[21] R. L. Sprott, "Biomarkers of aging and disease: introduction and definitions," *Experimental Gerontology*, vol. 45, pp. 2–4, 2010.

[22] V. Montalvo, C. C. Chan, I. Gery et al., "Complement deposits on ocular tissues adjacent to sites of inflammation," *Current Eye Research*, vol. 32, no. 11, pp. 917–922, 2007.

[23] M. Nozaki, B. J. Raisler, E. Sakurai et al., "Drusen complement components C3a and C5a promote choroidal neovascularization," *Proceedings of the National Academy of Sciences of the United States of America*, vol. 103, no. 7, pp. 2328–2333, 2006.

[24] R. D. Semba, E. J. Nicklett, and L. Ferrucci, "Does accumulation of advanced glycation end products contribute to the aging phenotype?," *The Journals of Gerontology Series A, Biological Sciences and Medical Sciences*, vol. 65A, pp. 963–975, 2010.

[25] G. Tezel, C. Luo, and X. Yang, "Accelerated aging in glaucoma: immunohistochemical assessment of advanced glycation end products in the human retina and optic nerve head," *Investigative Ophthalmology & Visual Science*, vol. 48, no. 3, pp. 1201–1211, 2007.

[26] D. R. Sell and V. M. Monnier, "Aging of long-lived proteins: extracellular matrix (collagens, elastins, proteoglycans) and lens crystallins," *Comprehensive Physiology*, 2011.

[27] R. H. Nagaraj, M. Linetsky, and A. W. Stitt, "The pathogenic role of Maillard reaction in the aging eye," *Amino Acids*, vol. 42, no. 4, pp. 1205–1220, 2010.

[28] C. T. Raghavan, M. Smuda, A. J. Smith et al., "AGEs in human lens capsule promote the TGFβ2-mediated EMT of lens epithelial cells: implications for age-associated fibrosis," *Aging Cell*, vol. 15, 2016.

[29] E. Leclerc, G. Fritz, S. W. Vetter, and C. W. Heizmann, "Binding of S100 proteins to RAGE: an update," *Biochimica et Biophysica Acta (BBA)-Molecular Cell Research*, vol. 1793, no. 6, pp. 993–1007, 2009.

[30] M. Babizhayev, "Generation of reactive oxygen species in the anterior eye segment. Synergistic codrugs of N-acetylcarnosine lubricant eye drops and mitochondria-targeted antioxidant act as a powerful therapeutic platform for the treatment of cataracts and primary open-angle glaucoma," *BBA Clinical*, vol. 6, 2016.

[31] E. Ganea and J. J. Harding, "Glutathione-related enzymes and the eye," *Current Eye Research*, vol. 31, no. 1, pp. 1–11, 2006.

[32] M. A. Babizhayev and Y. E. Yegorov, "Reactive oxygen species and the aging eye: specific role of metabolically active mitochondria in maintaining lens function and in the initiation of the oxidation-induced maturity onset cataract - a novel platform of mitochondria-targeted antioxidants with broad therapeutic potential for redox regulation and detoxification of oxidants in eye diseases," *American Journal of Therapeutics*, vol. 23, no. 1, pp. e98–e117, 2016.

[33] V. I. Pérez, C. M. Lew, L. A. Cortez et al., "Thioredoxin 2 haploinsufficiency in mice results in impaired mitochondrial function and increased oxidative stress," *Free Radical Biology & Medicine*, vol. 44, no. 5, pp. 882–892, 2008.

[34] H. Matsui, L. R. Lin, Y. S. Ho, and V. N. Reddy, "The effect of up- and downregulation of MnSOD enzyme on oxidative stress in human lens epithelial cells," *Investigative Ophthalmology & Visual Science*, vol. 44, no. 8, pp. 3467–3475, 2003.

[35] V. N. Reddy, E. Kasahara, M. Hiraoka, L. R. Lin, and Y. S. Ho, "Effects of variation in superoxide dismutases (SOD) on oxidative stress and apoptosis in lens epithelium," *Experimental Eye Research*, vol. 79, no. 6, pp. 859–868, 2004.

[36] M. A. Babizhayev, A. I. Deyev, V. N. Yermakova, I. V. Brikman, and J. Bours, "Lipid peroxidation and cataracts: N-acetylcarnosine as a therapeutic tool to manage age-related cataracts in human and in canine eyes," *Drugs in R&D*, vol. 5, no. 3, pp. 125–139, 2004.

[37] L. Huang, V. Grami, Y. Marrero et al., "Human lens phospholipid changes with age and cataract," *Investigative Ophthalmology & Visual Science*, vol. 46, no. 5, pp. 1682–1689, 2005.

[38] Z. Huang, J. Jiang, V. A. Tyurin et al., "Cardiolipin deficiency leads to decreased cardiolipin peroxidation and increased resistance of cells to apoptosis," *Free Radical Biology & Medicine*, vol. 44, no. 11, pp. 1935–1944, 2008.

[39] V. Bantseev, A. P. Cullen, J. R. Trevithick, and J. G. Sivak, "Optical function and mitochondrial metabolic properties in damage and recovery of bovine lens after in vitro carbonyl cyanide m-chlorophenylhydrazone treatment," *Mitochondrion*, vol. 3, no. 1, pp. 1–11, 2003.

[40] S. C. Saccà, S. Gandolfi, A. Bagnis et al., "The outflow pathway: a tissue with morphological and functional unity," *Journal of Cellular Physiology*, vol. 231, 2016.

[41] M. A. Babizhayev and Y. E. Yegorov, "Senescent phenotype of trabecular meshwork cells displays biomarkers in primary open-angle glaucoma," *Current Molecular Medicine*, vol. 11, no. 7, pp. 528–552, 2011.

[42] S. Kaushik and A. M. Cuervo, "Proteostasis and aging," *Nature Medicine*, vol. 21, no. 12, pp. 1406–1415, 2015.

[43] F. M. Menzies, A. Fleming, and D. C. Rubinsztein, "Compromised autophagy and neurodegenerative diseases," *Nature Reviews Neuroscience*, vol. 16, no. 6, pp. 345–357, 2015.

[44] I. Milisav, D. Šuput, and S. Ribarič, "Unfolded protein response and macroautophagy in Alzheimer's, Parkinson's and prion diseases," *Molecules*, vol. 20, no. 12, pp. 22718–22756, 2015.

[45] M. Komatsu, S. Waguri, T. Chiba et al., "Loss of autophagy in the central nervous system causes neurodegeneration in mice," *Nature*, vol. 441, no. 7095, pp. 880–884, 2006.

[46] M. Mehrpour, A. Esclatine, I. Beau, and P. Codogno, "Overview of macroautophagy regulation in mammalian cells," *Cell Research*, vol. 20, no. 7, pp. 748–762, 2010.

[47] M. Tsukada and Y. Ohsumi, "Isolation and characterization of autophagy-defective mutants of *Saccharomyces cerevisiae*," *FEBS Letters*, vol. 333, pp. 169–174, 1993.

[48] L. S. Frost, C. H. Mitchell, and K. Boesze-Battaglia, "Autophagy in the eye: implications for ocular cell health," *Experimental Eye Research*, vol. 124, pp. 56–66, 2014.

[49] H. Meng, M. Matthaei, N. Ramanan et al., "L450W and Q455K Col8a2 knock-in mouse models of Fuchs endothelial corneal dystrophy show distinct phenotypes and evidence for altered autophagy," *Investigative Ophthalmology & Visual Science*, vol. 54, pp. 1887–1897, 2013.

[50] S. I. Choi, B. Y. Kim, S. Dadakhujaev et al., "Impaired autophagy and delayed autophagic clearance of transforming growth factor β-induced protein (TGFBI) in granular corneal dystrophy type 2," *Autophagy*, vol. 8, pp. 1782–1797, 2012.

[51] G. Petrovski, R. Albert, K. Kaarniranta et al., "Autophagy in the eye: a double-edged sword," in *Autophagy: Principles, Regulation and Roles in Disease*, Nova Science Publishers, Inc., 2012.

[52] Y. Chen, O. Sawada, H. Kohno et al., "Autophagy protects the retina from light-induced degeneration," *The Journal of Biological Chemistry*, vol. 288, pp. 7506–7518, 2013.

[53] K. G. Lyamzaev, O. K. Nepryakhina, V. B. Saprunova et al., "Novel mechanism of elimination of malfunctioning mitochondria (mitoptosis): formation of mitoptotic bodies and extrusion of mitochondrial material from the cell," *Biochimica et Biophysica Acta (BBA) - Bioenergetics*, vol. 1777, no. 7-8, pp. 817–825, 2008.

[54] D. Mijaljica, M. Prescott, and R. Devenish, "Nibbling within the nucleus: turnover of nuclear contents," *Cellular and Molecular Life Sciences: CMLS*, vol. 64, no. 5, pp. 581–588, 2007.

[55] J. Chen, Z. Ma, X. Jiao et al., "Mutations in FYCO1 cause autosomal-recessive congenital cataracts," *American Journal of Human Genetics*, vol. 88, pp. 827–838, 2011.

[56] L. A. Brennan, W. L. Kantorow, D. Chauss et al., "Spatial expression patterns of autophagy genes in the eye lens and induction of autophagy in lens cells," *Molecular Vision*, vol. 18, pp. 1773–1786, 2012.

[57] M. J. Costello, L. A. Brennan, S. Basu et al., "Autophagy and mitophagy participate in ocular lens organelle degradation," *Experimental Eye Research*, vol. 116, pp. 141–150, 2013.

[58] J. Cejkova and C. Cejka, "Trehalose–current applications in ophthalmology and future perspectives," *Global Journal for Research Analysis*, vol. 4, no. 8, 2016.

[59] S. I. Wada, S. I. Ohba, T. Someno, M. Hatano, and A. Nomoto, "Structure and biological properties of lentztrehalose: a novel trehalose analog," *The Journal of Antibiotics*, vol. 67, no. 4, pp. 319–322, 2014.

[60] L. G. Friedman, Y. H. Qureshi, and W. H. Yu, "Promoting autophagic clearance: viable therapeutic targets in Alzheimer's disease," *Neurotherapeutics*, vol. 12, no. 1, pp. 94–108, 2014.

[61] A. Hill-Bator, M. Misiuk-Hojło, K. Marycz, and J. Grzesiak, "Trehalose-based eye drops preserve viability and functionality of cultured human corneal epithelial cells during desiccation," *BioMed Research International*, vol. 2014, Article ID 292139, 8 pages, 2014.

Hindawi
Journal of Ophthalmology
Volume 2017, Article ID 1909348, 9 pages
https://doi.org/10.1155/2017/1909348

Research Article

New Objective Refraction Metric Based on Sphere Fitting to the Wavefront

Mateusz Jaskulski,[1] Andreí Martínez-Finkelshtein,[2] and Norberto López-Gil[1]

[1]*Facultad de Óptica y Optometría, University of Murcia, Murcia, Spain*
[2]*Department of Mathematics, University of Almería, Almería, Spain*

Correspondence should be addressed to Mateusz Jaskulski; mateusz.jaskulski@gmail.com

Received 7 February 2017; Revised 9 May 2017; Accepted 11 July 2017; Published 20 September 2017

Academic Editor: Hema Radhakrishnan

Purpose. To develop an objective refraction formula based on the ocular wavefront error (WFE) expressed in terms of Zernike coefficients and pupil radius, which would be an accurate predictor of subjective spherical equivalent (SE) for different pupil sizes. *Methods*. A sphere is fitted to the ocular wavefront at the center and at a variable distance, t. The optimal fitting distance, t_{opt}, is obtained empirically from a dataset of 308 eyes as a function of objective refraction pupil radius, r_0, and used to define the formula of a new wavefront refraction metric (MTR). The metric is tested in another, independent dataset of 200 eyes. *Results*. For pupil radii $r_0 \leq 2$ mm, the new metric predicts the equivalent sphere with similar accuracy (<0.1D), however, for $r_0 > 2$ mm, the mean error of traditional metrics can increase beyond 0.25D, and the MTR remains accurate. The proposed metric allows clinicians to obtain an accurate clinical spherical equivalent value without rescaling/refitting of the wavefront coefficients. It has the potential to be developed into a metric which will be able to predict full spherocylindrical refraction for the desired illumination conditions and corresponding pupil size.

1. Introduction

Objective wavefront refraction is a computational technique which can be used to obtain a spherocylindrical prescription that best corrects the subject's vision from a single measurement of ocular wavefront aberrations [1, 2]. The goal is to match the clinical subjective refraction, which has long been the gold standard in optometric practice [1–6], in spite of being a lengthy procedure of relatively poor precision (95% limits of interexaminer agreement of the spherical equivalent 0.62 to 0.75D [4–7]—roughly twice the value reported for wavefront refractions) [4, 7, 8].

In a perfect optical system, a spherical wavefront from an object point should converge to a single point at the desired image location, such as the retina of the eye. In the presence of optical aberrations, however, the wavefront becomes distorted from its spherical shape which degrades the quality of the retinal images [7]. The wavefront error (WFE) is the optical path difference between the aberrated and the ideal, unaberrated wavefront. Because the WFE is measured for the whole area of the pupil, wavefront aberrometers are especially useful for the evaluation of refractive surgery cases, customized ablations, orthokeratology, and similar applications [4, 9, 10]. In daily optometric practice, however, wavefront refraction with these devices tends only to be used to estimate a starting point for subjective refraction [11].

Objective wavefront refraction is based on fitting a reference wavefront produced by an optimum, spherocylindrical lens to a two-dimensional ocular wavefront aberration function measured for a subject's eye. As described by Thibos et al. [7], there are two main categories of methods (hereafter called "metrics") of finding such spherocylindrical lens.

The first category, which they refer to as "refraction based on the principle of equivalent quadratic" is based on fast and relatively simple computations of Zernike coefficients, which

are used to describe the wavefront aberration function in the plane of the pupil. The second category, called "refraction based on maximizing optical or visual quality" is based on far more computationally intensive calculations of optical transfer functions and analyses of images in the plane of the retina using Fourier or geometrical optics. For instance, the VSOTF (visual Strehl ratio calculated from the optical transfer function [7, 12–15]) method can easily take a modern machine 1000 times longer to compute (e.g., 500 ms), as it involves many intermediate steps, such as calculations of normal and diffraction-limited pupil functions, their Fourier transforms, and ratio.

Additionally, the image-plane metrics are no longer directly tied by means of a mathematical formula to basic ocular aberrations, such as defocus, astigmatism, or SA, which are fundamental at the time of prescribing a refraction correction. All these methods from both categories have been widely used to predict subjective refraction not only in normal eyes studies [12–15] but also in peripheral refraction studies [16, 17], in eyes that have undergone refractive surgery [18], contact lenses [19], and even to study the accommodation response [20–22], among many others.

Although the continued development of aberrometers has made wavefront refraction a fast procedure with even better repeatability and precision [1, 4, 7], the accuracy of the technique is still a problem without a simple solution. Thibos (Indiana University) illustrated this by saying "We are aiming a gun (objective refraction) that does not shoot straight at a moving target (subjective refraction)." The "gun" does not shoot straight because objective refraction depends on the metric that is used to obtain it from the WFE, and these are known to suffer from bias [7]. On the other hand, the "target" is moving because subjective refraction changes with pupil size, especially in the presence of spherical aberration (SA), and depends on the level of illumination during measurement [23, 24]. Consequently, the spherocylindrical correction obtained via subjective refraction in clinical conditions does not exactly correspond to the best correction obtained using an aberrometer under different conditions (target size, illumination, cycloplegia, and so forth).

The purposes of the present study were to develop an objective refraction metric based on Zernike coefficients and pupil radius, which would be an accurate predictor of clinical, subjective refraction, and to address the variability between subjective and objective wavefront refraction. We propose a relatively simple pupil-plane formula of a metric that can provide a clinician with an accurate refraction value for a known pupil radius that the subject will typically have. Image-plane metrics were not considered in the present study, which does not in any way deny their huge usefulness in fundamental research, image processing, and other applications. In addition, given that the equivalent sphere is, in most cases, the most important value in the refraction, the study is limited for the sake of simplicity to the prediction of the SE. At the end of the Introduction section, formulas to extend the methodology and to apply it to the whole spherocylindrical refraction are provided ((14) and (15)).

2. Methods

2.1. Overview of the Datasets. The database of eyes of the present study is an amalgamation of wavefront and subjective refraction data from 4 independent, previously published datasets; the summary of which is presented in Table 1. All subjects were free of any kind of ocular disease and have never had refractive surgery. The data consisted of pupil diameters, signed Zernike coefficients through the fifth or sixth order, and subjective refraction data (sphere, axis, and cylinder) for each individual eye. Subjective refractions were in all cases performed manually, starting from autorefraction, using the standard optometric protocol of maximum plus, to the best visual acuity.

Out of the whole database of 2560 eyes collected by Salmon and van de Pol [25], only the A dataset was included because it contained subjective refraction data compatible with the present study. The eyes were not dilated, and the subjective refraction pupil radius was not known. In case of the H dataset, the eyes were dilated with 1% tropicamide, and the subjective refractions were performed at the same pupil size as the wavefront measurements. In case of the M dataset, the eyes were not dilated and the subjective refraction pupil radius was not known. Six eyes out of 180 had to be excluded from the original dataset, because an in-depth data analysis revealed that the subjects did not perform the accommodation task of the original study correctly. Together, the three datasets formed the AHM dataset of 308 eyes, which was used to develop the objective refraction metric proposed by the present study.

The IND dataset of 200 eyes was used to independently validate the results because the methodology to obtain the data was distinct. After performing initial subjective refractions, accommodation was paralyzed with 0.5% cyclopentolate. The eyes were then optimally corrected for astigmatism, and their hyperfocal points were conjugated with the retina with trial lenses. This correction was worn by the subjects during the subsequent aberrometry. This experimental design emphasized the effects of higher-order aberrations by minimizing the presence of uncorrected second-order aberrations.

The effects of longitudinal chromatic aberration between the wavelength of the infrared measurement beam and visible light, depth of diffuse reflection of infrared light in the choroid [27], and any other internal offsets of the apparatus were taken into account in the data.

2.2. Traditional Pupil-Plane Metrics of Objective Wavefront Refraction. The two metrics most widely used in practice, which belong to the category of *wavefront refraction based on the principle of equivalent quadratic*, are paraxial curvature matching at the pupil center (paraxial or Seidel refraction) and paraboloid least squares fitting over the full pupil area (minimum RMS or Zernike refraction) [7]. In both cases, the equivalent sphere is computed from Zernike coefficients C_n^m and pupil radius r_0. Aberrometers typically express the wavefront as an expansion of coefficients up to the sixth order [28].

Table 1: Summary of datasets of eyes included in the study.

Dataset	Number of eyes OD/OS (total)	Mean age	Cycloplegia	Pupil diameter	Aberrometer
Army [25] (A)	47/47(94)	29.9 ± 7.6	No	5.0 mm	COAS
Houston [26] (H)	20/20(40)	26.4 ± 7.7	Tropicamide 1%	7.4 ± 0.5 mm	COAS
Murcia [20] (M)	87/87(174)	35.0 ± 12.4	No	5.5 ± 0.9 mm	irx3
(AHM)	154 subjects, 308 eyes				
Indiana [7] (IND)	100/100(200)	26.1 ± 5.6	Cyclopentolate 0.5%	>7.5 mm (140 eyes) >6.0 mm (60 eyes)	Custom

Zernike refraction (hereafter called the "minRMS metric," with equivalent sphere M_{minRMS}) takes into account the Zernike higher-order aberrations (HOA). For this metric, the equivalent sphere is computed as follows:

$$M_{\text{minRMS}} = \frac{-4\sqrt{3}C_2^0}{r_0^2}, \tag{1}$$

where C_2^0 is the Zernike defocus coefficient and r_0 is the actual pupil radius.

The minRMS metric fits a paraboloid of revolution to the measured ocular wavefront in such a way that the root mean square error between the two is minimized for the whole area of the pupil. It was found to exhibit a systematic, myopic bias of roughly 0.4D [7] and becomes more myopic in the presence of large values of SA [29, 30].

Paraxial refraction (hereafter called the "paraxial metric," with equivalent sphere M_{paraxial}) takes into account only the curvature of the wavefront at the pupil center. It is not affected by SA because it does not take into account the peripheral rays. There is evidence, however, that for large pupils, high-contrast objects (as is the case in night vision), and in presence of fourth-order SA, the refractive error may become negative as the eye becomes more myopic [31]. In this case, the paraxial metric yields a hyperopic prediction of subjective refraction.

$$M_{\text{paraxial}} = \frac{-4\sqrt{3}C_2^0 + 12\sqrt{5}C_4^0 - 24\sqrt{7}C_6^0}{r_0^2}, \tag{2}$$

where C_4^0 and C_6^0 are, respectively, the fourth- and sixth-order Zernike spherical aberration coefficients, which contribute to the central curvature of the wavefront because they are *balanced* [32]. This gives rise to a difference of the values of equivalent spheres predicted by both metrics when SA is present in the eye.

In the absence of higher-order aberrations, minRMS and paraxial refractions are identical [13]. Both metrics give predictions of equivalent spheres that match for small pupils, and Campbell [6] reported their excellent agreement with subjective refractions for 4 mm pupils. Both metrics can be expressed by a more general formula in (3). For example, the minRMS equivalent sphere formula from (1) can be obtained from it when $n = 1$.

$$M_{\text{paraxial}} = \frac{2}{r_0^2}\sum_{n=1}^{\infty}(-1)^n\frac{(n+1)!}{(n-1)!}\sqrt{2n+1}C_{2n}^0, \tag{3}$$

where C_{2n}^0 is the radially symmetrical Zernike coefficients of the wavefront, r_0 is the actual pupil radius, and n is the Zernike order.

In the case of aberrated eyes, Thibos et al. [7] suggest that the clinical subjective refraction should lie somewhere between the paraxial and minRMS refractions, which is in agreement with other reports [14, 15].

2.3. Analytical Derivation of the New Objective Wavefront Refraction Metric. To compute an equivalent sphere from a two-dimensional wavefront aberration function, it is first expressed in terms of Zernike polynomials [28].

$$W(r) = \sum_{n=0}^{\infty} C_{2n}^0 Z_{2n}^0\left(\frac{r}{r_0}\right), \tag{4}$$

where C_{2n}^0 is the Zernike coefficients of the wavefront, $\rho = r/r_0$ is the normalized distance from the origin in the pupil plane, r_0 is the actual pupil radius, and $r \in [-r_0, r_0]$. Z_{2n}^m is a radially symmetric basis functions.

$$\begin{aligned} Z_2^0(\rho) &= \sqrt{3}\left(2\rho^2 - 1\right), \\ Z_4^0(\rho) &= \sqrt{5}\left(6\rho^4 - 6\rho^2 + 1\right), \\ Z_6^0(\rho) &= \sqrt{7}\left(20\rho^6 - 30\rho^4 + 12\rho^2 - 1\right), \ldots. \end{aligned} \tag{5}$$

For the sake of simplicity, the present study is focused on finding the equivalent sphere, the derivation is limited to terms with radial symmetry ($m = 0$, and n is even), and the coefficients are truncated after the sixth order [32, 33].

The equivalent sphere is found by approximating the wavefront in (4) by a sphere of radius R, centered at $(R, 0, 0)$.

$$S(r) = W(0) + R - \sqrt{R^2 - r^2} = W(0) + \frac{r^2}{R + \sqrt{R^2 - r^2}}. \tag{6}$$

The equivalent sphere, $M = -1/R$, is expressed as a function of both the Zernike coefficients and the pupil radius r_0. One simple way to approximate the wavefront by a sphere is to make them coincide in three prescribed points (nodes): the origin and the two points symmetrical with respect to the origin, located within the interval $[-r_0, r_0]$.

The position of the nodes can be written as $-r_0 t, 0$, and $+r_0 t$, where $t \in [0, 1]$ is a parameter that controls the distance from the origin, at which the wavefront is "matched," or interpolated. Seeking an explicit expression

for M, both equations (W and S) are replaced by their corresponding second-order interpolating polynomials, matching both the wavefront and the fitted sphere at each of the three nodes.

The polynomial interpolating S at the three nodes is formed by substituting r with $r_0 t$.

$$\widehat{S}(r) = W(0) + \frac{r^2}{R + \sqrt{R^2 - r_0^2 t^2}}. \tag{7}$$

Both $S(r)$ and its interpolating polynomial $S(r)$ take the same values at 0 and $\pm r_0 t$.

Similarly, the polynomial interpolating W at the three nodes is

$$\widehat{W}(r) = W(0) + \frac{2\Delta(t)}{r_0^2} r^2, \tag{8}$$

where

$$\Delta(t) \coloneqq \sqrt{3}C_2^0 + 3\sqrt{5}C_4^0\left(t^2 - 1\right) + \sqrt{7}C_6^0\left(10t^4 - 15t^2 + 6\right). \tag{9}$$

Well-known formulas for the Lagrange interpolation can be used to calculate $\widehat{W}(r)$; however, it is easier to verify the expression in (9) by taking into account that both $W(r)$ truncated after the sixth order and its interpolating polynomial $W(r)$ take the same values at 0 and $\pm r_0 t$.

As the last step or the derivation, S and W are equated and solved for R.

$$R(t) = \mathrm{t}^2\Delta(t) + \frac{r_0^2}{4\Delta(t)} \approx \frac{r_0^2}{4\Delta(t)}. \tag{10}$$

The term $t^2\Delta(t)$ can be dropped in case of a human eye, as it is much smaller than the term following it, because r_0 is several millimeters and $\Delta(t)$ is of an order of microns.

Finally, the formula for the spherical equivalent M is as follows:

$$M(t) = \frac{-1}{R}(t) = \frac{-4\Delta(t)}{r_0^2} = \frac{-4\sqrt{3}C_2^0 - 12\sqrt{5}C_4^0\left(t^2 - 1\right) - 4\sqrt{7}C_6^0\left(10t^4 - 15t^2 + 6\right)}{r_0^2}. \tag{11}$$

This formula defines a one-parameter family of spherical equivalents: the parameter t controls the position of the nodes at which the equivalent sphere matches the wavefront aberration function (Figure 1), and so, the previously described minRMS and paraxial metrics can be obtained from (11), depending on the value of t.

(a) When $t = 0$, the sphere is fit at the center of the wavefront, and (11) becomes identical to (2) (paraxial metric).

(b) When $t = 1$, the sphere is fit to the center and extremes of the wavefront (Figure 1) and (11) corresponds approximately to (1) (minRMS metric).

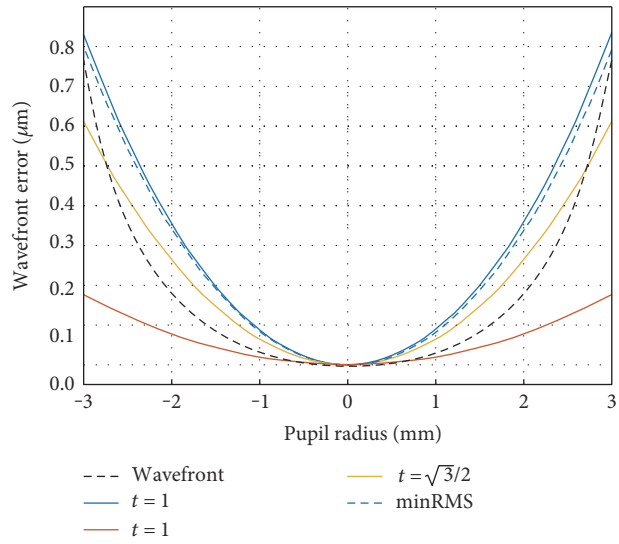

Figure 1: Example profiles of spherical and paraboloid fits (dashed blue line: minRMS; red line: $t = 0$; blue line: $t = 1$; orange line: $t = \sqrt{3}/2$) to radially symmetrical wavefront (represented by the black dotted line, where $C_2^0 = 0.220\,\mu$m, $C_4^0 = 0.050\,\mu$m, $C_6^0 = 0.0025\,\mu$m, and $r_0 = 3$ mm).

$$M(1) = \frac{-4\sqrt{3}C_2^0 - 4\sqrt{7}C_6^0}{r_0^2} \approx \frac{-4\sqrt{3}C_2^0}{r_0^2}. \tag{12}$$

The approximation by means of dropping the last term is justified by the fact that sixth-order SA is usually very low in human eyes [33]. This approximation is shown in Figure 1 and validated experimentally later (Figure 2).

(c) When an intermediate value is used, for instance $t = \sqrt{3}/2$, (11) becomes

$$M\left(\frac{\sqrt{3}}{2}\right) = \frac{-4\sqrt{3}C_2^0 + 3\sqrt{5}C_4^0 + 36\sqrt{7}C_6^0}{r_0^2}. \tag{13}$$

In this case, the nodes $-\sqrt{3}/2$, 0, and $+\sqrt{3}/2$ correspond to the zeros of the cubic Chebyshev polynomial of the second kind, which are known to provide a quasi-optimal set of interpolation nodes [34].

Figure 1 shows the example profiles of spherical and paraboloid fits to a radially symmetrical wavefront, described by (4). All of the profiles have been fixed to coincide at the apex of the wavefront.

The paraxial fit ($t = 0$) matches the wavefront well at the pupil center but does not take into account the shape of the wavefront for intermediate and peripheral areas of the pupil. On the other hand, the minRMS fit ($t = 1$) matches the wavefront well at the edge of the pupil but not at intermediate areas. The Chebyshev fit ($t = \sqrt{3}/2$) matches the wavefront at a predefined, intermediate distance from the center of the pupil.

Given a wavefront described by a set of Zernike coefficients C_2^0, C_4^0, and C_6^0 for a given r_0, (11) can be used to find

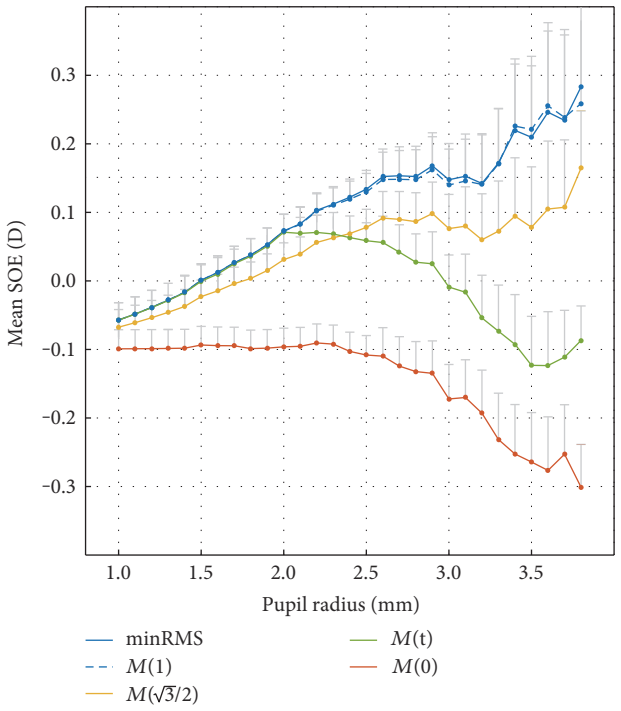

Figure 2: Mean SOE in function of the pupil radius for all 308 subjects of the AHM dataset, and for $t = 0$, 1, $\sqrt{3}/2$, $t(r)$, and additionally, the minRMS metric. The error bars represent +1 SEM.

the optimal value t_{opt}, such that $M(t_{opt})$ best approximates the $M_{subjective}$. In the present study, this approach is applied to a large database of objective and subjective refractions of real subjects.

The same methodology that was used to analytically derive the equivalent sphere M can be extended to take into account the whole spherocylindrical refraction by using power vectors [35]. Because of their orthogonality, the derivation can be performed for two orthogonal directions, corresponding to the higher and lower curvatures of the wavefront. The values of J_0 and J_{45} can be obtained in a similar way as M in (11), by taking into account the constant coefficients that multiply $\rho^2 \cos(\theta)$ and $\rho^2 \sin(\theta)$ within each Zernike polynomial.

$$J_0(t) = \frac{-2\sqrt{6}C_2^2 - 6\sqrt{10}C_4^2\left(t^2-1\right) - 2\sqrt{14}C_6^2\left(10t^4 - 15t^2 + 6\right)}{r_0^2}. \tag{14}$$

$$J_{45}(t) = \frac{-2\sqrt{6}C_2^{-2} - 6\sqrt{10}C_4^{-2}\left(t^2-1\right) - 2\sqrt{14}C_6^{-2}\left(10t^4 - 15t^2 + 6\right)}{r_0^2}. \tag{15}$$

The complete spherocylindrical refraction can be obtained using (11), together with (14) and (15), as described by Thibos et al. [35] (see Equation 23 hither).

2.4. Numerical Definition of the New Objective Wavefront Refraction Metric. In the previous section, the analytical relationship between a fitted equivalent sphere $M(t_{opt})$ that optimally approximates $M_{subjective}$ was established. In order to find the relationship between the parameter t_{opt} and objective refraction pupil radius r_0 (while subjective refraction pupil radius is unknown), the following data processing methodology was applied to the AHM dataset of 308 eyes:

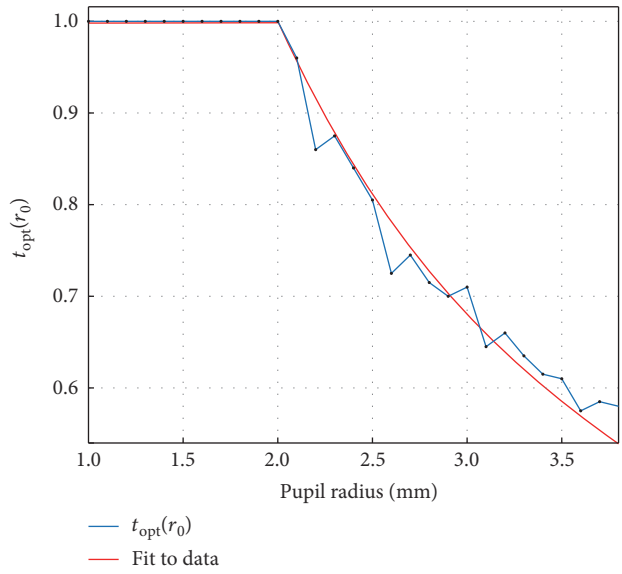

Figure 3: Change of the optimum value of t with objective pupil radius r_0 and the segmented fit of the data.

(a) For each value of pupil radius r_0 from 1.0 mm to 3.8 mm (increment of 0.1 mm) and each value of parameter t from 0 to 1 (increment of 0.05), (11) was applied to the Zernike coefficients of every eye to obtain equivalent sphere values.

(b) The difference between subjective and objective refraction (hereafter called subjective minus objective error (SOE)) was calculated for each eye and the combination of r_0 and t.

(c) For each value of r_0, the mean absolute SOE for all eyes was calculated, and the value of parameter t that minimized that mean was selected as t_{opt} for that pupil radius.

In order to obtain the Zernike coefficients corresponding to each pupil radius in step (a), rescaling [36, 37] was performed from larger to smaller pupil radii [38]. Figure 3 presents the change of t_{opt} in function of objective refraction pupil radius r_0 and a segmented fit to the data.

Figure 3 illustrates that for pupils that were small during aberrometry, t_{opt} approaches 1 (minRMS metric), while for large pupils, it decreases, and the slope becomes less negative as the pupil gets larger. A segmented fit to the discrete values of the function $t_{opt}(r_0)$ was performed, and finally, the MTR metric in (17) was obtained.

$$\text{MTR} = \frac{-4\sqrt{3}C_2^0 - 12\sqrt{5}C_4^0\left(t^2-1\right) - 4\sqrt{7}C_6^0\left(10t^4 - 15t^2 + 6\right)}{r_0^2}, \tag{16}$$

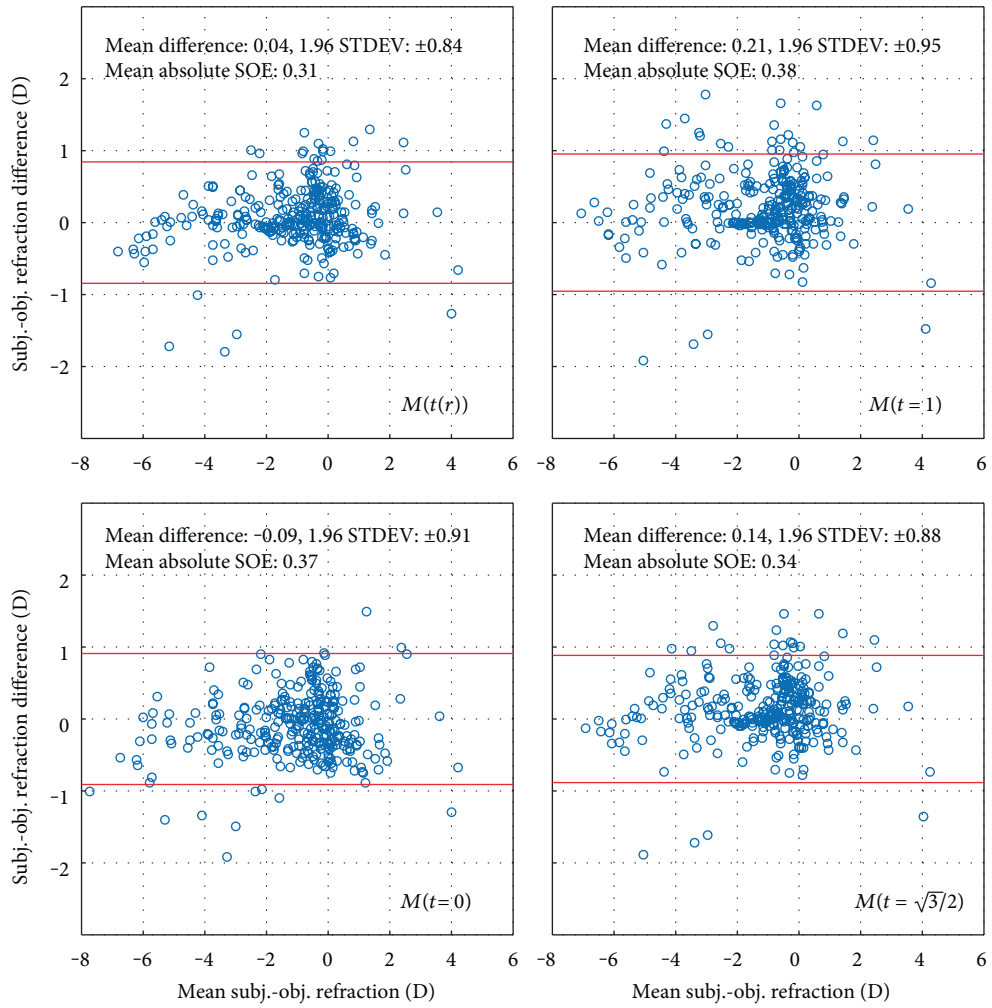

FIGURE 4: Bland-Altman plots [39] illustrating the accuracy of the prediction of subjective refraction in the AHM dataset for different values of parameter t. The data was obtained from WFE without any rescaling of the pupil radii to a common value.

$$t_{\text{opt}}(r_0) = \begin{cases} 1, & r_0 < 2 \\ \dfrac{2}{r_0}, & r_0 \geq 2 \end{cases}, \tag{17}$$

which gives the result in diopters when C_2^0, C_4^0, and C_6^0 are expressed in microns and the pupil radius, r_0, is in millimeters.

As described in Section 2.2, the traditional minRMS and paraxial metrics can be obtained from (11), by using fixed values of $t = 0$ and $t = 1$, respectively. The special case where the parameter t is a function of r_0, is hereafter referred to as $M[t(r)]$ or, for short, the MTR metric. When the plural form "MTR metrics" is used, the whole family of metrics, where t can be either a discrete value or a function of the pupil radius, is being referred to.

3. Results

Figure 4 presents the accuracy of the prediction of subjective refraction in the AHM dataset for different values of parameter t in form of Bland-Altman plots [39], where the difference between the subjective and objective refraction is plotted in the function of their mean value. Data for the minRMS metric is not shown because the results are practically identical (Figures 1 and 2) to those obtained with the $M(t = 1)$ metric. No rescaling of Zernike coefficients to a common value of the pupil radius was performed. Each data point represents the SOE value of a corresponding eye, calculated from the Zernike coefficients of the natural pupil radius.

Figure 2 shows the mean SOE as a function of the pupil radius for all 308 subjects of the AHM dataset, for $t = 0$, 1, and $\sqrt{3}/2$, $t_{\text{opt}} = f(r_0)$, and additionally, the classic minRMS metric.

Finally, in order to validate the results using an independent dataset, Figure 5 shows the mean SOE values calculated using the four MTRs for $t = 0$, $\sqrt{3}/2$, and 1 and $t_{\text{opt}} = f(r_0)$ in the IND dataset of 100 left and 100 right eyes (Table 1). This dataset is called independent because it has not been included in the numerical definition of the MTR metric described in Section 2.1.

As described in Section 2.1, the eyes in the IND dataset were paralyzed using 0.5% cyclopentolate, and optimally corrected for astigmatism. Their hyperfocal points were

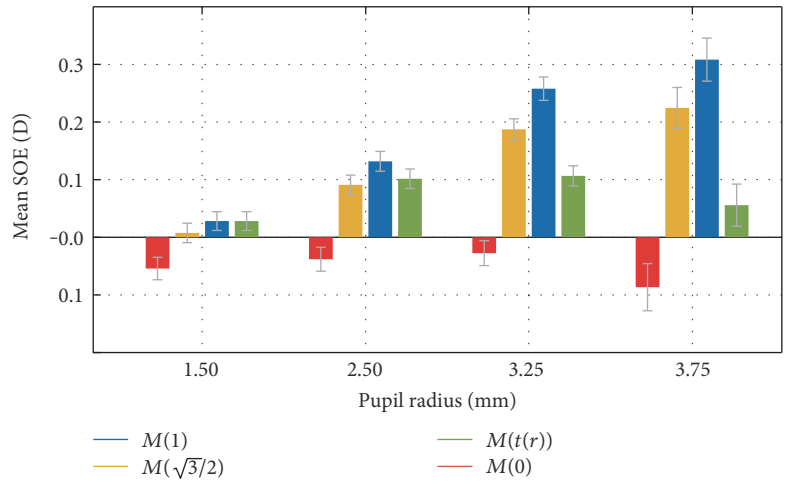

Figure 5: Application of the four MTR metrics to an independent IND dataset (Indiana in Table 1). The error bars represent ±1 SEM.

conjugated with the retina with trial lenses. Consequentially the values of $M_{\text{subjective}}$ were 0D for this dataset, and the mean SOE in Figure 5 represents the objective spherical equivalent values with the opposite sign. Even though the 100 left and 100 right eyes in the IND dataset cannot be treated as 200 independent eyes, there were no significant differences between the results obtained with the 4 metrics when they were applied to the subsets of 100 left and 100 right eyes separately.

4. Discussion

The present study presents an analytical derivation of a new, general formula (11) for the calculation of the spherical equivalent from the WFE. The formula includes the paraxial metric and a close approximation of the minRMS metric (12) as particular cases, where the value of the parameter t is a scalar number (0 and 1, resp.). Additionally, a relation between the optimum value of the parameter t and the objective refraction pupil radius r_0 is presented as the function $t_{\text{opt}}(r_0)$ ((17), illustrated in Figure 3). This function was obtained empirically from subjective refraction data from 308 eyes, measured following standard clinical protocols and under standard illumination conditions.

The Bland-Altman plots in Figure 4 show that for natural pupil radii (without rescaling the WFE), the mean difference between the values of subjective and objective refraction was the smallest for the MTR metric, although not by a large margin.

Figure 2 presents the mean intersubject SOE in the function of the pupil radius, which was obtained by rescaling [36, 37] the WFE before calculating the metrics. For small pupil radii (up to 2 mm), the HOA are small and do not noticeably affect the objective refraction, so that all of the metrics give similar results. For example, for $r_0 = 1$ mm, the difference between predictions of subjective refraction between the minRMS and paraxial metrics is merely 0.05D. For pupil radii up to 2 mm, the minRMS metric predicts subjective refraction slightly better than the paraxial metric. For such small pupils, the absolute SOE is similar for both the minRMS and paraxial metrics, and both predict subjective refraction better than the clinical precision of 0.25D.

Furthermore, Figure 2 indicates that rescaling the wavefront to correspond to the radius of 1.5 mm and applying the minRMS metric can be very successfully used to calculate refraction. This result is in agreement with results obtained by others [6, 26, 40] who found that Zernike refraction is a good predictor of subjective refraction when SA is low. Indeed, (17) indicates that $t_{\text{opt}} \cdot r_0 = 2$ for $r_0 \geq 2$ mm and the MTR metric corresponds to a sphere fitted to the wavefront at 0 and ±2 mm. This means that it predicts a similar equivalent sphere as the one obtained by the minRMS metric to a wavefront rescaled to correspond to a pupil radius of 2 mm [6]. In this case, the SOE calculated for the IND dataset was 0.06 ± 0.03D, which is practically the same as the mean SOE for the MTR metric without rescaling. In Figure 5, it can be seen that its mean SOE indeed does not exceed 0.1D, even for a large pupil radii of 3.75 mm.

It is important to note, however, that the SOE of the paraxial metric $M(t = 0)$ remains constant at −0.1D for pupil radii from 1 mm to 2.5 mm. This possibly reveals an empirical calibration offset favoring the minRMS metric in aberrometer devices and demonstrates that the calibration of the apparatus used to obtain the WFE data can play a very important role in the determination of the function $t_{\text{opt}}(r_0)$, shown in Figure 3.

For large pupil radii, the refraction calculated using the paraxial metric $M(t = 0)$ is not expected to change with pupil radius (as it is based on paraxial curvature matching to the pupil center), and its increase in the hyperopic direction for $r_0 \geq 2$ mm indicates that subjective spherical equivalent slightly changes with the pupil radius. We found this change to be very small (~0.1D), and it should not affect vision in any way. Charman et al. [41] found a similar effect of the decrease of refraction with pupil size, but it was so small that they concluded that refraction practically did not change. This may explain why paraxial refraction usually gives results in good agreement with subjective refraction for large pupil radii [7, 15]. Within the same range of r_0, the $M(t = 1)$ metric suffers from a myopic increase of SOE. This trend can be

predicted from (12), by taking into account that C_4^0 and C_6^0 spherical aberration coefficients increase their values exponentially with pupil radius and their average values are positive in the AHM database, which is usually the case for normal eyes [30]. For pupil radii over 2 mm, there are clear differences in the predictions of subjective refraction depending on the value of t. In particular, for $r > 3.5$ mm, the difference can be more than 0.5D, which is clinically significant.

5. Conclusions

The present study indicates that for pupil radii less than 2 mm, all of the wavefront refraction metrics are similarly accurate in predicting the equivalent sphere (mean SOE < 0.1D). For large pupil radii, however, the mean absolute SOE can increase beyond 0.25D for traditional metrics, which is clinically significant. This is caused by two factors. First, the effects of SA for large pupil radii cause the minRMS objective refraction to become significantly too myopic. Secondly, subjective refraction increases slightly in the myopic direction for large pupil radii, which increases the SOE for paraxial objective refraction in the hyperopic direction (Figure 2).

The new MTR objective wavefront refraction metric (16-17) is designed to depend on the objective refraction pupil radius, applying more or less weight to the SA coefficients in the function of r_0.

The benefit of this methodology lies in the fact that the MTR metric allows clinicians to obtain an accurate clinical spherical equivalent value without rescaling/refitting of the wavefront coefficients. It has the potential to be developed into a metric which will be able to predict full spherocylindrical refraction for the desired illumination conditions and corresponding pupil size. Several formulas can be applied to determine the pupil size from illumination, subject's age, and type of task to be performed [42].

Disclosure

A preliminary version of this work has been presented at the VIII European Meeting on Visual and Physiological Optics (VPO 2016) and included in the proceedings.

Conflicts of Interest

All authors declare no commercial relationships and that there is no conflict of interest regarding the publication of this paper.

Acknowledgments

Mateusz Jaskulski is supported by the Marie Curie ITN grant "AGEYE" 608049 to Norberto López-Gil. The publication of the manuscript has been supported by the SACCO-ERC-2012-StG-309416 grant to Norberto López-Gil. Andrei Martínez-Finkelshtein has been supported in part by the Spanish Government together with the European Regional Development Fund (ERDF) under Grant no. MTM2014-53963-P (from MINECO), by Junta de Andalucía (the Excellence Grant no. P11-FQM-7276 and the Research Group Grant no. FQM-229), and by the Campus de Excelencia Internacional del Mar (CEIMAR) of the University of Almería. The authors would like to acknowledge and thank the following research groups and peers for kindly contributing the datasets to the present study, specifically: Gareth D. Hastings, Jason D. Marsack, L. Chi Nguyen, Han Cheng, Raymond A. Applegate (for the Houston dataset); Larry N. Thibos, Xin Hong, Arthur Bradley, and Xu Cheng (for the Indiana dataset); Vicente Fernández-Sánchez, Francisco Lara (for the Murcia dataset); Tom Salmon (for the Army dataset); and Darío Ramos López.

References

[1] L. N. Thibos, N. Himebaugh, and C. D. Coe, "Wavefront refraction," in *Borish's Clinical Refraction. Chapter 19*, W. J. Benjamin, Ed., pp. 765–787, Elsevier, Oxford, 2006.

[2] N. López-Gil, C. D. Albarrán, L. N. Thibos, and H. C. Howland, "Refracción Objetiva," in *Optometría: Principios Básicos y Aplicación Clínica. Capítulo 13*, R. Montés-Micó, Ed., Elsevier, 2011.

[3] R. B. Rabbetts and M. EAH, "Accommodation and near vision. The inadequate stimulus myopias," in *Bennett & Rabbett's Clinical Visual Optics*, R. B. Rabbetts, Ed., pp. 125–153, Elsevier, Oxford, 2007.

[4] K. Pesudovs, K. E. Parker, H. Cheng, and R. A. Applegate, "The precision of wavefront refraction compared to subjective refraction and autorefraction," *Optometry and Vision Science*, vol. 84, no. 5, pp. 387–392, 2007.

[5] T. W. Raasch, K. B. Schechtman, L. J. Davis, K. Zadnik, and CLEK Study Group. Collaborative Longitudinal Evaluation of Keratoconus Study, "Repeatability of subjective refraction in myopic and keratoconic subjects: results of vector analysis," *Ophthalmic & Physiological Optics*, vol. 21, pp. 376–383, 2001.

[6] C. E. Campbell, "Determining spherocylindrical correction. Using four different wavefront error analysis methods: comparison to manifest refraction," *Journal of Refractive Surgery*, vol. 26, no. 11, pp. 881–890, 2010.

[7] L. N. Thibos, X. Hong, A. Bradley, and R. A. Applegate, "Accuracy and precision of objective refraction from wavefront aberrations," *Journal of Vision*, vol. 4, pp. 329–351, 2004.

[8] T. O. Salmon, R. W. West, W. Gasser, and T. Kenmore, "Measurement of refractive errors in young myopes using the COAS Shack-Hartmann aberrometer," *Optometry and Vision Science*, vol. 80, pp. 6–14, 2003.

[9] E. Moreno-Barriuso, J. M. Lloves, S. Marcos, R. Navarro, L. Llorente, and S. Barbero, "Ocular aberrations before and after myopic corneal refractive surgery: LASIK-induced changes measured with laser ray tracing," *Investigative Ophthalmology & Visual Science*, vol. 42, pp. 1396–1403, 2001.

[10] M. Faria-Ribeiro, R. Navarro, N. López-Gil, and J. M. González-Méijome, "Morphology, topography, and optics of the orthokeratology cornea," *Journal of Biomedical Optics*, vol. 21, article 75011, 2016.

[11] K. A. Lebow and C. E. Campbell, "A comparison of a traditional and wavefront autorefraction," *Optometry and Vision Science*, vol. 91, no. 10, pp. 1191–1198, 2014.

[12] R. A. Applegate, J. D. Marsack, and L. N. Thibos, "Metrics of retinal image quality predict visual performance in eyes with

20/17 or better visual acuity," *Optometry and Vision Science*, vol. 83, no. 9, pp. 635–640, 2006.

[13] J. Martin, B. Vasudevan, N. Himebaugh, A. Bradley, and L. Thibos, "Unbiased estimation of refractive state of aberrated eyes," *Vision Research*, vol. 51, no. 17, pp. 1932–1940, 2011.

[14] A. Guirao and D. R. Williams, "A method to predict refractive errors from wave aberration data," *Optometry and Vision Science*, vol. 80, no. 1, pp. 36–42, 2003.

[15] X. Cheng, A. Bradley, and L. N. Thibos, "Predicting subjective judgement of best focus with objective image quality metrics," *Journal of Vision*, vol. 4, pp. 310–321, 2004.

[16] D. A. Bernsten, D. O. Mutti, and K. Zadnik, "Validation of aberrometry-based relative peripheral refraction measurements," *Ophthalmic and Physiological Optics*, vol. 28, no. 1, pp. 83–90, 2008.

[17] R. C. Bakaraju, C. Fedtke, K. Ehrmann, D. Falk, V. Thomas, and B. A. Holden, "Peripheral refraction and higher-order aberrations with cycloplegia and fogging lenses using the BHVI-EyeMapper," *Journal of Optometry*, vol. 9, no. 1, pp. 5–12, 2016.

[18] K. P. Thompson, P. R. Staver, J. R. Garcia, S. A. Burns, R. H. Webb, and R. D. Stulting, "Using interWave aberrometry to measure and improve the quality of vision in LASIK surgery," *Ophthalmology*, vol. 111, no. 7, pp. 1368–1379, 2004.

[19] N. López-Gil, J. F. Castejón-Mochón, and V. Fernández-Sánchez, "Limitations of the ocular wavefront correction with contact lenses," *Vision Research*, vol. 49, pp. 1729–1737, 2009.

[20] N. López-Gil, V. Fernández-Sánchez, L. N. Thibos, and R. Montés-Micó, "Objective amplitude of accommodation computed from optical quality metrics applied to wavefront outcomes," *Journal of Optometry*, vol. 2, pp. 223–234, 2009.

[21] N. López-Gil and V. Fernández-Sánchez, "The change of spherical aberration during accommodation and its effect on the accommodation response," *Journal of Vision*, vol. 10, no. 13, p. 12, 2010.

[22] F. Lara, P. Bernal-Molina, V. Fernández-Sánchez, and N. López-Gil, "Changes in the objective amplitude of accommodation with pupil size," *Optometry and Vision Science*, vol. 91, no. 10, pp. 1215–1220, 2014.

[23] C. A. Johnson, "Effects of luminance and stimulus distance on accommodation and visual resolution," *Journal of the Optical Society of America A*, vol. 66, pp. 138–142, 1976.

[24] J. M. Otero, L. Plaza, and M. Ríos, "Influencia de la aberración monocromática de apertura en la miopía nocturna," *Anales de Física y Química*, vol. 44, pp. 293–304, 1948.

[25] T. O. Salmon and C. van de Pol, "Normal-eye Zernike coefficients and root-mean-square wavefront errors," *Journal of Cataract and Refractive Surgery*, vol. 32, no. 12, pp. 2064–2074, 2006.

[26] G. D. Hastings, J. D. Marsack, H. Cheng, L. C. Nguyen, and R. A. Applegate, "Evaluating objective refraction optimized with the visual Strehl image quality metric," *Investigative Ophthalmology & Visual Science*, vol. 57, no. 6255, 2016.

[27] D. F. Teel, R. J. Jacobs, J. Copland, D. R. Neal, and L. N. Thibos, "Differences between wavefront and subjective refraction for infrared light," *Optometry and Vision Science*, vol. 9, no. 10, pp. 1158–1166, 2014.

[28] American National Standards Institute (ANSI), "For ophthalmics—methods for reporting optical aberrations of eyes ANSI Z80.28 2004," 2013, http://webstore.ansi.org/.

[29] A. Bradley, R. Xu, L. N. Thibos, G. Marin, and M. Hernandez, "Influence of spherical aberration, stimulus spatial frequency, and pupil apodization on subjective refractions," *Ophthalmic & Physiological Optics*, vol. 34, no. 3, pp. 309–320, 2014.

[30] Y. Benard, N. Lopez-Gil, and R. Legras, "Optimizing the subjective depth-of-focus with combinations of fourth- and sixth-order spherical aberration," *Vision Research*, vol. 51, pp. 2471–2477, 2011.

[31] N. López-Gil, S. C. Peixoto-de-Matos, L. N. Thibos, and J. M. González-Méijome, "Shedding light on night myopia," *Journal of Vision*, vol. 12, no. 5, p. 4, 2012.

[32] V. N. Mahajan, "Systems with circular pupils," in *Aberration Theory Made Simple*, V. N. Mahajan, Ed., pp. 105–133, SPIE, 2011.

[33] G. M. Dai, "Ocular Wavefront representation," in *Wavefront Optics for Vision Correction*, G. M. Dai, Ed., SPIE, 1st edition, 2008.

[34] L. N. Trefethen, "Chebyshev polynomials and series," in *Approximation Theory and Approximation Practice. Chapter 3*, pp. 7–11, SIAM, Philadelphia, 2013.

[35] L. N. Thibos, W. Wheeler, and D. Horner, "Power vectors: an application of Fourier analysis to the description and statistical analysis of refractive error," *Optometry and Vision Science*, vol. 74, no. 6, pp. 367–375, 1997.

[36] J. Schwiegerling, "Scaling Zernike expansion coefficients to different pupil sizes," *Journal of the Optical Society of America A, Optics, Image Science, and Vision*, vol. 19, no. 10, pp. 1937–1945, 2002.

[37] L. Lundström and P. Unsbo, "Transformation of Zernike coefficients: scaled, translated, and rotated wavefronts with circular and elliptical pupils," *Journal of the Optical Society of America A*, vol. 24, no. 3, pp. 569–577, 2007.

[38] S. Bará, E. Pailos, J. Arines, N. López-Gil, and L. Thibos, "Estimating the eye aberration coefficients in resized pupils: is it better to refit or to rescale?," *Journal of the Optical Society of America A*, vol. 31, pp. 114–123, 2014.

[39] J. M. Bland and D. G. Altman, "Statistical methods for assessing agreement between two methods of clinical measurement," *Lancet*, vol. 1, no. 8476, pp. 307–310, 1986.

[40] X. Cheng, L. N. Thibos, and A. Bradley, "Estimating visual quality from wavefront aberration measurements," *Journal of Refractive Surgery*, vol. 19, pp. S579–S584, 2003.

[41] W. N. Charman, J. A. Jennings, and H. Whitefoot, "The refraction of the eye in the relation to spherical aberration and pupil size," *The British Journal of Physiological Optics*, vol. 32, pp. 78–93, 1978.

[42] A. B. Watson and J. I. Yellott, "A unified formula for light-adapted pupil size," *Journal of Vision*, vol. 12, no. 10, p. 12, 2012.

Hindawi
Journal of Ophthalmology
Volume 2017, Article ID 2190347, 10 pages
https://doi.org/10.1155/2017/2190347

Research Article

Steeper Iris Conicity Is Related to a Shallower Anterior Chamber: The Gutenberg Health Study

Alexander K. Schuster,[1] Norbert Pfeiffer,[1] Stefan Nickels,[1] Andreas Schulz,[2] Philipp S. Wild,[2,3,4] Maria Blettner,[5] Karl Lackner,[6] Manfred E. Beutel,[7] Thomas Münzel,[4,8] and Urs Vossmerbaeumer[1]

[1]*Department of Ophthalmology, University Medical Center of the Johannes Gutenberg-University Mainz, Mainz, Germany*
[2]*Preventive Cardiology and Preventive Medicine, Center for Cardiology, University Medical Center of the Johannes Gutenberg-University Mainz, Mainz, Germany*
[3]*Center for Thrombosis and Hemostasis, University Medical Center of the Johannes Gutenberg-University Mainz, Mainz, Germany*
[4]*DZHK (German Center for Cardiovascular Research), Partner Site Rhine-Main, Mainz, Germany*
[5]*Department of Biomedical Statistics, University Medical Center of the Johannes Gutenberg-University Mainz, Mainz, Germany*
[6]*Institute for Clinical Chemistry and Laboratory Medicine, University Medical Center of the Johannes Gutenberg-University Mainz, Mainz, Germany*
[7]*Department of Psychosomatic Medicine and Psychotherapy, University Medical Center of the Johannes Gutenberg-University Mainz, Mainz, Germany*
[8]*Center for Cardiology, University Medical Center of the Johannes Gutenberg-University Mainz, Mainz, Germany*

Correspondence should be addressed to Alexander K. Schuster; alexander.k.schuster@gmx.de

Received 2 April 2017; Revised 14 June 2017; Accepted 16 July 2017; Published 11 September 2017

Academic Editor: Alejandro Cerviño

Purpose. To report the distribution of iris conicity (steepness of the iris cone), investigate associated factors, and test whether pseudophakia allows the iris to sink back. *Methods.* A population-based cross-sectional study was carried out. Ophthalmological examination including objective refraction, biometry, noncontact tonometry, and Scheimpflug imaging (Pentacam®, Oculus) was performed including automated measurement of iris conicity. 3708 phakic subjects, 144 subjects with bilateral and 39 subjects with unilateral pseudophakia were included. Multivariable analyses were carried out to determine independently associated systemic and ocular factors for iris conicity in phakic eyes. *Results.* Mean iris conicity was $8.28^\circ \pm 3.29^\circ$ (right eyes). Statistical analysis revealed associations between steeper iris conicity and shallower anterior chamber depth, thicker human lens and higher corneal power in multivariable analysis, while older age was related to a flatter iris conicity. Refraction, axial length, central corneal thickness, pupil diameter, and intraocular pressure were not associated with iris conicity. Pseudophakia resulted in a 5.82° flatter iris conicity than in the fellow phakic eyes. *Conclusions.* Associations indicate a correlation between iris conicity with risk factors for angle-closure, namely, shallower anterior chamber depth and thicker human lens. In pseudophakic eyes, iris conicity is significantly lower, indicating that cataract surgery flattens the iris.

1. Introduction

Early in the history of glaucomatology, the geometry of the iris has been identified as an important factor for the understanding of aqueous humor outflow pathology, namely, for the risk of angle-closure glaucoma [1] and for the development of pigment-dispersion syndrome [2].

For almost a century, the analysis of the iris structure was restricted to examination by slit-lamp examination and gonioscopy. With the development of ultrasound biomicroscopy, quantitative examination of the anterior segment and the iris profile became possible [3, 4]. Scheimpflug imaging and anterior-segment optical coherence tomography (AS-OCT) enable the quantitative assessment of the anterior

segment, and the iris geometry acquired by noncontact examination [5, 6].

The traditional mode of thinking as trained in en face gonioscopic observation of the chamber angle was transferred into the quantitative assessment of the chamber angle revealing at the same time the restrictions of such analysis by demonstrating that the chamber angle is not a geometrically well-defined entity but rather a steeply curved surface. Our study would like to open a larger view making full use of anterior segment cross-sectional imaging modalities by introducing iris conicity as a novel term into the discussion of the anatomical architecture.

The geometry of the iris is important in several anterior segment pathologies: convex iris configuration is reported in patients with primary angle-closure, is linked to age, and is inversely to anterior chamber depth [7]. On the other hand, concave iris configuration is reported in patients with pigment dispersion syndrome and is investigated with different techniques, such as AS-OCT or ultrasound biomicroscopy [8–10].

The purpose of this study is to test the potential of Scheimpflug imaging for the assessment of the iris position in the anterior chamber (iris conicity) within an epidemiological study, but not to analyze the shape of the iris (i.e., iris convexity). The relationship between Scheimpflug imaging of the iris position and anthropometric parameters, as well as parameters of the anterior segment, is analyzed. Our hypothesis is that hyperopia is linked to a steeper conicity of the entire iris, while pseudophakia allows the iris to sink back from the cornea. The rationale behind this hypothesis is that patients with acute angle-closure are more likely to by hyperopic and a shallower anterior chamber angle might be linked to a steeper iris cone. The idea behind the "pseudophakia-hypothesis" was a recent finding by the EAGLE study [11]. This study showed that clear lens extraction is able to treat angle-closure comparable or even better than standard treatment with laser iridotomy. In addition, Siak et al. [12] reported an opening of the anterior chamber angle after cataract surgery. Therefore, one can assume that the iris sinks back by cataract surgery.

2. Materials and Methods

The Gutenberg Health Study (GHS) is a population-based, prospective, observational cohort study conducted in the Rhine-Main region in Midwestern Germany.

This study was approved by the ethics committee (Ethics Commission of the State Chamber of Physicians of Rhineland-Palatinate). According to the tenets of the Declaration of Helsinki, written informed consent was obtained from all participants prior to entering the study. The GHS is a joint project of internal medicine, ophthalmology, clinical chemistry, psychosomatic medicine, and epidemiology at the Johannes Gutenberg-University Mainz, Germany.

2.1. Study Sample. This study sample was recruited from the five-year follow-up of the GHS cohort including subjects with an age of 40 to 80 years at the time of examination. For the 5-year re-examination, Scheimpflug imaging was added. We included the first third of the total study population in this analysis; this study proportion was designed to be the representative for the region of Mainz/Mainz-Bingen at baseline examination.

We included 6138 eyes of 3708 phakic subjects (48.4% women) with a mean age of 58.7 ± 10.4 years (range 40 to 80 years) having data on Scheimpflug imaging. A detailed description of the systemic and ocular characteristics of the study population is shown in Table 1. Participants who only had cataract surgery in the past were included in the pseudophakic study group.

2.2. Exclusion Criteria. Participants with previous ocular surgery including cataract surgery were excluded from the general distribution and association analysis. Subjects with an exclusive history of cataract surgery were included in the pseudophakia study group.

2.3. Examinations. For each participant, a comprehensive ophthalmological work-up was performed including anterior segment Scheimpflug imaging (Pentacam HR, Oculus, Wetzlar, Germany) under mesopic light conditions and analysis of iris position. In addition, objective refraction (Humphrey Automated Refractor/Keratometer (HARK) 599, Carl Zeiss Meditec AG, Jena, Germany), and biometry (Lenstar LS900, Haag-Streit Diagnostics, Koeniz, Switzerland) were performed. One scan was performed per eye with each of these devices always starting with the right eye. Noncontact tonometry (Nidek NT-2000, Nidek Co., Japan) was carried out also starting with the right eye. The mean of three measurements within a 3 mmHg range was obtained for each eye. Examinations were performed by experienced study nurses in accordance with standardized operation procedures. More details of the ophthalmological study design were described by Hohn et al. [13].

Age was calculated as the difference between date of birth and date of examination. Date of birth, sex, and smoking habits were surveyed in a computer-assisted personal interview. Body height and body weight measures were performed with calibrated digital scales (Seca 862, Seca, Hamburg, Germany) and a measuring stick (Seca 220, Seca, Hamburg, Germany).

2.4. Data and Statistical Analysis. The Pentacam Scheimpflug imaging device comes with a software tool (Pentacam, v1.20r41, Oculus, Wetzlar, Germany) to measure a parameter termed "iris convexity": This is programmed to draw a straight line across the anterior profile of the iris in a way to reach equal areas under the curve above and behind this level. The crossing angle alpha of the lines of the opposite iris profiles is divided by two to reach a figure which is meant to describe "iris convexity" (Oculus, Wetzlar, Germany, personal communication). From a geometrical point of view, this describes the conicity of the iris, that is, the mean circular slope of the iris against the connecting line between the opposed chamber angles, which is mathematically the slant angle of a truncated cone (Figure 1). This means that a low value describes a gently inclined cone, while a high value represents a steep cone. We decided to use the term conicity

Table 1: Characteristics of the study sample of the Gutenberg Health Study. Means (standard deviations) and proportions in percentage (*n*/*N*) for dichotomous variables in the total cohort for males and females. CCT: central corneal thickness; IOP: intraocular pressure; OD: right eyes; OS: left eyes.

Variable	All (3708)	Men (1913)	Women (1795)
Sex (women)	48.4% (1795/3708)	0% (0/1913)	100.0% (1795/1795)
Age (y)	58.7 (10.4)	59.2 (10.4)	58.1 (10.3)
Smoking (yes)	16.4% (605/3680)	16.7% (318/1899)	16.1% (287/1781)
Body mass index (kg/m^2)	27.5 (4.8)	27.9 (4.2)	27.0 (5.4)
Height (m)	1.70 (0.09)	1.77 (0.07)	1.64 (0.07)
Weight (kg)	80.0 (16.2)	87.3 (14.2)	72.1 (14.5)
Eyes			
Spherical equivalent (dpt) (OD)	−0.41 (2.51)	−0.44 (2.52)	−0.38 (2.49)
Spherical equivalent (dpt) (OS)	−0.42 (2.53)	−0.46 (2.55)	−0.37 (2.52)
CCT (μm) (OD)	549 (35)	553 (35)	546 (35)
CCT (μm) (OS)	550 (35)	552 (35)	547 (35)
IOP (mmHg) (OD)	14.88 (2.93)	14.97 (3.00)	14.78 (2.85)
IOP (mmHg) (OS)	14.99 (2.95)	15.17 (2.98)	14.80 (2.91)
Axial length (mm) (OD)	23.7 (1.2)	24.0 (1.2)	23.4 (1.2)
Axial length (mm) (OS)	23.7 (1.3)	24.0 (1.3)	23.4 (1.2)
Lens thickness (mm) (OD)	4.37 (0.36)	4.38 (0.37)	4.36 (0.35)
Lens thickness (mm) (OS)	4.42 (0.35)	4.44 (0.36)	4.41 (0.34)
Corneal power (dpt) (OD)	44.0 (1.6)	43.6 (1.6)	44.4 (1.5)
Corneal power (dpt) (OS)	44.0 (1.6)	43.6 (1.6)	44.4 (1.5)
Anterior chamber depth (mm) (OD)	2.70 (0.36)	2.75 (0.37)	2.64 (0.34)
Anterior chamber depth (mm) (OS)	2.69 (0.36)	2.74 (0.36)	2.63 (0.35)
Mean pupil diameter (mm) (OD)	2.69 (0.45)	2.63 (0.44)	2.75 (0.46)
Mean pupil diameter (mm) (OS)	2.67 (0.44)	2.61 (0.42)	2.73 (0.45)
Iris conicity			
Iris conicity mean (°) (OD)	8.28 (3.29)	8.45 (3.26)	8.09 (3.31)
Iris conicity mean (°) (OS)	8.51 (3.27)	8.65 (3.22)	8.36 (3.32)

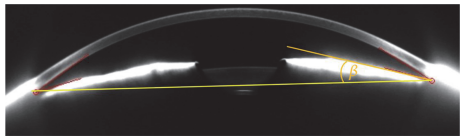

Figure 1: Illustration of iris conicity measurement. The iris surface is approximated by linear slopes (orange line). For illustration purposes, iris conicity is demonstrated. The opposite anterior chamber angles are connected by a plane (yellow line). Iris conicity is defined as the angle beta between these two lines. This corresponds to Pentacam "iris convexity" measure. Pentacam "iris convexity" is defined as half of the intersection angle of the linear slopes through the anterior surface of opposite iris cross-sections.

as it is more apt to describe the architecture of the anterior segment, while convexity by definition describes the curvature of a surface. This parameter is calculated as mean value of the Scheimpflug images.

Only Scheimpflug images with high quality were included, and all Scheimpflug measurements with a low value in the Pentacam quality score were excluded. A plausibility check was performed for all extreme values ("iris convexity" < −10° and "iris convexity" > 15°). Additionally, centration of the Scheimpflug imaging on the central cornea and opening of the eyelids were checked. Pupil size was measured simultaneously with Scheimpflug imaging. Central corneal thickness, corneal power, anterior chamber depth, lens thickness, and axial length were measured with Lenstar LS900 (Haag-Streit Diagnostics, Koeniz, Switzerland). Refraction (Humphrey Automated Refractor/Keratometer (HARK) 599, Carl Zeiss Meditec AG, Jena, Germany) was included as spherical equivalent in the analysis.

Data were processed by statistical analysis software (R version 3.3.1 [June 21, 2016]). Medians and interquartile ranges were calculated for all variables. For variables found to be nearly normally distributed, means and standard deviations were computed. Pearson's correlation coefficients were computed comparing right to left eyes with all primary and secondary variables.

Distribution of the iris conicity was evaluated using histograms. Associated factors were evaluated using linear regression models with generalized estimating equation (GEE) with consideration of the correlation structure between both eyes of the subjects. This model is applied to estimate the parameters of a generalized linear model.

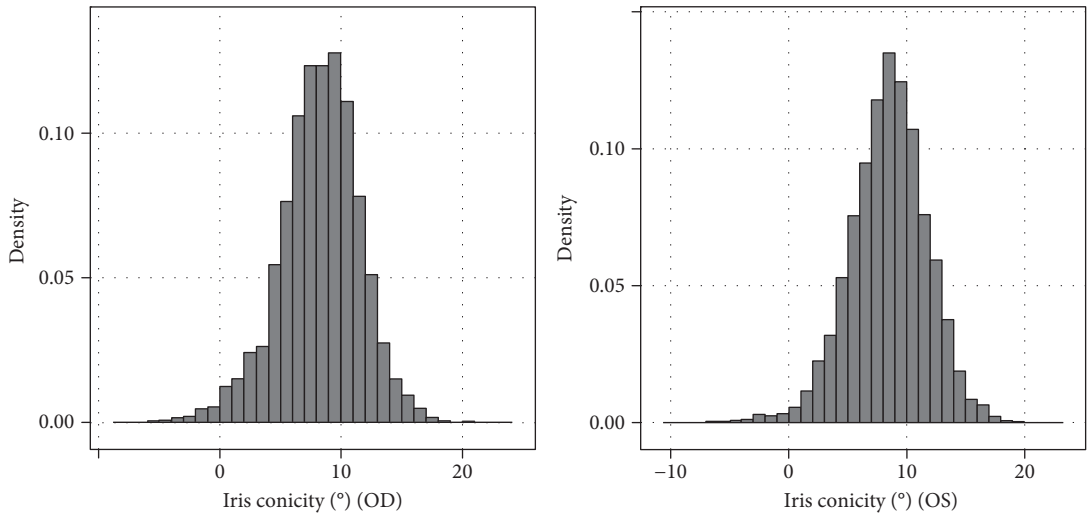

Figure 2: Distribution of iris conicity ("iris convexity," Pentacam) in the German population: the Gutenberg Health Study. (a) Right eyes. (b) Left eyes. Density is displayed as the proportion to the total study population (right eyes: 3060; left eyes: 3078).

We performed a three-step analysis: in the first model, sex, age, body height, body weight, and smoking status were included as independent variables to investigate associations to general anthropometric characteristics. In the second model, we include general ocular characteristics (intraocular pressure and spherical equivalent) as well. In the third model, anthropometric and biometric characteristics of the eye and intraocular pressure were included: The independent variables in this model were sex, age, height, weight, smoking, central corneal thickness, intraocular pressure, pupil diameter, corneal power of the steep meridian, anterior chamber depth, lens thickness, and axial length. Measurement of refraction was not included in this model due to collinearity. Multicollinearity was investigated by exploring pairwise Pearson's correlations.

Sensitivity analysis was carried out to determine the effect of refractive error by including only emmetropic eyes (sphere: $-0.5\,\text{D} \leq \times \leq 0.5\,\text{D}$), myopic eyes (sphere $< -0.5\,\text{D}$), and hyperopic eyes (sphere $> 0.5\,\text{D}$). In addition, the impact of astigmatism was evaluated with including only subjects with astigmatism $\leq -1.0\,\text{D}$ and with $> -1.0\,\text{D}$. In addition, we included corneal power instead of refraction in the multivariable model to evaluate the influence of image projection of the cornea.

This study was performed as an explorative study to analyze distribution and associations with iris conicity. All p values should be regarded as a continuous parameter which reflect the level of statistical evidence and are therefore reported exactly.

3. Results

Mean iris conicity was $8.28^\circ \pm 3.29^\circ$ (right eyes) and $8.51^\circ \pm 3.27^\circ$ with a range from -7° to 22° (Figure 2). A negative iris conicity indicates a positioning of the iris surface backwards (towards the vitreous cavity).

Comparing right to left eyes, iris conicity was highly correlated between both sides ($p < 0.001$), showing a correlation coefficient of 0.83.

Associated factors with the iris conicity were examined by a generalized estimating equation model and including only phakic eyes. The first model using sex, age, height, weight, and smoking status as independent variables showed sex ($p = 0.004$) and age ($p < 0.001$) as associated factors. The measurement of the conicity revealed a 0.35° (95% confidence interval (CI): -0.59 to -0.11; $p = 0.004$) lower inclination in women compared to men. Older subjects had a slightly flatter inclination. Each decade of age was associated with a 0.18° smaller iris conicity (per 10 years: beta $= -0.18$; 95% CI: -0.27 to -0.09; $p < 0.001$).

The second analysis model including anthropometric characteristics and general ocular characteristics, namely, intraocular pressure and refraction (spherical equivalent) showed the same associated factors as in model number 1 (Table 2), neither refraction nor intraocular pressure was associated.

The third analysis also included biometrics of the eye. It revealed that a shallower anterior chamber, higher corneal power, a thicker human lens, and younger age were associated with a steeper inclination of the iris (conicity). There was no common association with body height, body weight, smoking status, central corneal thickness, axial length, intraocular pressure, and pupil diameter in this multivariable model (Table 3). Pairwise correlation coefficients were low, indicating that there is no clear evidence for multicollinearity.

Sensitivity analysis revealed that association of iris conicity with age and lens thickness is independent of refractive status: comparable associations were found in the myopic, emmetropic, hyperopic subgroup, as in the subgroup with high astigmatism (Table 4). Interestingly, axial length was only associated with iris conicity in emmetropic and hyperopic eyes, but not in myopic eyes. In contrast, anterior chamber depth was only associated with iris conicity in the myopic subgroup, but not in the other subgroups.

Anterior chamber angle was inversely associated with iris conicity in phakic eyes (Pearson's correlation coefficient: $r = -0.46$, $p < 0.001$).

Table 2: Associations of iris conicity and anthropometric characteristics and intraocular pressure (IOP) and refraction in the Gutenberg Health Study using a generalized estimating equation model to incorporate correlations between right and left eyes. CI: confidence interval.

Iris conicity (°)	Beta estimate	Lower 95% CI	Upper 95% CI	p value
Sex (female)	−0.36	−0.61	−0.11	**0.005**
Age (y)	−0.02	−0.02	−0.01	**0.00**2
Height (m)	−0.59	−2.00	0.83	0.42
Weight (kg)	0.00	−0.01	0.01	0.95
Smoking	0.25	0.01	0.49	**0.045**
Intraocular pressure (mmHg)	−0.02	−0.05	0.01	0.18
Spherical equivalent (dpt)	0.00	−0.04	0.04	0.95

Table 3: Associations of iris conicity and anthropometric and ocular characteristics including ocular geometric parameters in the Gutenberg Health Study. We used a generalized estimating equation model to consider correlations between right and left eyes in our statistical model. CI: confidence interval.

Iris conicity (°)	Beta estimate	Lower 95% CI	Upper 95% CI	p value
Sex (female)	−0.32	−0.56	−0.07	**0.011**
Age (y)	−0.07	−0.08	−0.06	**<0.001**
Height (m)	0.99	−0.40	2.38	0.16
Weight (kg)	0.00	0.00	0.01	0.51
Smoking	0.03	−0.20	0.26	0.79
Intraocular pressure (mmH)	−0.03	−0.07	0.00	0.052
Corneal power (dpt)	0.09	0.03	0.16	**0.003**
Anterior chamber depth (mm)	−0.71	−1.05	−0.37	**<0.001**
Central corneal thickness (μm)	0.00	0.00	0.00	0.53
Lens thickness (mm)	2.77	2.43	3.10	**<0.001**
Axial length (mm)	−0.05	−0.15	0.04	0.26
Mean pupil diameter (μm)	−0.10	−0.31	0.11	0.34

Mean iris conicity was $0.74 \pm 2.52^\circ$ in right pseudophakic eyes and $0.77 \pm 2.61^\circ$ in left pseudophakic eyes. When comparing right phakic ($n = 2914$) to right pseudophakic eyes ($n = 135$), iris conicity was 7.54° lower in the pseudophakic eyes ($p < 0.001$). A similar finding was detected in left eyes: iris conicity was 7.74° lower in pseudophakic left eyes ($n = 144$) compared to phakic left eyes ($n = 2936$; $p < 0.001$).

When analyzing subjects with one phakic eye and the fellow eye being pseudophakic ($n = 39$), iris conicity was 5.82° smaller in the pseudophakic eyes (95% confidence interval: -7.66°; -3.98°; paired t test: $p < 0.001$) (Figure 3). An example is given in Figure 4.

4. Discussion

To the best of our knowledge, this is the first study to quantitatively analyze iris conicity in a population-based setting using Scheimpflug imaging. We found a mean iris conicity of $8.28^\circ \pm 3.29^\circ$ for right eyes and $8.51^\circ \pm 3.27^\circ$ for left eyes.

When analyzing anthropometric and ocular parameters (refraction, intraocular pressure), the model showed female gender and higher age as independent associated factors with a flatter iris conicity in the multivariable model, showing that both are related to iris conicity. To our surprise, refraction was not found to be associated with iris conicity. Corneal curvature was associated with iris conicity: a 10-diopter higher corneal power was associated with a 0.9° steeper iris inclination which may, however, not be of clinical relevance.

While several studies investigated anterior chamber angle width using Scheimpflug imaging, AS-OCT, or ultrasound biomicroscopy [14–19], little is known about the iris position in the anterior segment. The anterior chamber angle is formed by the posterior corneal surface and the peripheral anterior iris surface and therefore a close association between a steeper forward inclination of the iris profile and a smaller anterior chamber angle may appear likely. In agreement with this consideration, we found an inverse correlation between anterior chamber angle width and iris conicity.

Bearing this close correlation in mind, findings of our third analytical model investigating biometric parameters of the eye seem plausible. A more marked forward slope (steeper iris conicity) was independently associated with a shallower anterior chamber, higher corneal power, and a thicker crystalline lens. Similar findings for a smaller anterior chamber angle were previously reported by other groups [20, 21]. These results are similar to observations in patients with angle-closure glaucoma who tend to have a shallower anterior chamber and a thicker crystalline lens [22]. While a shallower

Table 4: Associations of iris conicity and anthropometric and ocular characteristics including ocular geometric parameters in the Gutenberg Health Study separated for refractive error (myopic eyes (sphere < −0.5 D), emmetropic eyes (sphere: −0.5 D ≤ × ≤ 0.5 D), hyperopic eyes (sphere > 0.5 D), and eyes with astigmatism >−1.0D. CI: confidence interval.

(a) Analysis of myopic subjects (N = 1688 eyes)

Iris conicity (°) ~	Beta estimate	Lower 95% CI	Upper 95% CI	p value
Sex	−0.45	−0.88	−0.02	**0.04**
Age (y)	−0.08	−0.10	−0.06	**<0.0001**
Height (m)	1.75	−0.63	4.14	0.15
Weight (kg)	0.00	−0.01	0.01	0.53
Smoking	0.23	−0.21	0.67	0.31
IOP (mmHg)	−0.02	−0.08	0.04	0.48
Corneal power (dpt)	0.04	−0.07	0.15	0.46
Anterior chamber depth (mm)	−0.77	−1.36	−0.17	**0.01**
CCT (μm)	−0.00	−0.01	0.00	0.40
Lens thickness (mm)	2.57	2.00	3.14	**<0.0001**
Axial length (mm)	−0.04	−0.20	0.13	0.67
Mean pupil diameter (mm)	−0.22	−0.59	0.15	0.25

(b) Analysis of emmetropic subjects (N = 1613 eyes)

Iris conicity (°) ~	Beta estimate	Lower 95% CI	Upper 95% CI	p value
Sex	−0.15	−0.60	0.30	0.52
Age (y)	−0.06	−0.08	−0.04	**<0.0001**
Height (m)	1.77	−0.86	4.40	0.19
Weight (kg)	0.01	−0.01	0.02	0.30
Smoking	−0.31	−0.69	0.06	0.10
IOP (mmHg)	−0.02	−0.08	0.04	0.54
Corneal power (dpt)	−0.09	−0.25	0.08	0.31
Anterior chamber depth (mm)	−0.31	−0.97	0.36	0.37
CCT (μm)	0.00	−0.00	0.01	0.59
Lens thickness (mm)	3.02	2.37	3.66	**<0.0001**
Axial length (mm)	−0.56	−0.95	−0.16	**0.006**
Mean pupil diameter (mm)	−0.08	−0.46	0.30	0.69

(c) Analysis of hyperopic subjects (N = 1980 eyes)

Iris conicity (°) ~	Beta estimate	Lower 95% CI	Upper 95% CI	p value
Sex	−0.51	−0.90	−0.11	**0.01**
Age (y)	−0.06	−0.07	−0.04	**<0.0001**
Height (m)	0.10	−2.17	2.36	0.93
Weight (kg)	−0.00	−0.01	0.01	0.80
Smoking	0.28	−0.11	0.67	0.15
IOP (mmHg)	−0.06	−0.11	−0.01	**0.02**
Corneal power (dpt)	−0.05	−0.17	0.08	0.49
Anterior chamber depth (mm)	−0.37	−0.96	0.23	0.23
CCT (μm)	−0.00	−0.01	0.00	0.47
Lens thickness (mm)	2.70	2.18	3.22	**<0.0001**
Axial length (mm)	−0.55	−0.80	−0.30	**<0.0001**
Mean pupil diameter (mm)	−0.09	−0.43	0.25	0.59

(d) Analysis of subjects with high astigmatism ($N = 659$ eyes)

Iris conicity (°) ~	Beta estimate	Lower 95% CI	Upper 95% CI	p value
Sex	0.13	−0.61	0.85	0.74
Age (y)	−0.10	−0.13	−0.07	**<0.0001**
Height (m)	1.76	−2.31	5.84	0.40
Weight (kg)	0.00	−0.01	0.02	0.90
Smoking	0.18	−0.48	0.83	0.60
IOP (mmHg)	0.04	−0.05	0.13	0.42
Corneal power (dpt)	0.09	−0.06	0.23	0.25
Anterior chamber depth (mm)	−0.89	−1.80	0.02	0.056
CCT (μm)	−0.01	−0.02	−0.00	**0.03**
Lens thickness (mm)	2.97	2.01	3.94	**<0.0001**
Axial length (mm)	0.08	−0.13	0.30	0.45
Mean pupil diameter (mm)	−0.07	−0.65	0.51	0.81

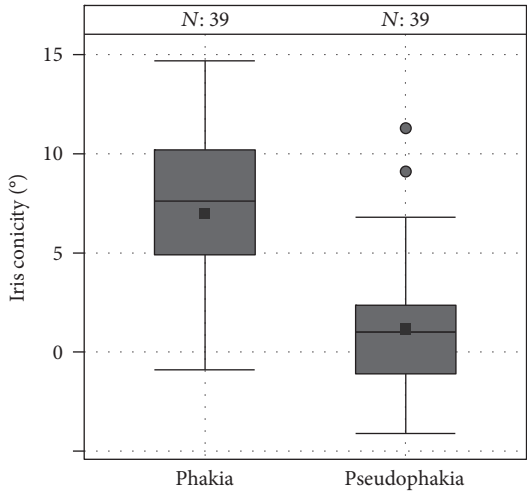

Figure 3: Box plots of iris conicity of intraindividual comparison of phakic and pseudophakic eyes in the GHS study population (N is the number of subjects with one eye having pseudophakia and the fellow eye being phakic in our study population).

anterior chamber depth was related to a steeper iris conicity in the main analysis, stratification on refractive error did yield that this is primarily visible in myopic eyes but not in emmetropic and hyperopic eyes. A decisive geometrical parameter may be the distance between the iris pigment epithelium and the anterior capsule of the crystalline lens. This however may not be approached by current noncontact imaging methods. We hence cannot state whether the observed iris conicity is determined by the flow of the aqueous humor between the anterior surface of the lens and the posterior surface of the iris or rather as a primary anatomical parameter by the intrinsic configuration of iris tissue.

Interestingly, axial length was not associated with iris conicity in the main analysis, while several studies reported an association between shorter axial length and a smaller anterior chamber angle and angle-closure glaucoma [15, 18, 23]. Nevertheless, subgroup analysis revealed an association in emmetropic and hyperopic eyes but not in myopic eyes, indicating that there might be a relationship in the physiological range of axial length. One may speculate that myopia is mainly linked to a relative elongation of the posterior segment of the eye, and therefore, a direct association may remain elusive. Also, the position of the iris root may be a determinant for the absolute conicity of the iris in so far as the accommodative state of the ciliary muscle may exert a subtle deformation. Moreover, it remains speculative whether the actual thickness of the crystalline lens is larger in a hyperopic eye compared to a myopic eye of the same absolute refractive error.

Similarly, iris conicity was not associated with central corneal thickness which is known to be linked with anterior chamber angle aperture [19, 24]. These findings indicate that iris conicity follows other rules than the mere chamber angle. While the anterior chamber angle is measured peripherally, the iris conicity indicates a spatial position of the iris in the anterior segment. However, both parameters are a geometrical reduction of complex microanatomical structure which do not lend themselves easily to a description by two straight crossing lines.

Iris configuration rather than iris position was investigated in several other studies. Iris concavity was reported to be present in pigment dispersion syndrome and pigmentary glaucoma [8]. In those eyes, peripheral sagging of the iris tissue is so marked that it leads to chafing of the pigment epithelium on the reverse side against the anterior lens capsule and zonular fibres [9]. Moderate myopia is associated with such a concave iris configuration [9, 10]. Iris contour itself is known to be changed by several physiological mechanisms, such as blinking [3], accommodation [25–28], and exercise [29, 30]. In addition, dynamic analysis of iris configuration shows changes in dark and bright light conditions [31]. Whether these factors do also influence iris position in the anterior segment is not fully understood.

There are methodological limitations to the study. First, we were not able to adjust for the potential influence of the pupil diameter on iris conicity under different lighting conditions. Imaging of the anterior segment was performed under mesopic lighting conditions without dilation of the pupil.

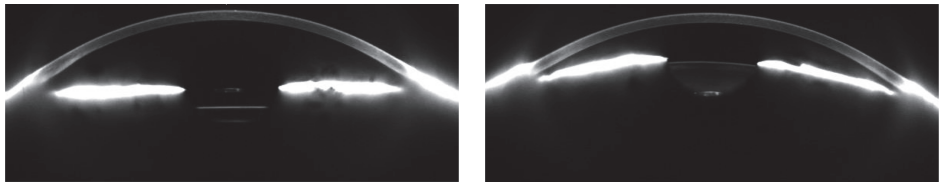

(a) (b)

Figure 4: Example of Scheimpflug images of an intraindividual comparison of a pseudophakic right eye (a) and a phakic left eye (b) in the GHS study population. Please observe the different light reflexes by the artificial intraocular lens and the crystalline lens. The iris is flat in the pseudophakic eye (a), while it is positioned towards the cornea in the phakic eye (b). This is described by iris conicity: iris conicity was −1° in the pseudophakic eye and 11° in the phakic eye.

Nevertheless, Scheimpflug imaging uses bright light source. Furthermore, we did not assess objective refraction under cycloplegic conditions; therefore, findings with respect to hyperopia might be underestimated. Also, accommodation might have influenced our results on lens thickness. However, our study cohort had an age range from 40 to 80 years. In the older age groups, the geometrical effect of accommodation on the lens configuration is limited. Also, we reported a cross-sectional analysis of associations with iris conicity and did not refer to actual changes of the iris geometry over time. Therefore age-related changes do not refer to individual changes over time. A critical look should be taken at the measurement method. We used the built-in measurement tool and performed a plausibility check for inappropriate values. Furthermore, the iris structure itself is approximated by a linear slope and intersection of opposite slopes are used to calculate the iris conicity. This measurement does not incorporate the iris profile (convex or concave configuration, plateau iris) but approximates the average iris position in the anterior segment. While this algorithm is less prone to errors than the identification of the anterior chamber angle, its value in glaucomatology is not yet established. In addition, we did not analyze a real object, namely, the iris, but its image projected by the cornea. Sensitivity analysis with incorporation of corneal power did not alter our findings. As most of our study participants were Caucasians, our conclusions should be regarded as valid for this ethnicity only.

The distribution of ocular parameters in our study population should be considered when interpreting our findings. Mean central corneal thickness (right eyes: 549 μm) was higher in the German population than in other studies [32, 33], as previously discussed [34].

Anterior chamber depth was also slightly shallower when comparing to literature. Our study showed a mean anterior chamber depth of 2.70 mm (right eyes), while Pan et al. [35] reported mean measurements of 3.15 mm for anterior chamber depth in Indian ethnicity and Lim et al. [36] 3.10 mm in Malay ethnicities. Axial length was comparable to other studies analyzing urban populations [35, 36], while in rural China and central India, axial length is shorter [37, 38]. With regard to lens thickness, our distribution was similar to literature when taking age distribution into account. The Central India Eye and Medical Study reported a lens thickness of 3.95 mm analyzing participants being a decade younger [39]. In a Burmese population for instance, lens thickness is slightly thicker (mean lens thickness 4.52 mm) than in our study [40]. Measurements of intraocular pressure are lower in our study compared to literature, as described for the baseline examination by Hoehn et al. [41] and being also true in the follow-up examination. Overall, distributions of ocular parameters in our study population were comparable to urban population, except for intraocular pressure.

In summary, we report the distribution of iris conicity using Scheimpflug imaging in a population-based study. A steeper conicity was independently associated with a shallow anterior chamber, and a thicker crystalline lens, while older persons had a flatter iris conicity. In pseudophakic eyes, iris conicity approaches 0°, showing that cataract surgery flattens the iris position.

Disclosure

Parts of this work have been presented at the ARVO Annual Meeting 2017 as a poster (Steeper iris conicity is related to a shallower anterior chamber but not to higher intraocular pressure—the Gutenberg Health Study (Schuster et al.). Investigative Ophthalmology & Visual Science June 2017, Vol. 58, 4806.).

Conflicts of Interest

The authors declare that they have no conflicts of interest.

Acknowledgments

The Gutenberg Health Study is funded through the government of Rhineland-Palatinate ("Stiftung Rheinland-Pfalz für Innovation," Contract AZ 961-386261/733) and the research programs "Wissen schafft Zukunft" and "Center for Translational Vascular Biology (CTVB)" of the Johannes Gutenberg-University of Mainz and its contract with Boehringer Ingelheim and PHILIPS Medical Systems, including an unrestricted grant for the Gutenberg Health Study. Philipp S. Wild is funded by the Federal Ministry of Education and Research (BMBF 01EO1503) and is a PI of the German Center for Cardiovascular Research (DZHK). Norbert Pfeiffer received financial support and grants from Novartis, Ivantis, Santen, Thea, Boehringer Ingelheim Deutschland GmbH & Co. KG, Alcon, and Sanoculis. Alexander K. Schuster, Stefan Nickels, Höhn R, Binder H, Andreas Schulz, Thomas Münzel, Manfred E. Beutel, and Urs Vossmerbaeumer received no funding. Alexander K. Schuster received educational support

by Santen Pharmaceutical Co., Ltd. (Osaka, Japan). Stefan Nickels received reimbursement of travel expenses from Novartis Pharma GmbH. Philipp S. Wild received research grants from Boehringer Ingelheim Deutschland GmbH & Co. KG, Daiichi Sankyo Deutschland GmbH, Bayer HealthCare-Bayer-Vital GmbH, Portavita BV, Sanofi-Aventis Deutschland GmbH, the German Ministry of Research, and the Ministry of Health of Rhineland-Palatinate. Thomas Münzel received speaker honorary from Boehringer Ingelheim Deutschland GmbH & Co. KG, Servier Deutschland GmbH, Actavis Deutschland GmbH, and Berlin Chemie Deutschland and, currently, research grants from the German Ministry of Research and the government of Rhineland-Palatinate. The authors thank all the study participants for their willingness to provide data for this research project, and they are indebted to all their coworkers for their enthusiastic commitment.

References

[1] T. Aung, W. P. Nolan, D. Machin et al., "Anterior chamber depth and the risk of primary angle closure in 2 East Asian populations," *Archives of Ophthalmology*, vol. 123, pp. 527–532, 2005.

[2] D. G. Campbell and R. M. Schertzer, "Pathophysiology of pigment dispersion syndrome and pigmentary glaucoma," *Current Opinion in Ophthalmology*, vol. 6, pp. 96–101, 1995.

[3] J. M. Liebmann, C. Tello, S. J. Chew, H. Cohen, and R. Ritch, "Prevention of blinking alters iris configuration in pigment dispersion syndrome and in normal eyes," *Ophthalmology*, vol. 102, pp. 446–455, 1995.

[4] C. J. Pavlin, K. Harasiewicz, and F. S. Foster, "An ultrasound biomicroscopic dark-room provocative test," *Ophthalmic Surgery*, vol. 26, pp. 253–255, 1995.

[5] L. Liu, E. L. Ong, and J. Crowston, "The concave iris in pigment dispersion syndrome," *Ophthalmology*, vol. 118, pp. 66–70, 2011.

[6] A. K. Schuster, J. E. Fischer, and U. Vossmerbaeumer, "Curvature of iris profile in spectral domain optical coherence tomography and dependency to refraction, age and pupil size - the MIPH Eye&Health Study," *Acta Ophthalmologica*, vol. 95, pp. 175–181, 2017.

[7] A. Nonaka, T. Iwawaki, M. Kikuchi, M. Fujihara, A. Nishida, and Y. Kurimoto, "Quantitative evaluation of iris convexity in primary angle closure," *American Journal of Ophthalmology*, vol. 143, pp. 695–697, 2007.

[8] F. N. Kanadani, S. Dorairaj, A. M. Langlieb et al., "Ultrasound biomicroscopy in asymmetric pigment dispersion syndrome and pigmentary glaucoma," *Archives of Ophthalmology*, vol. 124, pp. 1573–1576, 2006.

[9] F. Aptel, S. Beccat, V. Fortoul, and P. Denis, "Biometric analysis of pigment dispersion syndrome using anterior segment optical coherence tomography," *Ophthalmology*, vol. 118, pp. 1563–1570, 2011.

[10] S. Asrani, M. Sarunic, C. Santiago, and J. Izatt, "Detailed visualization of the anterior segment using fourier-domain optical coherence tomography," *Archives of Ophthalmology*, vol. 126, pp. 765–771, 2008.

[11] A. Azuara-Blanco, J. Burr, C. Ramsay et al., "Effectiveness of early lens extraction for the treatment of primary angle-closure glaucoma (EAGLE): a randomised controlled trial," *Lancet*, vol. 388, pp. 1389–1397, 2016.

[12] J. Siak, D. Quek, M. E. Nongpiur et al., "Anterior chamber angle and intraocular pressure changes after phacoemulsification: a comparison between eyes with closed-angle and open-angle glaucoma," *Journal of Glaucoma*, vol. 25, pp. e259–e264, 2016.

[13] R. Hohn, U. Kottler, T. Peto et al., "The ophthalmic branch of the Gutenberg health study: study design, cohort profile and self-reported diseases," *PLoS One*, vol. 10, article e0120476, 2015.

[14] Y. Barkana, I. Dekel, Y. Goldich, Y. Morad, I. Avni, and D. Zadok, "Angle closure in Caucasians—a pilot, general ophthalmology clinic-based study," *Journal of Glaucoma*, vol. 21, pp. 337–341, 2012.

[15] Y. Y. Kim, J. H. Lee, M. D. Ahn, C. Y. Kim, Namil Study Group, and Korean Glaucoma Society, "Angle closure in the Namil study in Central South Korea," *Archives of Ophthalmology*, vol. 130, pp. 1177–1183, 2012.

[16] S. Senthil, C. Garudadri, R. C. Khanna, and K. Sannapaneni, "Angle closure in the Andhra Pradesh eye disease study," *Ophthalmology*, vol. 117, pp. 1729–1735, 2010.

[17] S. H. van Romunde, G. Thepass, and H. G. Lemij, "Is hyperopia an important risk factor for PACG in the Dutch population?-a case control study," *Journal of Ophthalmology*, vol. 2013, Article ID 630481, 6 pages, 2013.

[18] L. Vijaya, R. George, H. Arvind et al., "Prevalence of angle-closure disease in a rural southern Indian population," *Archives of Ophthalmology*, vol. 124, pp. 403–409, 2006.

[19] A. K. Schuster, N. Pfeiffer, S. Nickels et al., "Distribution of anterior chamber angle width and correlation with age, refraction, and anterior chamber depth-the Gutenberg health study," *Investigative Ophthalmology & Visual Science*, vol. 57, pp. 3740–3746, 2016.

[20] H. Hashemi, M. Khabazkhoob, S. Mohazzab-Torabi et al., "Anterior chamber angle and anterior chamber volume in a 40- to 64-year-old population," *Eye & Contact Lens*, vol. 42, pp. 244–249, 2016.

[21] J. I. Fernandez-Vigo, J. A. Fernandez-Vigo, A. Macarro-Merino, C. Fernández-Pérez, J. M. Martínez-de-la-Casa, and J. García-Feijoó, "Determinants of anterior chamber depth in a large Caucasian population and agreement between intra-ocular lens Master and Pentacam measurements of this variable," *Acta Ophthalmologica*, vol. 94, pp. e150–e155, 2016.

[22] S. Yazdani, S. Akbarian, M. Pakravan, A. Doozandeh, and M. Afrouzifar, "Biometric parameters in different stages of primary angle closure using low-coherence interferometry," *Optometry and Vision Science*, vol. 92, pp. 343–349, 2015.

[23] R. F. Lowe, "Aetiology of the anatomical basis for primary angle-closure glaucoma. Biometrical comparisons between normal eyes and eyes with primary angle-closure glaucoma," *The British Journal of Ophthalmology*, vol. 54, pp. 161–169, 1970.

[24] L. Xu, W. F. Cao, Y. X. Wang, C. X. Chen, and J. B. Jonas, "Anterior chamber depth and chamber angle and their associations with ocular and general parameters: the Beijing eye study," *American Journal of Ophthalmology*, vol. 145, pp. 929–936, 2008.

[25] R. S. Adam, C. J. Pavlin, and L. J. Ulanski, "Ultrasound biomicroscopic analysis of iris profile changes with accommodation in pigmentary glaucoma and relationship to age," *American Journal of Ophthalmology*, vol. 138, pp. 652–654, 2004.

[26] S. Dorairaj, C. Oliveira, A. K. Fose et al., "Accommodation-induced changes in iris curvature," *Experimental Eye Research*, vol. 86, pp. 220–225, 2008.

[27] C. J. Pavlin, K. Harasiewicz, and F. S. Foster, "Posterior iris bowing in pigmentary dispersion syndrome caused by accommodation," *American Journal of Ophthalmology*, vol. 118, pp. 114–116, 1994.

[28] M. O. Balidis, C. Bunce, C. J. Sandy, R. P. Wormald, and M. H. Miller, "Iris configuration in accommodation in pigment dispersion syndrome," *Eye*, vol. 16, pp. 694–700, 2002.

[29] P. K. Jensen, O. Nissen, and S. V. Kessing, "Exercise and reversed pupillary block in pigmentary glaucoma," *American Journal of Ophthalmology*, vol. 120, pp. 110–112, 1995.

[30] B. Haargaard, P. K. Jensen, S. V. Kessing, and O. I. Nissen, "Exercise and iris concavity in healthy eyes," *Acta Ophthalmologica Scandinavica*, vol. 79, pp. 277–282, 2001.

[31] C. Y. Cheung, S. Liu, R. N. Weinreb et al., "Dynamic analysis of iris configuration with anterior segment optical coherence tomography," *Investigative Ophthalmology & Visual Science*, vol. 51, pp. 4040–4046, 2010.

[32] A. Tomidokoro, M. Araie, and A. Iwase, "Corneal thickness and relating factors in a population-based study in Japan: the Tajimi study," *American Journal of Ophthalmology*, vol. 144, pp. 152–154, 2007.

[33] T. Eysteinsson, F. Jonasson, H. Sasaki et al., "Central corneal thickness, radius of the corneal curvature and intraocular pressure in normal subjects using non-contact techniques: Reykjavik eye study," *Acta Ophthalmologica Scandinavica*, vol. 80, pp. 11–15, 2002.

[34] E. M. Hoffmann, J. Lamparter, A. Mirshahi et al., "Distribution of central corneal thickness and its association with ocular parameters in a large central European cohort: the Gutenberg health study," *PLoS One*, vol. 8, article e66158, 2013.

[35] C. W. Pan, T. Y. Wong, L. Chang et al., "Ocular biometry in an urban Indian population: the Singapore Indian eye study (SINDI)," *Investigative Ophthalmology & Visual Science*, vol. 52, pp. 6636–6642, 2011.

[36] L. S. Lim, S. M. Saw, V. S. Jeganathan et al., "Distribution and determinants of ocular biometric parameters in an Asian population: the Singapore Malay eye study," *Investigative Ophthalmology & Visual Science*, vol. 51, pp. 103–109, 2010.

[37] T. Fu, Y. W. Song, Z. Q. Chen et al., "Ocular biometry in the adult population in rural central China: a population-based, cross-sectional study," *International Journal of Ophthalmology*, vol. 8, pp. 812–817, 2015.

[38] J. B. Jonas, R. Iribarren, V. Nangia et al., "Lens position and age: the Central India eye and medical study," *Investigative Ophthalmology & Visual Science*, vol. 56, pp. 5309–5314, 2015.

[39] J. B. Jonas, V. Nangia, R. Gupta, A. Sinha, and K. Bhate, "Lens thickness and associated factors," *Clinical and Experimental Ophthalmology*, vol. 40, pp. 583–590, 2012.

[40] S. Warrier, H. M. Wu, H. S. Newland et al., "Ocular biometry and determinants of refractive error in rural Myanmar: the Meiktila eye study," *The British Journal of Ophthalmology*, vol. 92, pp. 1591–1594, 2008.

[41] R. Hoehn, A. Mirshahi, E. M. Hoffmann et al., "Distribution of intraocular pressure and its association with ocular features and cardiovascular risk factors: the Gutenberg health study," *Ophthalmology*, vol. 120, pp. 961–968, 2013.

Hindawi
Journal of Ophthalmology
Volume 2017, Article ID 4165706, 5 pages
https://doi.org/10.1155/2017/4165706

Research Article

Accommodative Stimulus-Response Curve with Emoji Symbols

Robert Montés-Micó,[1,2] José J. Esteve Taboada,[1,2] Paula Bernal-Molina,[1,2] and Teresa Ferrer-Blasco[1,2]

[1]*Department of Optics and Optometry and Visual Sciences, University of Valencia, 46100 Burjassot, Spain*
[2]*Interuniversity Laboratory for Research in Vision and Optometry, Mixed Group UVEG-UMU, Valencia, Spain*

Correspondence should be addressed to José J. Esteve Taboada; josejuan.esteve@uv.es

Received 11 May 2017; Accepted 25 July 2017; Published 10 September 2017

Academic Editor: Antonio Queiros

Purpose. To evaluate the static measurement of the accommodative stimulus-response curve with emoji symbols. *Methods.* The accommodative stimulus-response curve was measured in 18 subjects using a Hartmann-Shack sensor to obtain the objective accommodative response from the Zernike defocus term. Measurements were acquired at different accommodative demands, from 0 to 3 D with a step of 0.5 D. Detailed and nondetailed emoji targets were used with two different sizes, corresponding to the two most common visual angles used in smartphones. *Results.* A regression analysis was performed to fit the mean results obtained for each target. The determination coefficient was $R^2 \geq 0.988$ for all targets. For the detailed targets, the slopes for the averaged stimulus-response curve were 0.65 and 0.66 for the bigger and smaller sizes, respectively. For the nondetailed targets, the slopes were 0.60 and 0.58 for the bigger and smaller sizes, respectively. p values for these slopes were statistically significant for the two types of targets ($p < 0.01$). *Conclusions.* Our results reveal that the replacement of a word or several words by detailed or nondetailed emoji symbols seems not to provoke a different accommodative response in normal subjects and under standard viewing conditions in the use of smartphones.

1. Introduction

Over the last few years, there has been a significant increase in the use of Internet-based instruments such as tablets and/or smartphones. Around two billion phones are estimated as currently in use worldwide, and this number is expected to double by 2020 [1]. The number of hours of use in front of a tablet or smartphone screen is increasing, both in adults and children. In addition, the reading distance may vary since smaller screen size implies that the user tends to get closer for its use. Bababekova et al. [2] reported that the mean viewing distance for reading text messages on a smartphone is 4 cm closer than for Internet viewing, in both cases closer than that usually adopted for other computer devices. Also, there is a study that shows that the viewing distance of a smartphone may vary depending on the time spent reading, being closer after 60 minutes [3].

Smartphones can be used for different visual tasks such as reading the Internet, viewing videos, and writing and reading messages in social networks or messaging applications. These activities are changing quickly, and it may be now found that some written text is replaced by emojis. An emoji is defined as a pictograph (graphic symbol) that represents not only a facial expression but also concepts and ideas [4] and is frequently used to replace some words in messages. To replace a word or several words by an emoji may provoke a different accommodative response (AR) depending on the details included in the emoji symbol. The assessment of the AR by means of the accommodative stimulus-response curve may provide information regarding some relevant clinical aspects. The analysis of this curve is important for the assessment of the relationship between accommodation and myopia or amblyopia development [5–8].

Therefore, the purpose of the present study is to evaluate the accommodative stimulus-response curve using a wavefront-sensing optical system in order to assess the effect of detailed and nondetailed emoji symbols used in messaging applications frequently found in smartphones.

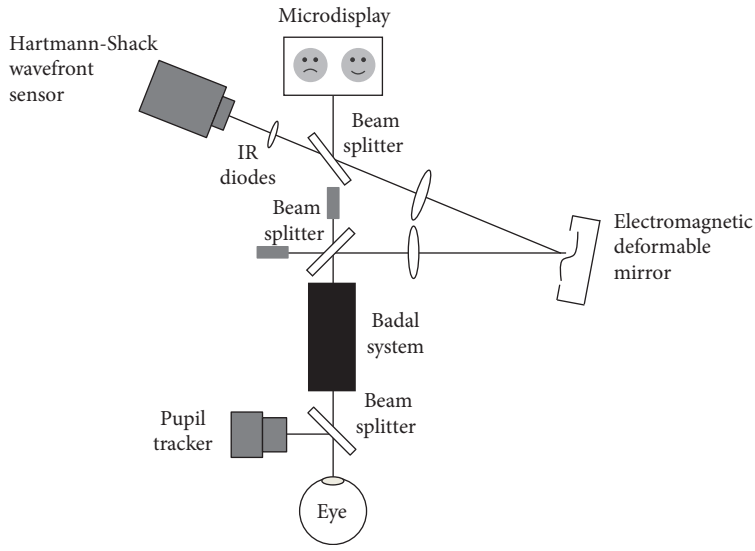

Figure 1: Schematic diagram of the wavefront-sensing optical system.

2. Methods

2.1. Subjects. Eighteen young adult subjects with a mean age of 28.6 ± 8.2 years were recruited for this experiment. The mean spherical equivalent refractive error was -0.16 ± 1.30 diopters (D). Astigmatism was limited to ≤1.00 D and anisometropia <2.00 D. All subjects had a best-corrected visual acuity of 20/20 or better, showed no ocular pathology, no previous conducted ocular surgery, and normal clinical amplitudes of accommodation for their ages. The study followed the Declaration of Helsinki and was approved by the Ethics Committee of the Institution. The subjects were verbally informed about the details and possible consequences of the study, and a signed formal consent was obtained from each subject.

2.2. Experimental System. A wavefront-sensing optical system was used to carry out the measurements. Figure 1 shows a detailed description of the experimental setup used. The system is composed of a Hartmann-Shack wavefront sensor (Haso 32, Imagine Eyes, France) and a 52-actuator deformable mirror (Mirao 52, Imagine Eyes, France) that was used to compensate for the internal aberrations of the optical system [9]. The wavefront sensor employs a square array of 1024 microlenses and a near-infrared light source with a wavelength of 850 nm. An internal microdisplay is used to project the target, while the Badal system is employed to change the accommodation demand. A precise alignment of the subject's pupil is required, which was controlled with an additional camera. Head movements were reduced employing a chin and forehead rest. The subject's right eye viewed the target and the left eye was patched. All measurements were taken using the analysis and simulation software library and software development kits provided by the manufacturer (Imagine Eyes, France).

2.3. Experimental Procedure. Measurements were acquired at different accommodative demands (AD), from 0 to 3 D with a step of 0.5 D. Detailed (happy and sad smileys) and nondetailed (heart and star) emoji targets, so classified depending on the level of details included in the emoji symbols, were used with two different sizes (21 and 30 arc min), corresponding to the two most common visual angles used in smartphones at a standard distance of 30 cm. These two sizes were selected according to the most used configuration for viewing messages in end-to-end instant messaging applications. Detailed emojis are supposed to require higher visual acuity than nondetailed ones (see Figure 2 for a description of both emoji targets). The accommodative stimulus-response curve was measured under four different conditions, combining both the type and the size of emojis. Subjects were also allowed to rest between trials.

2.4. Data Analysis. Wavefront data were exported as Zernike coefficients up to the 6th order. In order to identify the AR of the eyes to the accommodation stimuli only, Zernike defocus was used. AR was determined in diopters by using the equation that follows:

$$\mathrm{AR} = \mathrm{AD} - \frac{C_2^0 4\sqrt{3}}{r^2}, \tag{1}$$

where C_2^0 is the second-order Zernike coefficient for defocus, expressed in μm, and r is the pupil radius, expressed in mm [10].

Mean data for each of the different conditions were fitted into linear models. For each regression analysis, the following values were recorded: intercept n, slope m, determination coefficient R^2, and p values. Besides these values, the accommodative error index I was obtained for each condition [11]. This metric is defined as the mean of the response error

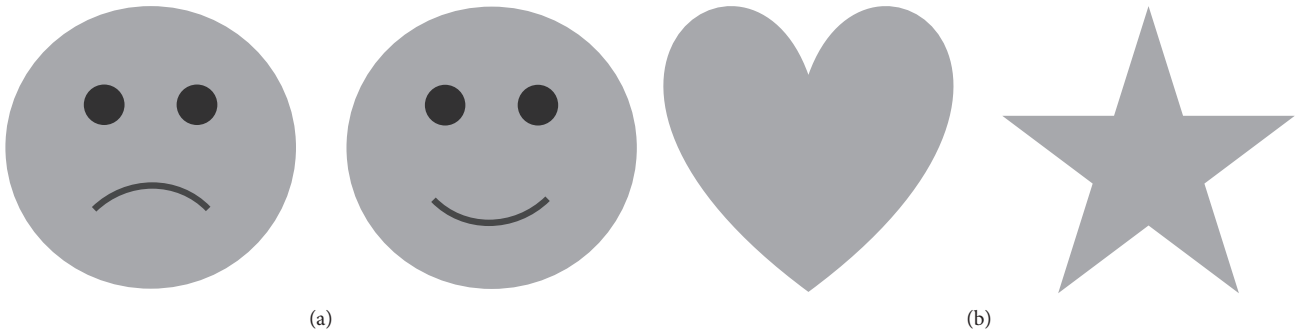

(a) (b)

Figure 2: Detailed (a) and nondetailed (b) emoji symbols used for the experiment.

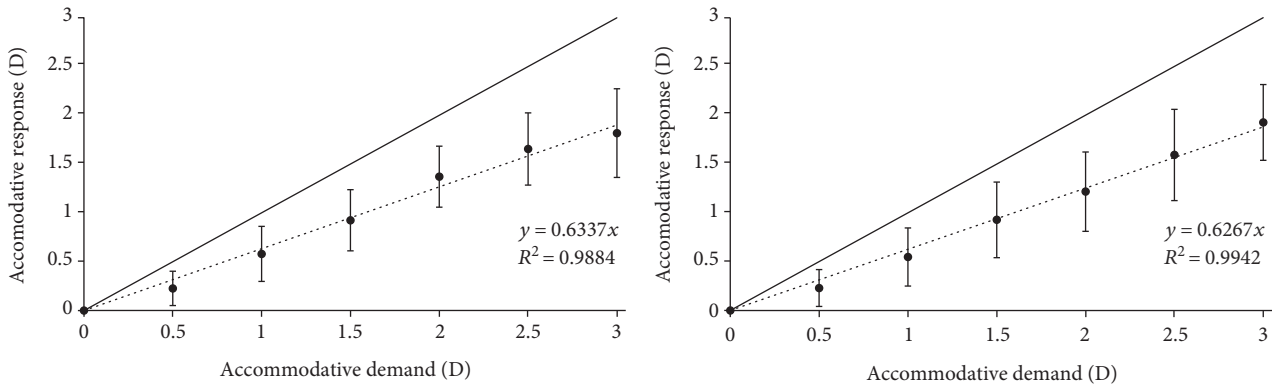

(a) (b)

Figure 3: Mean accommodative response obtained with the detailed (happy and sad smileys) emoji targets for 30 (a) and 21 (b) arc min. Each data point represents the mean ± standard deviation (SD) at each accommodative demand. The solid line represents the theoretical accommodative response while the dotted line represents the fitted linear model.

magnitude divided by the squared correlation coefficient. The accommodative error index is defined therefore as

$$I = \frac{|(1-m)((x_1+x_2)/2)-n|}{R^2}, \quad (2)$$

where x_1 and x_2 correspond to the stimulus levels defining the range over which the regression fit applies. Slope values themselves are not valid to characterize a stimulus-response curve, since a curve with $m = 1$ does not necessarily coincide with the ideal line and important lags or leads may still be present, and therefore, the accommodative error index was introduced to consider both the extent to which responses deviate from ideal and the goodness of fit of data points to the regression line. The accommodative error index I value increases with the numerator value, that is, when the discrepancy between the regression line fitted to the measured accommodative responses and the ideal line increases (measured by the normalized area between both lines). The value of I also increases as the denominator decreases, that is, when the degree of correlation between stimulus and response is not high.

An additional ANCOVA analysis using MATLAB 2015b (The MathWorks Inc., Natick, MA, USA) was also carried out in order to determine whether the slopes of the four different conditions were significantly different. A p value lower than 0.05 was considered as statistically significant.

3. Results

Figure 3 shows the mean AR obtained for all the subjects for each AD, starting from 0 D and ending at 3 D of AD with a 0.5 D step with the detailed (happy and sad smileys) emoji targets for 30 (top) and 21 (bottom) arc min. The slopes for the averaged stimulus-response curve were 0.634 and 0.627 for the bigger and smaller sizes, respectively. The p values for these slopes were statistically significant for the two sizes ($p < 0.01$). The determination coefficient in both cases was $R^2 \geq 0.988$.

Figure 4 shows the averaged AR obtained with the nondetailed (heart and star) emoji targets for 30 (top) and 21 (bottom) arc min. The slopes for the averaged stimulus-response curve were 0.566 and 0.544 for the bigger and smaller sizes, respectively. The p values for these slopes were statistically significant for the two sizes ($p < 0.01$). The determination coefficient in both cases was $R^2 \geq 0.988$.

The solid line in both figures shows the theoretical ideal response of the accommodation process (i.e., equal AR for each AD). In this case, there was a difference towards the same direction between all AR and the theoretical line, showing accommodative lag for all subjects and AD. The accommodative error index I values for the different conditions assessed were the following: 0.56 and 0.56 for the detailed emoji targets for 30 and 21 arc min, respectively

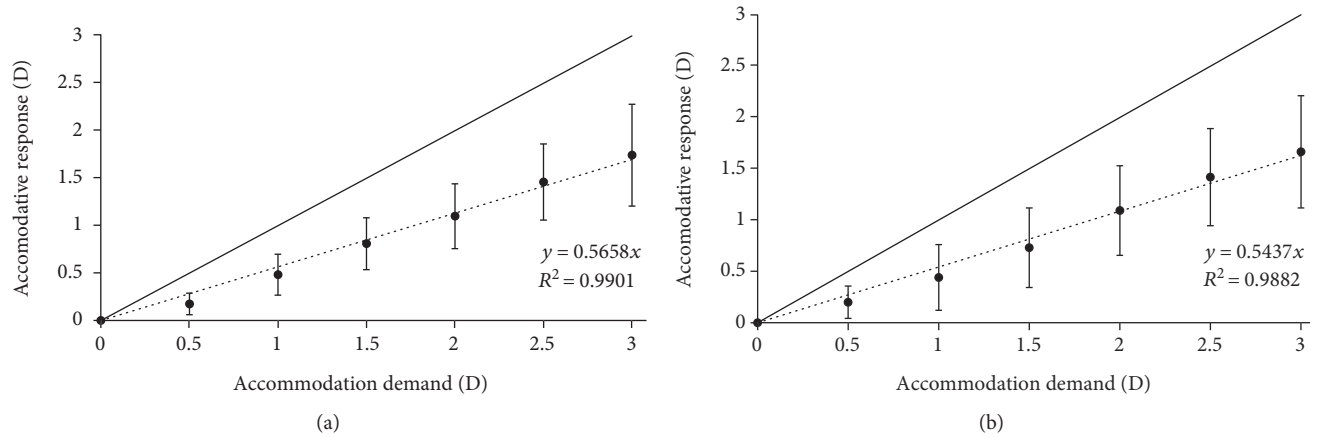

Figure 4: Mean accommodative response obtained with the nondetailed (heart and star) emoji targets for 30 (a) and 21 (b) arc min. Each data point represents the mean ± standard deviation (SD) at each accommodative demand. The solid line represents the theoretical accommodative response while the dotted line represents the fitted linear model.

and 0.66 and 0.69 for the nondetailed emoji targets for 30 and 21 arc min, respectively.

An ANCOVA statistical analysis was conducted to analyze if the measurements obtained for the four different conditions were statistically different or not. This analysis revealed that the slopes of the AR for the four conditions were not significantly different from each other ($p = 0.06$). Despite no statistically significant differences were found in the slope values, the outcomes for the detailed emoji targets were slightly larger than the ones obtained for the nondetailed emoji targets.

4. Discussion

As we have introduced, there is a general trend worldwide to increase the number of hours using handheld devices such as smartphones or tablets. The use of these devices, specifically by children and young individuals, may produce a change in their AR. It is interesting to note, for example, that smartphone gaming has risen dramatically in recent years [12]. Specifically, smartphone gaming and frequent use patterns are associated with smartphone addiction [13]. For example, Haug et al. [14] indicated that smartphone addiction occurred in 16.9% of a sample of 1519 students from Switzerland. Then, the excessive use of a smartphone can be described as a type of behavioural addiction that changes several aspects of information reading and communication. The addiction that is actually reported in the literature produces inevitably an increasing number of hours of use that may affect the AR.

The use of instant messaging applications frequently found in smartphones is one of the main factors that contributes in increasing the number of hours of use. An emoji, defined as a pictograph that describes concepts, ideas, and emotions, is one of the communication elements most used in these applications, to such an extent that frequently the communication between individuals only considers emoji symbols. Then, when text is replaced by an emoji symbol, this may also affect the AR and should be evaluated. In addition, it becomes important for the user of these applications to pay detailed attention to the emoji symbol used, since, for instance, emojis representing different emotions or feelings differ only in small details (see, for example, happy and sad smileys in Figure 2(a)).

Therefore, the aim of the present study focuses on the analysis of the accommodative stimulus-response curve using a wavefront-sensing optical system in order to properly analyze the effect of emoji symbols on the accommodative system of the human eye. Due to the importance of the details in some emojis to properly communicate the message, we have considered the analysis with two different groups of emojis (detailed and nondetailed) requiring different visual demanding tasks.

Our results revealed that under all the conditions of the experiments that were carried out there was an accommodative lag for all subjects evaluated. Mean lag values for all the experimental conditions increased for higher vergences, ranging from 0.3 (at 0.5 D) to 1.3 D (at 3 D). These results agree with previous literature showing that accommodative lag increases with AD [7, 15–17]. We have to note that there have been reported differences in the accommodative stimulus-response curves depending on the measurement method used [7, 17]. Recently, Chen et al. [17] measured monocularly this curve using three methods: dynamic and static measurements using a motorised Badal system and the minus lens technique. They concluded that the results are method-dependent, and that using dynamic measurements, accommodative behaviour varies with the speed of dioptric change of the stimulus. In our experiment, we have used a Hartmann-Shack wavefront sensor with a Badal lens, and the accommodation measurement was based on the Zernike defocus term (see (1)).

Figures 3 and 4 show the data for the detailed and nondetailed emoji symbols used. Specifically, Figure 3 shows the happy and sad smiley emoji targets for 30 and 21 arc min. The slopes for both types of symbols were higher than 0.6 and the determination coefficient $R^2 \geq 0.988$, being statistically significant for the two sizes evaluated ($p < 0.01$). Similar

outcomes were found for the heart and star emoji targets (see Figure 4). The slopes were higher than 0.5 and the determination coefficient $R^2 \geq 0.988$, being statistically significant for the two sizes evaluated ($p < 0.01$). The ANCOVA analysis revealed that there were no statistically significant differences between the results obtained for the slopes in the four experimental conditions ($p = 0.06$), although it is interesting to point out that the slopes for the detailed emoji targets (Figure 3) were slightly larger than the ones obtained for the nondetailed emoji targets (Figure 4). This response may be due to the fact that detailed targets may require higher AR to reduce the accommodative lag and increase the quality of the retinal image [16]. In relation to the emoji sizes, our results revealed that there were no differences between the slopes (see Figures 3 and 4). Some instant messaging applications that are commonly used worldwide increase the size of the emoji when it is displayed alone, without text. Despite the fact that there are no differences in the AR, this different size may allow for a better visualization increasing the reading speed or message comprehension, for example. In relation to the accommodative error index, the results obtained revealed and confirmed that the detailed emoji targets require larger AR to reduce the accommodative lag. Note, for example, that the accommodative error index for nondetailed targets is about 25% higher than the values obtained for the detailed targets.

One of the limitations in our study is that we have used some specific emojis. However, there are a lot of them and new ones appear every day. Besides, the use of a particular emoji symbol changes frequently by users. In this regard, for example, the website Emojitracker (http://emojitracker.com/), that monitors the use of emojis on Twitter in real time, shows how the frequency of use for a particular emoji changes with time. Future studies should be done with more emoji types.

In conclusion, we have measured the accommodative stimulus-response curve under different conditions combining both the type and the size of emoji symbols. Our results reveal that the replacement of a word or several words by detailed or nondetailed emoji symbols seems not to provoke a different AR in normal subjects and under standard viewing conditions in the use of smartphones. However, further research should be carried out in order to evaluate the use of other emoji symbols that appear continuously.

Conflicts of Interest

The authors declare that they have no conflict of interest.

Acknowledgments

This study was funded by the European Research Council Starting Grant ERC-2012-StG-309416.

References

[1] T. McIlroy, "Planet of the phones," *The Economist*, 2015, http://www.economist.com/news/leaders/21645180-smartphone-ubiquitous-addictive-and-transformative-planet-phones.

[2] Y. Bababekova, M. Rosenfield, J. Hue, and R. R. Huang, "Font size and viewing distance of handheld smartphones," *Optometry and Vision Science*, vol. 88, pp. 795–797, 2011.

[3] J. Long, R. Cheung, S. Duong, R. Paynter, and L. Asper, "Viewing distance and eyestrain symptoms with prolonged viewing of smartphones," *Clinical & Experimental Optometry*, vol. 100, pp. 133–137, 2017.

[4] P. Kralj Novak, J. Smailović, B. Sluban, and I. Mozetič, "Sentiment of emojis," *PLoS One*, vol. 10, article e0144296, 2015.

[5] K. J. Ciuffreda, S. C. Hokoda, G. K. Hung, and J. L. Semmlow, "Accommodative stimulus/response function in human amblyopia," *Documenta Ophthalmologica*, vol. 56, pp. 303–326, 1984.

[6] N. A. McBrien and M. Millodot, "The relationship between tonic accommodation and refractive error," *Investigative Ophthalmology & Visual Science*, vol. 28, pp. 997–1004, 1987.

[7] M. L. Abbott, K. L. Schmid, and N. C. Strang, "Differences in the accommodation stimulus response curves of adult myopes and emmetropes," *Ophthalmic and Physiological Optics*, vol. 18, pp. 13–20, 1998.

[8] B. C. Jiang and J. M. White, "Effect of accommodative adaptation on static and dynamic accommodation in emmetropia and late-onset myopia," *Optometry and Vision Science*, vol. 76, pp. 295–302, 1999.

[9] A. I. Moulakaki, A. J. Del Águila-Carrasco, J. J. Esteve-Taboada, and R. Montés-Micó, "Effect of even and odd-order aberrations on the accommodation response," *International Journal of Ophthalmology*, vol. 10, pp. 955–960, 2017.

[10] L. N. Thibos, X. Hong, A. Bradley, and R. A. Applegate, "Accuracy and precision of objective refraction from wavefront aberrations," *Journal of Vision*, vol. 4, pp. 329–351, 2004.

[11] K. Chauhan and W. N. Charman, "Single figure indices for the steady-state accommodative response," *Ophthalmic and Physiological Optics*, vol. 15, pp. 217–221, 1995.

[12] Y. H. Lin, S. H. Lin, C. C. H. Yang, and T. B. J. Kuo, "Psychopathology of everyday life in the 21st Century: smartphone addiction," in *Internet addiction: neuroscientific approaches and therapeutical implications including smartphone addiction*, C. Montag and M. Reuter, Eds., Springer International Publishing AG, Switzerland, 2017.

[13] C. H. Liu, S. H. Lin, Y. C. Pan, and Y. H. Lin, "Smartphone gaming and frequent use pattern associated with smartphone addiction," *Medicine*, vol. 95, article e4068, 2016.

[14] S. Haug, R. P. Castro, M. Kwon, A. Filler, T. Kowatsch, and M. P. Schaub, "Smartphone use and smartphone addiction among young people in Switzerland," *Journal of Behavioral Addictions*, vol. 4, pp. 299–307, 2015.

[15] H. A. Anderson, A. Glasser, K. K. Stuebing, and R. E. Manny, "Minus lens stimulated accommodative lag as a function of age," *Optometry and Vision Science*, vol. 86, pp. 685–694, 2009.

[16] V. Sreenivasan, E. Aslakson, A. Kornaus, and L. N. Thibos, "Retinal image quality during accommodation in adult myopic eyes," *Optometry and Vision Science*, vol. 90, pp. 1292–1303, 2013.

[17] Y. Chen, W. Jin, Z. Zheng et al., "Comparison of three monocular methods for measuring accommodative stimulus-response curves," *Clinical & Experimental Optometry*, vol. 100, pp. 155–161, 2017.

Hindawi
Journal of Ophthalmology
Volume 2017, Article ID 7935406, 8 pages
https://doi.org/10.1155/2017/7935406

Research Article

Evaluation of Cholinergic Deficiency in Preclinical Alzheimer's Disease Using Pupillometry

Shaun Frost,[1,2] Liam Robinson,[1,2] Christopher C. Rowe,[3] David Ames,[4,5,6] Colin L. Masters,[5] Kevin Taddei,[7] Stephanie R. Rainey-Smith,[7,8] Ralph N. Martins,[7,8,9,10] and Yogesan Kanagasingam[1,2]

[1]*Commonwealth Scientific and Industrial Research Organisation (CSIRO), Perth, WA, Australia*
[2]*Australian e-Health Research Centre, Perth, WA, Australia*
[3]*Department of Nuclear Medicine and Centre for PET, Austin Health, Melbourne, VIC, Australia*
[4]*Department of Psychiatry, University of Melbourne, Melbourne, VIC, Australia*
[5]*The Mental Health Research Institute (MHRI), University of Melbourne, Melbourne, VIC, Australia*
[6]*National Ageing Research Institute, Melbourne, VIC, Australia*
[7]*School of Medical and Health Sciences, Edith Cowan University, Joondalup, WA, Australia*
[8]*Sir James McCusker Alzheimer's Disease Research Unit, Hollywood Private Hospital, Perth, WA, Australia*
[9]*School of Biomedical Sciences, Macquarie University, North Ryde, NSW, Australia*
[10]*School of Psychiatry and Clinical Neurosciences, University of Western Australia, Crawley, WA, Australia*

Correspondence should be addressed to Shaun Frost; shaun.frost@csiro.au

Received 28 April 2017; Accepted 4 June 2017; Published 15 August 2017

Academic Editor: Alejandro Cerviño

Cortical cholinergic deficiency is prominent in Alzheimer's disease (AD), and published findings of diminished pupil flash response in AD suggest that this deficiency may extend to the visual cortical areas and anterior eye. Pupillometry is a low-cost, noninvasive technique that may be useful for monitoring cholinergic deficits which generally lead to memory and cognitive disorders. The aim of the study was to evaluate pupillometry for early detection of AD by comparing the pupil flash response (PFR) in AD ($N = 14$) and cognitively normal healthy control (HC, $N = 115$) participants, with the HC group stratified according to high ($N = 38$) and low ($N = 77$) neocortical amyloid burden (NAB). Constriction phase PFR parameters were significantly reduced in AD compared to HC (maximum acceleration $p < 0.05$, maximum velocity $p < 0.0005$, average velocity $p < 0.005$, and constriction amplitude $p < 0.00005$). The high-NAB HC subgroup had reduced PFR response cross-sectionally, and also a greater decline longitudinally, compared to the low-NAB subgroup, suggesting changes to pupil response in preclinical AD. The results suggest that PFR changes may occur in the preclinical phase of AD. Hence, pupillometry has a potential as an adjunct for noninvasive, cost-effective screening for preclinical AD.

1. Introduction

The ocular pupil controls retinal illumination and responds dynamically to a bright flash of light by rapid constriction followed by redilation (Figure 1). Pupillometry investigates this response by delivering a flash of light into the eye and accurately detecting and measuring pupil size changes over time.

Pupil size and response are controlled by the opposing action of the sphincter and dilator muscles of the iris. The constriction phase of the pupil response (Figure 1) is primarily driven by the cholinergic system [1], with acetylcholine (ACh) being the neurotransmitter involved in projections between the Edinger-Westphal nucleus, ciliary ganglion, and sphincter muscle [2]. Thus, pupillometry provides a practical, noninvasive approach with which to evaluate cholinergic deficiency.

Pupillometry has been used to identify a cholinergic deficiency in a number of disorders including Alzheimer's

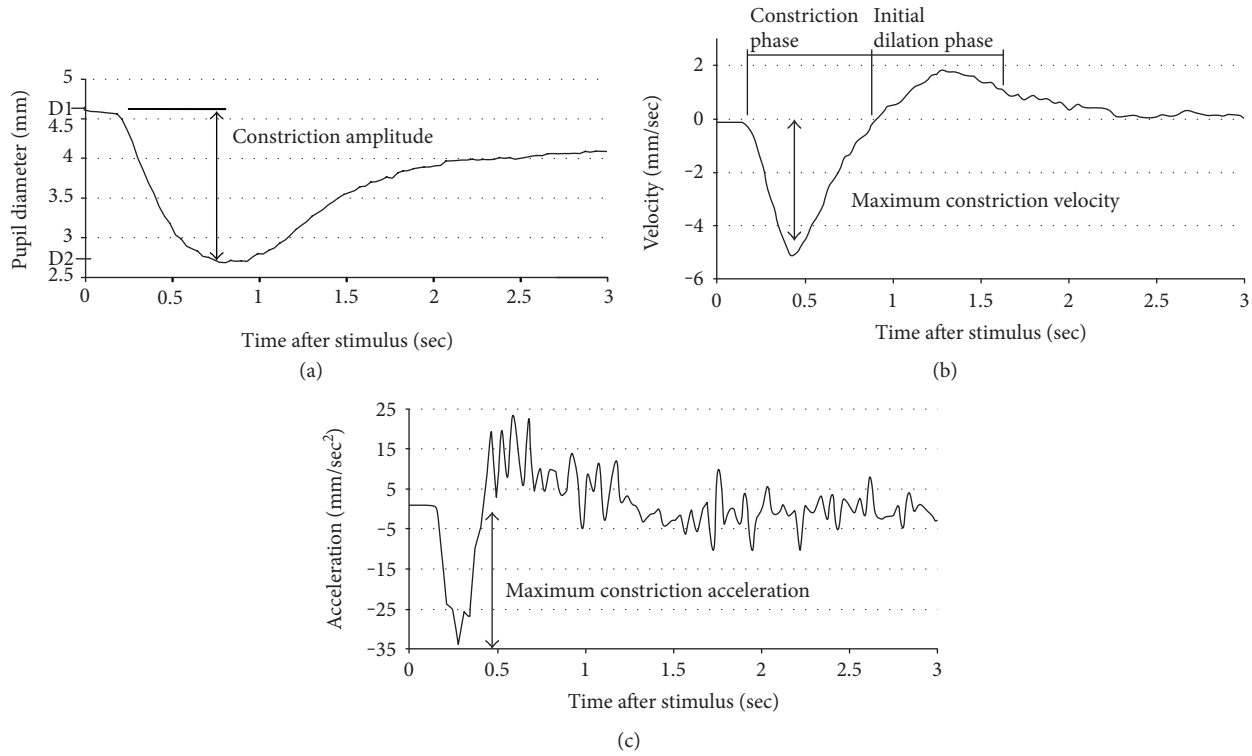

Figure 1: Illustration of pupil flash response and parameters measured. (a) Pupil diameter over time after stimulus at time zero. (b) Pupil velocity (rate of change of pupil diameter). (c) Pupil acceleration (rate of change of velocity). The constriction phase lasts from stimulus to minimum pupil size; parameters calculated during this phase are the constriction amplitude, maximum and average constriction velocity, and maximum constriction acceleration.

disease (AD) [3–8] and Parkinson's disease [5, 9]. As the primary neurotransmitter deficit in AD is ACh [10–12], the constriction phase of the pupil flash response (PFR) has gained interest for evaluating cholinergic deficiency and for early detection, diagnosis, and monitoring of AD. The majority of study results to date indicate a slower and reduced pupil response in AD, with reduced velocities, accelerations, and constriction amplitude, and increased latencies. The work of Ferrario et al. [6] on only constriction acceleration stands in contrast, possibly due to different methodology and participant selection. Some studies indicate a faster recovery after stimulus in AD, despite slower constriction and dilation velocities, probably due to the reduced amplitude [3, 13].

Our prior study [8] found a weaker pupil constriction response in AD, consistent with the hypothesis of a cholinergic deficit in the peripheral parasympathetic pathway in AD. Significant differences were found between AD and cognitively normal healthy control (HC) participants in 10 different calculated PFR parameters, with the greatest differences coming from the constriction phase: maximum constriction acceleration, maximum constriction velocity, mean constriction velocity, and constriction amplitude. These promising preliminary results warranted further investigation into whether pupil response changes occur early in AD, possibly providing a test for early detection or monitoring of the disease.

AD is characterized clinically by a progressive decline in memory, learning, and executive function and neuropathologically by the presence of cerebral extracellular amyloid deposits (plaques), intracellular neurofibrillary tangles, and cerebral (in particular hippocampal) atrophy. In addition to the debilitating symptoms endured by AD patients, the disease imposes a huge social and economic burden on society [14].

AD cognitive symptoms arise only after extensive, irreversible neural deterioration has already occurred. As a result, diagnosis is usually made late in the disease process, limiting both the efficacy of available treatments and the evaluation of new treatments. Biomarkers for early detection of AD include cerebrospinal fluid concentrations of beta-amyloid ($A\beta$), total tau and phosphorylated tau peptides [15–18], and brain $A\beta$ plaque burden imaged using positron emission tomography (PET) [16, 18–20]. Research demonstrates that plaque burden can be detected over 20 years before cognitive symptoms begin [21]. However, while these are valuable diagnostic and secondary screening biomarkers, they are not suitable as primary screening technologies for AD. A screening process that could provide early, accurate diagnosis or a prognosis of AD would enable earlier intervention, facilitate cost-effective screening into treatment trials, and allow current and future treatments to be more effective.

The present study investigated constriction phase pupil response in AD and HC participants, with a particular focus on PFR changes in preclinical AD as determined by high neocortical amyloid burden (NAB).

2. Materials and Methods

2.1. Participants. Participants for the study were recruited from the Australian Imaging, Biomarkers, and Lifestyle (AIBL) study of ageing in Australia. The AIBL study has two sites: Melbourne (Victoria) and Perth (Western Australia). The pupillometry study was conducted only at the Perth site. A previous report details the AIBL study design and baseline cohort [22]. Briefly, the AIBL study integrates data from neuroimaging, biomarkers, lifestyle, clinical, and neuropsychological domains for eligible volunteers older than 60 years who are fluent in English. AIBL classifies participants into 3 groups: (1) individuals meeting the criteria for AD based on the NINCDS-ADRDA (National Institute of Neurological and Communicative Disorders and Stroke-Alzheimer's Disease and Related Disorders Association) [23], (2) individuals meeting the criteria for mild cognitive impairment [24, 25], and (3) cognitively normal healthy control individuals.

The following were part of the AIBL exclusion criteria: a history of non-AD dementia, schizophrenia, bipolar disorder, significant current (but not past) depression (geriatric depression scale above 5/15), Parkinson's disease, cancer (other than basal cell skin carcinoma) within the last 2 years, symptomatic stroke, uncontrolled diabetes, diagnosed obstructive sleep apnoea, or current regular alcohol use exceeding 2 standard drinks per day for women or 4 per day for men.

AIBL participants were excluded from the pupil response study if they did not have PET data available; if they had pupillary malformations, severe cataract, self-reported history of glaucoma in either eye, penetrating eye wounds to both eyes, and eye surgery to both eyes that involved the muscle; if they used cholinesterase inhibitors or prescribed ocular medications; or if they were unable to complete the task without excessive blinking.

All participants provided written informed consent, and all PFR procedures were approved by the Hollywood Private Hospital Research Ethics Committee according to the Helsinki Declaration. Approval for the parent AIBL study was obtained from the Austin Health Human Research Ethics Committee, the Hollywood Private Hospital Research Ethics Committee, the St. Vincent Hospital Research Ethics Committee, and the Edith Cowan University Human Research Ethics Committee.

The present study draws upon data generated from the AIBL study, including neuroimaging and genetic test results. The methodology for these AIBL procedures is reported elsewhere [22] and summarized below.

2.2. Neuroimaging. Neuroimaging methodology is reported in more detail elsewhere [26]. Briefly, participants were neuroimaged for the presence of fibrillar brain Aβ using PET with 2 different radiotracers: 11C-Pittsburgh compound B (PiB) and 18F-flutemetamol (FLUTE). Previous reports describe the PET methodology for each tracer in detail [20, 27]. For semiquantitative analysis, a volume of interest template was applied to the summed and spatially normalized PET images to obtain a standardized uptake value (SUV). The images were then scaled to the SUV of each tracer's recommended reference region to generate a tissue ratio termed SUV ratio (SUVR). A global measure of NAB was computed using the mean SUVR in the frontal, superior parietal, lateral temporal, occipital, and anterior and posterior cingulate regions of the brain. For PiB, the SUV was normalized to the cerebellar cortex, whereas the pons was used as the reference region for FLUTE [28]. SUVR was stratified into a dichotomous variable classified as high or low based on neuropathologically validated thresholds for each tracer. We considered participants who underwent FLUTE imaging to have high NAB when the SUVR was 0.62 or higher [28], and for PiB imaging, when the SUVR was 1.4 or higher [29].

2.3. Genotyping. APOE genotyping was performed according to the following protocol: fasting blood samples were obtained using standard venepuncture of the antecubital vein and collected into EDTA tubes containing prostaglandin E1 (PGE: 33.3 ng/ml; Sapphire Bioscience, NSW, Australia) to prevent platelet activation. Extraction of DNA from 5 ml of whole blood was undertaken using QIAamp DNA Blood Maxi Kits (Qiagen, Hilden, Germany) as per the manufacturer's instructions. Specific TaqMan® (Thermo Fisher Scientific, Waltham, MA, USA) genotyping assays were used for ascertaining APOE genotype (rs7412, assay ID: C____904973_10; rs429358, assay ID: C___3084793_20), which were performed on a QuantStudio 12K Flex™ real-time PCR system (Thermo Fisher Scientific, Waltham, MA, USA) using the TaqMan GTXpress™ Master Mix (Thermo Fisher Scientific, Waltham, MA, USA).

2.4. System of Pupillometry. A record of the pupil's response to a flash of light was collected for each participant using a commercial pupillometer. The PFR was collected using a NeurOptics™ VIP™-200 Pupillometer. This is a commercial, monocular device providing fully automated operation and calculation of response parameters. The device produces a white flash stimulus and then measures the pupil size for 5 seconds using infrared illumination. The video frame rate is 33 Hz, the stimulus/pulse intensity is 180 μW, and the stimulus/pulse duration is 31 ms. The pupillometer produces diffuse light over the whole visual field.

The room was darkened for 2 minutes prior to testing. The test was practiced once before recording. Occasionally, an extra trial was needed to achieve a recording without blinks or artefacts. Data was rejected if artefacts were present. The right eye was used for all participants, except where there was injury or pathology to the right eye only or a suitable pupil response could not be obtained with the right eye, in which case the left eye was used ($N = 1$). The pupillometer provided automatic calculation of the following pupil response parameters: resting pupil diameter (D1, mm), minimum pupil diameter (D2, mm), average constriction velocity (CV, mm/sec), maximum constriction velocity (MCV, mm/sec), and constriction amplitude (AMP, mm), which was calculated as the difference between resting pupil diameter and minimum pupil diameter (D1 – D2, mm). A record of the pupil's diameter as a function of time was exported from the pupillometer. From this record, maximum constriction

Table 1: Demographics and descriptive PFR analysis for HC and AD groups, with ANOVA, χ^2 test, and GLM analysis.

	Healthy control	Alzheimer's disease	p value
Number of participants [N]	115	14	
Age: years [mean (±SD)]	72.9 (±5.3)	77.4 (±5.4)	**0.002**$^{\sim}$
Sex: male [N (%)]	56 (49)	10 (61)	0.11†
APOE ε4 carrier [N (%)]	27 (23)	12 (86)	**0.000001**†
MCA [mm/sec^2, mean (±SD)]	31.12 (±6.56)	26.84 (±4.23)	**0.030**‡
MCV [mm/sec, mean (±SD)]	4.22 (±0.65)	3.41 (±0.55)	**0.00045**‡
CV [mm/sec, mean (±SD)]	3.02 (±0.49)	2.53 (±0.44)	**0.0015**‡
AMP [mm, mean (±SD)]	1.46 (±0.28)	1.15 (±0.28)	**0.0030**‡

$^{\sim}$Analysis of variance (ANOVA) for the continuous age demographic variable ($p < 0.05$ considered significant). $^{\dagger}\chi^2$ test for categorical demographic variables (gender and *APOE* ε4 carrier status) ($p < 0.05$ considered significant). $^{\ddagger}p$ value from generalised linear model analysis of differences between groups (including significant confounders). Bold values significant after adjustment for false discovery rate (FDR) using the Benjamini and Hochberg method. *APOE* ε4 carrier status refers to carrier/noncarrier of an apolipoprotein E ε4 allele. SD refers to standard deviation, mm refers to millimetres, sec refers to seconds, PFR refers to pupil flash response, HC refers to healthy control, AD refers to Alzheimer's disease, GLM refers to generalised linear methods, MCA refers to maximum constriction acceleration, MCV refers to maximum constriction velocity, CV refers to average constriction velocity, and AMP refers to constriction amplitude.

acceleration (MCA, mm/sec^2) was calculated by masked operators using fully automated computer algorithms. PFR trials with artefacts or excessive blinking were discarded. A computer algorithm was used to remove minor blinks.

2.5. Statistical Analysis. Descriptive statistics including means and standard deviations (SD) for the full cohort and clinical group are shown in Table 1. Demographic comparisons were performed using a χ^2 test (Fisher's exact calculation where necessary) for categorical variables (gender and *APOE* ε4 status), and analysis of variance (ANOVA) for the continuous age variable ($p < 0.05$ considered significant). Pupil response measures were compared between groups using generalised linear modelling, with confounding variables reduced via the stepAIC method (a stepwise model selection by Akaike information criterion). Confounders considered included age, sex, and *APOE* ε4 status (the major genetic risk factor for sporadic AD [30]). Statistical significance was defined as $p < 0.05$. All statistical analyses were conducted in the R statistical environment [31]. The likelihood of false-positive results was minimised by comparing p values to adjusted critical values according to the Benjamini and Hochberg false discovery rate (FDR) method [32]. Receiver-operating characteristic (ROC) curve analysis was also performed to further illustrate the classification accuracy of the PFR parameters. The area under the curve (AUC) of the ROC curves was estimated, an AUC of 1 indicates perfect classification ability, whereas an AUC near 0.5 indicates poor (random) classification ability. Logistical models combining PFR measures were created to assess combined classification performance.

3. Results

Eligible AIBL participants in Perth with PET data available numbered 206 (182 HC, 24 AD). $N = 180$ (87%) were willing to participate in the pupillometry study. Participants were excluded from the pupil response study if they had pupillary malformations, severe cataract ($N = 5$), self-reported history of glaucoma in either eye, penetrating eye wounds to both eyes, and eye surgery to both eyes that involved the muscle; if they used cholinesterase inhibitors or prescribed ocular medications ($N = 36$); or if they were unable to complete the task without excessive blinking ($N = 10$). All participants were white Caucasians.

The pupillometry study thus included $N = 129$ participants (115 HC, 14 AD). Table 1 shows the demographic comparisons between HC and AD groups, Table 2 shows the same for the HC group stratified according to NAB status, and Table 3 shows the same for the 37 HC participants with longitudinal pupillometry results available, again stratified according to NAB status.

There was a significantly greater proportion of *APOE* ε4 carriers in the AD group (Table 1, $p = 0.000001$), consistent with *APOE* ε4 being the major genetic risk factor for sporadic AD. The AD group was also older (mean age 77.4 years) compared to the HC group (mean age 72.9 years) ($p = 0.002$).

PFR parameters were not significantly different between males and females, or between *APOE* ε4 carriers and noncarriers, but they did exhibit an age dependence (MCV $p = 0.00002$, CV $p = 0.00001$, MCA $p = 0.002$, and AMP $p = 0.02$).

Significant differences in pupil response were found between the AD and HC groups (Table 1). Specifically, the AD group exhibited reduced MCV ($p = 0.00045$, Figure 2), AMP ($p = 0.0030$), MCA ($p = 0.030$), and CV ($p = 0.0015$). All results were significant after adjustment using the Benjamini and Hochberg FDR method [32].

MCV provided the greatest clinical classification accuracy with sensitivity 100%, specificity 67%, and AUC 0.85 (CI [0.76–0.93]). Combining PFR parameters into a logistic model did not improve classification performance, as the parameters were highly correlated. However, adding age and *APOE* ε4 carrier status improved classification performance to sensitivity 91.7%, specificity 93.1%, and AUC 0.94 (CI [0.87–1]).

Stratifying the HC group according to NAB, the low-NAB group consisted of 77 participants of mean age 72.3 years, while the high-NAB group consisted of 38 participants of mean age 74.0 years. Demographics and results of this

Table 2: Demographics and descriptive PFR analysis for the HC group stratified according to neocortical amyloid burden (NAB), with ANOVA, χ^2 test, and GLM analysis.

	Healthy control [low NAB]	Healthy control [high NAB]	p value
Number of participants [N]	77	38	
Age: years [mean (±SD)]	72.3 (±5.2)	74.0 (±5.3)	0.05734$^{\sim}$
Sex: male [N (%)]	35 (49)	20 (53)	0.433†
APOE ε4 carrier: [N (%)]	10 (13)	17 (45)	**0.000202**†
MCA [mm/sec^2, mean (±SD)]	32.97 (±5.96)	30.08 (±7.2)	0.067‡
MCV [mm/sec, mean (±SD)]	4.48 (±0.63)	4.05 (±0.62)	**0.021**‡
CV [mm/sec, mean (±SD)]	3.23 (±0.47)	2.92 (±0.42)	0.12‡
AMP [mean (±SD)]	1.54 (±0.29)	1.41 (±0.26)	0.77‡

$^{\sim}$Analysis of variance (ANOVA) for the continuous age demographic variable ($p < 0.05$ considered significant). $^{\dagger}\chi^2$ test for categorical demographic variables (gender and *APOE* ε4 carrier status) ($p < 0.05$ considered significant). $^{\ddagger}p$ value from the generalised linear model analysis of differences between groups (including significant confounders). Bold values significant after adjustment for false discovery rate (FDR) using the Benjamini and Hochberg method. *APOE* ε4 carrier status refers to carrier/noncarrier of an apolipoprotein E ε4 allele. NAB refers to neocortical amyloid burden, SD refers to standard deviation, mm refers to millimetres, sec refers to seconds, PFR refers to pupil flash response, HC refers to healthy control, AD refers to Alzheimer's disease, GLM refers to generalised linear methods, MCA refers to maximum constriction acceleration, MCV refers to maximum constriction velocity, CV refers to average constriction velocity, and AMP refers to constriction amplitude.

Table 3: Demographics and descriptive PFR analysis for the longitudinal HC group stratified according to neocortical amyloid burden (NAB), with ANOVA, χ^2 test, and GLM and ROC analyses.

	Healthy control [low NAB]	Healthy control [high NAB]	p value
Number of participants [N]	19	11	
Age: years [mean (±SD)]	72.2 (±0.31)	72.1 (±4.3)	0.97$^{\sim}$
Sex: male [N (%)]	7 (37)	8 (73)	**0.00026**†
APOE ε4 carrier [N (%)]	4 (21)	10 (91)	**0.035**†
Change in MCA [mm/sec^2, mean (±SD)]	−1.49 (±1.80)	−5.66 (±3.10)	**0.0068**‡
Change in MCV [mm/sec, mean (±SD)]	−0.19 (±0.17)	−0.55 (±0.42)	0.047‡
Change in CV [mm/sec, mean (±SD)]	−0.52 (±0.75)	−0.21 (±0.1)	0.62‡
Change in AMP [mm, mean (±SD)]	−0.24 (±0.32)	−0.13 (±0.09)	0.24‡

$^{\sim}$Analysis of variance (ANOVA) for the continuous age demographic variable ($p < 0.05$ considered significant). $^{\dagger}\chi^2$ test for categorical demographic variables (gender and *APOE* ε4 carrier status) ($p < 0.05$ considered significant). $^{\ddagger}p$ value from the generalised linear model analysis of differences between groups (including significant confounders). Bold values significant after adjustment for false discovery rate (FDR) using the Benjamini and Hochberg method. *APOE* ε4 carrier status refers to carrier/noncarrier of an apolipoprotein E ε4 allele. NAB refers to neocortical amyloid burden, SD refers to standard deviation, mm refers to millimetres, sec refers to seconds, PFR refers to pupil flash response, HC refers to healthy control, AD refers to Alzheimer's disease, GLM refers to generalised linear methods, MCA refers to maximum constriction acceleration, MCV refers to maximum constriction velocity, CV refers to average constriction velocity, and AMP refers to constriction amplitude.

comparison are presented in Table 2. There was a significantly greater proportion of *APOE* ε4 carriers in the high-NAB group ($p = 0.0002$), again consistent with *APOE* ε4 being the major genetic risk factor for sporadic AD. MCV was reduced in the high-NAB group ($p = 0.021$). The remaining PFR parameters exhibited nonsignificant trends for reduced values in the high-NAB group. Combining MCV and MCA into a logistic model provided classification accuracy for high NAB with sensitivity 57.1%, specificity 71.6%, and AUC 0.63 (CI [0.52–0.75]). Adding age and *APOE* ε4 carrier status improved the performance of the model to sensitivity 60%, specificity 88%, and AUC 0.74 (CI [0.63–0.84]).

Thirty HC participants (19 low NAB, 11 high NAB) underwent longitudinal pupillometry, with PFR data collected using the same device and an intermeasurement period ranging 27–36 months prior to this study [8]. The change in PFR parameters between visits was calculated. Demographics and results of this comparison are presented in Table 3. There was again a significantly greater proportion of *APOE* ε4 carriers in the high-NAB group ($p = 0.035$). The high-NAB group also had a greater percentage of males (73%) compared to the low-NAB group (37%) ($p = 0.00026$). PFR parameters were not significantly correlated with the exact interval between longitudinal measurements.

Group means for each PFR parameter change were negative, indicating a weaker PFR at the more recent pupillometry test. The reduction in MCA and MCV was more pronounced in the high-NAB group ($p = 0.0068$, $p = 0.047$, resp.). The MCA result was still significant after Benjamini and Hochberg FDR adjustment [32]; however, the maximum velocity result was not. Combining MCA and MCV in a logistic model provided a classification accuracy for high NAB with sensitivity 73%, specificity 100%, and AUC 0.90

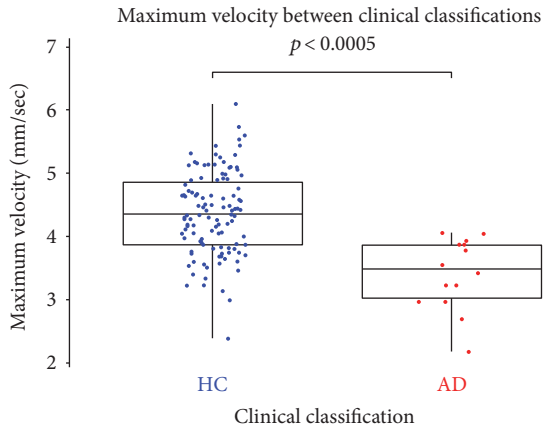

Figure 2: Comparison across clinical groups of the maximum velocity in the constriction phase of the pupil flash response. HC refers to healthy control participants, AD refers to Alzheimer's disease, mm refers to millimetres, and sec refers to seconds.

(CI [0.75–1]). Adding age and *APOE* $\varepsilon 4$ carrier status improved the performance of the model to sensitivity 91%, specificity 100%, and AUC 0.99 (CI [0.96–1.0]).

4. Discussion

The results are indicative of a weaker constriction phase pupil response in AD, consistent with earlier studies [3–5, 9]. Possible causes of the PFR changes in AD are degeneration in relays in the midbrain or central cholinergic depletion [11, 12]. The four PFR parameters considered in this study are all measures of the constriction phase of the PFR which is primarily a parasympathetic cholinergic response [1]. These four PFR parameters were also the same parameters that were most significantly altered in AD in prior studies [3–8]. The results therefore suggest cholinergic deficits in the peripheral parasympathetic pathway in AD. AD patients receiving pharmacological treatment with anticholinesterase agents (such as Donepezil) have been excluded from this study, due to the likely effect of these drugs on the PFR. The necessary exclusion of those on anticholinesterase agents introduces some bias as it is possible that those not so treated are going to be different in some way from the 60–70% of AD subjects who do receive such therapy; for example, reported results from other studies indicate that Donepezil may normalize PFR in some AD patients [4, 5]. If PFR changes in AD relate to neurotransmitter status, then PFR testing may be useful as an objective, noninvasive monitor with which to follow disease progression and treatment efficacy.

As therapeutic trials in AD have shifted to earlier, preclinical intervention [33, 34], the need has grown for a practical screening test to identify those individuals on the pathway to symptomatic AD. Clinicopathologic studies at autopsy support the hypothesis of a protracted asymptomatic stage of AD, with the slow buildup of Aβ protein plaques beginning about 10–20 years prior to diagnosis [35–41]. PET Aβ neuroimaging provides a semiquantitative measure of NAB [16, 18–20]. However, while it is a valuable diagnostic and secondary screening biomarker, the procedure is not suitable as a primary screening technology for AD, due to cost, availability of PET scanners, invasiveness, and radiation dose. There is consequently a need for a noninvasive, cost-effective population-based AD screening technology to triage those requiring more extensive screening. Recent results from Aβ immunotherapy trials have shown promise, both for clearance of Aβ from the brain and for slowing cognitive decline in early or preclinical AD [33, 34], clearly underscoring the need for early detection.

To investigate pupillometry as a potential component of such an AD screening test, the present study investigated constriction phase pupil response in cognitively normal healthy control individuals stratified according to PET-determined NAB. The low-NAB group consists of cognitively and neuropathologically normal healthy control participants, while the high-NAB group consists of participants who have AD neuropathology but are still cognitively normal, suggesting they are in the preclinical phase of AD.

Since the cross-sectional data suggest a weaker pupil response in the high-NAB group, we hypothesized that longitudinal monitoring of pupil response may perform better at detecting preclinical AD. Natural variation in PFR between individuals may limit the utility of a single PFR test for AD screening; hence, it is possible that longitudinal monitoring might facilitate more accurate preclinical detection or monitoring of AD. Hence, we also investigated longitudinal changes in PFR over approximately 3 years. As the group means for each PFR parameter change were negative, the results suggested a decline in PFR over the period, consistent with the observed age-dependence of PFR parameters in the full cohort. The reduction in MCA was more pronounced in the high-NAB group, with a similar trend for MCV (not significant after multiple testing adjustment). Longitudinal change in MCA and MCV provided good classification accuracy (AUC 0.9); hence, pupillometric changes over time may have utility in detecting preclinical AD. The value of PFR testing may be in its use for providing a noninvasive monitor of physiological abnormality with which to follow disease progression and treatment efficacy.

Overall, the results add to the evidence of a weaker pupil flash response in AD and suggest that some PFR changes may occur in preclinical AD. To our knowledge, we are the only group to report on PFR differences with respect to NAB and preclinical AD. Cholinergic depletion may occur in preclinical AD, and pupillometry may have utility as a component of a practical screening test for early detection of AD. Additionally, longitudinal pupillometry could provide a practical monitoring test for disease progression or response to therapy.

The constriction phase of the PFR is primarily a parasympathetic response of the autonomic nervous system; hence, constriction PFR parameters can be used as an accurate method to assess the function of the neurotransmitter involved, acetylcholine [1, 3, 42]. Studies have suggested that PFR is sensitive to early cholinergic depletion which can lead to a decline in cognitive function. Cholinergic depletion may also occur in other diseases such as Parkinson's disease [43], which has also been reported to influence PFR [5, 9]. Hence,

the specificity of the PFR changes in AD needs further investigation using cohorts which include individuals with other disorders that may affect the cholinergic system and PFR.

A major strength of this study is the well characterized cohorts, including the presence of neuroimaging data that enable deeper interrogation of associations between PFR parameters and AD. A limitation was the small number of participants ($N = 27$) in the longitudinal study; the results warrant further investigation with a similarly well-characterized, larger cohort.

5. Conclusions

This study demonstrates relationships between pupil response parameters, neocortical amyloid plaque load, and AD. Some PFR changes that are associated with diagnosed AD also occur in preclinical AD.

Pupillometry demonstrates potential as an adjunct (possibly together with blood or other biomarkers) (1) for accurate diagnosis of AD and monitoring of disease progress and response to therapy and (2) for low-cost and noninvasive detection of preclinical AD, recruitment into preclinical AD therapeutic trials and also monitoring response in these trials.

The results of this study suggest that PFR monitoring, rather than a single PFR test, might be more powerful as part of an early screening test for AD and for monitoring disease progress and response to intervention. Pupillometry is a low-cost, noninvasive technology that may reflect early cholinergic deficits preceding memory and cognitive decline.

Conflicts of Interest

All authors report no conflict of interest.

Acknowledgments

The authors wish to thank the Australian Imaging, Biomarker and Lifestyle (AIBL) Study Team (http://www.aibl.csiro.au/about/aibl-research-team) for referring participants to the study. They also wish to thank the participants of the AIBL study for their commitment and dedication in helping advance research into the early detection and causation of AD. Funding for the study was provided by the CSIRO Flagship Collaboration Fund and the Science and Industry Endowment Fund (SIEF) in partnership with Edith Cowan University (ECU), the Florey Institute of Neuroscience and Mental Health, Alzheimer's Australia (AA), National Ageing Research Institute (NARI), Austin Health, CogState Ltd., Hollywood Private Hospital, and Sir Charles Gairdner Hospital. The study also received funding from the National Health and Medical Research Council (NHMRC), the Dementia Collaborative Research Centres program (DCRC2), the Cooperative Research Centre (CRC) for Mental Health—funded through the CRC program (an Australian Government Initiative, Grant ID 20100104), the McCusker Alzheimer's Research Foundation, and Operational Infrastructure Support from the Government of Victoria. Shaun Frost received funding support from the National Health and Medical Research Council (NHMRC) of Australia, in the form of a Dementia Research Fellowship.

References

[1] I. E. Loewenfeld, *The Pupil: Anatomy, Physiology, and Clinical Applications*, 1999.

[2] H. Guyton, *Textbook of Medical Physiology*, W.B. Saunders Company Publications, Philadelphia, 9th edition, 1996.

[3] D. F. Fotiou, C. G. Brozou, A. B. Haidich et al., "Pupil reaction to light in Alzheimer's disease: evaluation of pupil size changes and mobility," *Aging Clinical and Experimental Research*, vol. 19, no. 5, pp. 364–371, 2007.

[4] F. Fotiou, K. N. Fountoulakis, M. Tsolaki, A. Goulas, and A. Palikaras, "Changes in pupil reaction to light in Alzheimer's disease patients: a preliminary report," *International Journal of Psychophysiology*, vol. 37, no. 1, pp. 111–120, 2000.

[5] E. Granholm, S. Morris, D. Galasko, C. Shults, E. Rogers, and B. Vukov, "Tropicamide effects on pupil size and pupillary light reflexes in Alzheimer's and Parkinson's disease," *International Journal of Psychophysiology*, vol. 47, no. 2, pp. 95–115, 2003.

[6] E. Ferrario, M. Molaschi, L. Villa, O. Varetto, C. Bogetto, and R. Nuzzi, "Is videopupillography useful in the diagnosis of Alzheimer's disease?" *Neurology*, vol. 50, no. 3, pp. 642–644, 1998.

[7] A. Tales, T. Troscianko, D. Lush, J. Haworth, G. K. Wilcock, and S. R. Butler, "The pupillary light reflex in aging and Alzheimer's disease," *Aging (Milano)*, vol. 13, no. 6, pp. 473–478, 2001.

[8] S. Frost, Y. Kanagasingam, H. Sohrabi et al., "Pupil response biomarkers for early detection and monitoring of Alzheimer's disease," *Current Alzheimer Research*, vol. 10, no. 9, pp. 931–939, 2013c.

[9] D. F. Fotiou, V. Stergiou, D. Tsiptsios, C. Lithari, M. Nakou, and A. Karlovasitou, "Cholinergic deficiency in Alzheimer's and Parkinson's disease: evaluation with pupillometry," *International Journal of Psychophysiology*, vol. 73, no. 2, pp. 143–149, 2009.

[10] P. Davies and A. J. Maloney, "Selective loss of central cholinergic neurons in Alzheimer's disease," *Lancet*, vol. 2, no. 8000, p. 1403, 1976.

[11] K. Herholz, S. Weisenbach, G. Zündorf et al., "In vivo study of acetylcholine esterase in basal forebrain, amygdala, and cortex in mild to moderate Alzheimer disease," *NeuroImage*, vol. 21, no. 1, pp. 136–143, 2004.

[12] H. Tohgi, T. Abe, K. Hashiguchi, M. Saheki, and S. Takahashi, "Remarkable reduction in acetylcholine concentration in the cerebrospinal fluid from patients with Alzheimer type dementia," *Neuroscience Letters*, vol. 177, no. 1-2, pp. 139–142, 1994.

[13] R. Prettyman, P. Bitsios, and E. Szabadi, "Altered pupillary size and darkness and light reflexes in Alzheimer's disease," *Journal of Neurology, Neurosurgery, and Psychiatry*, vol. 62, no. 6, pp. 665–668, 1997.

[14] Alzheimer's Disease International, *The Global Impact of Dementia 2013–2050*, 2013.

[15] K. Blennow, H. Hampel, M. Weiner, and H. Zetterberg, "Cerebrospinal fluid and plasma biomarkers in Alzheimer disease," *Nature Reviews Neurology*, vol. 6, no. 3, pp. 131–144, 2010.

[16] A. M. Fagan, M. A. Mintun, R. H. Mach et al., "Inverse relation between in vivo amyloid imaging load and cerebrospinal fluid

Abeta42 in humans," *Annals of Neurology*, vol. 59, no. 3, pp. 512–519, 2006.

[17] T. Sunderland, G. Linker, N. Mirza et al., "Decreased beta-amyloid1-42 and increased tau levels in cerebrospinal fluid of patients with Alzheimer disease," *Journal of the American Medical Association*, vol. 289, no. 16, pp. 2094–2103, 2003.

[18] L. J. Thal, K. Kantarci, E. M. Reiman et al., "The role of biomarkers in clinical trials for Alzheimer disease," *Alzheimer Disease and Associated Disorders*, vol. 20, no. 1, pp. 6–15, 2006.

[19] J. C. Morris, C. M. Roe, E. A. Grant et al., "Pittsburgh compound B imaging and prediction of progression from cognitive normality to symptomatic Alzheimer disease," *Archives of Neurology*, vol. 66, no. 12, pp. 1469–1475, 2009.

[20] C. C. Rowe, K. A. Ellis, M. Rimajova et al., "Amyloid imaging results from the Australian Imaging, Biomarkers and Lifestyle (AIBL) study of aging," *Neurobiology of Aging*, vol. 31, no. 8, pp. 1275–1283, 2010.

[21] V. L. Villemagne, S. Burnham, P. Bourgeat et al., "Amyloid beta deposition, neurodegeneration, and cognitive decline in sporadic Alzheimer's disease: a prospective cohort study," *Lancet Neurology*, vol. 12, no. 4, pp. 357–367, 2013.

[22] K. A. Ellis, A. I. Bush, D. Darby et al., "The Australian Imaging, Biomarkers and Lifestyle (AIBL) study of aging: methodology and baseline characteristics of 1112 individuals recruited for a longitudinal study of Alzheimer's disease," *International Psychogeriatrics*, vol. 21, no. 4, pp. 672–687, 2009.

[23] G. McKhann, D. Drachman, M. Folstein, R. Katzman, D. Price, and E. M. Stadlan, "Clinical diagnosis of Alzheimer's disease: report of the NINCDS-ADRDA Work Group under the auspices of Department of Health and Human Services Task Force on Alzheimer's disease," *Neurology*, vol. 34, no. 7, pp. 939–944, 1984.

[24] R. C. Petersen, G. E. Smith, S. C. Waring, R. J. Ivnik, E. G. Tangalos, and E. Kokmen, "Mild cognitive impairment: clinical characterization and outcome," *Archives of Neurology*, vol. 56, no. 3, pp. 303–308, 1999.

[25] B. Winblad, K. Palmer, M. Kivipelto et al., "Mild cognitive impairment—beyond controversies, towards a consensus: report of the International Working Group on Mild Cognitive Impairment," *Journal of Internal Medicine*, vol. 256, no. 3, pp. 240–246, 2004.

[26] P. Bourgeat, G. Chételat, V. L. Villemagne et al., "Beta-amyloid burden in the temporal neocortex is related to hippocampal atrophy in elderly subjects without dementia," *Neurology*, vol. 74, no. 2, pp. 121–127, 2010.

[27] R. Vandenberghe, K. Van Laere, A. Ivanoiu et al., "18F-flutemetamol amyloid imaging in Alzheimer disease and mild cognitive impairment: a phase 2 trial," *Annals of Neurology*, vol. 68, no. 3, pp. 319–329, 2010.

[28] L. Thurfjell, J. Lilja, R. Lundqvist et al., "Automated quantification of 18F-flutemetamol PET activity for categorizing scans as negative or positive for brain amyloid: concordance with visual image reads," *Journal of Nuclear Medicine*, vol. 55, no. 10, pp. 1623–1628, 2014.

[29] V. Villemagne, K. Pike, M. Fodero-Tavoletti et al., "Age dependent prevalence of beta-amyloid positive 11C-PiB PET in healthy elderly subjects parallels neuropathology findings," *Journal of Nuclear Medicine*, vol. 49, no. 5, MeetingAbstracts_1, p. 34, 2008.

[30] E. H. Corder, A. M. Saunders, W. J. Strittmatter et al., "Gene dose of apolipoprotein E type 4 allele and the risk of Alzheimer's disease in late onset families," *Science*, vol. 261, no. 5123, pp. 921–923, 1993.

[31] R_Development_Core_Team, *R: A Language and Environment for Statistical Computing*, R Foundation for Statistical Computing, Vienna, Austria, 2013.

[32] Y. Benjamini and Y. Hochberg, "Controlling the false discovery rate - a practical and powerful approach to multiple testing," *Journal of Royal Statistical Society B Methodological*, vol. 57, no. 1, pp. 289–300, 1995.

[33] J. Sevigny, P. Chiao, T. Bussière et al., "The antibody aducanumab reduces Abeta plaques in Alzheimer's disease," *Nature*, vol. 537, no. 7618, pp. 50–56, 2016.

[34] B. Vellas, M. C. Carrillo, C. Sampaio et al., "Designing drug trials for Alzheimer's disease: what we have learned from the release of the phase III antibody trials: a report from the EU/US/CTAD task force," *Alzheimer's & Dementia*, vol. 9, no. 4, pp. 438–444, 2013.

[35] H. Braak and E. Braak, "Frequency of stages of Alzheimer-related lesions in different age categories," *Neurobiology of Aging*, vol. 18, no. 4, pp. 351–357, 1997.

[36] C. M. Hulette, K. A. Welsh-Bohmer, M. G. Murray, A. M. Saunders, D. C. Mash, and L. M. McIntyre, "Neuropathological and neuropsychological changes in "normal" aging: evidence for preclinical Alzheimer disease in cognitively normal individuals," *Journal of Neuropathology and Experimental Neurology*, vol. 57, no. 12, pp. 1168–1174, 1998.

[37] W. R. Markesbery, "Neuropathologic alterations in mild cognitive impairment: a review," *Journal of Alzheimers Disease*, vol. 19, no. 1, pp. 221–228, 2010.

[38] W. R. Markesbery, F. A. Schmitt, R. J. Kryscio, D. G. Davis, C. D. Smith, and D. R. Wekstein, "Neuropathologic substrate of mild cognitive impairment," *Archives of Neurology-Chicago*, vol. 63, no. 1, pp. 38–46, 2006.

[39] J. C. Morris and J. L. Price, "Pathologic correlates of nondemented aging, mild cognitive impairment, and early-stage Alzheimer's disease," *Journal of Molecular Neuroscience*, vol. 17, no. 2, pp. 101–118, 2001.

[40] J. L. Price, A. I. Ko, M. J. Wade, S. K. Tsou, D. W. McKeel, and J. C. Morris, "Neuron number in the entorhinal cortex and CA1 in preclinical Alzheimer disease," *Archives of Neurology-Chicago*, vol. 58, no. 9, pp. 1395–1402, 2001.

[41] T. GomezIsla, J. L. Price, D. W. McKeel, J. C. Morris, J. H. Growdon, and B. T. Hyman, "Profound loss of layer II entorhinal cortex neurons occurs in very mild Alzheimer's disease," *Journal of Neuroscience*, vol. 16, no. 14, pp. 4491–4500, 1996.

[42] H. Wilhelm and B. Wilhelm, "Clinical applications of pupillography," *Journal of Neuro-Ophthalmology*, vol. 23, no. 1, pp. 42–49, 2003.

[43] B. Dubois, B. Pillon, F. Lhermitte, and Y. Agid, "Cholinergic deficiency and frontal dysfunction in Parkinson's disease," *Annals of Neurology*, vol. 28, no. 2, pp. 117–121, 1990.

Hindawi
Journal of Ophthalmology
Volume 2017, Article ID 5649532, 12 pages
https://doi.org/10.1155/2017/5649532

Review Article

Changes in Intraocular Straylight and Visual Acuity with Age in Cataracts of Different Morphologies

Sonia Gholami,[1] Nicolaas J. Reus,[2] and Thomas J. T. P. van den Berg[3]

[1]*Rotterdam Ophthalmic Institute, Rotterdam, Netherlands*
[2]*Amphia Hospital, Breda, Netherlands*
[3]*Netherlands Institute for Neuroscience and Royal Netherlands Academy of Arts and Sciences, Amsterdam, Netherlands*

Correspondence should be addressed to Sonia Gholami; sonia.gholami@googlemail.com

Received 13 March 2017; Accepted 7 June 2017; Published 31 July 2017

Academic Editor: Jose M. González-Meijome

Purpose. To investigate the significance of difference in straylight of cataract eyes with different morphologies, as a function of age and visual acuity. *Methods*. A literature review to collect relevant papers on straylight, age, and visual acuity of three common cataract morphologies leads to including five eligible papers for the analysis. The effect of morphology was incorporated to categorize straylight dependency on the two variables. We also determined the amount of progression in a cataract group using a control group. *Results*. The mean straylight was 1.22 log units ± 0.20 (SD) in nuclear (592 eyes), 1.26 log units ± 0.23 in cortical (776 eyes), and 1.48 log units ± 0.34 in posterior subcapsular (75 eyes) groups. The slope of straylight-age relationship was 0.009 ($R^2 = 0.20$) in nuclear, 0.012 ($R^2 = 0.22$) in cortical, and 0.014 ($R^2 = 0.11$) in posterior subcapsular groups. The slope of straylight-visual acuity relationship was 0.62 ($R^2 = 0.25$) in nuclear, 0.33 ($R^2 = 0.13$) in cortical, and 1.03 ($R^2 = 0.34$) in posterior subcapsular groups. *Conclusion*. Considering morphology of cataract provides a better insight in assessing visual functions of cataract eyes, in posterior subcapsular cataract, particularly, in spite of notable elevated straylight, visual acuity might not manifest severe loss.

1. Introduction

The eye is an optical system with imperfections. Entering this optical system, light is refracted by the ocular media (e.g., cornea and crystalline lens) to form an image on the retina. However, part of this light is scattered by optical imperfections. Depending on the direction of scattering (forward or backward), it can have different influences on vision. The forward light scattering causes (intraocular) straylight or disability glare [1]. It produces undesired veiling of the retinal image which leads to reduced vision, glare, and other visual impairments. In young healthy eyes, almost 10% of the inbound light is scattered [2]. However, in eyes older than 50 years of age, this number increases considerably [3]. A phakic norm curve has been established that can be used as a reference for clinical practice [3]. Some pathological conditions, in particular cataract, increase the amount of intraocular straylight above normal. In clinical practice, a patient's visual complaints, ophthalmic examination with a slit-lamp, and measurement of visual acuity are the predominant scales for managing cataract. It should be noted that a slit-lamp examination provides only backscatter-based assessments. As the correlation between forward and backward light scattering has been shown to be small, methods that measure the amount of backscatter, such as slit-lamp examination, cannot reliably quantify straylight and glare [4–7]. Various studies have shown that straylight is a vision impairment that is not directly related to visual acuity and is only weakly correlated to it [3, 8]. A computerized purpose-built device, called C-Quant (Oculus Optikgeräte GmbH), measures the amount of ocular straylight and renders a parameter in the logarithmic unit (log(s)) with good reliability and repeatability [9–11].

As mentioned earlier, visual acuity is an important criterion in the cataract surgical decision-making process. However, various studies [12, 13] have shown that in a significant number of cataract cases, visual acuity is not an adequate measure to judge visual performance. Subsequent studies have supported this notion [14, 15]. Moreover, there have

been reports of no change or even an increase in straylight after cataract surgery when the decision was made solely based on visual acuity [16]. The reason for this is that visual acuity only evaluates the impact of narrow-angle light spreading due to refractive errors and therefore can only measure a limited part of a patient's vision [13, 17]. Elliot et al. [7] expressed that additional visual tests were needed that could mirror visual loss but at the same time should be unrelated to visual acuity. They acknowledged the direct compensation method to quantify straylight as a standard technique to evaluate the validity of disability glare tests.

Recently, a literature review [18] established a norm curve for pseudophakic eyes and also a reference curve to estimate the amount of straylight to be expected after cataract surgery by introducing *straylight improvement* as a function of age and preoperative straylight. Although this reference is a good measure for cataract management in an average eye, it may overlook the influence of the type, location, and intensity of the cataract on the outcome because the type of cataract was not specified in the norm curve. To establish morphologically categorized references, we need a phakic norm stratified to the type of cataract. In the present study, we performed a literature review to identify relevant papers on straylight, age, and visual acuity in three common types of cataract. In addition, we recalculated the significance of the relation between straylight and visual acuity with taking cataract morphology into account. The published studies included in this literature review were evidenced individually that such correlation varies from one type of cataract to another. The population sizes and severities of the cataracts were different across these studies. We consider the relatively large final number of observations and their diverse degrees of cataract intensity as the strength of this study to improve the generalizability of the results.

2. Materials and Methods

This study includes two parts. The first part encompasses a comprehensive literature review to study the effect of different cataract morphologies on straylight and to determine models for straylight values as a function of age for different types of cataract. Second, we calculated the correlations between straylight and visual acuity, the amount of progression of straylight and visual acuity from those of a normal group, and the ratios of straylight to age and visual acuity in each cataract group.

A literature examination was carried out including all available studies that reported straylight values, measured with a C-Quant instrument (Oculus Optikgeräte GmbH), in cataract eyes with specification of its morphology. The language of the articles and age, gender, and race of the participants had no influence in this process. All papers provided information on intraocular straylight, age, and visual acuity of participants with the specification of the type of cataract. All papers had excluded patients with a history of ocular surgery or diseases, diabetic retinopathy, glaucoma, and age-related macular degeneration. We considered data with expected standard deviation (ESD) of 0.12 log units or less reliable for analysis.

Table 1: Red circles show deficient data, and green circles show available data in each individual study.

Cataract	Study (year)	Age	SL	VA
Nuclear	Filgueira et al. (2016)	🟢	🟢	🟢
	Congdon et al. (2012)	🟢	🟢	🟢
	Bal et al. (2011)	🟢	🟢	🟢
	Nischler et al. (2010)	🟢	🟢	🟢
	de Waard et al. (1992)	🔴	🟢	🟢
Cortical	Filgueira et al. (2016)	🔴	🔴	🔴
	Congdon et al. (2012)	🔴	🔴	🔴
	Bal et al. (2011)	🟢	🟢	🟢
	Nischler et al. (2010)	🟢	🟢	🟢
	de Waard et al. (1992)	🔴	🟢	🟢
Posterior subcapsular	Filgueira et al. (2016)	🟢	🟢	🟢
	Congdon et al. (2012)	🔴	🔴	🔴
	Bal et al. (2011)	🟢	🟢	🟢
	Nischler et al. (2010)	🟢	🟢	🟢
	de Waard et al. (1992)	🔴	🟢	🟢

PubMed, Medline, and Google Scholar were the scientific databases we screened using the following keywords: *straylight, C-Quant, age, visual acuity, cataract, cataract morphology, cataract classification, LOCS III, nuclear cataract, cortical cataract and posterior subcapsular cataract (PSC)*. In case of overlapping data in the studies, the one with the larger population was included for the review. Five papers met the eligibility criteria: de Waard et al., Nischler et al., Bal et al., Congdon et al., and Filgueira et al. [6, 19–22]. Because of lack of the desired data in four cases, we contacted the corresponding authors. In one case, there was no response; therefore GSYS2.4 (a graph digitizing system developed by Nuclear Reaction Data Center, University of Hokkaido, Japan) was used to extract data from the published graphs. Table 1 shows which data were reported by the five included studies. It has to be noted that the various studies classified the types of cataract differently based on LOCS (Table 2).

Data from all five articles were used to develop the log(s)-age normative curves for the three types of cataract. The correlations between the two variables were calculated and compared with each other. We calculated the normally expected mean straylight value for each cataract type, all types of cataract combined and the control group by using the log(s)-age normative equation obtained by van den Berg et al. [23], which reads

$$\begin{aligned}\log(\text{straylight parameter}) &= \log(s) \\ &= 0.9 + \log\left(1 + (\text{age}/65)^4\right).\end{aligned} \quad (1)$$

Table 2: Range of intensity defined for each type of cataract in the studies.

Study	Cataract definition
Filgueira et al. (2016)	Early age-related cataracts: nuclear (NO = 1 and 2), posterior subcapsular (P = 1 and 2)
Congdon et al. (2012)	Nuclear (NO ≥ 3)
Bal et al. (2011)	Nuclear (NO > 2, NC > 2, $C \leq 2$, $P \leq 1$), cortical (NO ≤ 2, NC ≤ 2, $C > 2$, $P \leq 1$), posterior subcapsular ($C \leq 2$, $P > 1$)
Nischler et al. (2010)	Nuclear ($2 \leq$ NO ≤ 4, $2 \leq$ NC ≤ 4, $C < 2$, $P \leq 1.5$), cortical (NO < 2, NC < 2, $2 \leq C \leq 4$, $P \leq 1.5$), posterior subcapsular (NO < 2, NC < 2, $C < 2$, $1.5 \leq P \leq 4$)
de Waard et al. (1992)	Advanced age-related cataracts (morphologically not categorized)

The results were compared with the measured straylight values. The residuals are displayed by using histograms. To study the possible differentiative impact of morphology on the progressive process of cataract, we used the largest control group—which belonged to Nischler et al.—with the best straylight and visual acuity values. We then compared the straylight and visual acuity of each cataract group in each study by connecting the mean values to those of the control group using arrows to show the magnitude and direction of progression. The slopes and lengths of the arrows were compared with each other. The correlations between log(s) and logMAR visual acuity values were calculated and compared with each other. We also calculated the ratio of straylight to age and visual acuity for each type of cataract; the results are illustrated using box-and-whisker plots. The log(s)-logMAR normative curves for each type of cataract are also derived using data from all five articles.

Linear regression analysis was performed with Excel software (2010, Microsoft Corporation) and SPSS Statistics 21 (IBM Corporation) on the straylight values—log(s)—to describe it as a function of age and logMAR visual acuity. Unpaired t-tests were used to calculate the significance of differences in means (±95% CI) between each study and the normative curve of each cataract type. The significance level was set at P value less than 0.05.

3. Results

3.1. Comprehensive Review. As explained in Materials and Methods, five reports fulfilled the eligibility criteria. Table 3 shows a summary of outcomes of each study. Table 4 shows the outcomes for each type of cataract, all types of cataract combined, and the control group. Figure 1 illustrates age, visual acuity, and straylight distributions in each cataract group.

The evaluations concerning log(s)-logMAR-related analyses were based on 776 total observations, with mean visual acuity of 0.02 ± 0.18 log units (range −0.30 to 0.70 log units) and mean straylight of 1.23 ± 0.22 log units (range 0.61 to 2.09 log units). The total number of cataract eyes was 725 for evaluations concerning log(s)-age-related analyses with a mean age of 63 ± 9 years (range 44 to 85 years of age). Figures 2 and 3 show the log(s)-age and log(s)-logMAR linear regressions for studies comprising the required data.

3.2. Effect of Cataract Morphology on Straylight. Straylight varied as a function of cataract morphology (Table 3); it was significantly higher in the three cataract groups (1.22 ± 0.20 log units in nuclear cataract, 1.26 ± 0.23 log units in cortical cataract, and 1.48 ± 0.34 log units in PSC) compared to the control group (1.12 ± 0.16 log units, $P < 0.05$). In addition, in all cataracts combined, straylight was significantly increased (1.26 ± 0.12 log units) relative to the control group ($P < 0.05$).

3.3. Correlation with Age. Straylight showed the highest correlation with age in Congdon et al.'s nuclear group ($R^2 = 0.36$, $P < 0.05$), and it showed no to a very weak correlation in several other groups (Table 3). Figure 1 shows phakic normative curves for each type of cataract; the data were derived from 574 eyes of nuclear, 93 of cortical, and 58 eyes of PSC. Overall, cortical cataract showed the highest correlation between log(s) and age ($R^2 = 0.22$, $P < 0.05$), and the overall PSC showed the lowest correlation between the two variables ($R^2 = 0.11$, $P < 0.05$) (Table 4). Figure 2 shows reference curves for cataracts and control group. The overall relationships read as

$$\begin{aligned} &\text{straylight value} = 0.009 \times \text{age} + 0.60 \\ &\qquad \left(\text{nuclear group}; R^2 = 0.20, P < 0.05\right), \\ &\text{straylight value} = 0.012 \times \text{age} + 0.50 \\ &\qquad \left(\text{cortical group}; R^2 = 0.22, P < 0.05\right), \\ &\text{straylight value} = 0.014 \times \text{age} + 0.53 \\ &\qquad \left(\text{PSC group}; R^2 = 0.11, P < 0.05\right), \end{aligned} \tag{2}$$

whereas that of the control group reads

$$\begin{aligned} &\text{straylight value} = 0.007 \times \text{age} + 0.68 \\ &\qquad \left(\text{control group}; R^2 = 0.17, P < 0.05\right). \end{aligned} \tag{3}$$

Mean straylight values are displayed in Tables 2 and 3. The figures show differences in different studies.

The mean age of each group is depicted in Figure 3. Using the log(s)-age norm curve equation obtained by van den Berg et al. [23], we calculated the expected mean straylight for each cataract type of each study, overall cataract types, all cataract types combined, and control groups. The results were compared with the measured straylight values. The residuals are

Table 3: Overview of the analysis on the data derived from raw data or published plots of each individual study (NC: nuclear cataract; CC: cortical cataract; and PSC: posterior subcapsular cataract).

Cataract	First author (year)	Eyes (n)	Age (Y)	Mean ± SD VA (logMAR)	SL (log(s))	log(s)-age Dependency	R^2	log(s)-logMAR Dependency	R^2
NC	Filgueira (2016)	14	69 ± 18	0.10 ± 0.08	1.33 ± 0.21	log(s) = 0.008 × age + 0.75	0.02	log(s) = 0.14 × logMAR − 0.08	0.14
	Congdon (2012)	24	65 ± 10	0.22 ± 0.14	1.36 ± 0.33	log(s) = 0.019 × age + 0.12	0.36	log(s) = 0.82 × logMAR + 1.17	0.13
	Bal (2011)	23	67 ± 9	0.28 ± 0.18	1.50 ± 0.24	log(s) = 0.001 × age + 1.54	0.00	log(s) = 0.51 × logMAR + 1.36	0.14
	Nischler (2010)	512	63 ± 9	−0.05 ± 0.12	1.19 ± 0.17	log(s) = 0.008 × age + 0.65	0.21	log(s) = 0.44 × logMAR + 1.21	0.10
	de Waard (1992)	18	NA	0.39 ± 0.14	1.54 ± 0.16	NA	NA	log(s) = 0.01 × logMAR + 1.42	0.08
CC	Filgueira (2016)	NA	NA	NA	NA	NA	NA	NA	NA
	Congdon (2012)	NA	NA	NA	NA	NA	NA	NA	NA
	Bal (2011)	15	67 ± 7	0.25 ± 0.20	1.48 ± 0.29	log(s) = 0.020 × age + 0.13	0.26	log(s) = − 0.28 × logMAR + 1.55	0.04
	Nischler (2010)	78	62 ± 8	−0.06 ± 0.09	1.20 ± 0.17	log(s) = 0.008 × age + 0.69	0.17	log(s) = 0.13 × logMAR + 1.21	0.00
	de Waard (1992)	16	NA	0.24 ± 0.13	1.34 ± 0.29	NA	NA	log(s) = 1.22 × logMAR + 1.04	0.29
PSC	Filgueira (2016)	20	56 ± 5	0.03 ± 0.05	1.17 ± 0.27	log(s) = 0.013 × age + 0.42	0.06	log(s) = 0.04 × logMAR − 0.02	0.11
	Congdon (2012)	NA	NA	NA	NA	NA	NA	NA	NA
	Bal (2011)	20	64 ± 9	0.30 ± 0.22	1.79 ± 0.20	log(s) = 0.001 × age + 1.77	0.00	log(s) = 0.13 × logMAR + 1.76	0.02
	Nischler (2010)	18	61 ± 8	0.02 ± 0.11	1.30 ± 0.27	log(s) = 0.000 × age + 1.19	0.00	log(s) = 1.02 × logMAR + 1.28	0.17
	de Waard (1992)	17	NA	0.26 ± 0.18	1.67 ± 0.21	NA	NA	log(s) = 0.33 × logMAR + 1.58	0.08

Table 4: Overview of the analysis on collected data from individual studies for each cataract group.

Group	Number of eyes		Mean ± SD			log(s)-age		log(s)-logMAR	
	SL-age	SL-VA	Age (year)	VA (logMAR)	SL (log(s))	Dependency	R^2	Dependency	R^2
Nuclear	573	592	63 ± 9	−0.01 ± 0.16	1.22 ± 0.20	$\log(s) = 0.009 \times \text{age} + 0.60$	0.20	$\log(s) = 0.62 \times \text{logMAR} + 1.22$	0.25
Cortical	93	109	62 ± 8	0.03 ± 0.18	1.26 ± 0.23	$\log(s) = 0.012 \times \text{age} + 0.50$	0.22	$\log(s) = 0.33 \times \text{logMAR} + 1.24$	0.13
Posterior	58	75	60 ± 8	0.15 ± 0.20	1.48 ± 0.34	$\log(s) = 0.015 \times \text{age} + 0.53$	0.11	$\log(s) = 1.03 \times \text{logMAR} + 1.32$	0.34
All cataracts	724	776	63 ± 9	0.02 ± 0.18	1.23 ± 0.22	$\log(s) = 0.009 \times \text{age} + 0.64$	0.14	$\log(s) = 0.68 \times \text{logMAR} + 1.24$	0.26
Control	1761	1761	57 ± 8	−0.07 ± 0.11	1.12 ± 0.16	$\log(s) = 0.008 \times \text{age} + 0.68$	0.17	$\log(s) = 0.25 \times \text{logMAR} + 1.14$	0.03

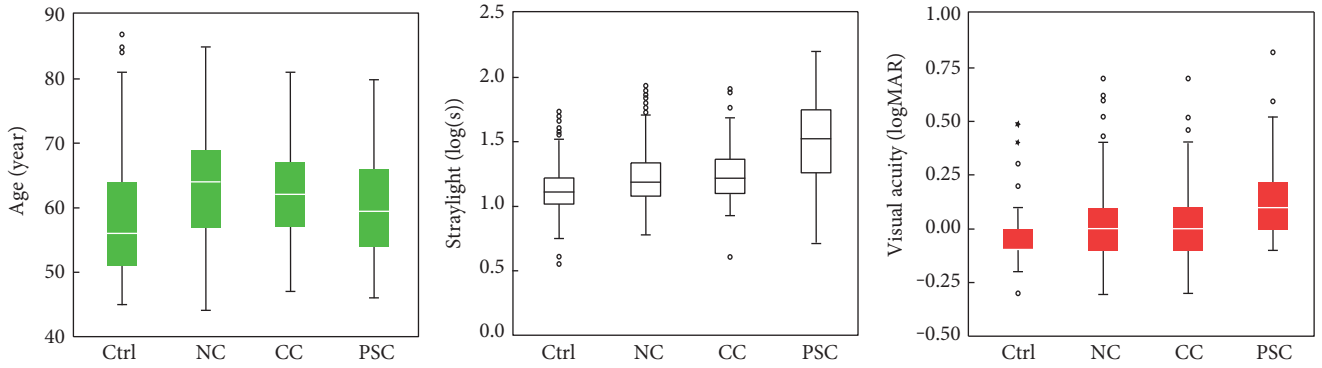

Figure 1: Age, intraocular straylight, and best-corrected visual acuity plotted for cataract and control groups. Straylight and visual acuity differed significantly from PSC to the other cataracts and control group. (NC: nuclear cataract; CC: cortical cataract; and PSC: posterior subcapsular cataract).

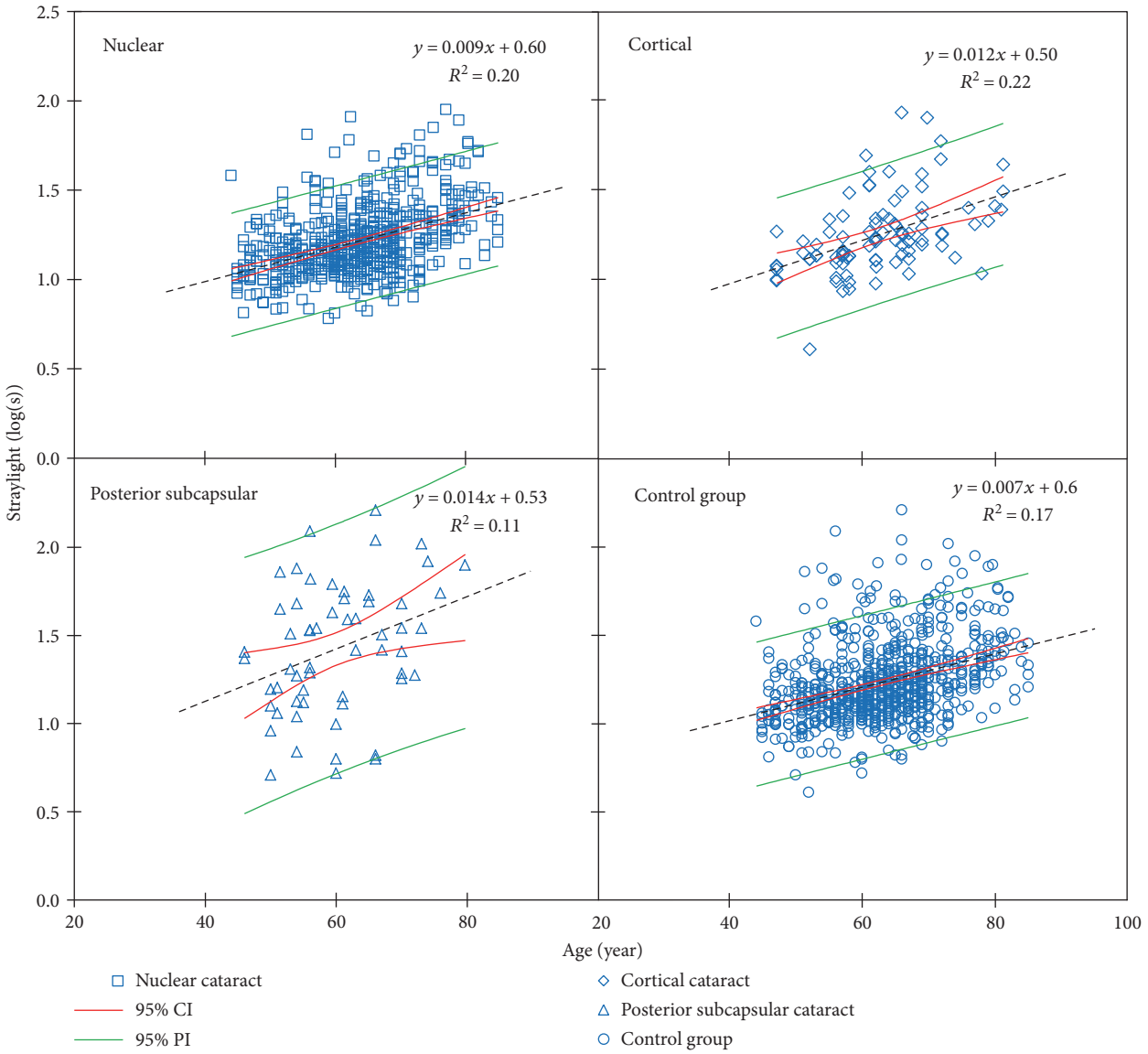

Figure 2: Linear models of log(s)-age dependency for nuclear cataract derived from four studies, cortical cataract derived from two studies, posterior subcapsular cataract derived from three studies and control group are plotted. Black dotted lines are the regression lines.

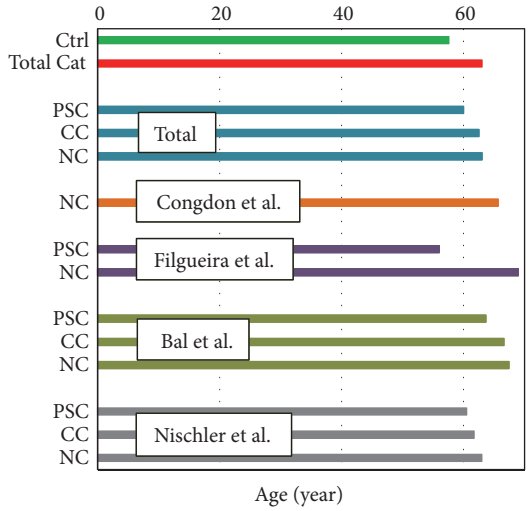

Figure 3: Mean age of each type of cataract in each published study. In average, patients with PSC cataract are the youngest. (Ctrl: control group; NC: nuclear cataract; Total cat: all cataract groups combined; CC: cortical cataract; and PSC: posterior subcapsular cataract).

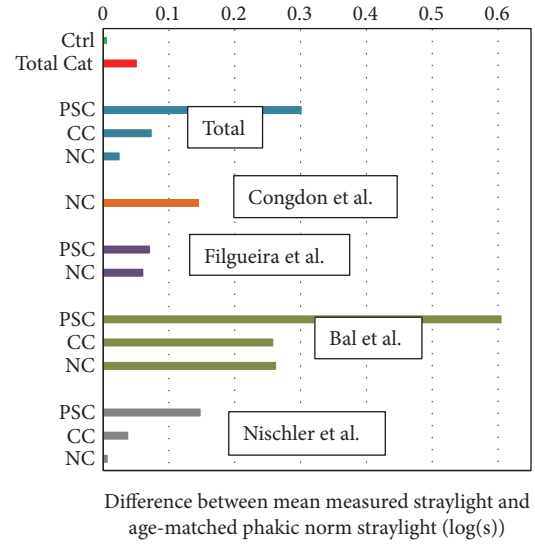

Figure 4: Differences between the mean straylight value in patients with different types of cataract for the various studies and the age-matched straylight value derived from the phakic norm curve by van den Berg et al. [23] are plotted. In all data, straylight in patients with PSC cataract showed the highest deviation from that of a noncataract (phakic) group. (Ctrl: control group; Total cat: all cataract groups combined; NC: nuclear cataract; CC: cortical cataract; and PSC: posterior subcapsular cataract).

displayed in Figure 4. We must remind the reader that not every study provided information on age (Table 1). Among three cataract groups, the mean straylight of PSC group showed the highest difference from the expected mean straylight of an age-matched phakic group; by contrast, nuclear group showed the smallest difference. The same figure shows negligible difference between measured and expected straylight in control group.

3.4. Correlation with Visual Acuity. Straylight showed the highest correlation with logMAR visual acuity in de Waard et al.'s cortical group ($R^2 = 0.29$, $P < 0.05$) and the lowest correlation in Nischler et al.'s cortical group ($R^2 = 0.00$, $P = 0.99$). Overall, PSC showed the highest correlation between straylight and logMAR visual acuity ($R^2 = 0.34$, $P < 0.05$) and cortical cataract showed the lowest correlation, however significant, between the two variables ($R^2 = 0.13$, $P < 0.05$). The relations and correlation coefficients between log(s) and logMAR visual acuity are reported in Tables 3 and 4.

Figure 5 shows log(s)-logMAR reference curves for cataracts and control group. The overall relationships read as

$$\begin{aligned}
&\text{straylight value} = 0.62 \times \text{visual acuity} + 1.22 \\
&\qquad \left(\text{nuclear group}; R^2 = 0.25, P < 0.05\right), \\
&\text{straylight value} = 0.33 \times \text{visual acuity} + 1.24 \\
&\qquad \left(\text{cortical group}; R^2 = 0.13, P < 0.05\right), \\
&\text{straylight value} = 1.03 \times \text{visual acuity} + 1.34 \\
&\qquad \left(\text{PSC group}; R^2 = 0.34, P < 0.05\right),
\end{aligned} \tag{4}$$

whereas the norm of the control group reads as

$$\begin{aligned}
&\text{straylight value} = 0.25 \times \text{visual acuity} + 1.14 \\
&\qquad \left(\text{control group}; R^2 = 0.03, P < 0.05\right).
\end{aligned} \tag{5}$$

From the above relationships, one can see that straylight varies as a function of morphology. Patients with PSC for a similar logMAR visual acuity have a higher straylight than the other cataracts and control group.

3.5. Cataract: Progression from Healthy Eyes. We estimated the amount of progression of mean straylight and mean visual acuity from those of the control group in each individual study and cataract groups. The progression lines are demonstrated in Figure 6. Data showed that PSC in Bal et al. had the highest progression from noncataract status in terms of both straylight ($\Delta SL = 0.68$ log units) and visual acuity ($\Delta VA = 0.37$ log units). However, with respect to the progression of individual variables, the mean visual acuity increased the most in de Waard et al.'s nuclear group ($\Delta VA = 0.46$ log units), whereas its mean straylight value increased ($\Delta SL = 0.42$ log units) less than that of Bal et al.'s PSC group. The mean visual acuity deteriorated the least in Nischler et al.'s nuclear and cortical groups.

3.6. Ratio between Straylight and Age and Visual Acuity. The ratios between straylight and age and between straylight and visual acuity are illustrated using box-and-whisker plots (Figure 7). The median of straylight parameter (s)/age (year) had the lowest value in nuclear cataract group and the highest value in PSC group, albeit with a rather more skewed distribution comparing the two other cataract groups. The differences in medians of the PSC group and the other two cataract groups were statistically significant. The median of log(s)-logMAR showed similarly lower values in nuclear and cortical groups in comparison to that of PSC group.

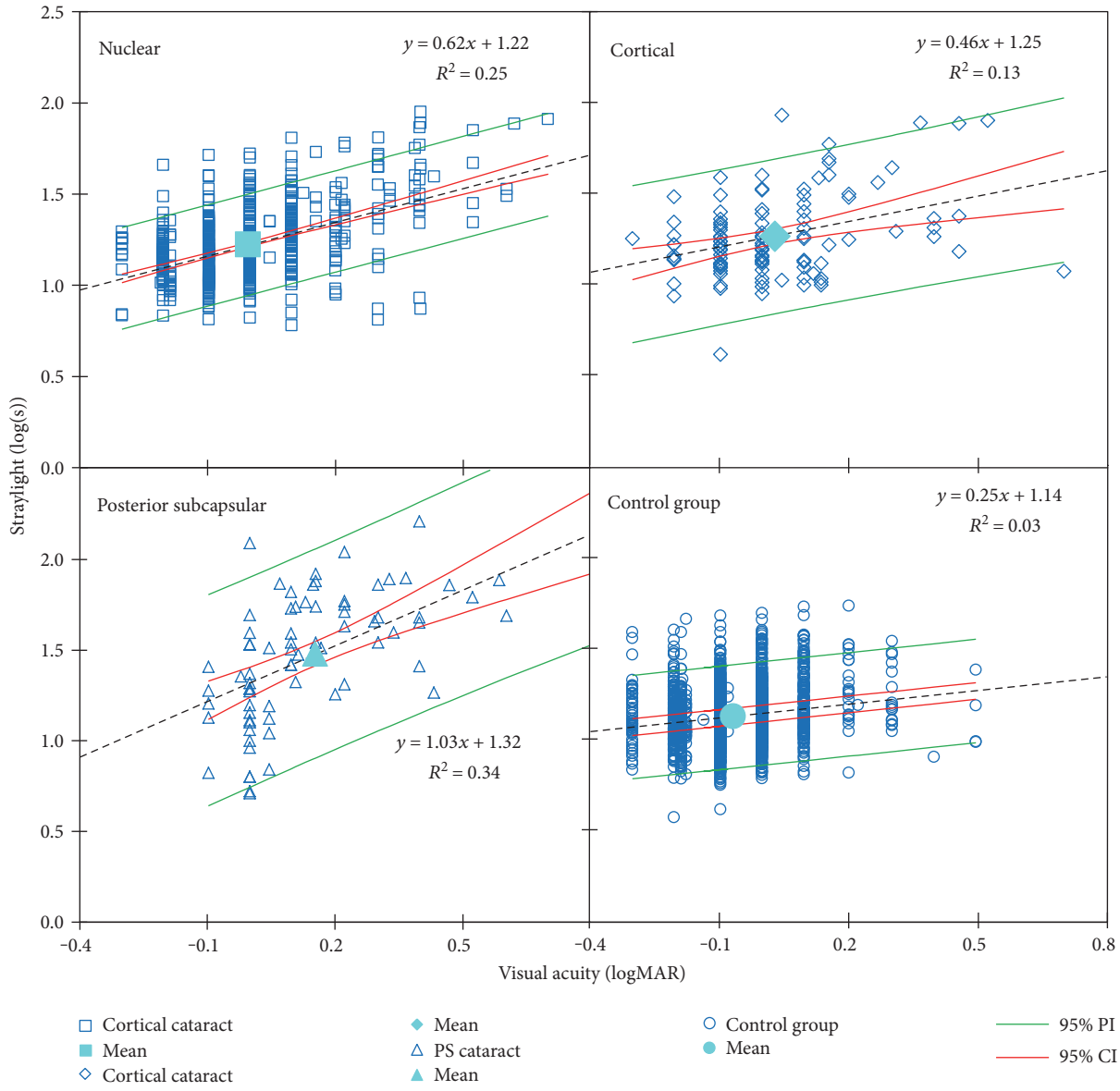

Figure 5: Linear models of log(s)-logMAR visual acuity dependency for nuclear cataract derived from five studies, cortical cataract derived from three studies, PSC cataract derived from four studies and control group are plotted. Black dotted lines are the regression lines.

4. Discussion

The application of the findings of this literature review is limited by the restricted range of the severity of cataracts and the difference in age between the studies. However, it is a good place to start studying the distinctive relationship between cataract morphology and visual functions. There is a strong correlation between cataract morphology, the intensity of lens opacification, and impairment of visual functions (i.e., straylight and visual acuity).

From the results, we found that PSC population was generally younger, which is in agreement with the literature [24–27] reporting that the average age of the population developing or undergoing surgery for PSC is younger than that for other types of cataract.

In the present study, the log(s)-age dependencies were obtained for cataracts of different morphologies. Among five published articles used in this literature review, four could be used for the nuclear, three for the PSC, and two for the cortical log(s)-age dependency equations (Table 1). These equations cannot be considered normative reference curves, because the different studies made a severity selection of the cataract populations. This must have influenced (weakened) the dependencies. The slopes of the dependency equations varied from one cataract group to another, but the differences were not statistically significant. The slope of the dependency function of the nuclear cataract was close to that of the control group. The reason is that Nischler et al.'s nuclear group with patients with rather good vision was remarkably larger than the rest. The differences between cataracts and control

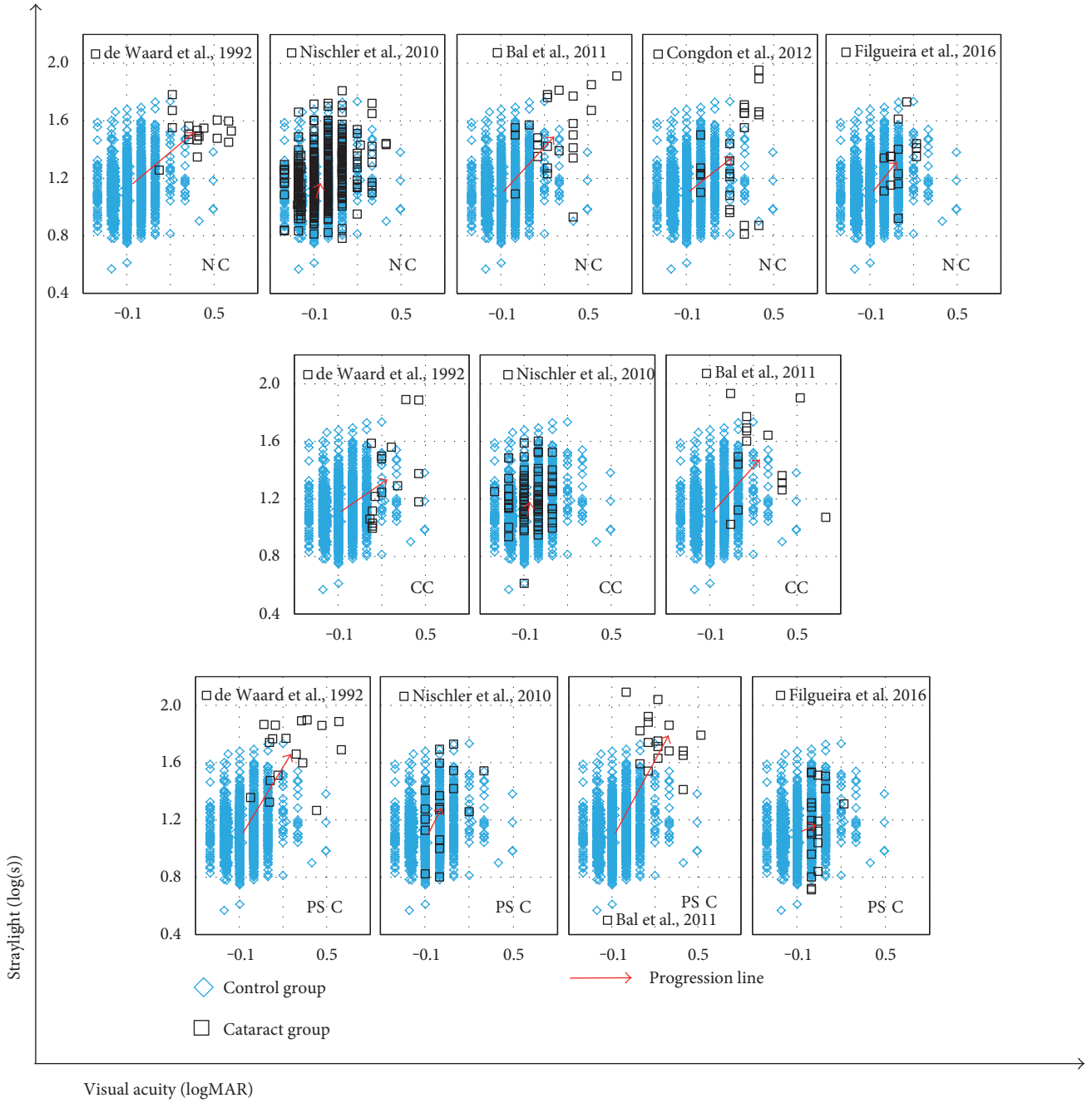

Figure 6: Progression of cataracts from control group is illustrated by arrows originating from mean straylight and mean visual acuity of the control group towards those of each type of cataract in each individual study. (NC: nuclear cataract; CC: cortical cataract; and PSC: posterior subcapsular cataract).

groups, as mentioned earlier, were small, with large overlap between the cataract and control populations. This points at limited validity of the LOCS cataract grading. Although LOCS serves to improve the grading and classifying slit-lamp observation, it is not precise for assessing function. As mentioned in the introduction, there is a weak relation between backscatter and forward scatter; therefore, a slit-lamp-based measurement cannot be a reliable means to quantify forward scatter. The correlation between log(s) and age also varied between cataract groups and control group; it was the highest in cortical cataract and the lowest in PSC.

In each cataract group, the difference in the mean straylight values of individual studies and the respective dependency function was significant. This can be explained by different levels of cataract severity and significant difference in the number of eyes of the largest study and the rest. Such difference was not observed between the slopes of each study and the respective dependency functions. It appeared that the mean straylight values of the reference curves were

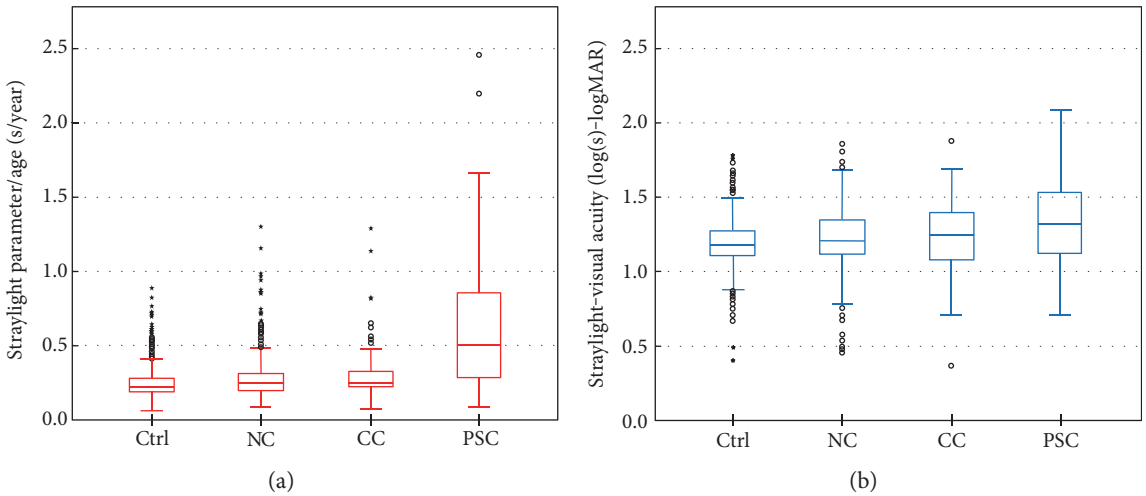

Figure 7: (a) Ratio between straylight parameter and age for each type of cataract: the median of such ratio is significantly higher in the PSC group. (b) The same is valid for straylight-visual acuity. Both cases suggest that straylight is highest in the patients with PSC group albeit lower and/or similar age and visual acuity than/as the other cataracts. (Ctrl: control group; NC: nuclear cataract; CC: cortical cataract; and PSC: posterior subcapsular cataract).

moderately closer to those of Nischler et al.'s nuclear and cortical groups. Nischler et al. covered the major part of the overall data in these two groups; therefore, it is no surprise that it leads the outcomes. The reason Nischler et al. had the lowest mean values in straylight and visual acuity may be due to the fact that the patients were active drivers; therefore, they had comparatively better vision than their age-equivalent peers in other studies. The lowest straylight belonged to Filgueira et al.'s PSC. This is a deviant behavior as PSC in every other study had the highest straylight value. This group's visual acuity was almost as low as that of Nischler et al. Recruiting patients with eyes at the early stage of cataract in these two studies can explain these results (Table 2). When we left out data from Nischler et al. and Filgueira et al., the difference in means of cataract groups became very small, whereas the mean straylight of PSC was approximately 0.3 log units higher than that of other cataracts. This is in agreement with the finding by Elliott et al. [28, 29] that in the advanced stages of cataracts, for patients with PSC, visual acuity alone is not an adequate assessment of visual performance and cataract management. The straylight curve established for normal phakic eyes [23] shows that straylight increases strongly with age with a logarithmic relation (to the power of 4). The change in straylight shows stable behavior in young eyes and considerably increases over 50 years of age. However, our findings showed rather linear relationship between log(s) and age. This may be related to the selection based on severity. We also found that the control group in Figure 4 shows the phakic reference norm works very well.

The correlation between log(s) and logMAR visual acuity varied from none to a moderate one in individual studies and within cataract types, but it never was strong. Overall, no type of cataract showed strong log(s)-logMAR correlation. In clinical practice, this means straylight cannot be predicted on the basis of visual acuity for any type of cataract. Figure 6 shows that, overall, in PSC group straylight deteriorated faster than visual acuity. Some studies [30, 31] found that with increasing the severity of posterior capsule opacification (PCO), visual acuity and straylight deteriorate, albeit with different rates; the PCO severity-log(s) relation is linear, whereas the PCO severity-logMAR is curvilinear [31]. Therefore, straylight is more sensitive to the changes in PCO severity than visual acuity. Kruijt and van den Berg [32] also discussed this difference for localized processes.

Regardless of severity of cataracts, the present study supports the notion that the straylight is the highest in PSC. Fluctuations in density and discontinuous refractive index can be responsible for such amplification [33, 34]. The difference between log(s)-logMAR dependency slopes of cataracts of different morphologies and their correlation coefficients is notable. The distinction between PSC and noncataract eyes is especially remarkable. The log(s)-logMAR progression of cataracts from a control group in our study also showed that PSC deteriorated the most in terms of visual functions. Therefore, it can be inferred that patients with this type of cataract would benefit the most from surgery. However, to draw definite conclusion, further studies on the improvement of visual functions after cataract surgery considering cataract morphologies are necessary. The results presented in Figure 4 show that the age-corrected mean straylight values of Bal et al. in every cataract groups are higher than those of other studies. Unlike patients recruited in the other studies, these patients were listed for cataract surgery. When Bal et al.'s patients were excluded from analysis, PSC had the worst visual acuity; the change in visual acuity in all cataract groups was in average 0.03 log units. The changes in straylight of nuclear and cortical groups were negligible, but it decreased about 0.11 log units in PSC. Therefore, the difference in mean straylight of PSC remained remarkably higher than the other cataracts and the correlation with age decreased ($R^2 = 0.04$, $P = 0.22$). The slopes of the new reference curves remained almost

unchanged. We observed no change in the new log(s)-logMAR correlation in any cataract group, whereas the slopes changed, albeit insignificantly, with the average change of 0.06. Although the effect of excluding Bal et al.'s data on our analysis was unimportant, one needs to recognize the relatively small size of this study as an effective factor in this context.

It should be noted that correlations that were significant in one or some studies, and were not in the other(s), were in fact significant in the whole cataract group. However, this cannot be said about the whole data (different types of cataracts combined), because of different morphologies and eventually different optical dynamics.

5. Conclusion

We confirm that straylight in cataract eyes varies rather independently from age and best-corrected visual acuity. The independence of these two aspects of crystalline lens was speculated to be caused by different optical processes of remarkably different scales [3]. We found that, in accordance to the literature, to assess visual functions of cataracts, the analysis should consider cataract morphology. This becomes more crucial in PSC, where the general visual acuity might not show severe loss, but a remarkable increase of straylight above the cutoff value of 1.40 log units [35] can have negative effect on the quality of life. The norm curves obtained in this literature review serve to distinguish the particular effect of each type of cataract, from early-stage to mild, on visual impairment. However to generalize our results, scrutinize their validity in more severe cataracts, and to develop postoperative straylight improvement references, further studies are needed.

Conflicts of Interest

The Netherlands Academy of Arts and Sciences owns a patent on straylight measurement, with Dr. Thomas J. T. P. van den Berg as the inventor and licenses that to Oculus Optikgeräte GmbH for the C-Quant instrument. None of the other authors has a financial or proprietary interest in any material or method mentioned.

Acknowledgments

This research has been possible thanks to the *AGEYE Marie Curie Initial Training Network*, funded by the European Commission (FP7-PEOPLE-ITN-2013-608049). The authors thank Professor Robert Montés-Micó and Dr. Alejandro Cerviño from the University of Valencia for their cooperation and support.

References

[1] J. J. Vos, "Disability glare—a state of the art report," *CIE Journal*, vol. 3, no. 2, pp. 39–53, 1984.

[2] T. J. T. P. van den Berg, "Analysis of intraocular straylight, especially in relation to age," *Optometry and Vision Science*, vol. 72, no. 2, pp. 52–59, 1995.

[3] T. J. T. P. van den Berg, L. J. van Rijn, R. Michael et al., "Straylight effects with aging and lens extraction," *American Journal of Ophthalmology*, vol. 144, no. 3, pp. 358–363, 2007.

[4] D. Yager, T. Hage, R. Yuan, S. Mathews, and M. Katz, "The relations between contrast threshold, lens back scatter, and disability glare. Noninvasive assessment of the visual system," *OSA Technical Digest Series*, vol. 3, pp. 168–171, 1990.

[5] D. B. Elliott, S. Mitchell, and D. Whitaker, "Factors affecting light scatter in contact lens wearers," *Optometry and Vision Science*, vol. 68, no. 8, pp. 629–633, 1991.

[6] P. W. T. de Waard, J. K. Uspeerf, T. J. T. P. van den Berg, and P. T. V. A. de Jong, "Intraocular light scattering in age-related cataracts," *Investigative Ophthalmology & Visual Science*, vol. 33, no. 3, pp. 618–625, 1992.

[7] D. B. Elliott, D. Fonn, J. Flanagan, and M. Doughty, "Relative sensitivity of clinical tests to hydrophilic lens-induced corneal thickness changes," *Optometry and Vision Science*, vol. 70, no. 12, pp. 1044–1048, 1993.

[8] R. Michael, L. J. van Rijn, T. J. T. P. van den Berg et al., "Association of lens opacities, intraocular straylight, contrast sensitivity and visual acuity in European drivers," *Acta Ophthalmologica*, vol. 87, no. 6, pp. 666–671, 2009.

[9] J. E. Coppens, L. Franssen, L. J. van Rijn, and T. J. T. P. van den Berg, "Reliability of the compensation comparison stray-light measurement method," *Journal of Biomedical Optics*, vol. 11, no. 3, pp. 1–9, 2006.

[10] A. Cervino, R. Montes-Mico, and S. L. Hosking, "Performance of the compensation comparison method for retinal straylight measurement: effect of patient's age on repeatability," *The British Journal of Ophthalmology*, vol. 92, no. 6, pp. 788–791, 2008.

[11] I. Guber, L. M. Bachmann, J. Guber, F. Bochmann, A. P. Lange, and M. A. Thiel, "Reproducibility of straylight measurement by C-Quant for assessment of retinal straylight using the compensation comparison method," *Graefe's Archive for Clinical and Experimental Ophthalmology*, vol. 249, no. 9, pp. 1367–1371, 2011.

[12] D. B. Elliott and M. A. Hurst, "Simple clinical techniques to evaluate visual function in patients with early cataract," *Optometry and Vision Science*, vol. 67, no. 11, pp. 822–825, 1990.

[13] D. B. Elliott, "Evaluating visual function in cataract," *Optometry and Vision Science*, vol. 70, no. 11, pp. 896–902, 1993.

[14] R. W. Massof and G. S. Rubin, "Visual function assessment questionnaires," *Survey of Ophthalmology*, vol. 45, no. 6, pp. 531–548, 2001.

[15] G. S. Rubin, K. Bandeen-Roche, G. H. Huang et al., "The association of multiple visual impairments with self-reported visual disability: SEE project," *Investigative Ophthalmology & Visual Science*, vol. 42, no. 1, pp. 64–72, 2001.

[16] I. J. E. van der Meulen, J. Gjertsen, B. Kruijt et al., "Straylight measurements as an indication for cataract surgery," *Journal of Cataract and Refractive Surgery*, vol. 38, no. 5, pp. 840–848, 2012.

[17] D. B. Elliott, M. A. Bullimore, and I. L. Bailey, "Improving the reliability of the Pelli-Robson contrast sensitivity test," *Clinical Vision Science*, vol. 6, no. 6, pp. 471–475, 1991.

[18] G. Łabuz, N. J. Reus, and T. J. T. P. van den Berg, "Ocular straylight in the normal pseudophakic eye," *Journal of Cataract and Refractive Surgery*, vol. 41, no. 7, pp. 1406–1415, 2015.

[19] C. Nischler, R. Michael, C. Wintersteller et al., "Cataract and pseudophakia in elderly European drivers," *European Journal of Ophthalmology*, vol. 20, no. 5, pp. 892–901, 2010.

[20] T. Bal, T. Coeckelbergh, J. van Looveren, J. J. Rozema, and M. J. Tassignon, "Influence of cataract morphology on straylight and contrast sensitivity and its relevance to fitness to drive," *Ophthalmologica*, vol. 225, no. 2, pp. 105–111, 2011.

[21] N. Congdon, X. Yan, D. S. Friedman et al., "Visual symptoms and retinal straylight after laser peripheral iridotomy," *Ophthalmology*, vol. 119, no. 7, pp. 1375–1382, 2012.

[22] C. P. Filgueira, R. F. Sánchez, L. A. Issolio, and E. M. Colombo, "Straylight and visual quality on early nuclear and posterior subcapsular cataracts," *Current Eye Research*, vol. 41, no. 9, pp. 1209–1215, 2016.

[23] T. J. T. P. van den Berg, L. Franssen, B. Kruijt, and J. E. Coppens, "History of ocular straylight measurement: a review," *Zeitschrift für Medizinische Physik*, vol. 23, no. 1, pp. 6–20, 2013.

[24] N. A. P. Brown and A. R. Hill, "Cataract: the relation between myopia and cataract morphology," *The British Journal of Ophthalmology*, vol. 71, no. 6, pp. 405–414, 1987.

[25] I. Adamsons, B. Munoz, C. Enger, and H. R. Taylor, "Prevalence of lens opacities in surgical and general populations," *Archives of Ophthalmology*, vol. 109, no. 7, pp. 993–997, 1991.

[26] B. E. K. Klein, R. Klein, and S. E. Moss, "Incident cataract surgery: the beaver dam eye study," *Ophthalmology*, vol. 104, no. 4, pp. 573–580, 1997.

[27] J. Panchapakesan, P. Mitchell, K. Tumuluri, E. Rochtchina, S. Foran, and R. G. Cumming, "Five year incidence of cataract surgery: the Blue Mountains eye study," *The British Journal of Ophthalmology*, vol. 87, no. 2, pp. 168–172, 2003.

[28] D. B. Elliott, J. Gilchrist, and D. Whitaker, "Contrast sensitivity and glare sensitivity changes with three types of cataract morphology: are these techniques necessary in a clinical evaluation of cataract?" *Ophthalmic & Physiological Optics*, vol. 9, no. 1, pp. 25–30, 1989.

[29] T. J. T. P. van den Berg, L. Franssen, and J. E. Coppens, "Ocular media clarity and straylight," *Encyclopedia of the Eye*, vol. 3, pp. 173–183, 2010.

[30] W. R. Meacock, D. J. Spalton, J. Boyce, and J. Marshall, "The effect of posterior capsule opacification on visual function," *Investigative Ophthalmology & Visual Science*, vol. 44, no. 11, pp. 4665–4669, 2003.

[31] M. C. van Bree, T. J. van den Berg, and B. L. Zijlmans, "Posterior capsule opacification severity, assessed with straylight measurement, as main indicator of early visual function deterioration," *Ophthalmology*, vol. 120, no. 1, pp. 20–33, 2013.

[32] B. Kruijt and T. J. T. P. van den Berg, "Optical scattering measurements of laser induced damage in the intraocular lens," *PloS One*, vol. 7, no. 2, article e31764, 2012.

[33] D. Tang, D. Borchman, A. K. Schwarz et al., "Light scattering of human lens vesicles in vitro," *Experimental Eye Research*, vol. 76, no. 5, pp. 605–612, 2003.

[34] H. Pau, "Cortical and subcapsular cataracts: significance of physical forces," *Ophthalmologica*, vol. 220, no. 1, pp. 1–5, 2006.

[35] L. J. van Rijn, C. Nischler, R. Michael et al., "Prevalence of impairment of visual function in European drivers," *Acta Ophthalmologica*, vol. 89, no. 2, pp. 124–131, 2011.

Hindawi
Journal of Ophthalmology
Volume 2017, Article ID 6030793, 8 pages
https://doi.org/10.1155/2017/6030793

Research Article

Intraocular Telescopic System Design: Optical and Visual Simulation in a Human Eye Model

Georgios Zoulinakis[1,2] and Teresa Ferrer-Blasco[1,2]

[1]*Department of Optics and Optometry and Visual Sciences, Physics Faculty, University of Valencia, C/ Dr. Moliner 50, 46100 Valencia, Spain*
[2]*Interuniversity Laboratory for Research in Vision and Optometry, Mixed Group University of Valencia-University of Murcia, Valencia, Spain*

Correspondence should be addressed to Georgios Zoulinakis; zoulinakisg@gmail.com

Received 19 December 2016; Accepted 26 February 2017; Published 2 April 2017

Academic Editor: Van C. Lansingh

Purpose. To design an intraocular telescopic system (ITS) for magnifying retinal image and to simulate its optical and visual performance after implantation in a human eye model. *Methods.* Design and simulation were carried out with a ray-tracing and optical design software. Two different ITS were designed, and their visual performance was simulated using the Liou-Brennan eye model. The difference between the ITS was their lenses' placement in the eye model and their powers. Ray tracing in both centered and decentered situations was carried out for both ITS while visual Strehl ratio (VSOTF) was computed using custom-made MATLAB code. *Results.* The results show that between 0.4 and 0.8 mm of decentration, the VSOTF does not change much either for far or near target distances. The image projection for these decentrations is in the parafoveal zone, and the quality of the image projected is quite similar. *Conclusion.* Both systems display similar quality while they differ in size; therefore, the choice between them would need to take into account specific parameters from the patient's eye. Quality does not change too much between 0.4 and 0.8 mm of decentration for either system which gives flexibility to the clinician to adjust decentration to avoid areas of retinal damage.

1. Introduction

Retinal damage results in localized vision loss, and frequently, visual rehabilitation implies optimizing the remaining vision by means of image magnification and/or decentration to non-affected areas. Age-related macular degeneration (AMD) is a retinal condition that causes a progressive loss of central vision, and its prevalence is being increased due to ageing of the world population and sedentary. Patients diagnosed with AMD face significant and progressive visual loss, which may lead to legal and social blindness [1]. In this situation, patients need to use the peripheral field of view in order to track moving objects and to move in their environment [2–4]. This adds up to the fact that many AMD patients are also afflicted by cataract, where both conditions decrease visual acuity.

Cataract extraction and intraocular lens implantation not only solves satisfactorily the visual decrease caused by the cataract [5] but also improves visual acuity and quality of life in AMD patients, while not influencing the progression of the disease [6]. In this situation, implanting an intraocular telescopic system (ITS) might be an option to consider for optimizing the remaining visual capability of the eye.

An ITS is a miniaturized telescopic device that can be implanted in the human eye. Several trials and research studies have reported the good clinical outcomes, safety, and improved quality of life after implantation [7–10]. These ITS may be grouped into two types: the first one is composed of 2 lenses with high optical power (Galilean telescope) [11] and the second one is composed of mirrors (Cassegrain telescope) [12]. Both ITS project a magnified image, with a magnification of ×2 or ×3, but there is a large variety of different magnifications used in common practice.

Within the Galilean-type ITS, a further division can be made in two more subtypes. The first subtype would be

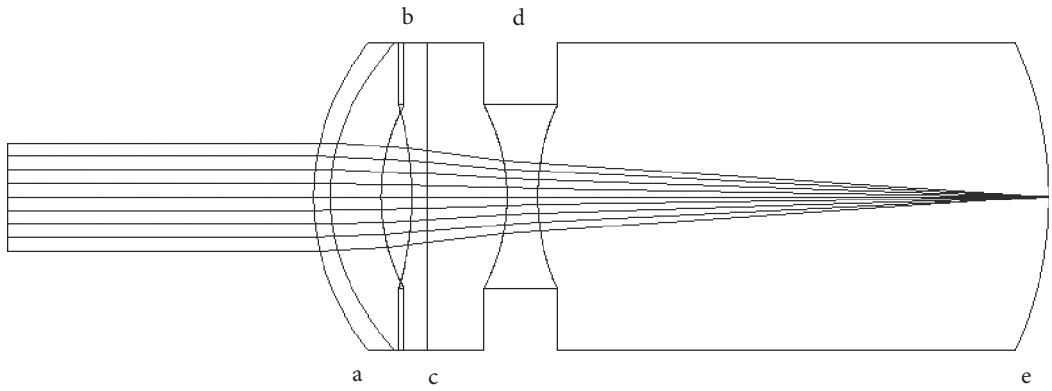

Figure 1: Liou-Brennan eye model with intraocular telescope ITS 1. a, cornea; b, anterior positive lens; c, pupil; d, posterior negative lens; e, retina.

positioned between the anterior and posterior chamber of the eye, while the second one would be positioned completely in the posterior chamber, behind the pupil. The optimal position, distance between the lenses, and magnification provided by these ITS have been reported previously [7, 11, 13].

The purpose of the present study is to design one Galilean telescope of each subtype and simulate optical and visual outcomes in a human eye model to test vision at different vergences. There is also a study and comparison of the quality offered with the decentration of the lenses of each system.

2. Materials and Methods

Ray-tracing and optical design software (ZEMAX, USA) was used to design and study the optical and visual quality of the ITS proposed. The human eye model introduced by Liou and Brennan in 1997 [14] was used for the calculations. This eye model is simple enough for the needs of the present study, and while more complicated and recent models could also be used [15–19], the results would follow the same pattern if the model simulates an emmetropic human eye. On the other hand, the main difference between the different theoretical eye models is the way the crystalline lens is designed. For the purposes of this study, as further explained later in the manuscript, the crystalline lens was removed, and therefore, there is no major difference in using one eye model or the other. Unless otherwise stated in the paper, all the parameters of the model used were the same as stated in the original work by Liou and Brennan.

To carry out the simulations, a central incoming field of rays of green light (587.6 nm) passing through a pupil of 3 mm in diameter was used. Two different target vergences were used: a target for distance and a target for near at reading distance (0.41 m). As the target distance decreased, the distance between the lenses had to increase for the image to remain focused.

2.1. ITS Design. The ITS studied consists of an anterior positive and a posterior negative lens (Galilean telescope). Both lenses were of high optical power as described later in the manuscript. The first ITS designed has the positive lens in front of the pupil and the negative lens behind, while the second one is completely positioned behind the pupil. None of the designs correspond to an existing design, material, or patent. The *ITS through pupil* (ITS 1) was designed following the work of Felipe et al. [11] and the model is shown in Figure 1. The crystalline lens was removed from the eye model, and the empty space was given the refractive index of the aqueous (1.336). The system is composed of a positive anterior lens of 53 diopters (D) and a negative posterior lens of −64 D. The anterior lens was designed and located 1.66 mm from the posterior corneal surface and 0.5 mm in front of the pupil, with a refractive index of 1.55 and thickness of 1 mm. The anterior surface of the lens was given 33 D of power while the posterior surface was calculated to be 20.44 D, to give a total power of 53 D. This power was calculated from the effective power formula

$$D = P_a + P_p - \frac{t}{n} P_a P_p. \quad (1)$$

In this formula, D represents the total optical power in diopters; P_a, P_p represent the optical powers of the anterior and posterior surface of the lens, respectively; t represents the lens thickness; and n represents the refractive index of the lens.

The posterior lens was designed to be located 2.6 mm behind the pupil, with a total power of −64 D. The anterior surface was given a power of −34 D, and the posterior surface was calculated to be −29.36 D. The same thickness and refractive index were used for the power calculation as before. The total distance between both lenses was 3.1 mm for distance and 3.65 mm for near.

The *ITS behind the pupil* (ITS 2) design was based on the work description of Tabernero et al. [13], and the model is shown in Figure 2. As done previously, the crystalline lens was removed from the eye model. The empty space was given the refractive index of the aqueous, and the whole telescopic system was designed behind the pupil, in the posterior chamber. This system is composed of a positive anterior lens of 66 D and a negative posterior lens of −66 D. For the positive lens, the anterior surface was designed with 36 D and the posterior surface 30.71 D of dioptric power. For the negative lens, the anterior surface was designed with −36 D and the posterior −29.32 D of dioptric power. All calculations were

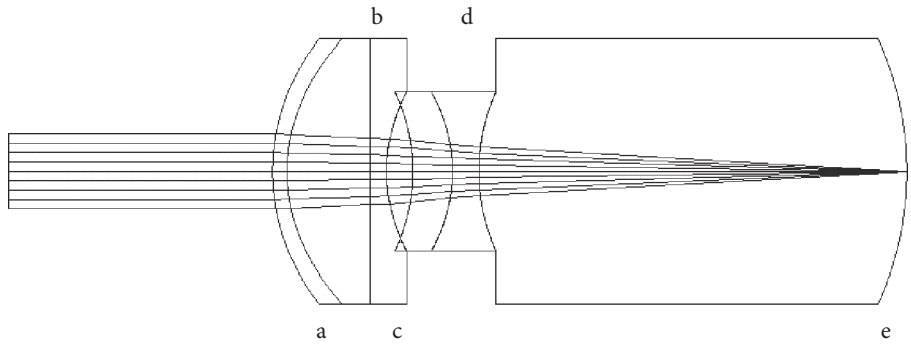

Figure 2: Liou-Brennan eye model with intraocular telescope ITS 2. a, cornea; b, pupil; c, anterior positive lens; d, posterior positive lens; e, retina.

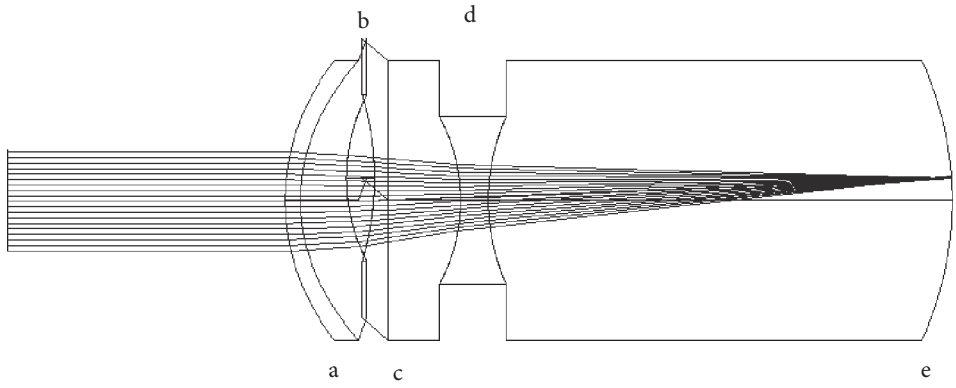

Figure 3: ITS 1 with decentered anterior lens. a, cornea; b, anterior positive lens; c, pupil; d, posterior negative lens; e, retina.

carried out as with the previous design, using the formula for thick lenses. Both lenses had a thickness of 1 mm and a refractive index of 1.55. The distance between the lenses in this system was 1.5 mm for distance and 1.95 mm for near.

2.1.1. Optimization and Decentration of the Lenses. Both ITS were studied under optimized and nonoptimized situations. The optimization process was done using the optimization tool provided by the software. This tool optimizes the system by changing the variables selected by the user in order to get the least root mean square (RMS) wavefront error of the whole optical system. The variables used in this study were the conic constant, the second and fourth asphericity term of the anterior surface of the positive lens of the system. These were selected in order to study the differences between an ITS with spherical lenses and an ITS that also corrects the aberrations produced by the cornea.

The effect of decentration of the ITS lenses was also explored. In the case of a nonfunctional macula, redirecting the image to a healthy region is one option to be considered. Decentration of the image is provided by a prism effect produced by the decentration of the two lenses. The anterior lens of each ITS was decentered up to 1 mm in 0.2 mm steps. The decentration was done for both optimized and nonoptimized systems. Decentration was induced in one direction only (y-axis), since the eye model used is rotationally symmetric. In a customized model (with astigmatism and decentered surfaces), the direction of the decentration would have to be chosen according to the astigmatism and the retinal area where the image needs to be projected on. Figures 3 and 4 show the decentered ITS 1 and 2 designs, respectively.

In order to decenter the lenses, two more surfaces were added on top of the surfaces of each lens. These surfaces are called *coordinate break surfaces*, and they help the user to decenter the lens from the optical axis. They do not alter the final optical and visual quality outcomes in any way, as they only serve as a tool for changing the position of each lens. After performing ray tracing through the optical design software, resulting wavefront RMS error and Zernike coefficients were collected and fed into a custom-made program in MATLAB to calculate a metric called visual Strehl ratio (VSOTF) [20, 21]. The VSOTF is based on the optical transfer function of the whole optical system. It is considered to be one of the best metrics for assessing retinal image quality and has been used in research studies [22, 23]. It is calculated as a ratio of the system's integrated optical transfer function modulated by the contrast sensitivity function to its equivalent for a diffraction-limited system,

$$\mathrm{VSOTF} = \frac{\int_{-\infty}^{\infty}\int_{-\infty}^{\infty} \mathrm{CSF_N}(f_x, f_y) * \mathrm{OTF}(f_x, f_y)\, df_x df_y}{\int_{-\infty}^{\infty}\int_{-\infty}^{\infty} \mathrm{CSF_N}(f_x, f_y) * \mathrm{OTF_{DL}}(f_x, f_y)\, df_x df_y}, \quad (2)$$

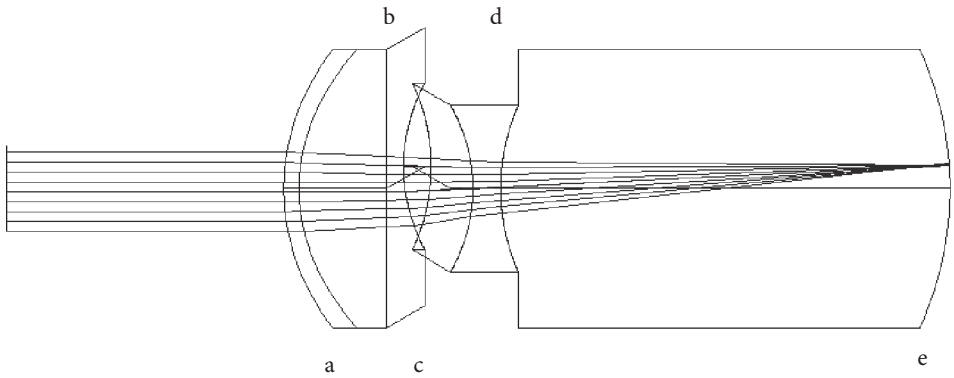

Figure 4: ITS 2 with decentered anterior lens. a, cornea; b, pupil; c, anterior positive lens; d, posterior positive lens; e, retina.

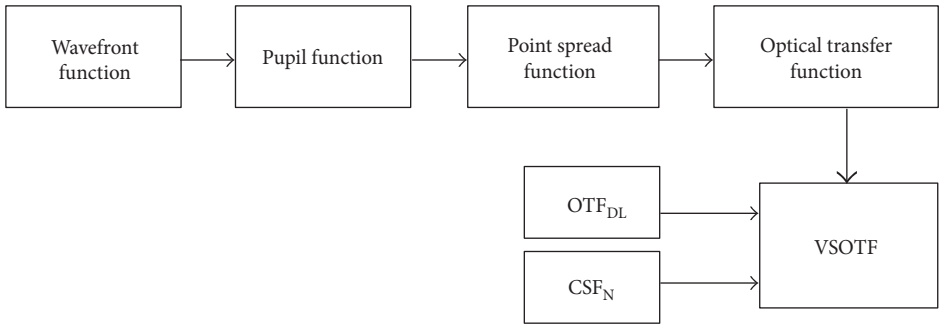

Figure 5: A schematic diagram of the custom algorithm written in MATLAB.

where $\mathrm{OTF}(f_x,f_y)$ represents the optical transfer function, $\mathrm{OTF}_{\mathrm{DL}}(f_x,f_y)$ represents the diffraction-limited optical transfer function, $\mathrm{CSF}_{\mathrm{N}}(f_x,f_y)$ is the neural contrast sensitivity function, and (f_x,f_y) are the spatial frequency coordinates [21].

The software program uses the wavefront function, which is produced from the optics of the model eye, the telescope, and the pupil function implemented in the software (circular with 3 mm in diameter). By combining these, it calculates the pupil function that, after Fourier transformation, provides the point-spread function. A secondary Fourier transform yields the optical transfer function (OTF) of the system. The program also calculates the diffraction-limited OTF ($\mathrm{OTF}_{\mathrm{DL}}$) and the neural contrast sensitivity function ($\mathrm{CSF}_{\mathrm{N}}$) of the system [24]. Finally, it combines the OTF, $\mathrm{OTF}_{\mathrm{DL}}$, and $\mathrm{CSF}_{\mathrm{N}}$ in order to calculate the VSOTF of the system. Figure 5 provides a graphical approach to the algorithm.

3. Results

The optical quality was measured in terms of total wavefront RMS error (for 587.6 nm wavelength) and the visual quality in terms of VSOTF metric. Results for both optimized and nonoptimized telescopic systems were gathered, with either centered or decentered lenses in order to study the impact of decentration in the quality of vision.

Table 1 presents the results for both telescopic systems at far target distance.

Figure 6 represents graphically the optical quality results for distance in terms of wavefront RMS error. The wavefront RMS error results were calculated through the ray-tracing software, and they were measured for 587.6 nm wavelength. Figure 6 also shows the visual quality results for distance in terms of the visual Strehl ratio. The VSOTF results were calculated through a pupil of 3 mm diameter.

Table 2 presents the results for the first and second telescopic systems at near target distance. Figure 7 shows graphically the optical and visual results for both telescopic systems focused at near.

When the lenses of each ITS were decentered, the image was also moving towards the peripheral area of the fovea. This image decentration was also measured in the software, and the results for the nonoptimized ITS are shown in Table 3. The same table also compiles the results for the optimized ITS image decentration for distance and near.

4. Discussion

Retinal conditions such as AMD have compromised vision in the central field and benefit from magnifying the retinal image or relocating it in order to optimize the remaining visual capabilities. A telescopic system that magnifies and/or projects the image to a healthy part of the retina could be a satisfactory option. In the present study, two different ITS were designed and compared. The first one is composed of an anterior lens of +53 D optical power, positioned in front of the pupil, and a posterior lens of −64 D optical power, placed behind the pupil. The second telescope is totally positioned behind the pupil and is composed of an anterior lens

Table 1: Optical and visual results for both telescopic systems (far target distance).

	Decentration (mm)	Optimized system		Nonoptimized system	
		RMS (wavelengths)	VSOTF	RMS (wavelengths)	VSOTF
ITS 1	0.0	0.00017	0.99997	0.06621	0.67655
	0.2	0.04750	0.56845	0.12529	0.24763
	0.4	0.11107	0.27600	0.25315	0.09752
	0.6	0.20162	0.19473	0.44053	0.07813
	0.8	0.32587	0.17874	0.69565	0.10008
	1.0	0.48908	0.18612	1.02587	0.10115
ITS 2	0.0	0.00032	0.99997	0.04573	0.80058
	0.2	0.04446	0.65255	0.10011	0.25081
	0.4	0.12208	0.40203	0.25297	0.11908
	0.6	0.24940	0.37397	0.51092	0.14969
	0.8	0.43805	0.32400	0.88700	0.16121
	1.0	0.70249	0.09259	1.40018	0.00757

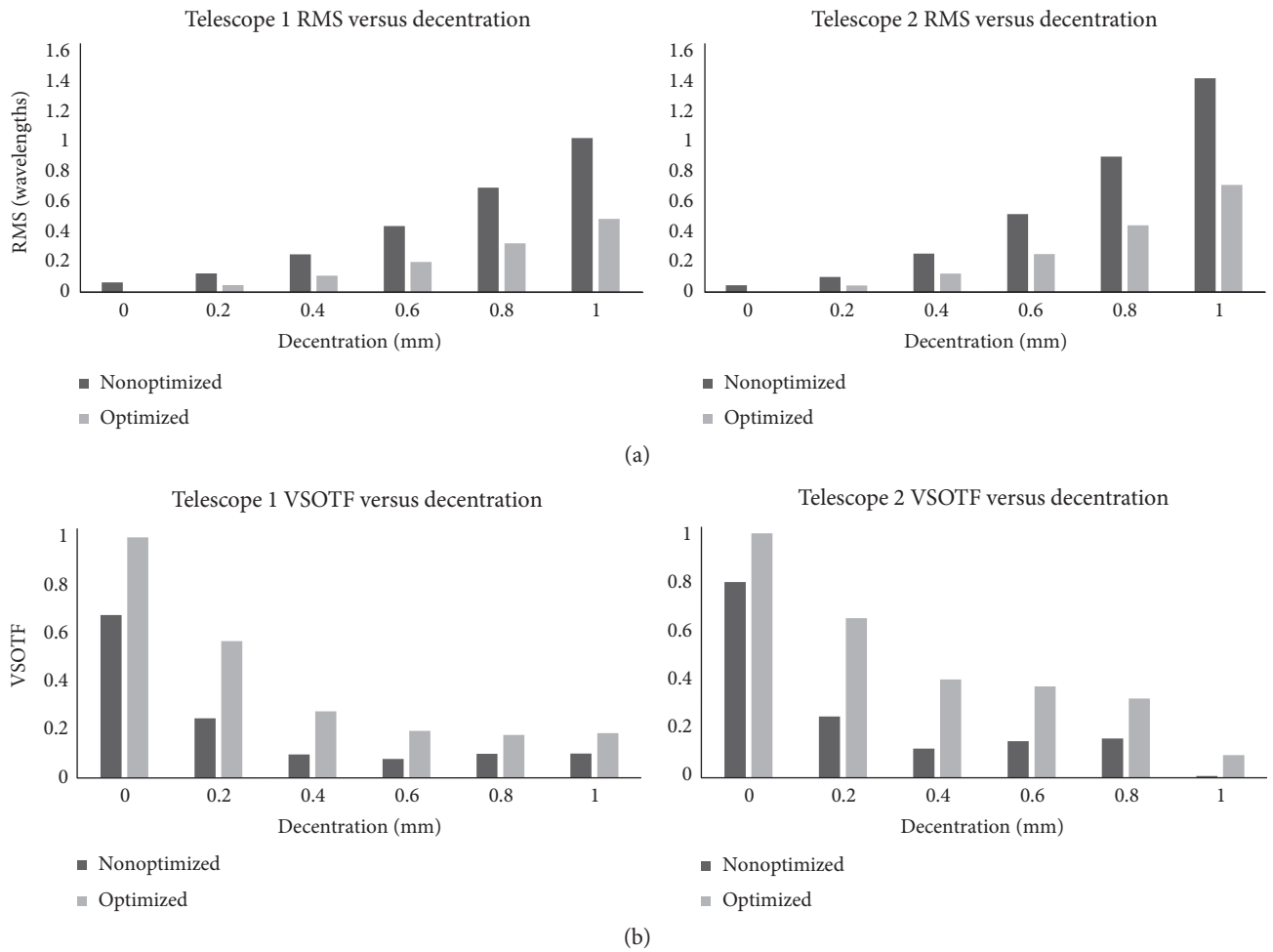

Figure 6: Telescope root mean square (RMS) wavefront error (a) and visual Strehl ratio (VSOTF) (b) versus decentration of the anterior lens.

with optical power +66 D and a posterior lens of −66 D. In order to focus at different distances, the distance between the lenses must change as well in both ITS proposed. For the ITS 1, when focused at distance, the distance between lenses was 3.1 mm, increasing to 3.65 mm for near targets. For ITS 2, the distance between lenses changed from 1.5 mm when focused at distance to 1.95 mm when focused at near.

Table 2: Optical and visual results for both telescopic systems (near target distance).

	Decentration (mm)	Optimized system		Nonoptimized system	
		RMS (wavelengths)	VSOTF	RMS (wavelengths)	VSOTF
ITS 1	0.0	0.00050	0.99997	0.08162	0.51337
	0.2	0.03162	0.75714	0.13343	0.20787
	0.4	0.07285	0.42921	0.25653	0.07948
	0.6	0.13094	0.29042	0.44222	0.05522
	0.8	0.21107	0.23356	0.69713	0.07219
	1.0	0.31791	0.21931	1.02795	0.09214
ITS 2	0.0	0.00058	0.99997	0.06363	0.64374
	0.2	0.03885	0.71124	0.12556	0.17792
	0.4	0.10720	0.44347	0.30485	0.07998
	0.6	0.22132	0.39109	0.60986	0.09826
	0.8	0.39469	0.37503	1.05769	0.14287
	1.0	0.64508	0.17847	1.67465	0.00579

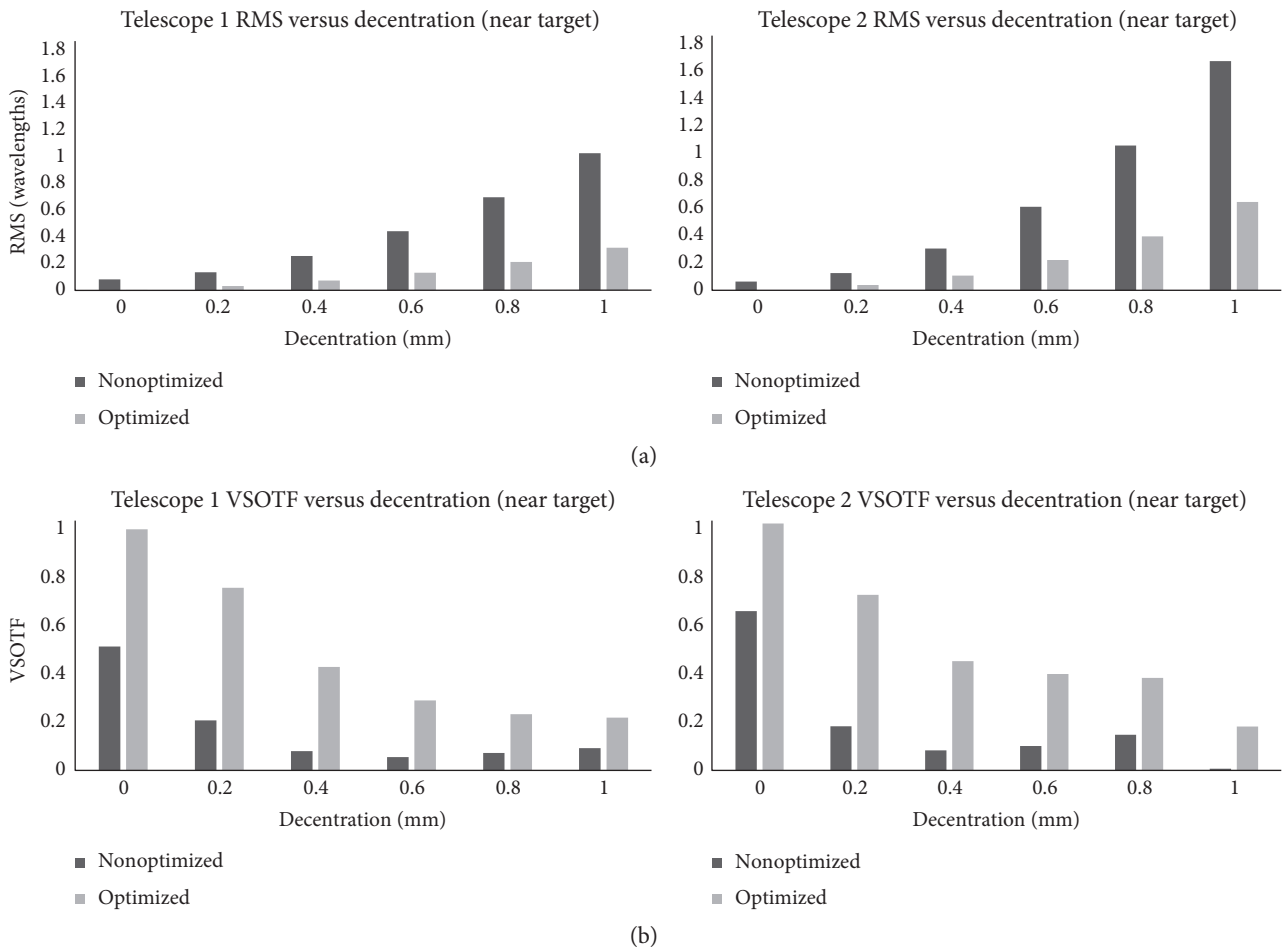

Figure 7: Telescope root mean square (RMS) wavefront error (a) and visual Strehl ratio (VSOTF) (b) versus decentration of the anterior lens for near target distance.

For both designs (see Figure 6), the optical and visual quality is better when using aspheric lenses in order to correct the aberrations induced by the cornea and the implantation procedure. ITS 2 provides better optical and visual results than ITS 1. The same observations can be done from Figures 4 and 5 for the near target results. Both ITS could provide equal quality of vision in AMD patients. The ITS 2 provides slightly better results, and the fact that the whole ITS is behind the

Table 3: Image decentration for both optimized and nonoptimized ITS over anterior lens decentration.

	Anterior lens decentration (mm)	ITS 1 (nonoptimized)		ITS 2 (nonoptimized)	
		Image decentration far target distance (mm)	Image decentration near target distance (mm)	Image decentration far target distance (mm)	Image decentration near target distance (mm)
Nonoptimized systems	0.2	0.1953	0.1991	0.2082	0.2152
	0.4	0.4016	0.3992	0.4222	0.4240
	0.6	0.6010	0.6017	0.6278	0.6440
	0.8	0.7952	0.7992	0.8346	0.8585
	1.0	1.0130	1.0020	1.0610	1.0810
Optimized systems	0.2	0.1953	0.2041	0.2110	0.2179
	0.4	0.4037	0.3992	0.4227	0.4324
	0.6	0.6051	0.6042	0.6304	0.6440
	0.8	0.7964	0.8042	0.8612	0.8585
	1.0	0.9876	1.0020	1.0780	1.0880

pupil and is smaller in length suggests it could be a better option for a real implant.

Another parameter that plays a significant role in the choice of an ITS would be the axial length of the eye. As Felipe et al. [11] stated in their study, longer eyes (myopic) would be more suitable for the ITS 1.

A further expansion of this study could be considered in order to optimize the asphericities of the anterior lens after the decentration of the lens. This could result in better optical and visual quality as previously done in the study by Tabernero et al. [13]. In this study, the optimization was done before the decentration of the lenses in order to test the image quality when the decentration of an already manufactured ITS needs to be selected.

For the near targets, the results follow the same trend with that for distance (Figure 7). The VSOTF decreases as decentration increases. Nevertheless, between 0.4 and 0.8 mm decentration, the difference between the results is minimal. This could indicate a range of selectable decentrations that would allow the clinician to relocate the retinal image without modifying significantly its quality.

In general, while the decentration increases, the quality decreases dramatically. There are astigmatic and coma aberrations induced because of the decentration of the lenses. As Tabernero et al. [13] proposed in their study, a cylinder lens could be used in order to fix the induced amount of astigmatism. On the other hand, as previously discussed, image quality is not significantly affected by decentrations between 0.4 and 0.8 mm for either distance or near targets (Table 3). This decentration induces a displacement of the retinal image within the central 3.5 degrees of the retina, which is within the foveal and parafoveal area.

According to these results, depending on the area of the retinal damage, the surgeon might choose a specific decentration for each patient without altering significantly the quality of the image. For ITS 2 particularly, the calculated VSOTF is above the 0.3 limit that represents the 0 logMAR, as proposed by Cheng et al. [25]. Obviously, as departing from the fovea, the image would be displaced to a retinal region with lower visual capabilities, and therefore, the final visual result might be even lower, but the optical quality provided by the ITS would be better than the visual threshold for that part of the retina.

Long-term results of recent studies [26] report visual results in agreement with our simulations. In the same study, it is also reported that younger patients showed even better results than the older ones, something that is expected as their vision is generally better. These young subjects also presented less adverse events from the application of such devices. In this way, the simulation of these telescopic systems could provide better results in terms of agreement with clinical studies and increase our knowledge in this research field.

In the end, biometric parameters must be determined before considering which of the designs should be considered to be used. Both systems can be used, but there is still space for more research in their designs and applications.

Conflicts of Interest

None of the authors has any financial or proprietary interest to disclose in relation with any of the materials or methods described.

Acknowledgments

This study is supported by the Marie Curie Grant FP7-LIFE-ITN-2013-608049-AGEYE.

References

[1] S. B. Bloch, M. Larsen, and I. C. Munch, "Incidence of legal blindness from age-related macular degeneration in Denmark: year 2000 to 2010," *American Journal of Ophthalmology*, vol. 153, no. 2, pp. 209–213, 2012, e202.

[2] R. D. Jager, W. F. Mieler, and J. W. Miller, "Age-related macular degeneration," *New England Journal of Medicine*, vol. 358, no. 24, pp. 2606–2617, 2008.

[3] L. S. Lim, P. Mitchell, J. M. Seddon, F. G. Holz, and T. Y. Wong, "Age-related macular degeneration," *The Lancet*, vol. 379, no. 9827, pp. 1728–1738, 2012.

[4] H. L. Cook, P. J. Patel, and A. Tufail, "Age-related macular degeneration: diagnosis and management," *British Medical Bulletin*, vol. 85, no. 1, pp. 127–149, 2008.

[5] D. Allen and A. Vasavada, "Cataract and surgery for cataract," *BMJ*, vol. 333, no. 7559, pp. 128–132, 2006.

[6] D. S. Ehmann and A. C. Ho, "Cataract surgery and age-related macular degeneration," *Current Opinion in Ophthalmology*, vol. 28, no. 1, pp. 58–62, 2017.

[7] M. A. Qureshi, S. J. Robbie, J. Tabernero, and P. Artal, "Injectable intraocular telescope: pilot study," *Journal of Cataract & Refractive Surgery*, vol. 41, no. 10, pp. 2125–2135, 2015.

[8] H. L. Hudson, R. D. Stulting, J. S. Heier et al., "Implantable telescope for end-stage age-related macular degeneration: long-term visual acuity and safety outcomes," *American Journal of Ophthalmology*, vol. 146, no. 5, pp. 664–673, 2008, e661.

[9] M. A. Singer, N. Amir, A. Herro, S. S. Porbandarwalla, and J. Pollard, "Improving quality of life in patients with end-stage age-related macular degeneration: focus on miniature ocular implants," *Clinical Ophthalmology*, vol. 6, pp. 33–39, 2012.

[10] S. S. Lane and B. D. Kuppermann, "The implantable miniature telescope for macular degeneration," *Current Opinion in Ophthalmology*, vol. 17, no. 1, pp. 94–98, 2006.

[11] A. Felipe, M. Díaz-Llopis, A. Navea, and J. M. Artigas, "Optical analysis to predict outcomes after implantation of a double intraocular lens magnification device," *Journal of Cataract & Refractive Surgery*, vol. 33, no. 10, pp. 1781–1789, 2007.

[12] A. Agarwal, I. Lipshitz, S. Jacob et al., "Mirror telescopic intraocular lens for age-related macular degeneration: design and preliminary clinical results of the Lipshitz macular implant," *Journal of Cataract & Refractive Surgery*, vol. 34, no. 1, pp. 87–94, 2008.

[13] J. Tabernero, M. A. Qureshi, S. J. Robbie, and P. Artal, "An aspheric intraocular telescope for age-related macular degeneration patients," *Biomedical Optics Express*, vol. 6, no. 3, pp. 1010–1020, 2015.

[14] H.-L. Liou and N. A. Brennan, "Anatomically accurate, finite model eye for optical modeling," *Journal of the Optical Society of America A*, vol. 14, no. 8, pp. 1684–1695, 1997.

[15] A. V. Goncharov and C. Dainty, "Wide-field schematic eye models with gradient-index lens," *Journal of the Optical Society of America A, Optics, image science, and vision*, vol. 24, no. 8, pp. 2157–2174, 2007.

[16] T. Eppig, K. Scholz, A. Löffler, A. Meßner, and A. Langenbucher, "Effect of decentration and tilt on the image quality of aspheric intraocular lens designs in a model eye," *Journal of Cataract & Refractive Surgery*, vol. 35, no. 6, pp. 1091–1100, 2009.

[17] J. J. Rozema, D. A. Atchison, and M.-J. Tassignon, "Statistical eye model for normal eyes," *Investigative Ophthalmology & Visual Science*, vol. 52, no. 7, pp. 4525–4533, 2011.

[18] J. Polans, B. Jaeken, R. P. McNabb, L. Hervella, P. Artal, and J. A. Izatt, "Wide-field schematic model of the human eye with asymmetrically tilted and decentered lens," *Investigative Ophthalmology & Visual Science*, vol. 56, no. 7, pp. 6019–6019, 2015.

[19] D. A. Atchison and L. N. Thibos, "Optical models of the human eye," *Clinical and Experimental Optometry*, vol. 99, no. 2, pp. 99–106, 2016.

[20] J. D. Marsack, L. N. Thibos, and R. A. Applegate, "Metrics of optical quality derived from wave aberrations predict visual performance," *Journal of Vision*, vol. 4, no. 4, pp. 322–328, 2004.

[21] D. R. Iskander, "Computational aspects of the visual Strehl ratio," *Optometry & Vision Science*, vol. 83, no. 1, pp. 57–59, 2006.

[22] Y. Benard, N. Lopez-Gil, and R. Legras, "Subjective depth of field in presence of 4th-order and 6th-order Zernike spherical aberration using adaptive optics technology," *Journal of Cataract & Refractive Surgery*, vol. 36, no. 12, pp. 2129–2138, 2010.

[23] A. A. Gallego, S. Bará, Z. Jaroszewicz, and A. Kolodziejczyk, "Visual Strehl performance of IOL designs with extended depth of focus," *Optometry & Vision Science*, vol. 89, no. 12, pp. 1702–1707, 2012.

[24] F. W. Campbell and D. G. Green, "Optical and retinal factors affecting visual resolution," *The Journal of Physiology*, vol. 181, no. 3, pp. 576–593, 1965.

[25] X. Cheng, A. Bradley, and L. N. Thibos, "Predicting subjective judgment of best focus with objective image quality metrics," *Journal of Vision*, vol. 4, no. 4, pp. 310–321, 2004.

[26] D. Boyer, K. B. Freund, C. Regillo, M. H. Levy, and S. Garg, "Long-term (60-month) results for the implantable miniature telescope: efficacy and safety outcomes stratified by age in patients with end-stage age-related macular degeneration," *Journal of Clinical Ophthalmology*, vol. 9, pp. 1099–1107, 2015.